Geologic Studies in Alaska by the U.S. Geological Survey, 1997

Edited by Karen D. Kelley

U.S. Geological Survey Professional Paper 1614

U.S. Department of the Interior
U.S. Geological Survey

U.S. Department of the Interior
Bruce Babbitt, Secretary

U.S. Geological Survey
Charles G. Groat, Director

For sale by U.S. Geological Survey, Information Services
Box 25286, Federal Center
Denver, CO 80225

This publication is also available online at:
http://greenwood.cr.usgs.gov/pub/ppapers/p1614/

Library of Congress Cataloging-in-Publication Data

Geologic studies in Alaska by the U.S. Geological Survey, 1997 /
edited by Karen D. Kelley.
p. cm.—(U.S. Geological Survey professional paper : 1614)
Includes bibliographical references.
Supt. of Docs. no.: I 19. 16: 1614
1. Geology—Alaska. I. Kelley, Karen D. II. Series.
QE83.G46 2000
557.98—dc219 9–41611
CIP

Contents

BIBLIOGRAPHIES

Contributors to this Professional Paper

Anchorage

Bradley, Dwight C.
Dumoulin, Julie A.

U.S. Geological Survey
4200 University Drive
Anchorage, Alaska 99508

York, Geoff S.

U.S. Geological Survey
Alaska Biological Science Center
1011 Tudor Road
Anchorage, Alaska 99503

Houle, Julie A.
Meyers, Mark D.

Alaska Department of Natural Resources
Division of Oil and Gas
Anchorage, Alaska 99503-5948

Denver

Flores, Romeo M., Mail Stop 939
Goldfarb, Richard J., Mail Stop 964
Kelley, Karen D., Mail Stop 964
Meier, Allen L., Mail Stop 973
Parnow, Cynthia C., Mail Stop 964
Siems, David F., Mail Stop 973
Stricker, Gary D., Mail Stop 939

U.S. Geological Survey
P.O. Box 25046, Mail Stop ____
Denver Federal Center
Denver, Colorado 80225

Fairbanks

Werdon, Melanie B.

Alaska Division of Geological and Geophysical Surveys
794 University Ave., Suite 200
Fairbanks, Alaska 99709-3645

Newberry, Rainer J.

Department of Geology
University of Alaska
Fairbanks, Alaska 99775

Menlo Park

Barnes, David F., Mail Stop 989
Brew, David A., Mail Stop 901
Fierstein, Judy, Mail Stop 910
Hildreth, Wes, Mail Stop 910
Lanphere, Marvin A., Mail Stop 937
Galloway, John P., Mail Stop 904
Toussaint, Susan, Mail Sop 955

U.S. Geological Survey
345 Middlefield Road, Mail Stop ____
Menlo Park, California 94025

Reston

Harris, Anita G., Mail Stop 926A
Repetski, John E., Mail Stop 926A

U.S. Geological Survey
National Center, Mail Stop ____
12201 Sunrise Valley Drive
Reston, Virginia 20192

Others

Cieutat, Barrett A.

ERM Southwest
3501 North Causeway Boulevard, Suite 200
Metairie, Louisiana 70002

Farmer, G. Lang

Department of Geology
University of Colorado
Boulder, Colorado 80302

Geologic Studies in Alaska by the U.S. Geological Survey, 1997

Edited by Karen D. Kelley

Introduction

By Karen D. Kelley

The eight papers that follow continue the series[1] of U.S. Geological Survey (USGS) reports on investigations in the geologic sciences in Alaska. The series presents new and sometimes preliminary findings that are of interest to earth scientists in academia, government, and industry; to land and resource managers; and to the general public. Reports presented in Geologic Studies in Alaska cover a broad spectrum of topics from all parts of the State (fig. 1), which serves to emphasize the diversity of USGS efforts to meet the Nation's needs for earth-science information in Alaska.

The papers in this volume are organized under the topics Resources, Geologic Framework, and Environment and Climate. Such an organization is intended to reflect the scope and objectives of USGS programs currently active in Alaska. Resource papers include one that presents detailed observations from a Mississippian Zn-Pb-Cu-Ag occurrence in the Brooks Range (Werdon). Mineralogic, chemical, and isotopic data provide the basis for a proposed relationship between this vein-breccia deposit and the shale-hosted massive sulfide deposit type, which includes the active Red Dog mine in the western Brooks Range. Also included under the topic of Resources is a paper that presents geochemical and isotopic data from the Greens Creek and Woewodski Island volcanogenic massive sulfide deposits in southeastern Alaska (Newberry and Brew). The depositional environment and sedimentological setting of Tertiary coal beds in the Matanuska and Susitna Valleys is the focus of a third paper under the topic of Resources (Flores and others).

Geologic Framework studies provide background information that is the scientific basis for present and future studies of the environment, mineral and energy resources, paleoclimate, and hazards in Alaska. One paper presents the results of sedimentologic and paleontologic comparisons of lower Paleozoic, deep-water-facies rock units in central Alaska (Dumoulin and others). The authors show which of these units are likely to correlate with one another, suggest likely source regions, and provide a structural restoration of units that have been fragmented by large fault motions. A second framework paper provides a map, rock descriptions, and chemical compositions of volcanic rocks in a newly recognized, geologically young volcanic center in the Aleutian volcanic arc (Hildreth and others). A third paper presents an interesting summary of gravity changes that occurred in south-central Alaska during the great earthquake of 1964 and for the following 25 years (Barnes). Gravity changes correlate with land-elevation changes in some cases, but not in others, which means that different processes are responsible for the gravity changes.

---

[1] From 1975 through 1988, the Geologic Studies in Alaska series was published as USGS Circulars, which were initially titled "The United States Geological Survey in Alaska: Accomplishments during 19xx." From 1989 to 1994, the series was published as the more formal USGS Bulletins. As a result of reorganization of USGS publications, beginning in 1995 the series has been published as USGS Professional Papers.

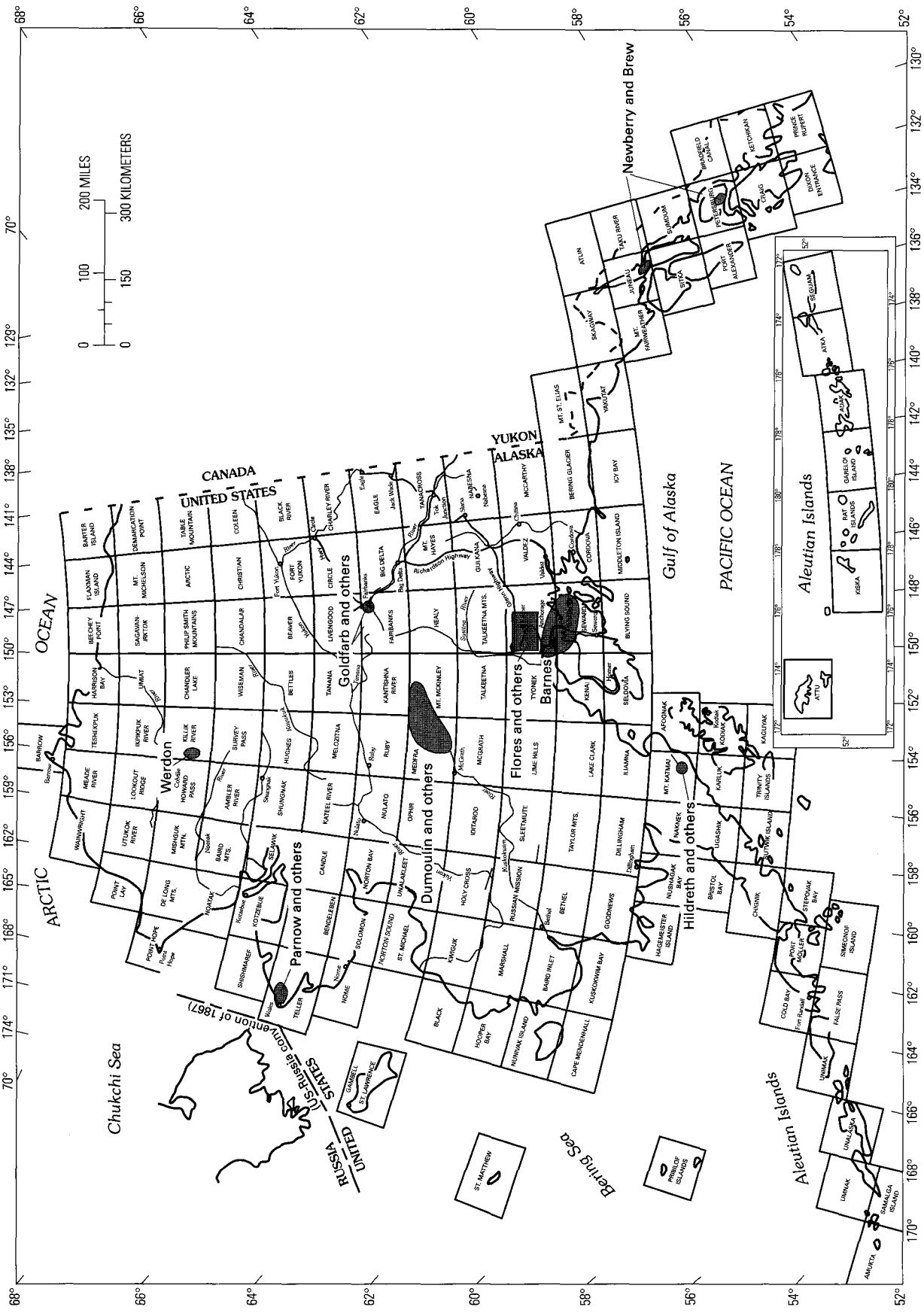

Figure 1. Index map of Alaska showing 1:250,000-scale quadrangles and locations of study areas discussed in this book.

Environmental studies are the focus of two papers. One study discusses the nature and origin of uncommonly high arsenic and heavy-metal concentrations in stream sediments of the northwestern Seward Peninsula, a region of traditional subsistence living (Parnow and others). A second study evaluates the chemical characteristics of natural waters north of Fairbanks, an area known for atypically high arsenic concentrations in ground waters (Goldfarb and others).

Two bibliographies at the end of the volume present reports about Alaskan earth sciences in USGS publications during 1997, and reports about Alaska by USGS authors in non-USGS publications during the same period.

Geologic Studies in Alaska by the
U.S. Geological Survey, 1997
U.S. Geological Survey Professional Paper 1614

Geologic Setting of Mississippian Vein-Breccias at the Kady Zn-Pb-Cu-Ag Prospect: Plumbing System for a Failed Sedex Deposit?

By Melanie B. Werdon

Abstract

The north-central and northwestern Brooks Range of Alaska hosts widespread Zn-Pb-Ag shale-hosted massive sulfide (Sedex), vein-breccia, and disseminated sulfide deposits. The vein-breccia and disseminated occurrences show no obvious igneous association and are hosted by a deformed, but only weakly metamorphosed, package of Upper Devonian to Lower Mississippian mixed continental and marine clastic rocks (the Endicott Group). The Sedex deposits (i.e., Red Dog, Drenchwater) are hosted by black siliceous carbonaceous shale and mudstone of the Mississippian to Pennsylvanian Kuna Formation. Previous studies have suggested that the vein-breccia zones are either Carboniferous or were formed along Mesozoic or post-Mesozoic faults. This study documents a Mississippian age for the Kady vein-breccia prospect and investigates the physical and chemical controls on ore formation.

Early diagenetic and hydrothermal features at the Kady Zn-Pb-Cu-Ag vein-breccia prospect provide insights into Carboniferous basinal dewatering of the Upper Devonian to Lower Mississippian Endicott Group in the northern Brooks Range, Alaska. Sulfides at Kady occur in several subparallel, quartz-dominated, linear vein-breccia zones (1–35 m wide, with a minimum strike length of about 800 m), which are offset by Mesozoic structures, and as permeability-controlled, strata-bound disseminated cements in gray sandstone in a 5-km by 3-km area. Sphalerite ($(Zn_{81.5\text{-}99.7}, Fe_{0.1\text{-}17.9}, Cd_{0.1\text{-}0.9})S$) is the dominant sulfide mineral, followed by galena, chalcopyrite, minor pyrite, trace bravoite and Ag+Sb±Pb sulfosalts, and extremely rare pyrrhotite. The relative proportion and volumetric abundance of the primary minerals varies widely within and between vein-breccia zones. Main stage quartz+sulfide (±late calcite) vein-breccia zones cut rare early ankerite and siderite veins. Sulfides and quartz precipitated during a steep drop in temperature, possibly during the change from lithostatic to hydrostatic pressure during extensional faulting, from a relatively low temperature (≤ 250°C), slightly acidic, carbon-destructive hydrothermal fluid. Textural and mineralogical data indicate that sulfides and quartz were deposited under evolving chemical conditions (i.e., increasing pH, fugacity of oxygen, and fugacity of sulfur).

The lack of known Sedex mineralization in the north-central Brooks Range suggests that Kady represents the hydrothermal fluid pathway below a failed or nonexistent Sedex system. Although early diagenetic processes within the Endicott Group were favorable for the mineral-destructive release of base metals from detrital minerals, base metals were not transported and deposited in overlying shales but, rather, were deposited within the Endicott Group. Unfavorable conditions may have existed for Sedex deposit formation above the Kady prospect including one or more combinations of the following: boiling above the level of the vein-breccia system leading to rapid precipitation of base metal sulfides in the vein-breccias; dispersion of buoyant, low-salinity, metal-bearing fluids (if they reached the sea floor) such that metals would not be deposited and accumulated in massive amounts; and a short-lived, low-temperature system.

Introduction

The Kady Zn-Pb-Cu-Ag vein-breccia and disseminated sulfide prospect is located in the southwestern part of the Killik River quadrangle in the north-central Brooks Range, Alaska (fig. 1). Kady is located within Gates of the Arctic National Park near the headwaters of a tributary to Outwash Creek at lat 68°12′N. and long 154°58′W. in T. 32 N., R. 17 E.

Numerous Zn-Pb-Ag vein-breccia and disseminated sulfide occurrences were discovered in the northern Brooks Range during reconnaissance studies by the U.S. Bureau of Mines and U.S. Geological Survey in the 1970's to 1990's (e.g., Jansons and Parke, 1981; Jansons, 1982; Meyer and Kurtak, 1992; Kelley and others, 1997). These vein-breccia and disseminated sulfide occurrences are hosted by arenaceous, mixed continental-marine clastic rocks of the Upper Devonian to Lower Mississippian Endicott Group and extend from the western Brooks Range, near Red Dog, eastward to the Killik River quadrangle. The Kady prospect was discovered in 1985 by tracing stream-sediment geochemical anomalies to their source (Duttweiler, 1987).

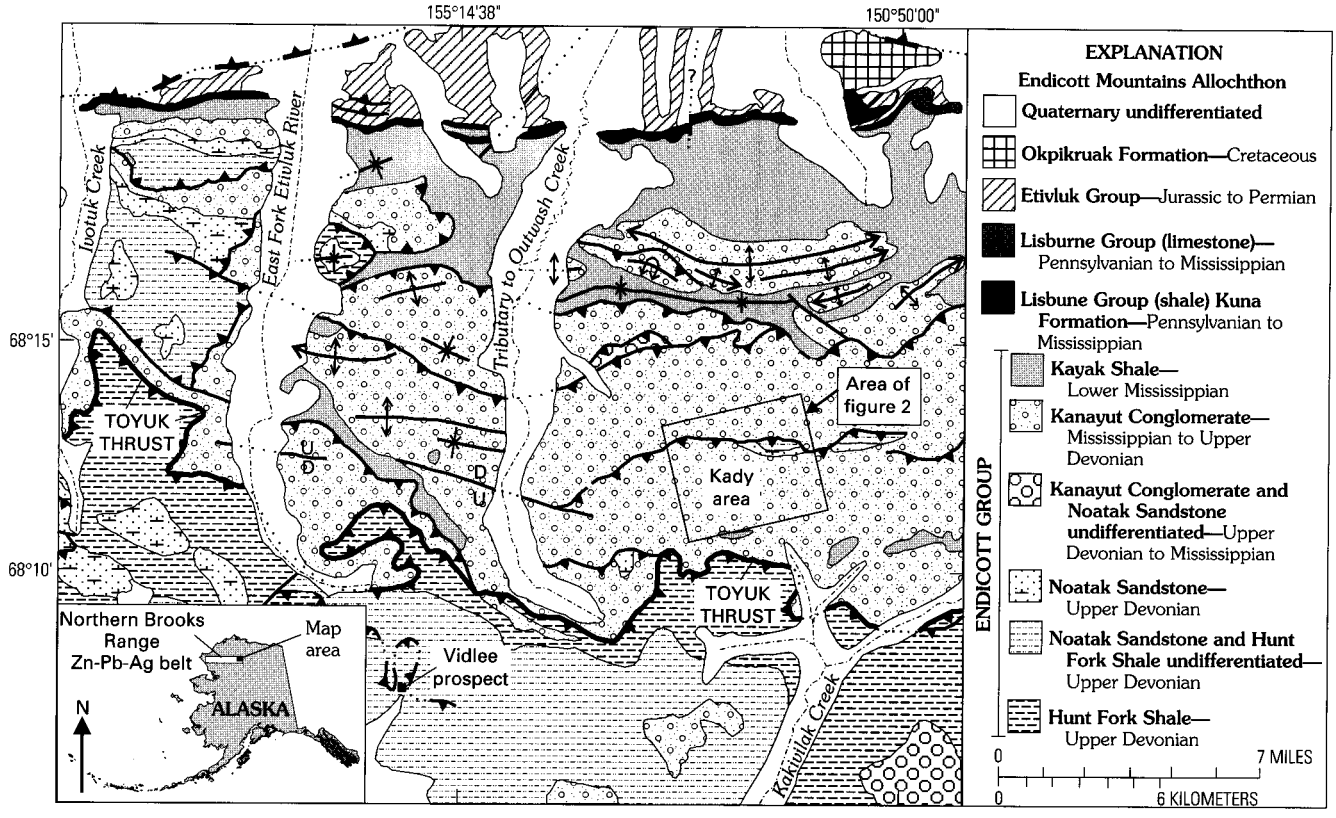

Figure 1. Geologic map of the southwest part of the Killik River quadrangle, north-central Brooks Range, Alaska. Geology modified from Mull and others (1994) and Mull and Werdon (1994).

Mineralized rocks at Kady occur within the Endicott Mountains allochthon, a regionally extensive package of predominantly sedimentary rocks of Devonian to Cretaceous age, which are part of the Brooks Range fold-and-thrust belt. Two tectonic events of significance have been recognized within (or have affected rocks of) the Endicott Mountains allochthon: (1) Mississippian to Pennsylvanian(?) extension, and (2) compression during the Late Jurassic to Early Cretaceous Brookian orogeny. Extension during Mississippian to Pennsylvanian(?) time in the northern Brooks Range is suggested by abrupt facies changes and inferred normal faults (Moore and others, 1986), shale-hosted stratiform or sedimentary exhalative (Sedex) massive sulfide deposits (Moore and others, 1986; Forrest, 1983), and regionally extensive, but volumetrically minor, volcanic tuffs and intrusions within Mississippian- to Pennsylvanian-age units (Werdon, 1996; Mull and Werdon, 1994). Alkaline volcanic rocks at the shale-hosted Red Dog and Drenchwater massive sulfide deposits have $^{40}Ar/^{39}Ar$ plateau ages ranging from 343 Ma to 336 Ma (Werdon and others, 1998). Northward emplacement of allochthons during the Mesozoic Brookian orogeny is related to convergence between the continental Arctic Alaska terrane and the interior of Alaska (Moore and others, 1994).

A reconnaissance study by Ellersieck and others (1990) has suggested that the vein-breccia occurrences may either be feeder zones to Carboniferous Sedex deposits or may have formed along Mesozoic or post-Mesozoic faults in the Brooks Range. Although the Zn-Pb-Ag geochemical signature and relative stratigraphic position of the vein-breccia occurrences suggests that they may be genetically related to the Sedex hydrothermal event, previous studies have not provided evidence documenting a Carboniferous age for the vein-breccia occurrences. The timing of Sedex and vein-breccia mineralization in the northern Brooks Range has recently been investigated by the $^{40}Ar/^{39}Ar$ laser step-heating method (Werdon and others, 1998). Volcanic tuffs, breccias, and small intrusions at Drenchwater have been cut and partially replaced by sulfide mineralization (Werdon, 1996). Biotite from the intrusions provides an estimate of the maximum age for the Sedex mineralizing event. A 3-m-thick, hydrothermal white mica altered igneous sill(?), which intrudes the Ikalukrok unit of the Upper Mississippian to Pennsylvanian(?) Kuna Formation, was also dated from the south side of the main Red Dog deposit. The igneous sill(?) consists of intergrown fine-grained white mica, clay(?), and granular quartz, and it is cut by hydrothermal quartz±sphaleriite±pyrite±galena±white mica veins. The plateau age of this whole-rock sample records the time at which temperatures cooled below the argon closure temperature of hydrothermally produced white mica (interpreted as representing the late stage of the hydrothermal system). The biotite from Drenchwater and the white mica from the sill(?) at Red Dog suggest that the maximum and minimum age limits for the Sedex mineralizing event are approximately 337 Ma and about 314 Ma, respectively (Werdon and others, 1998).

Recrystallized detrital white mica from sandstone adjacent to a quartz-sulfide vein at Kady was also dated by the $^{40}Ar/^{39}Ar$ laser step-heating method (Werdon and others, 1998). Plateau ages of 324±2 Ma and 325±2 Ma, and an isochron age of 324±3 Ma were obtained from three whole-rock sandstone chips from

the same hand specimen. Although these dates fall within the $^{40}Ar/^{39}Ar$ timing constraints for the Carboniferous Sedex mineralizing event, it could be argued that the ages represent a regional heating event if the field and petrographic data suggest that mineralization at Kady did not occur during Carboniferous time. In addition, lead isotopic compositions of galena at Kady (Gaccetta and Church, 1989; Werdon, 1998) are statistically indistinguishable at 2σ from those of galena in the shale-hosted Red Dog, Lik, and Drenchwater massive sulfide deposits (Gaccetta and Church, 1989). The isotopic similarity suggests a similar source for the lead in these deposits, and it suggests, but does not require, that these deposits are the same age because lead isotopic ratios do not change when physically remobilized.

The data presented in this paper document that the mineralization at the Kady vein-breccia prospect is Carboniferous in age. The physical and chemical controls on ore formation are also discussed. Unlike most vein-breccia occurrences in the northern Brooks Range, the Kady prospect is well exposed and the geologic and structural relationships are clear. The lack of extensive weathering allowed detailed examination of the mineralized zones and determination of the composition, cementation, diagenetic history, and hydrothermal alteration of the host rocks. Investigation of the host rocks was undertaken to (1) evaluate the local Endicott Group's potential as a source of Zn, Pb and Cu, (2) characterize wallrock alteration adjacent to the vein-breccia zones, and (3) investigate the stratigraphic controls of both disseminated and vein-breccia mineralization. The lack of known Sedex mineralization in the Killik River quadrangle suggests that the Kady prospect represents the hydrothermal fluid pathway below a failed or nonexistent Sedex system. Kady provides a good opportunity to examine why Sedex mineralization may not have formed.

Methods

Geologic and structural mapping of the Kady area was conducted at a scale of 1:15,840 during 19 days in the field. The size, texture(s), and mineralogy of each vein-breccia and disseminated sulfide zone was recorded. Forty-five doubly-polished thin sections of vein- and breccia-textured ore were examined by transmitted- and reflected-light petrography. Eight doubly-polished, 30-μm thin sections of sphalerite were quantitatively analyzed for Zn, Fe, Cd, Mn, and S using the University of Alaska-Fairbanks Cameca electron microprobe. Standards used for calibration include: MnS (Mn, S), $Fe_{40}Zn_{60}S$ (Fe), and CdSZnS (Cd, Zn). Analytical operating conditions include an accelerating potential of 25 keV, a beam current of 20 nA, and a beam diameter of 1 μm. Weight-percent analyses were converted to mole percent. Additionally, the sphalerite color for each point was recorded.

Selected hand samples of visibly mineralized rocks at Kady were analyzed for major and trace elements by inductively coupled plasma atomic emission spectroscopy (ICP-AES), and rocks suspected of containing elevated levels of Ag, Zn, Pb, and Cu were analyzed by fire assay (Meyer and Kurtak, 1992). All Au analyses were determined by the fire-assay method. Several pulps from this data set were also analyzed for trace elements by X-ray fluorescence (XRF) to confirm suspected interference problems (discussed in text). Interference problems in fire-assay analyses for Au occurred in samples that contain greater than 2 percent Pb.

Sphalerite, galena, chalcopyrite, and pyrite separates were made by cutting out selected areas with a trim saw, crushing to between 30 and 100 mesh, washing, and then hand-picking grains under high magnification to minimize contamination between phases. Sulfur isotopic analyses for sphalerite, galena, chalcopyrite, and ore-stage pyrite are reported as per mil variations with respect to the Canyon Diablo iron meteorite. Samples were analyzed by Geochron Laboratories, Inc., Cambridge, Mass., and have analytical uncertainties of ±0.2‰ at 2σ.

Hydrothermal quartz separates were made by cutting out selected pieces of quartz from both vein- and breccia-textured, sulfide-bearing samples. Oxygen isotopic compositions obtained from hydrothermal quartz are reported as per mil (‰) variations of $^{18}O/^{16}O$ with respect to standard mean ocean water (SMOW). Samples were analyzed by Dr. K.L. Shelton, University of Missouri-Columbia, and the analytical precision is generally better than ±0.1‰ at 1σ.

Approximately 115 clastic rocks and their cements at Kady were examined petrographically, by electron microprobe energy dispersive spectroscopy (EDS), and by cathodoluminescence (CL) (operated at 20–25 keV). The results are summarized in the Appendix.

Fluid-inclusion temperature and salinity data were obtained from vein quartz at Kady. The individual analyses are presented in Werdon (1998), along with a complete description of the samples, sample locations, and analytical methods.

Geology and Structure of the Kady Area

Stratigraphic units in the Kady area are part of the Lower Mississippian to Upper Devonian Endicott Group, which includes the Hunt Fork Shale, Noatak Sandstone, Kanayut Conglomerate, and Kayak Shale. The Hunt Fork Shale is exposed along a fault separating a south-dipping upright section of Noatak Sandstone to the south from an overturned, south-dipping section of the Noatak Sandstone to the north (fig. 2). The Hunt Fork Shale consists of brown, fine-grained, carbonate-cemented sandstone interbedded with variably micaceous, grayish-black, compact to fissile shale. The Hunt Fork Shale served as a large-scale detachment surface in the Kady area; therefore, stratigraphically underlying units are not present. The thickness of the Hunt Fork Shale is difficult to determine because it is typically structurally thickened or thinned, but it is estimated to be greater than 500 m thick in the Kady area (Mull and others, 1994).

The lower part of the Noatak Sandstone is exposed in the core of several anticlines (fig. 2). The lower part of the Noatak Sandstone in the Kady area consists of interbedded red-brown to black shale; red-brown siltstone; brown, fine- to medium-grained calcareous sandstone; and lesser orange-brown sandy limestone. It is characterized by distinctive, manganese-oxide-coated, carbonate-rip-up-clast layers (intra-formational lithoclast conglomerates) within calcareous sandstones, and small (less than 2 cm) brachiopods. The brachiopods are similar to brachiopods in Devonian units elsewhere in the northern Brooks

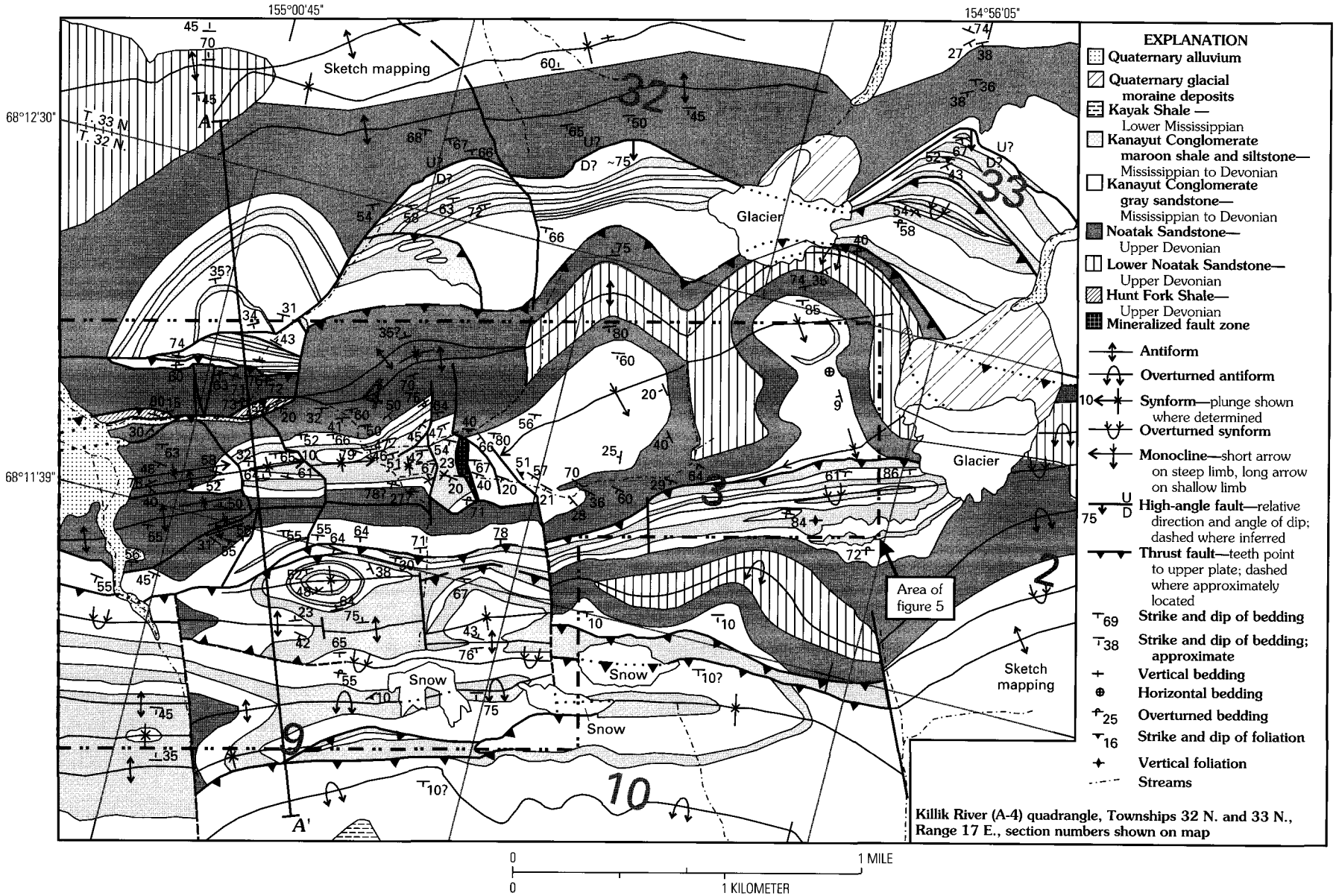

Figure 2. Geologic map of the Kady area.

Range (R. Blodgett, oral commun., 1993). The thickness of the lower part of the Noatak Sandstone is estimated to be approximately 50 m, and it is depositionally overlain by the upper part of the Noatak Sandstone.

The upper part of the Noatak Sandstone in the Kady area is a light greenish brown, medium-grained, thin wavy-bedded to crossbedded to massive, partially to completely carbonate-cemented sandstone (fig. 3*A*). It is characterized by patchy poikilitic carbonate cement, calcareous concretions (as large as 30 cm in diameter) (fig. 3*B*), thin black shale flasers, variably micaceous partings, and small patches of disseminated pyrite (fig. 3*C*). The thickness of the upper part of the Noatak Sandstone is estimated to be about 170 m. The carbonate cement content decreases as the Noatak Sandstone grades upward into the Kanayut Conglomerate.

The Kanayut Conglomerate in the Kady area consists of interbedded gray sandstone, red-brown siltstone and shale, and minor calcareous sandstone and quartz-chert-pebble conglomerate. It contains occasional limonite rip-up clasts, carbonaceous plant fragments, thin coal beds, and intergranular carbonaceous material that highlights bedding within sandstone. The gray sandstone at the base of the Kanayut Conglomerate is a distinctive marker bed; it forms massive, prominently outcropping ridges covered by black lichen. The gray sandstone is dominantly quartz cemented (generally less than or equal to 5 percent carbonate cement) and contains fining-upward sequences (fig. 3*D*), trough crossbedding, planar bedding, and minor, thin conglomerate beds (pebbles as large as 4 cm in diameter; average less than or equal to 2 cm) (fig. 3*E*). Thinner, erosion-resistant, gray sandstone layers are interbedded with reddish-brown siltstone, maroon to black shale, and conglomerate in the upper half of the Kanayut Conglomerate. The thickness of the Kanayut Conglomerate is estimated to be about 300 m. The Kayak Shale depositionally overlies the Kanayut Conglomerate, but it was not examined as part of this study.

Sedimentary rocks of the Endicott Group are complexly and spectacularly folded and faulted in the Kady area. The initial stages of Mesozoic compression produced kilometer-scale folds (open and overturned antiforms and synforms) (figs. 2, 3*F*). The axes of the folds trend roughly N. 75° E., and their axial planes

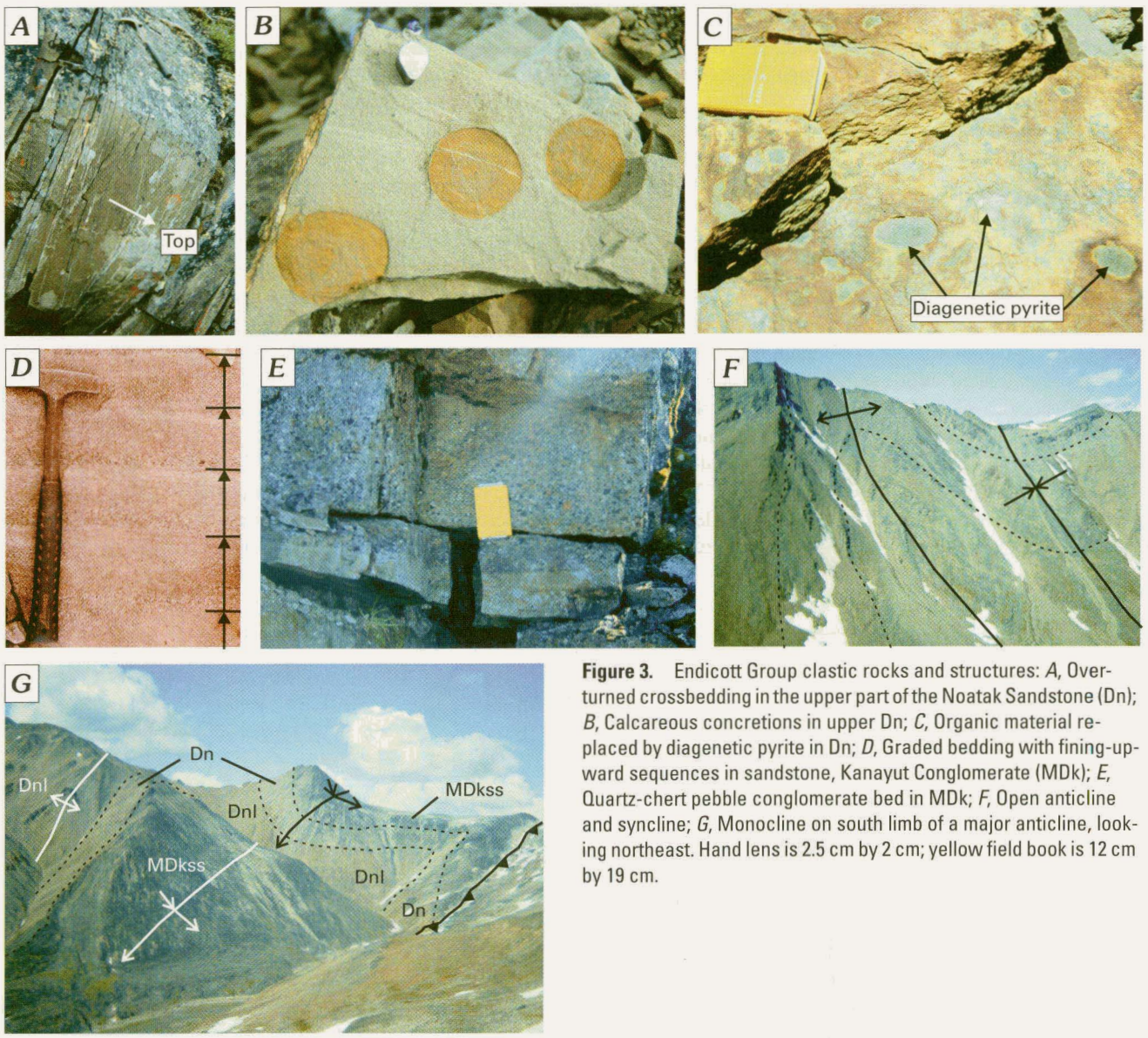

Figure 3. Endicott Group clastic rocks and structures: *A*, Overturned crossbedding in the upper part of the Noatak Sandstone (Dn); *B*, Calcareous concretions in upper Dn; *C*, Organic material replaced by diagenetic pyrite in Dn; *D*, Graded bedding with fining-upward sequences in sandstone, Kanayut Conglomerate (MDk); *E*, Quartz-chert pebble conglomerate bed in MDk; *F*, Open anticline and syncline; *G*, Monocline on south limb of a major anticline, looking northeast. Hand lens is 2.5 cm by 2 cm; yellow field book is 12 cm by 19 cm.

dip moderately to steeply to the south. A distinctive, west-plunging monocline occurs on the south flank of the large anticline in the central map area (fig. 3*G*). A structural cross section through the Kady area (fig. 4) shows the relatively incompetent Hunt Fork Shale overlain by the Noatak Sandstone and the sandstone-dominated lower part of the Kanayut Conglomerate, which form a relatively competent layer. Incompetent shale-rich units in the upper Kanayut Conglomerate are structurally thickened and internally folded within the cores of anticlines. Continued compression produced thrust faults subparallel to fold axes and a conjugate set of reverse faults. Offset on thrust faults in the Kady area is on the scale of a few hundred meters or less.

The Mesozoic structural style varies significantly from east to west. For example, the major anticline north of the monocline is overturned on its eastern end (fig. 2). To the west, the anticline progressively changes into an open fold, an open fold with an M-shaped core, and on the western end one limb is overturned and faulted away. Two north-northwest-trending, high-angle faults in the southern half of the map area (fig. 2) separate areas with different structural styles.

A late, east-trending normal(?) fault is present in the northern half of the map area (fig. 2). This fault is parallel to Mesozoic thrust faults and could also be interpreted as a thrust fault with younger-over-older-style displacement. One north-northwest-trending fault in the northern map area offsets the east-trending fold and fault structures.

Mineralization

Distribution and Field Description of Sulfide Mineralization

The Kanayut Conglomerate is the main host for vein-breccia and disseminated sulfide mineralization at Kady, with lesser amounts occurring in the Noatak Sandstone. Sulfide minerals include sphalerite, galena, chalcopyrite, and minor pyrite. Most mineralization occurs within a subparallel set of vein-breccia zones that strike approximately N. 25° W. and dip steeply west (fig. 5). Vein-breccia zone U is the widest (as wide as 37 m) and highest grade mineralized zone (figs. 6*A* and 6*B*). Vein-breccia zones B-C-E-F-G and L-K-H are interpreted to be formerly continuous and subparallel systems (fig. 6*C*)—both of these vein-breccia zones terminate at the Mesozoic thrust faults that bound their north and south sides, and the apparent changes in strike, in part, reflect topographic variations. Vein-breccia zone B-C-E-F-G is offset approximately 12 m along a small normal fault near C, and there is a thrust fault between F and G, and K and H. This structural evidence supports the interpretation that the vein-breccia zones were present before Mesozoic deformation. Vein-breccia zones U-V, M, P and possibly A (fig. 5) are also part of this subparallel set. Vein-breccia zones with approximately east-west orientations include D, AB, AC, and a small breccia zone near E (fig. 5). Vein-breccia zone D is parallel to the fold axis of an anticline, and its orientation may suggest that minor sulfide remobilization accompanied Mesozoic deformation.

Although most vein-breccia zones have an overall linear strike orientation, one vein at H is slightly folded (fig. 6*D*). Other veins at H occur in thin-sheeted vein sets (fig. 6*E*), or pinch out and are cut by late faults with minor slip (fig. 6*F*). Most veins at Kady are wider in brittle sandstone units and pinch out or disappear entirely in less competent shale units. The vein-breccia zones cross bedding at steep angles and are roughly perpendicular to the axial traces of large-scale Mesozoic folds and thrust faults (fig. 5). The approximately N. 55° E. trend is the extensional direction in the Mesozoic contractional event and could be interpreted as evidence for vein formation during or after Mesozoic deformation. The offset of Mesozoic fold axes along several of the western vein-breccia zones (figs. 2, 5) could either be interpreted as evidence (1) for vein formation after Mesozoic deformation, or (2) that Carboniferous mineralized zones acted as planes of weakness during Mesozoic deformation. Sheeted quartz veins at S are cut off by a later, inferred, Mesozoic fault. Mineralization has been variably deformed depending upon the competency of the host rock, degree of wallrock silica flooding, and the location within a given structure. Quartz-sulfide mineralization is often cut by penetrative cleavage, joints, and (or) stylolites.

Gray sandstone within the Kanayut Conglomerate contains sparse disseminated sphalerite and galena (generally less than 0.1 percent Zn+Pb), both adjacent to and distal from the vein-breccia zones (fig. 5). Sulfide-bearing sandstone is recognized

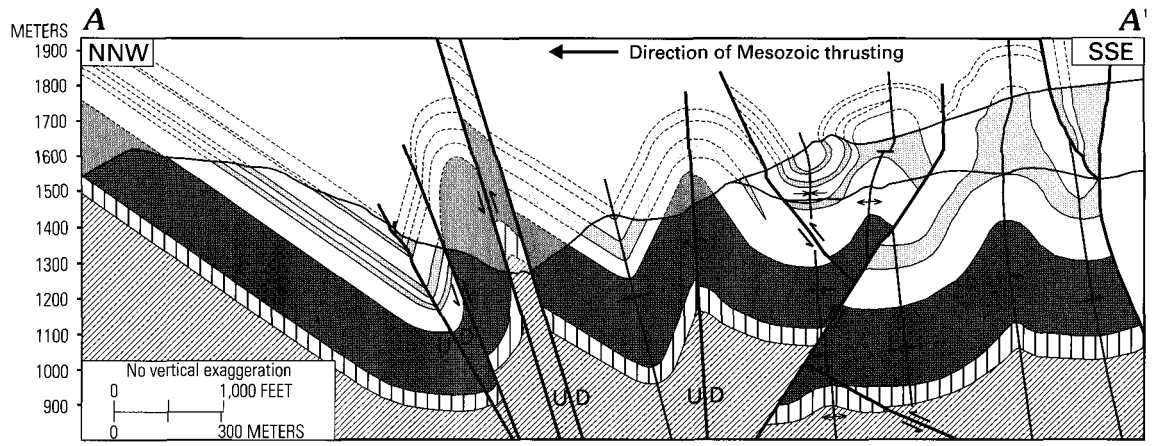

Figure 4. Structural cross section through the Kady area.

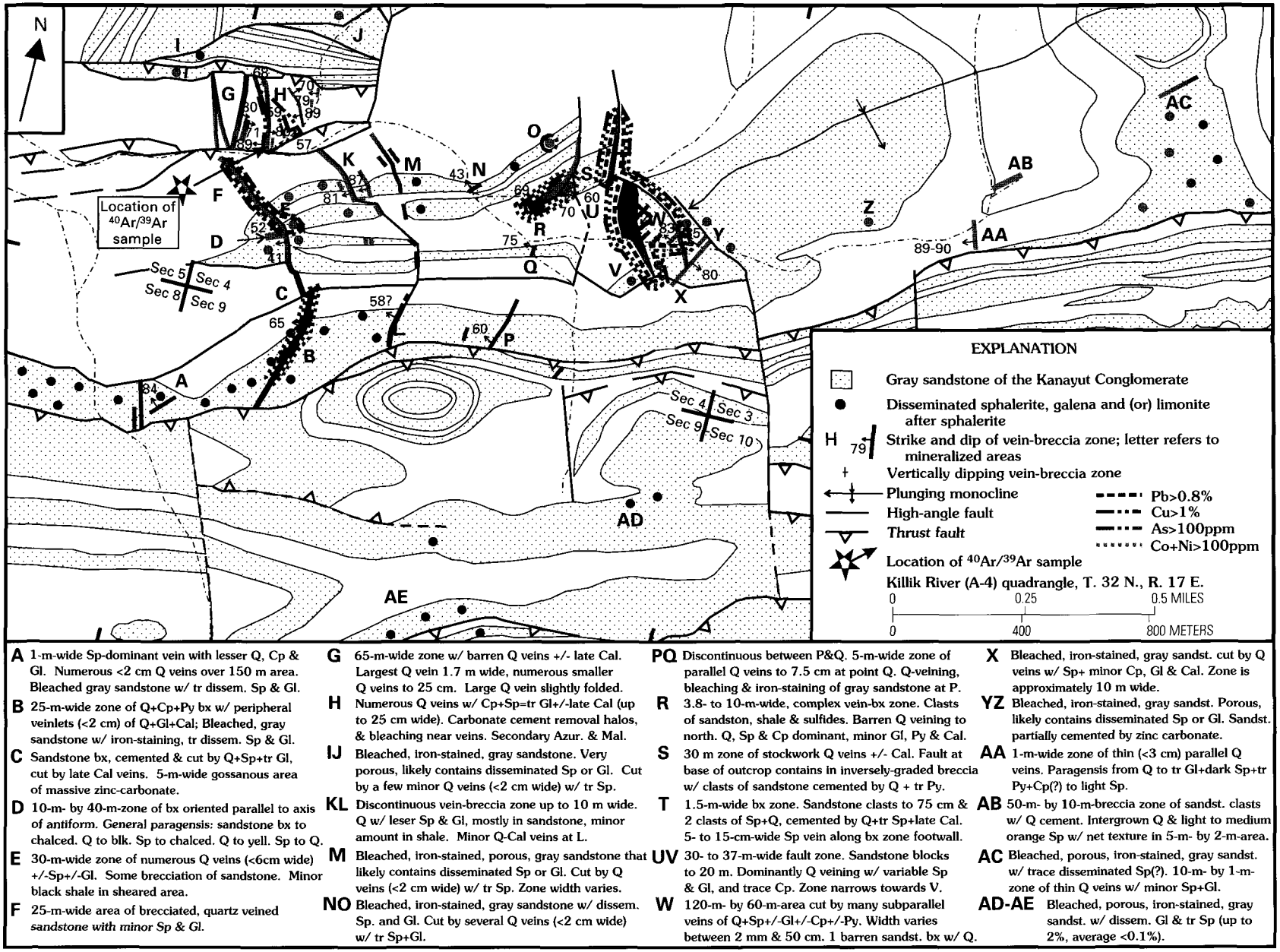

A 1-m-wide Sp-dominant vein with lesser Q, Cp & Gl. Numerous <2 cm Q veins over 150 m area. Bleached gray sandstone w/ tr dissem. Sp & Gl.

B 25-m-wide zone of Q+Cp+Py bx w/ peripheral veinlets (<2 cm) of Q+Gl+Cal; Bleached, gray sandstone w/ iron-staining, tr dissem. Sp & Gl.

C Sandstone bx, cemented & cut by Q+Sp+tr Gl, cut by late Cal veins. 5-m-wide gossanous area of massive zinc-carbonate.

D 10-m- by 40-m-zone of bx oriented parallel to axis of antiform. General paragensis: sandstone bx to chalced. Q to blk. Sp to chalced. Q to yell. Sp to Q.

E 30-m-wide zone of numerous Q veins (<6cm wide) +/-Sp+/-Gl. Some brecciation of sandstone. Minor black shale in sheared area.

F 25-m-wide area of brecciated, quartz veined sandstone with minor Sp & Gl.

G 65-m-wide zone w/ barren Q veins +/- late Cal. Largest Q vein 1.7 m wide, numerous smaller Q veins to 25 cm. Large Q vein slightly folded.

H Numerous Q veins w/ Cp+Sp=tr Gl+/-late Cal (up to 25 cm wide). Carbonate cement removal halos, & bleaching near veins. Secondary Azur. & Mal.

IJ Bleached, iron-stained, gray sandstone. Very porous, likely contains disseminated Sp or Gl. Cut by a few minor Q veins (<2 cm wide) w/ tr Sp.

KL Discontinuous vein-breccia zone up to 10 m wide. Q w/ leser Sp & Gl, mostly in sandstone, minor amount in shale. Minor Q-Cal veins at L.

M Bleached, iron-stained, porous, gray sandstone that likely contains disseminated Sp or Gl. Cut by Q veins (<2 cm wide) w/ tr Sp. Zone width varies.

NO Bleached, iron-stained, gray sandstone w/ dissem. Sp. and Gl. Cut by several Q veins (<2 cm wide) w/ tr Sp+Gl.

PQ Discontinuous between P&Q. 5-m-wide zone of parallel Q veins to 7.5 cm at point Q. Q-veining, bleaching & iron-staining of gray sandstone at P.

R 3.8- to 10-m-wide, complex vein-bx zone. Clasts of sandston, shale & sulfides. Barren Q veining to north. Q, Sp & Cp dominant, minor Gl, Py & Cal.

S 30 m zone of stockwork Q veins +/- Cal. Fault at base of outcrop contains in inversely-graded breccia w/ clasts of sandstone cemented by Q + tr Py.

T 1.5-m-wide bx zone. Sandstone clasts to 75 cm & 2 clasts of Sp+Q, cemented by Q+tr Sp+late Cal. 5- to 15-cm-wide Sp vein along bx zone footwall.

UV 30- to 37-m-wide fault zone. Sandstone blocks to 20 m. Dominantly Q veining w/ variable Sp & Gl, and trace Cp. Zone narrows towards V.

W 120-m- by 60-m-area cut by many subparallel veins of Q+Sp+/-Gl+/-Cp+/-Py. Width varies between 2 mm & 50 cm. 1 barren sandst. bx w/ Q.

X Bleached, iron-stained, gray sandst. cut by Q veins w/ Sp+ minor Cp, Gl & Cal. Zone is approximately 10 m wide.

YZ Bleached, iron-stained, gray sandst. Porous, likely contains disseminated Sp or Gl. Sandst. partially cemented by zinc carbonate.

AA 1-m-wide zone of thin (<3 cm) parallel Q veins. Paragensis from Q to tr Gl+dark Sp+tr Py+Cp(?) to light Sp.

AB 50-m- by 10-m-breccia zone of sandst. clasts w/ Q cement. Intergrown Q & light to medium orange Sp w/ net texture in 5-m- by 2-m-area.

AC Bleached, porous, iron-stained, gray sandst. w/ trace disseminated Sp(?). 10-m- by 1-m-zone of thin Q veins w/ minor Sp+Gl.

AD-AE Bleached, porous, iron-stained, gray sandst. w/ dissem. Gl & tr Sp (up to 2%, average <0.1%).

Figure 5. Map showing vein-breccia (gray lines) and disseminated (gray dots) sulfide mineralized areas. Gray sandstone within the Kanayut Conglomerate (stippled pattern) hosts most of the disseminated sulfides. Letters refer to individually described mineralized areas. Dips of mineralized vein-breccia zones are shown where measured. Map location shown in figure 2. Azur., azurite; Cal, calcite; Cp, chalcopyrite; Gl, galena; Mal., malachite; Py, pyrite; Q, quartz; Sp, sphalerite; amt., amount; blk., black; bx, breccia; chalced., chalcedonic; dissem., disseminated; sandst., sandstone; tr, trace; yell., yellow.

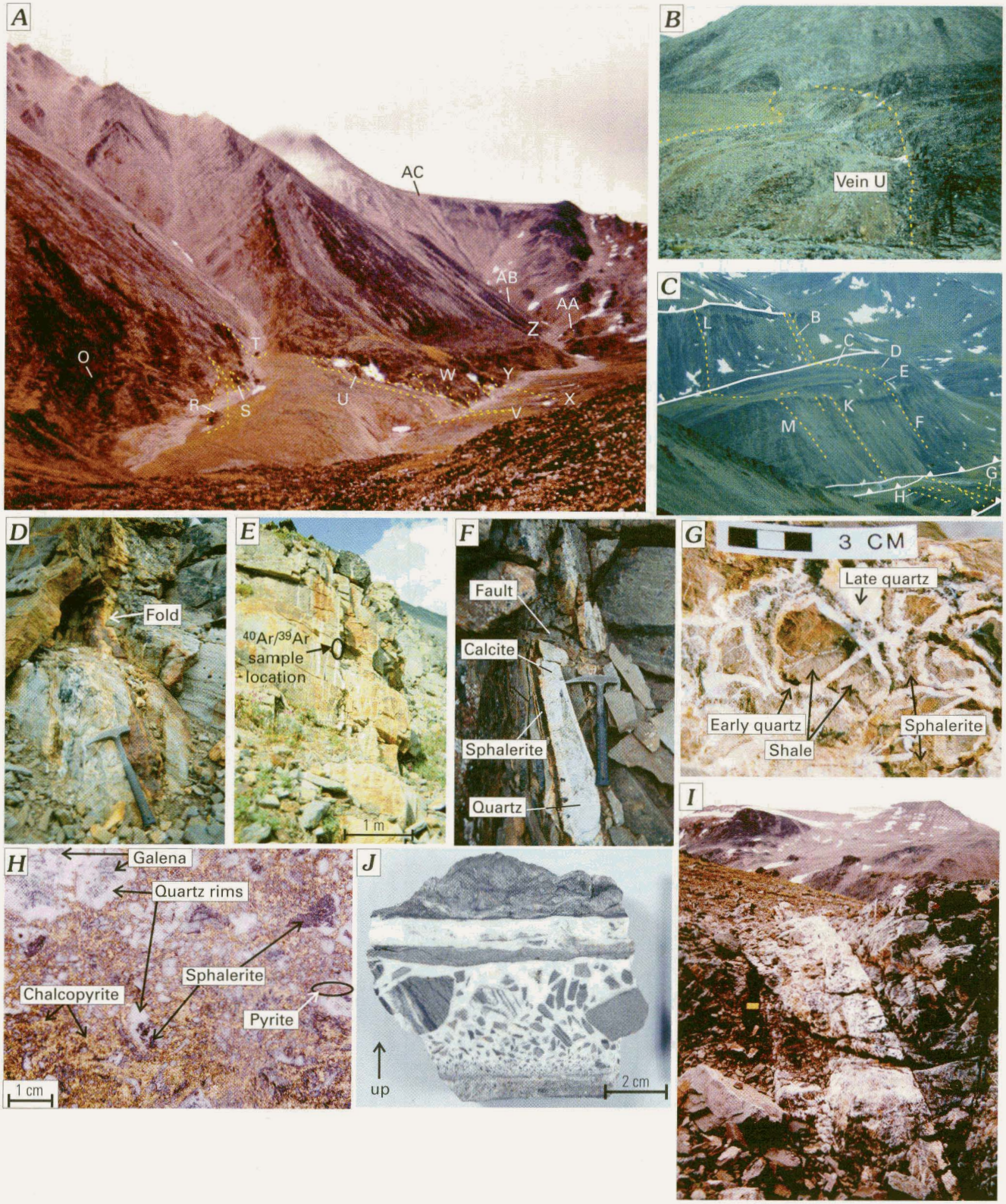

Figure 6. Vein-breccia zones and ore textures: *A*, View of vein-breccia zones looking east; *B*, Vein U viewed from area V (letters refer to individually described mineralized areas; see fig. 5); *C*, View of vein-breccia zones looking southwest; *D*, Folded quartz-sulfide vein in the Noatak Sandstone; *E*, Sheeted vein set at H; *F*, Pinched-out vein in shale bed in the Kanayut Conglomerate offset by late fault with minor slip, area H; *G*, Shale breccia clasts surrounded by milky quartz with open space between clasts filled with brown sphalerite and late quartz; *H*, Complex quartz-sulfide breccia, area R. Early galena, sphalerite, and pyrite fragments and (or) crystals are rimmed by milky quartz. Paragenetically late, intergrown chalcopyrite and quartz fill leftover open space; *I*, Sharp-edged vein-breccia zone, vein T; yellow field book is 12 cm by 19 cm; *J*, Inversely size graded breccia, area S.

in the field by its bleached, relatively light, gray color; iron staining (pale yellow to light orange red); highly reflective euhedral crystalline quartz faces inside pore spaces; and high porosity. Disseminated pyrite is sparsely distributed throughout the Kanayut Conglomerate and Noatak Sandstone, but its relationship (if any) to mineralization is unclear.

Texture and Mineralogy of Individual Vein-Breccia Zones

Individual vein-breccia zones vary in texture, width, and mineralogy (fig. 6). Textural variations include faulted host-rock blocks (as large as 20 m in vein U) cut by thin veins, host-rock breccias cemented by sulfides and quartz (fig. 6*G*), symmetrical veins, veinlets, and complex sulfide-in-sulfide breccias (fig. 6*H*). Most breccia clasts are host-rock fragments, but clasts of vein-type sphalerite in sandstone (as large as 25 cm in diameter) occur in vein T (fig. 6*I*). Host-rock breccias contain clasts that were torn from adjacent wallrocks and subsequently rotated and removed from their original locations. Vein S contains an unusual breccia with inversely size graded, rotated clasts, which is evidence for locally high fluid-flow rates (fig. 6*J*). A folded vein in area W has a tension gash that is symmetrically zoned with early brown sphalerite and late quartz. Sandstone along the margin of the vein is sheared, and there are peripheral barren quartz veins. The largest vein-breccia zones commonly have peripheral barren quartz veins and quartz-cemented host-rock breccias.

The relative proportions of the sulfides and their paragenetic sequences vary widely from vein to vein and within single vein-breccia zones. Locally, vein-breccia zones contain as much as 50 percent sulfides. If the entire length of the vein-breccia zones is considered (including barren quartz zones), the maximum sulfide content is less than 20 percent. Areas G, K, L, M, N, and Q average less than 1 percent sulfides. Sphalerite is the dominant sulfide mineral at Kady, followed in abundance by galena. Chalcopyrite is generally minor, but in vein-breccia zone B it is abundant (as much as 10.9 percent Cu) and constitutes as much as 98 percent of the sulfide present over a 2-m by 20-m area. The highest Zn and Pb grades occur in vein U, and the highest concentrations of Cu occur in the B, H, and R veins. Pyrite occurs in significant quantities only in the R and B veins. Rare submicroscopic grains of pyrrhotite occur within sphalerite in vein D, along with minor pyrite. Minor compositionally zoned pyrite and bravoite occur in vein U. Sulfosalts occur in trace amounts as microscopic blebs within galena.

Gangue minerals include abundant quartz, minor calcite, trace siderite and ankerite, and very rare chlorite. Vein quartz is usually crystalline and growth zoned but occasionally is dendritic, and there is an unusual area of chalcedonic banded quartz in vein D. Calcite, if present, always forms the paragenetically latest cement in the center of veins and breccias. Calcite is volumetrically most abundant in veins that cut carbonate-cemented sandstone, which suggests wallrock interaction buffered vein-fluid chemistry (pH). Calcite also occurs in sharp-edged veins that cut a sphalerite-cemented sandstone breccia in area C. Rare siderite and ankerite veins are paragenetically earlier than quartz-sulfide veins and only contain sulfides in area H. Siderite, ankerite, and calcite also occur in veins and breccias not spatially associated with quartz veins or sulfide mineralization. Gangue minerals developed in wallrocks due to reactions with mineralizing fluids include siderite, ankerite, and recrystallized white mica.

Supergene weathering of a chalcopyrite-quartz vein at H has leached copper from chalcopyrite and precipitated malachite and minor azurite on top of calcite and quartz. Secondary azurite and malachite are also intergrown with zinc carbonate and limonite in a sandstone breccia near H.

Sphalerite Descriptions and Compositional Variations

Sphalerite is the most common sulfide mineral at Kady, and it occurs throughout the paragenetic sequence of different vein-breccia zones. Most sphalerite is a dull to vitreous, medium-brown color in outcrop, with minor local resinous yellow sphalerite. In doubly polished thin sections, sphalerite colors range from clear through shades of yellow, orange, reddish orange, and dark reddish orange, to an almost opaque black. The black sphalerite is actually light to medium yellow under high magnification, and the apparent black color is due to abundant microscopic inclusions of chalcopyrite. Pale-yellow sphalerite rarely contains small, grayish-brown, intensely growth zoned areas. Yellow and orange are the predominant colors in most sphalerite samples. Vein sphalerite is typically color-banded parallel to growth zones. Sphalerite in breccia-textured ore is intergrown with quartz and may be color-banded (either around sandstone clasts or as broken fragments of growth-zoned sphalerite veins) (fig. 7*A*), irregularly zoned (fig. 7*B*), sector zoned (fig. 7*C*), patchy, and (or) uniform in color.

Sphalerite exhibits a range in composition ($Zn_{81.5\text{-}99.7}$, $Fe_{0.1\text{-}17.9}$, $Cd_{0.1\text{-}0.9}$)S, but most sphalerite falls within the compositional range ($Zn_{92.0\text{-}98.0}$, $Fe_{1.5\text{-}8.0}$, $Cd_{0.1\text{-}0.7}$)S (table 1). Most sphalerite did not contain Mn above the lower detection limit of 0.05 mole percent MnS at 2σ. Variation diagrams for mole percent CdS vs. FeS and mole percent FeS vs. sphalerite color (fig. 8) show the variety of sphalerite types and zoning. The color varies from clear to light yellow (0–2 mole percent FeS) through dark reddish orange (14–18 mole percent FeS) and is directly proportional to the iron content of the sphalerite.

Kady sphalerites fall into three different compositional groups (fig. 8). In group 1, sphalerite CdS values are highly variable, FeS values are uniformly low, and CdS does not vary with FeS. Sphalerite in vein H and late sphalerite in vein U occur in group 1. In group 2, sphalerite CdS values increase with FeS, and FeS values are less than 10 mole percent. The wide spread of values for vein R (fig. 8) may be due to redistribution of iron in sphalerite during extensive replacement by chalcopyrite. In group 3, sphalerite CdS values vary with FeS values but with a shallower slope than group-2 sphalerite. Sphalerites in group 3 also have higher FeS values. The three groups merge at low CdS and FeS values (fig. 8). The variety of sphalerite compositions may reflect varying chemical conditions in different parts of the Kady vein-breccia system.

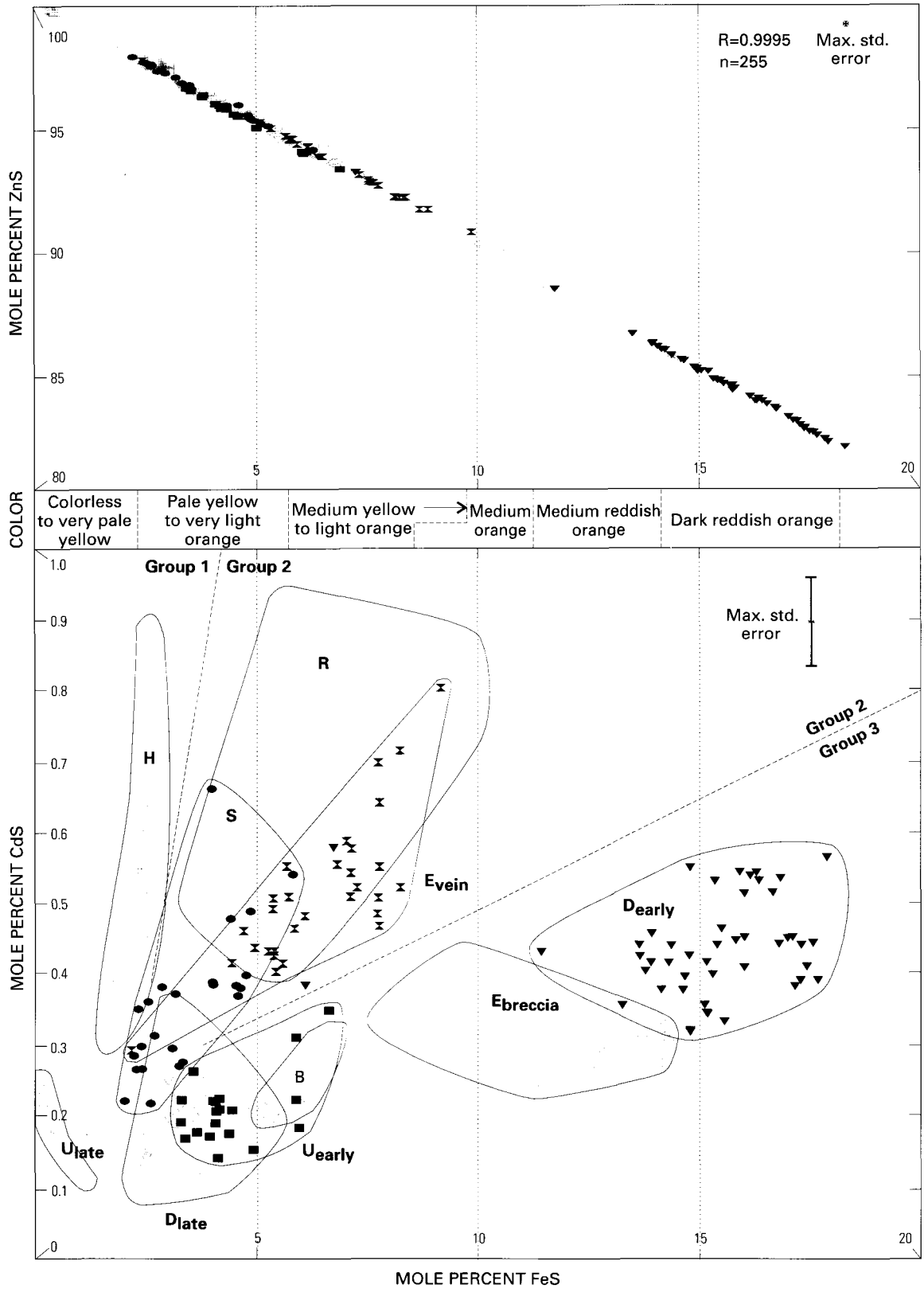

Figure 8. Mole percent FeS, CdS, ZnS and color variations in sphalerite. Letters refer to individual mapped veins shown in figure 5. The sphalerite color correlates with mole percent FeS. The three sphalerite groups are discussed in the text.

Table 1. Quantitative electron microprobe analyses of sphalerite.

Vein	Sample description	Sphalerite color(s) (in 30-μm-thick thin sections)	Composition (mole percent) (range / mean / median / 1 σ)
S	Brecciated, quartz-veined sandstone; angular, 1- to 2-mm sphalerite fragments floating in a randomly oriented mosaic of clear, non-growth zoned quartz crystals in a 0.5- to 1.0-cm-wide vein; minor chalcopyrite disease in sphalerite.	Irregular color zonation, colorless to pale yellow.	**ZnS** 93.6 - 97.7 / 96.2 / 96.4 / 1.1 **FeS** 2.0 - 5.8 / 3.5 / 3.2 / 1.1 **CdS** 0.2 - 0.7 / 0.4 / 0.4 / 0.1 **MnS** not above lower detection limit. **n**=24
B	Brecciated, quartz-veined sandstone; angular, 0.1- to 1.5-mm sphalerite fragments floating in a 2-cm-wide, clear to milky quartz vein; minor chalcopyrite disease in sphalerite; trace chlorite(?) in center of vein.	Poorly growth zoned, light to medium golden brown to yellow.	**ZnS** 92.8 - 94.6 / 93.8 / 93.7 / 0.6 **FeS** 5.2 - 6.8 / 6.0 / 6.1 / 0.6 **CdS** 0.2 - 0.3 / 0.3 / 0.3 / 0.1 **MnS** not above lower detection limit. **n**=10
R	Complex sulfide breccia with sphalerite (black in hand specimen), galena, chalcopyrite, pyrite, and quartz; abundant chalcopyrite disease and veins in sphalerite; clasts include sphalerite, galena-quartz mixtures, and pyrite-quartz mixtures; clasts are rimmed by quartz, with leftover open space filled by intergrown chalcopyrite and quartz.	Unusually colored sphalerite; appears black, gray, or brown due to abundant chalcopyrite inclusions, but it is mostly light to medium yellow under high magnification.	**ZnS** 89.3 – 96.0 / 94.0 / 94.4 / 1.6 **FeS** 3.5 - 9.9 / 5.5 / 5.1 / 1.5 **CdS** 0.4 - 0.9 / 0.6 / 0.5 / 0.1 **MnS** not above lower detection limit. **n**=36
H	5-cm-wide sphalerite (uniformly light brown in hand specimen) and quartz vein; sphalerite (early) cut and fragmented by irregular, symmetrically growth zoned milky quartz veins up to 0.5 cm wide; minor chalcopyrite disease	Clear, very light orange, and pale yellow w/ irregular color zonation.	**ZnS** 96.5 - 98.1 / 97.1 / 97.1 / 0.3 **FeS** 1.6 - 2.6 / 2.3 / 2.4 / 0.2 **CdS** 0.3 - 0.9 / 0.5 / 0.5 / 0.1 **MnS** not above lower detection limit. **n**=25
U	Quartz-dominant, sulfide-bearing, 5-cm-wide vein cutting sandstone; paragenetically early quartz followed by co-precipitated quartz, chalcopyrite, galena, and compositionally zoned pyrite-bravoite, followed by quartz, then dark sphalerite rimmed with light sphalerite, then an unknown gray carbonate and finally, late calcite; sphalerite is cut by a vein of iron sulfide but it is not diseased by chalcopyrite.	Growth zoned from early, light- and medium-orange sphalerite, to very light yellow, to late clear sphalerite.	Early, orange sphalerite. **ZnS** 93.0 - 96.5 / 95.4 / 95.7 / 1.0 **FeS** 3.3 - 6.7 / 4.4 / 4.1 / 1.0 **CdS** 0.1 - 0.4 / 0.2 / 0.2 / 0.1 **MnS** not above lower detection limit. **n**=20 Late, clear sphalerite. **ZnS** 98.8 - 99.7 / 99.5 / 99.5 / 0.3 **FeS** 0.1 - 1.1 / 0.3 / 0.2 / 0.3 **CdS** 0.1 - 0.3 / 0.2 / 0.2 / 0.0 **MnS** not above lower detection limit. **n**=10
D	Complex quartz-sphalerite-sandstone breccia; breccia contains clasts of sandstone, sphalerite, and sphalerite clasts with quartz rims; quartz-rimmed sandstone clasts (up to 4 cm) entrained with sphalerite clasts (up to 3 cm) in 10-m-wide vein-breccia zone; early reddish-orange sphalerite clasts (containing and partially rimmed by pyrite cubes) surrounded by granular to dendritic to growth-zoned quartz (with trace pyrite in quartz near early sphalerite); discontinuously overgrown by clear to yellow sphalerite crystals (no pyrite), surrounded by minor chalcedonic quartz and late, open-space-filling, coarse-grained, growth-zoned quartz.	Early sphalerite is medium to dark reddish orange w/ a couple of minor growth bands of medium yellow orange sphalerite. Late sphalerite is clear to medium yellow.	Early, reddish-orange sphalerite. **ZnS** 81.5 - 93.5 / 84.4 / 84.1 / 2.3 **FeS** 6.1 - 17.9 / 15.1 / 15.4 / 2.3 **CdS** 0.3 - 0.6 / 0.4 / 0.4 / 0.1 **MnS** not above lower detection limit. **n**=47 Late, clear to yellow sphalerite. **ZnS** 94.4 - 97.7 / 96.5 / 96.6 / 0.8 **FeS** 2.2 - 5.4 / 3.3 / 3.2 / 0.8 **CdS** 0.1 - 0.4 / 0.2 / 0.2 / 0.1 **MnS** not above lower detection limit. **n**=38

Table 1. Quantitative electron microprobe analyses of sphalerite—*Continued.*

Vein	Sample description	Sphalerite color(s) (in 30-μm-thick thin sections)	Composition (mole percent) (range / mean / median / 1 σ)
$E_{breccia}$	Angular, 0.1- to 1.5-mm fragments of sphalerite and sandstone floating, with pyrite crystals, in a 3- to 4-cm-wide quartz vein; minor to abundant chalcopyrite and iron sulfide disease with small patches of chalcopyrite replacing sphalerite.	Medium orange red to light orange, irregularly zoned.	**ZnS** 85.4 - 91.9 / 87.5 / 87.2 / 1.9 **FeS** 7.8 - 14.3 / 12.2 / 12.5 / 1.9 **CdS** 0.2 - 0.4 / 0.3 / 0.3 / 0.1 **MnS** up to 0.1 **n**=15
E_{vein}	Sphalerite-dominant vein with growth-zoned, vein-type sphalerite fragments enclosed in a matrix of finely crushed sphalerite intergrown with quartz; minor chalcopyrite and iron sulfide disease; some pyrite appears to replace sphalerite; pyrite is euhedral in quartz adjacent to sphalerite.	Mostly medium yellow to light orange; growth zoned; one sphalerite vein fragment is medium orange.	**ZnS** 90.0 - 97.5 / 93.1 / 93.0 / 1.6 **FeS** 2.2 - 9.2 / 6.4 / 6.5 / 1.5 **CdS** 0.3 - 0.8 / 0.5 / 0.5 / 0.1 **MnS** up to 0.1 **n**=30

XRF analyses (Werdon, 1998). Sn values occur within veins with high Zn concentrations, and there is a weak correlation between the elements. No Sn- or As-bearing minerals were observed in polished thin sections.

Isotopic Work

Sulfur Isotopes

Sulfur isotopic values (table 2) obtained for sulfides from vein-breccia zones W and R were used to estimate the temperature of sulfide deposition using the sulfur isotopic thermometer equations of Ohmoto and Rye (1979). Sulfur isotope geothermometry, based on the fractionation of sulfur isotopes between different sulfur-bearing compounds, assumes that equilibrium was obtained and preserved between two co-precipitated minerals. Sphalerite and galena in vein W are texturally intergrown and are interpreted to be co-precipitated. If isotopic equilibrium is assumed, the sulfide pair indicates a temperature of 209°±25°C during sulfide deposition. In vein-breccia zone R, sulfides occur in a complex breccia texture. Paragenetically early pyrite and sphalerite are overgrown by growth-zoned quartz. Paragenetically late galena, chalcopyrite, and quartz fill interstitial space left over between the pyrite-sphalerite-quartz clasts. If equilibrium at each stage is assumed, the early pyrite-sphalerite pair indicates a temperature of 251°±50°C, and the late galena-chalcopyrite pair indicates a temperature of 162°±35°C.

Oxygen Isotopes

Quartz was selected for oxygen isotopic analyses from both vein- and breccia-textured samples at Kady (table 3). Reliable oxygen-isotope compositions of ore-forming fluids are difficult to obtain from direct fluid-inclusion-extraction procedures because ore-forming fluids trapped in primary fluid inclusions can be contaminated by secondary fluid inclusions trapped during deformation. The oxygen-isotope composition of hydrothermal solutions can, however, be determined from quartz-water fractionation factors using fluid-inclusion homogenization temperatures and measured $\delta^{18}O$ values of hydrothermal quartz. Fluid-inclusion analyses from primary, two-phase (water-vapor) fluid inclusions indicate vein quartz at Kady was deposited from

Table 2. Sulfur isotopic analyses of sulfide minerals.

[Vein locations are shown on fig. 5. Sulfur isotopic analyses for sphalerite, galena, chalcopyrite, and ore-stage pyrite are reported as per mil variations with respect to the Canyon Diablo iron meteorite. Samples were analyzed by Geochron Laboratories, Inc., Cambridge, Mass., and have analytical uncertainties of ±0.2‰ at 2σ]

Vein	Mineral	^{34}S (‰)	Sample description
R	sphalerite	11.4	4-m-wide complex vein-breccia zone with quartz (70%), sphalerite (16%), chalcopyrite (8%), galena (1%), pyrite (3%) and calcite (2%).
R	chalcopyrite	10.9	
R	galena	7.8	
R	ore-stage pyrite	12.5	
W	sphalerite	12.7	0.37-m-wide vein of co-precipitated quartz (30%) and light- to medium-brown sphalerite (70%) with trace galena.
W	galena	9.6	

≤ 6 equivalent weight percent NaCl fluids at homogenization temperatures between 100°C and 145°C (not pressure corrected), and there is no evidence to suggest boiling (Werdon, 1998).

The $\delta^{18}O$ data from quartz (sample U-2), and primary fluid-inclusion homogenization temperatures in vein U are used to calculate the oxygen-isotope composition of the hydrothermal fluid at Kady using the quartz-water fractionation factor equation of Matsuhisa and others (1979):

$$\delta^{18}O_{qtz} - \delta^{18}O_f = \left(\frac{3.34\times10^6}{T^2}\right) - 3.31$$

where,

$\delta^{18}O_{qtz}$ is the $\delta^{18}O$ data from quartz,

$\delta^{18}O_f$ is the $\delta^{18}O$ composition of the hydrothermal fluid, and

T is the primary fluid-inclusion homogenization temperature in degrees Kelvin.

The fluid-inclusion measurements for vein U were taken on a different sample than the $\delta^{18}O$ measurements, but the quartz in both cases is spatially associated with chalcopyrite and galena. $\delta^{18}O$ values of the hydrothermal quartz range from 13.6‰ to 13.8‰ (table 3), and primary fluid-inclusion homogenization temperatures range from 118°C to 143°C (Werdon, 1998). This corresponds to a range of calculated $\delta^{18}O_f$ values between –4.9‰ and –2.2‰ for the hydrothermal fluid at Kady.

Although no isotopic values for hydrogen (δD) are available for the hydrothermal fluid at Kady, the calculated range of $\delta^{18}O_f$ values provides insight into the character and origin of the hydrothermal fluid. The source of the hydrothermal fluid at Kady can be modeled in two ways (fig. 10). The $\delta^{18}O_f$ values may suggest that the fluid was originally derived from a seawater and (or) a meteoric water source. The relative contribution of meteoric water and seawater cannot be determined, given the uncertainties in the ancient seawater field boundary (Sheppard, 1986). The other way to model the fluid is mixing between meteoric water and either a deep basinal brine or a metamorphic fluid.

Host-Rock Diagenesis and Alteration

Clastic Components, Early Cements, and Diagenesis

Clastic rocks of three Endicott-Group formations (Hunt Fork Shale, Noatak Sandstone, and Kanayut Conglomerate) distal to the vein-breccia zones (as far as 2 km away) were examined to determine which mineral assemblages characterized sedimentation, early cementation, and diagenesis. These features have a widespread distribution and show no spatial relationship to the vein-breccia zones.

Sandstones distal to the vein-breccia zones at Kady are predominantly (80–95 percent) composed of monocrystalline quartz (MCQ) and black chert fragments. The ratio of MCQ to chert varies from 50:50 to 95:5. Cherty argillite lithic fragments (1–10 percent) and white mica (1–10 percent) are common minor components. Plagioclase (1–4 percent), clay and (or) illite patches (0–13 percent), chlorite (0–2 percent), and accessory minerals (apatite, tourmaline, zircon, and rutile (anatase?)—less than or equal to 1 percent) are also present.

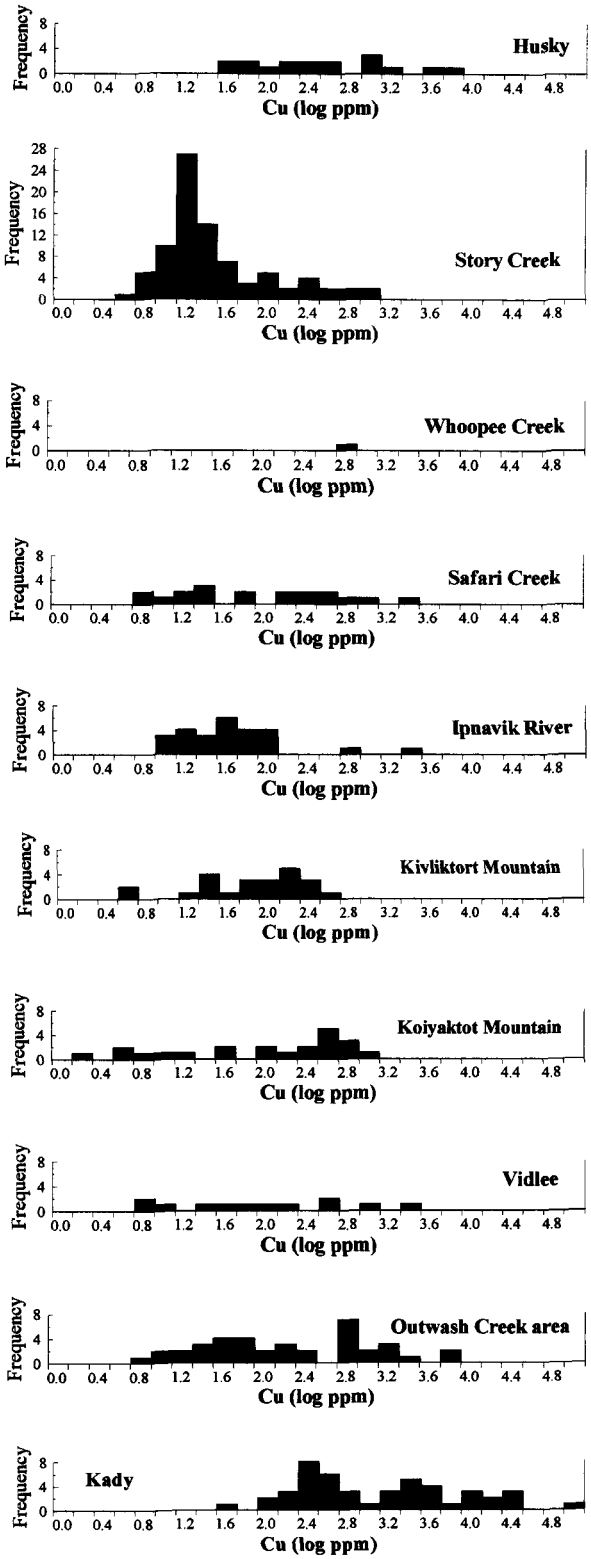

Figure 9. Histogram of copper analyses from mineralized hand samples from vein-breccia occurrences in the northern Brooks Range. Samples from Kady and the Outwash Creek area are more copper rich. Copper values are in log ppm units. ICP analyses are from Meyer and Kurtak (1992).

Table 3. Oxygen isotopic analyses of hydrothermal quartz.

[Oxygen isotopic compositions obtained from hydrothermal quartz are reported as per mil (‰) variations of $^{18}O/^{16}O$ with respect to standard mean ocean water (SMOW). Samples analyzed by Dr. K.L. Shelton, University of Missouri-Columbia. Analytical precision is generally better than ±0.1‰ at 1σ]

Vein	$\delta^{18}O$ (‰)	Sample description
AB	15.0	Breccia composed of light-gray, silicified siltstone fragments (10%) cemented by intergrown quartz (45%), medium reddish brown sphalerite (45%), and trace chalcopyrite.
S	13.1	Vein quartz from 8-cm-wide breccia-vein with sandstone clasts (<3%), quartz (45%), brown sphalerite (50%), and trace chalcopyrite (<1%) and pyrite (<1%).
S	15.2	Breccia quartz; same as above.
R	10.9	Quartz vein with granular, fine-grained pyrite and minor chalcopyrite (~5%).
A	10.8	1-m-wide vein of medium- to dark-brown sphalerite (94%) with lesser quartz (5%) and chalcopyrite (1%).
A	14.2	Light-gray, silicified siltstone fragments (20%) floating in mixed quartz (60%), chalcopyrite (15%), and medium-brown sphalerite (5%).
U-1	15.4	Vein of quartz (75%), medium- to dark-brown sphalerite (24%) and chalcopyrite (1%); quartz cross-cuts sphalerite subparallel to color banding.
U-2	13.6	Early quartz from a 6.5-cm-wide symmetrical vein with early quartz (3%) + trace chalcopyrite (<1%), growth-zoned late quartz (66%), and paragenetically late galena (30%).
U-2	13.8	Late quartz; same as above.

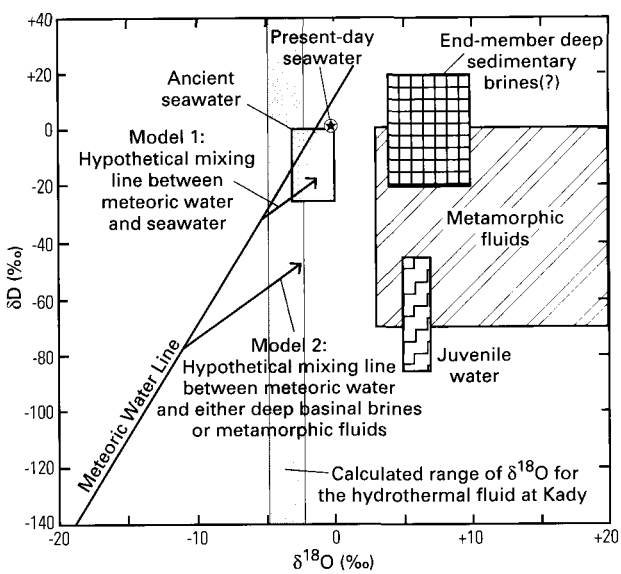

Figure 10. Calculated $\delta^{18}O_{fluid}$ values for Kady. δD refers to the isotopic composition of hydrogen in water. Field boundaries from Ohmoto (1986), Sheppard (1986).

Euhedral to irregularly shaped plagioclase grains are completely albitized. Clastic grain-shaped clay and (or) very fine grained illite patches are possibly pseudomorphs after K-feldspar, although no detrital K-feldspar was identified in any stratigraphic unit at Kady. Scattered patches of chlorite are probably pseudomorphs after biotite, as one chlorite grain had a zircon inclusion with a metamict halo and rare partially chlorite altered biotite is present in a few sandstones. Some chlorite patches may be hornblende pseudomorphs as well because high-temperature fractions in $^{40}Ar/^{39}Ar$ sandstone spectra have high Ca/K and Cl/K ratios (Werdon and others, 1998). Large rutile (anatase?) grains are probably detrital, but widely distributed small grains are probably products of biotite destruction.

If the diagenetic fluids were K-feldspar- and mafic-mineral-destructive, they may have derived metals from structurally bound sites in K-feldspar and mafic minerals by diagenetic processes. K-feldspar often contains structurally bound Pb^{+2} (which substitutes for K^{+1}), and mafic minerals can contain elevated levels of Cu^{+2} and Zn^{+2}. Therefore, sedimentary rocks of the Endicott Group may have provided a potential primary sedimentary source for base metals; however, mafic minerals are volumetrically minor, and K-feldspar may have been absent.

Organic plant material and fine-grained detrital carbonaceous fragments occur locally in the upper Noatak Sandstone, and more commonly in the Kanayut Conglomerate. Shales in the Kady area contain clay, quartz, chert, detrital white mica, limonite, and various carbonate minerals. Sandstone and shale in the Hunt Fork Shale and lower portion of the Noatak Sandstone are mineralogically similar to, but slightly less compositionally and texturally mature than, sandstone in the upper Noatak Sandstone and the Kanayut Conglomerate and exhibit similar diagenetic mineral-alteration assemblages.

Primary and early diagenetic cements identified petrographically and by energy dispersive spectroscopy (EDS) in the Endicott Group clastic rocks include: quartz, calcite, ankerite, siderite, an unidentified phosphate mineral, iron-manganese oxide/hydroxide, hematite, and organic material. The cement paragenesis of 117 individual samples is presented in the Appendix, and the overall cement paragenesis is summarized in figure 11. Quartz and ankerite are the most abundant early diagenetic cements.

Early diagenetic processes are very important in sandstone because the porosity can be significantly changed by early cementation or dissolution (development of secondary porosity) and because these processes influence later diagenetic and (or) hydrothermal processes. The distribution of carbonate in the Noatak Sandstone ranges from sandy limestone, to well-cemented calcareous sandstone, to concretionary and weakly carbonate cemented sandstone. The upper Noatak Sandstone contains small (2–6 mm), sparsely distributed, poikilitic ankerite crystals and minor early diagenetic quartz (EDQ) cement (fig. 12*A*). Early diagenetic ankerite often replaces chert grains inside poikilitic crystals. Gray sandstone in the Kanayut Conglomerate is weakly cemented by EDQ, as well as by disseminated carbonate (as much as 5 percent) in non-mineralized areas.

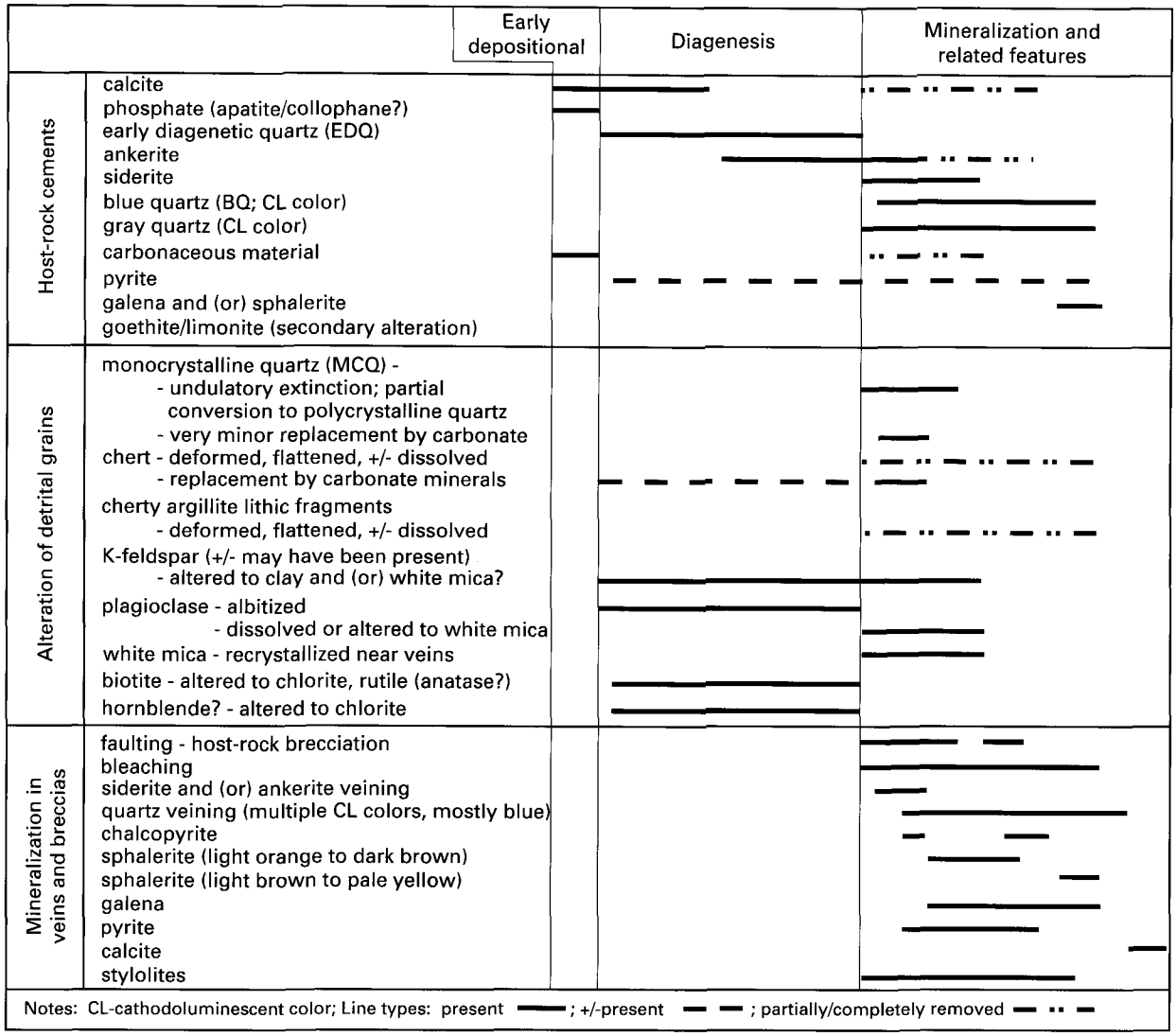

Figure 11. Summary of host-rock diagenesis and alteration, and ore paragenesis.

Hydrothermal Cements, Veins, and Vein-Related Alteration

Clastic rocks of the Endicott Group were examined to determine which mineral assemblages are related to the hydrothermal event. Interpreted alteration minerals are those that are spatially restricted to areas immediately adjacent to the vein-breccia zones (as much as 1 m away). Hydrothermal cements are present at varying distances from the vein-breccia zones, depending on the primary permeability of sandstone units.

Most sandstones in the Kanayut Conglomerate are partially to completely cemented by a combination of early diagenetic and hydrothermal quartz, which cannot be distinguished in transmitted light (fig. 12*B*). Cathodoluminescence is particularly useful for distinguishing early diagenetic quartz cement from later hydrothermal quartz cement. Unlike early diagenetic quartz, which is non-luminescent, hydrothermal quartz at Kady is typically light to medium neon blue (fig. 12*C*). The blue hydrothermal quartz is paragenetically later than early diagenetic quartz cement in the Kanayut Conglomerate and carbonate cement in the Noatak Sandstone.

The high permeability and porosity in both the upper, less well cemented part of the Noatak Sandstone and the sandstone of the Kanayut Conglomerate provided a site through which hydrothermal fluids could flow. Hydrothermal quartz, followed by disseminated galena and sphalerite, are paragenetically late cements in some gray sandstone units (fig. 5). Secondary goethite/limonite (±anomalous Zn) often occurs within pore spaces in the Kanayut Conglomerate, and zinc-carbonate cement occurs within the Noatak Sandstone in a small area near vein C.

In contrast to the relatively uniform color of hydrothermal cement, the cathodoluminescent color of hydrothermal quartz in veins is highly variable, including all shades of neon blue, gray, white, and pale brown (figs. 12*C*–12*E*). In larger, growth-zoned quartz veins, the cathodoluminescent colors alternate, particularly where there are alternating fluid-inclusion-rich and inclusion-poor bands. The cathodoluminescent colors in larger veins are relatively pale compared to very thin veins.

Extremely rare, paragenetically early siderite and ankerite veins hosted by the Noatak Sandstone are cut by later hydrothermal quartz veins (fig. 12*C*). Calcite occurs in veins that cut the Noatak Sandstone, and it occurs as the last mineral deposited in

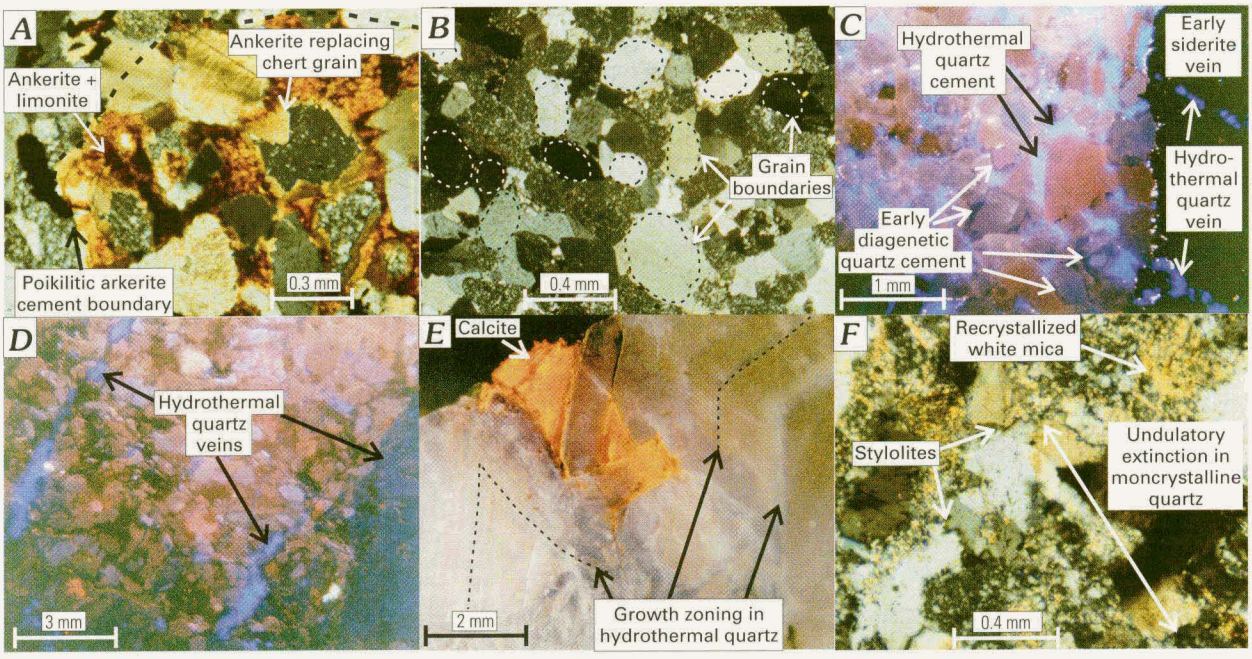

Figure 12. Petrographic and cathodoluminescent photos of host rocks and vein textures: *A*, Poikilitic ankerite cement in the Noatak Sandstone; chert clast partially replaced by ankerite; *B*, Texturally and compositionally mature, quartz-cemented sandstone in the Kanayut Conglomerate composed of monocrystalline quartz and chert grains; *C*, Sandstone cemented by sparse early-diagenetic quartz (non-luminescent) and late hydrothermal quartz (bright blue cathodoluminescent color). Late hydrothermal quartz veins cut an early siderite vein; *D*, Sandstone cut by a set of subparallel hydrothermal quartz veins; *E*, Faint cathodoluminescent color banding in growth-zoned hydrothermal quartz vein; *F*, Altered sandstone adjacent to vein H with structurally deformed clastic grains, stylolitization, and white mica (recrystallized and newly crystallized).

symmetrical veins and breccia-textured ore. The paragenetically late calcite in ore-related veins may have been locally derived from nearby carbonate-cemented units. There is an overall trend from relatively high iron carbonates (siderite and ankerite) in the early pre-sulfide stages to pure calcite in the post-sulfide stages of the hydrothermal system.

For alteration reactions to occur, the hydrothermal fluid must be at least slightly out of equilibrium with the wallrock sediments and the fluid must flow in volumetrically significant amounts. The clastic rocks at Kady are relatively siliceous and therefore alteration is not obvious in the field. Numerous subtle mineralogical, textural, and structural changes are observed in clastic rocks adjacent to the vein-breccia zones (fig. 11), and all of the features decrease in intensity with distance from the vein-breccia zones. The distance depends on the width of the vein-breccia zone and host-rock permeability but is generally limited to within 1 m of the vein-breccia zones.

The clastic rocks immediately adjacent to the vein-breccia zones are structurally deformed. In thin section, monocrystalline quartz grains and their quartz overgrowths exhibit undulatory extinction, and chert grains have been partially to completely flattened (fig. 12*F*). Thin barren quartz veins are commonly present immediately adjacent and subparallel to the vein-breccia zones (fig. 13).

Breccia clasts within the vein-breccia zones, adjacent clastic wallrocks, and disseminated Pb and (or) Zn-sulfide-bearing gray sandstones are typically bleached relative to the fresh rocks. The color change from light gray to grayish white is primarily due to dissolution of chert grains and (or) recrystallization of black detrital chert grains to exclude carbon(?). In areas of intense silica dissolution, a pseudo-foliation is observed in hand sample. In thin section, these areas have numerous stylolites cutting chert and monocrystalline quartz grains, as well as stylolitized grain boundaries (fig. 12*F*). Carbonaceous material is not present in bleached, mineralized, gray sandstone; it was either not present (unlikely) or it was removed by the hydrothermal fluid. Alteration is less extensive (generally occurs less than 2 cm from vein margins) in the less permeable carbonate-cemented sandstone and shale units. The carbonate-cemented sandstone and shale units are generally medium brown to maroon and are altered to lighter shades of these colors, or less commonly to light or medium forest green. The color change in these units is caused by the removal of iron carbonates, iron oxides, and (or) hydroxides.

To document chemical changes in carbonate minerals adjacent to mineralized vein-breccia zones, carbonate cements were semiquantitatively analyzed using EDS and cathodoluminescence. Carbonate cement in the Noatak Sandstone shows zoning (on a small scale) away from vein-breccia mineralization (figs. 13*A*–13*E*) in area H. In area H, 2- to 6-mm-wide green, carbonate-removal alteration halos surround the sulfide-bearing quartz veins. The small carbonate-removal halo suggests that the ore fluids were weakly acidic. This is followed sequentially outward by ankerite, ankerite with elevated Mn, calcite with trace Fe (iron oxide?), and finally a return to background ankerite about 0.5 m from the vein. The carbonate with the slightly elevated Mn content (fig. 13*D*) exhibits a much brighter orange color (Mn is a cathodoluminescent activator element and Fe is a suppressor). Carbonate flooding of wallrocks is only present adjacent to veins that cut the carbonate-cemented Noatak Sandstone.

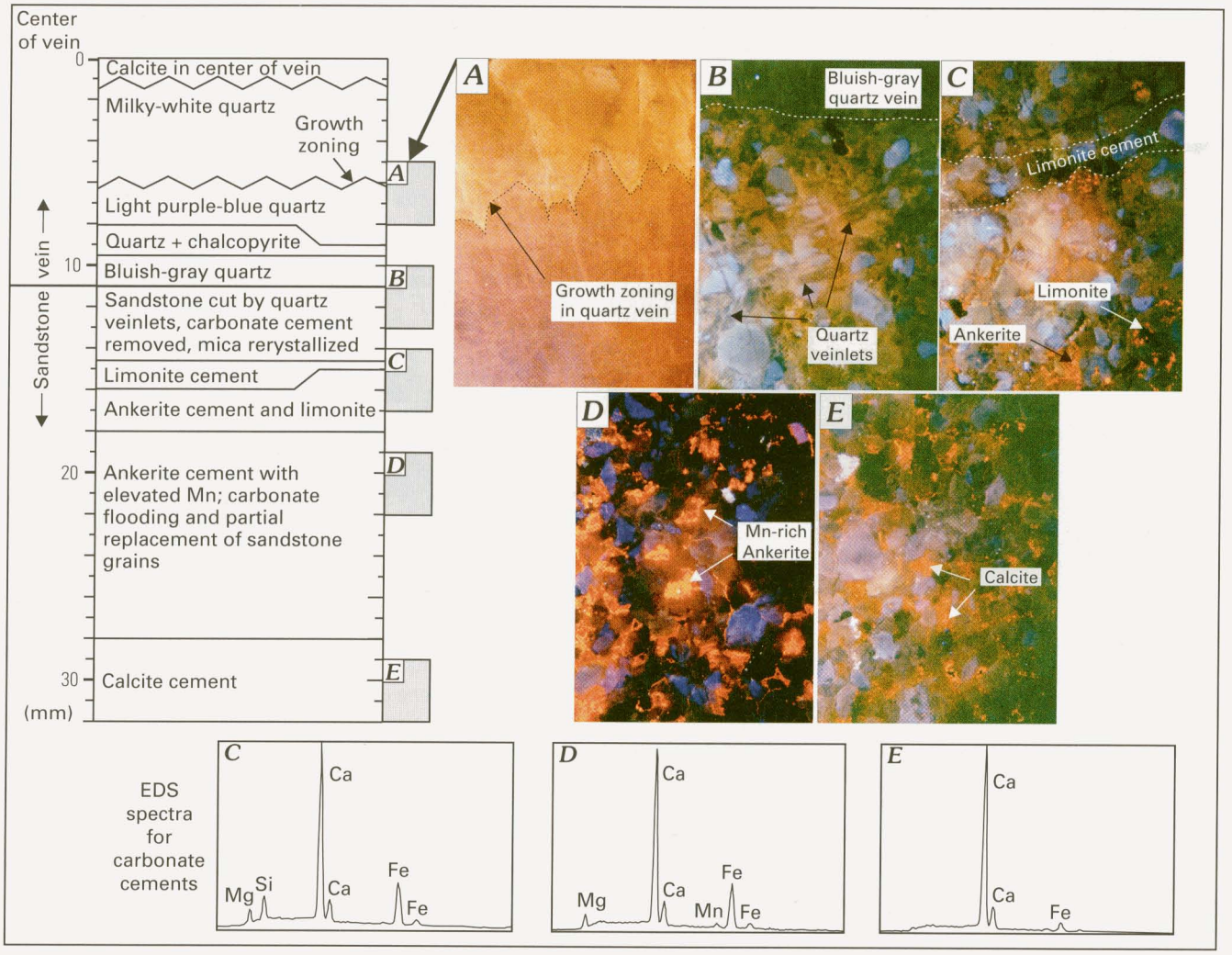

Figure 13. Alteration of carbonate cement in sandstone adjacent to vein H (see fig. 5 for location).

In these areas, ankerite replaces chert and, rarely, monocrystalline quartz grains. Compared to the Noatak Sandstone, carbonate cement within gray sandstone of the Kanayut Conglomerate is removed at greater distances (as much as 10? m) from vein-breccia zones, presumably due to the higher primary permeability.

An important mineralogical change accompanying vein-breccia formation is the recrystallization of white mica. Detrital white mica grains are partially to completely pseudomorphed by fine-grained, recrystallized, white mica (fig. 12*F*), and patches of illite often become coarser grained adjacent to vein margins. Plagioclase is not present in the 2- to 6-mm-wide alteration halos surrounding veins in area H, suggesting that it was either dissolved, or altered to white mica as well. Calculated vacuum-derived $^{40}Ar/^{39}Ar$ closure temperatures for hydrothermal sericite are between 220°C and 240°C (McMaster, 1987), which implies an estimated minimum temperature of about 220°C for the hydrothermal fluids in the veins. Recrystallized white mica in sandstone within the sheeted vein-set in area H (fig. 6*E*) was dated by the $^{40}Ar/^{39}Ar$ laser step-heating method (Werdon and others, 1998). It yielded Mississippian plateau ages of 324±2 Ma and 325±2 Ma, and an isochron age of 324±3 Ma. The presence of non-recrystallized detrital white mica distal to the vein-breccia zones argues against the $^{40}Ar/^{39}Ar$ ages reflecting a regional heating event.

Mineralization Model and Conclusions

Because the formation of sediment-hosted base-metal deposits is often intimately linked to the development of the basin in which they formed, the timing of deposit formation with respect to basin evolution must be considered. The Kady vein-breccia prospect is interpreted as part of a region-wide Zn-Pb-Ag hydrothermal mineralizing event estimated to be between 337 and about 314 Ma (Werdon and others, 1998). A Carboniferous age for the Kady prospect is supported by the Carboniferous $^{40}Ar/^{39}Ar$ ages of recrystallized white mica in wallrocks adjacent to the vein-breccia zones and by structural field evidence for a pre-Mesozoic age (offset by Mesozoic faults, minor folding). A period of regional extension, and volumetrically minor alkaline volcanic activity, occurred between 343 and 336 Ma (Werdon and others, 1998). This presumably set up an elevated geothermal gradient that heated basinal fluids.

Potential metal sources at Kady include the Endicott Group clastics and (or) underlying basement rocks. Because basement rocks are structurally removed, it is not possible to evaluate this potential source. Sedimentary sources for base metals could include metals adsorbed on clays and Fe-Mn oxide cements, or metals diagenetically released from structurally bound mineral sites (e.g., biotite (Zn^{+2}, Cu^{+2}) and

K-feldspar (Pb^{+2})). All of these potential sources might have been available within the Endicott Group, but the exact source(s) is difficult to determine because metal contents of Endicott-Group units distal to and within mineralized areas have not been determined. The replacement of biotite by chlorite shows that mafic minerals were out of equilibrium with pore fluids in the Endicott Group, indicating that it has a favorable diagenetic history for being a metal source.

The mineralized zones contain brecciated and veined sandstone produced by minor tectonic movement and (or) hydrofracturing. The vertical offset of bedding is difficult to assess due to Mesozoic reactivation. Mississippian offset appears to have been greatest along the U vein (perhaps 50 m?). The presence of strata-bound zones of very low grade disseminated sulfide mineralization adjacent to the vein-breccia zones suggests that silica- and base-metal-bearing fluids flowed through poorly cemented sandstone beds. Hydrothermal cementation of the sediments in the Endicott Group, along with a high fluid pressure (as evidenced by large, rotated, displaced, and (or) size-graded breccia clasts), helped support and preserve the fault structures. The subparallel mineralized zones at Kady are modeled as steeply dipping listric(?) faults along which up-flowing basinal fluids traveled and sulfides were deposited (fig. 14).

Carboniferous units stratigraphically above the Kanayut Conglomerate have been structurally and (or) erosionally removed in the Kady area (except for small pieces of the Kayak Shale); therefore, it is not known what Mississippian facies were present above the vein-breccia zones, or if it was an area of emergence and non-deposition. The offset on Mesozoic thrust faults in the Kady area is relatively minor (less than a few hundred meters). Although no detailed structural maps are available between Kady and the mountain front, if the structural style in this area is similar to that in the Kady area, and if thrust-fault offsets are also relatively minor, the Pennsylvanian to Mississippian facies along the mountain front (fig. 1) could potentially be similar to the facies formerly overlying the Endicott Group in the Kady area. If the Kady deposit was overlain by basinal shales of the Kuna Formation, the low thermal conductivity and low permeability of these shaley capping sediments could reduce both conductive and convective heat loss from the basin (Goodfellow and others, 1993), thereby maintaining elevated temperatures within the Endicott Group reservoir until faulting occurred. This proposed basin model would be physically similar to the Sedex model of Lydon (1983).

During faulting, the pressure (P) is interpreted to have changed from predominantly lithostatic to hydrostatic (fig. 14). Stratigraphic thickness estimates for units above the vein-breccia zones suggest that about 375 m of sediment may have been present over the top of the vein-breccia system. The depth of seawater covering the sediments is unknown. If the maximum temperature for the hydrothermal fluids was around 210°C to 250°C, boiling would occur between 190 m and 410 m below sea level. In other words, if the water depth was less than 190 m to 410 m, boiling would occur below the sea floor. Although the

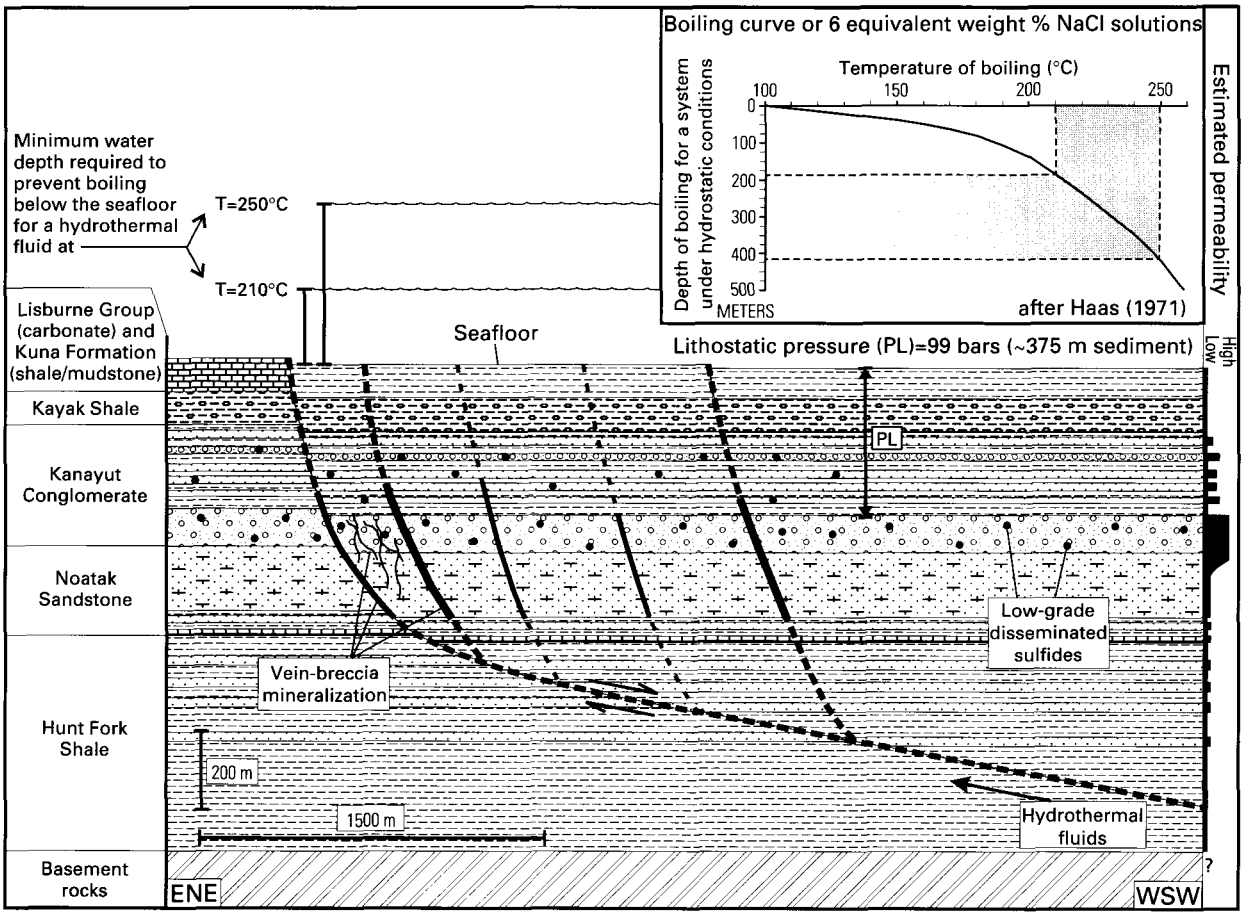

Figure 14. Schematic cross section and mineralization model for Kady.

possibility of boiling in the upper levels of the vein-breccia system is within stratigraphic-thickness, salinity, and sulfur-isotopic-temperature constraints, there is no evidence to suggest boiling in fluid inclusions from hydrothermal-vein quartz at Kady (Werdon, 1998).

Textural, mineralogical, and fluid-inclusion data indicate that sulfides and quartz were deposited from slightly acidic, low-salinity hydrothermal fluids under evolving chemical conditions (i.e., T, P, pH, fugacity of oxygen, fugacity of sulfur). A drop in temperature is suggested by the presence of dendritic quartz within some of the vein-breccia zones, the sulfur-pair temperature estimates in vein R, and relatively low fluid-inclusion homogenization temperatures in late, vein-textured quartz. Most vein-breccia zones formed within the stability field for pyrite, but areas D and E evolved starting at the pyrite-pyrrhotite boundary. The decrease in sphalerite mole percent FeS values in many of the veins suggests that both the sulfidation and oxidation state of the fluid increased with time. The relatively high levels of Cu at Kady suggest that the fluids were relatively oxidized because copper is essentially immobile under reducing conditions at low temperatures. The removal of carbonaceous material within the mineralized area is consistent with a relatively oxidizing hydrothermal fluid. The pH increased in the late stages of the hydrothermal event due to buffering by wallrock carbonate cement.

The evidence and models discussed above suggest several reasons why a sedimentary exhalative deposit likely did not form above the Kady vein-breccia prospect. Although sulfur isotopic pairs and white mica $^{40}Ar/^{39}Ar$ closure temperatures indicate sulfides at Kady formed at a temperature of at least 220°C (and possibly as high as 250°C), these relatively low temperatures cannot alone explain the lack of a Sedex deposit. Unlike the Red Dog and Drenchwater deposits, which are spatially associated with a few minor volcanic sills or dikes within and near mineralized areas, there are no volcanic sills or dikes within the Endicott Group in the Kady area. This could suggest that the Kady prospect had a shorter lived system of heat input to sustain hydrothermal fluid flow, but no data on how long the mineralizing systems were active is available.

The presence of sulfides within the Endicott Group suggests that metal-bearing solutions encountered changing physical and (or) chemical conditions that caused metals to drop out of solution before reaching the sea floor. Although there is no evidence for boiling within the vein-breccia system, the hydrostatic pressure may not have been great enough to keep the hydrothermal fluids from boiling in the subsurface above the level of the vein-breccia zones. If the water depth was great enough to prevent subsurface boiling, the low salinity values indicate that the ore fluid would be highly buoyant in seawater upon reaching the sea floor, and metals would be dispersed. The above information suggests that evaluation of Carboniferous facies, and water-depth estimates derived from them, are important to evaluating areas for their Sedex potential.

Acknowledgments

The Alaska Division of Geological and Geophysical Surveys and the U.S. Geological Survey provided financial support for this study. I wish to thank Rainer Newberry and Jeanine Schmidt for their numerous reviews and advice over the years on this project. Suggestions made by reviewers Gar Pessel, Ken Severin, Paul Layer, Jim Dover, and Karen Kelley also improved this paper. The help of Dennis Boyce in the field and discussions of Brooks Range geology with Gil Mull and Wes Wallace are also appreciated.

References Cited

Duttweiler, K.A., 1987, Use of factor analysis in locating base metal mineralization in the Killik River quadrangle, Alaska: U.S. Geological Survey Circular 998, p. 27-30.

Ellersieck, I., Tailleur, I.L., and Mull, C.G., 1990, Explanation to accompany reconnaissance geologic map of the Story Creek area, National Petroleum Reserve, Alaska: U.S. Geological Survey Open-File Report 90-533, 21 p.

Forrest, K., 1983, Geologic and isotopic studies of the Lik deposit and the surrounding mineral district, De Long Mountains, western Brooks Range, Alaska: University of Minnesota, unpub. Ph.D. dissertation, 161 p.

Gaccetta, J.D., and Church, S.E., 1989, Lead isotope data base for sulfide occurrences from Alaska: U.S. Geological Survey Open-File Report 89-688, 60 p.

Goodfellow, W.D., Lydon, J.W., and Turner, R.J.W., 1993, Geology and genesis of stratiform sediment-hosted (SEDEX) zinc-lead-silver sulfide deposits, *in* Kirkham, R.V., Sinclair, W.D., Thorpe, R.I., and Duke, J.M., eds., Mineral Deposit Modeling: Geological Association of Canada, Special Paper 40, p. 201-251.

Haas, J.L., 1971, The effect of salinity on the maximum thermal gradient of a hydrothermal system at hydrostatic pressure: Economic Geology, v. 66, p. 940-946.

Jansons, U., 1982, Zinc-lead occurrences in and near the National Petroleum Reserve in Alaska: U.S. Bureau of Mines Mineral Lands Assessment Report MLA 121-82, 55 p.

Jansons, U., and Parke, M.A., 1981, 1978 mineral investigations in the Misheguk Mountain and Howard Pass quadrangles, Alaska: U.S. Bureau of Mines Open-File Report 26-81, 195 p.

Kelley, K.D., Taylor, C.D., and Cieutat, B.A., 1997, Silver-lead-zinc mineral occurrences in the Howard Pass quadrangle, Brooks Range, Alaska, *in* Dumoulin, J., and Gray, J., eds., Geological Studies in Alaska by the U.S. Geological Survey, 1995: U.S. Geological Survey Professional Paper 1574, p. 101-110.

Lydon, J.W., 1983, Chemical parameters controlling the origin and deposition of sediment-hosted stratiform lead-zinc deposits, *in* Sangster, D.F., ed., Short Course in Sediment-Hosted Stratiform Lead-Zinc Deposits: Mineralogical Association of Canada, p. 175-250.

Matsuhisa, Y., Goldsmith, J.R., and Clayton, R.N., 1979, Oxygen isotopic fractionation in the system quartz-albite-anorthite-water: Geochimica et Cosmochimica Acta, v. 43, p. 1131-1140.

McMaster, D., 1987, A preliminary $^{40}Ar/^{39}Ar$ study of the thermal history and age of gold in the Red Lake greenstone belt: University of Toronto, unpub. M.S. thesis, 107 p.

Meyer, M.P., and Kurtak, J.M., 1992, Results of the 1991 U.S. Bureau of Mines Colville mining district study: U.S. Bureau of Mines Open-File Report 75-92, 101 p.

Moore, D.W., Young, L.E., Modene, J.S., and Plahuta, J.T., 1986, Geologic setting and genesis of the Red Dog zinc-lead-silver deposit, western Brooks Range, Alaska: Economic Geology, v. 81, p. 1696-1727.

Moore, T.E., Wallace, W.K., Bird, K.J., Karl, S.M., Mull, C.G., and Dillon, J.T., 1994, Geology of northern Alaska, *in* Plafker, G., and Berg, H.C., eds., The Geology of Alaska: Boulder, Colo., Geology of North America, v. G1, Geological Society of America, p. 49-140.

Mull, C.G., Moore, T.E., Harris, E.E., Tailleur, I.L., 1994, Geologic map of the Killik River quadrangle: U.S. Geological Survey Open-File Report 94-679, 1 sheet, scale 1:125,000.

Mull, C.G., and Werdon, M.B., 1994, Generalized geologic map of the western Endicott Mountains, central Brooks Range, Alaska: Alaska Division of Geological and Geophysical Surveys Public Data File 94-55, 1 sheet, scale 1:250,000.

Ohmoto, H., 1986, Stable isotope geochemistry of ore deposits, *in* Valley, J.W., Taylor, H.P., Jr., and O'Neil, J.R., eds., Stable Isotopes in High Temperature Geological Processes: Reviews in Mineralogy, v. 16, p. 491-559.

Ohmoto, H., and Rye, R.O., 1979, Isotopes of sulfur and carbon, *in* Barnes, H.L., ed., Geochemistry of Hydrothermal Ore Deposits (2nd ed.): New York, John Wiley and Sons, p. 509-567.

Sheppard, S.M.F., 1986, Characterization and isotopic variations in natural waters, *in* Valley, J.W., Taylor, H.P., Jr., and O'Neil, J.R., eds., Stable Isotopes in High Temperature Geological Processes: Reviews in Mineralogy, v. 16, p. 165-183.

Toulmin, P., III, Barton, P.B., Jr., and Wiggins, L.B., 1991, Commentary on the sphalerite geobarometer: American Mineralogist, v. 76, p. 1038-1051.

Werdon, M.B., 1996, Drenchwater, Alaska: Zn-Pb-Ag mineralization in a mixed black shale-volcanic environment, *in* Coyner, A.R., and Fahey, P.L., eds., Geology and Ore Deposits of the American Cordillera: Geological Society of Nevada Symposium, Reno/Sparks, Nevada, April 1995, Proceedings, p. 1341-1354.

Werdon, M.B., 1998, Lead isotopic ratios, ICP and XRF analyses, and fluid inclusion data for the Kady Zn-Pb-Cu-Ag vein-breccia prospect, northern Brooks Range, Alaska: Alaska Division of Geological and Geophysical Surveys Public Data File 98-43, 8 p.

Werdon, M.B., Newberry, R.J., and Layer, P.W., 1998, $^{40}Ar/^{39}Ar$ laser step-heating data and spectra from sandstone and volcanic rocks in the northern Brooks Range, Alaska: Alaska Division of Geological and Geophysical Surveys Public Data File 98-33, 25 p.

Reviewers: Jeanine Schmidt, Rainer Newberry, Jim Dover, Karen Kelley, Gar Pessel, Ken Severin, and Paul Layer.

Appendix 1. Summary of field, petrographic, energy dispersive spectroscopy (EDS), and cathodoluminescence data for clastic and lesser carbonate rocks and mineralization in the Kady area.

[Units include the Kayak Shale (Mk), Kanayut Conglomerate (MDk), Noatak Sandstone (Dn), lower Noatak Sandstone (Dnl), and Hunt Fork Shale (Dhf), as well as mineralization (Min). Colors in cement and vein and mineralization columns are cathodoluminescent colors. BQ, quartz with blue cathodoluminescent color; EDQ, early diagenetic quartz (non-cathodoluminescent colors); MCQ, monocrystalline quartz]

Sample number	Unit	Field description and petrographic observations	Cements (listed in paragenetic order)	Veins (minerals listed in paragenetic order)
1	Dn	Sandstone breccia: angular sandstone clasts (≤3 cm) floating in calcite. Light tan-gray, fine grained, disseminated pyrite (<1%), porous-leached.	EDQ, calcite.	Calcite.
2	Dn	Sandstone: gray-brown weathering, fine-medium grained, <1% disseminated pyrite, porous-leached, grains of MCQ (48%), chert (49%), white mica, lithics, chlorite (after biotite?) and fine-grained white mica/clay patches (3%).	EDQ, ankerite (partially replacing chert grains, ± altered to goethite), trace BQ.	BQ.
3	Min-Dn	Sandstone: gray-brown weathering, fine-grained, porous-leached sandstone, quartz vein is surrounded by carbonate flooding, grains of quartz, chert, and <3% white mica, fine-grained white mica patches, Al- and Si-clay grains, and lithics.	EDQ, ankerite, minor siderite, BQ; ankerite extensively replaced chert grains.	Sandstone cut by BQ veins (+ sphalerite + galena + pyrite + trace chalcopyrite? ± late calcite) that are folded by foliation. One micritic carbonate vein with late chlorite.
4	MDk	Sandstone: light gray-brown weathering, fine-grained sandstone with planar beds, minor shale partings, Al- and Si-clay patches (after feldspar?).	EDQ, ankerite(?), siderite, BQ.	
5	MDk	Siltstone and shale: maroon, tan, and minor black, very fine grained, highly foliated.	Goethite after siderite, small calcite patch.	
6	MDk	Shale: maroon.		
7	MDk	Sandstone: fine grained, abundant carbonate cement.	EDQ, siderite (replacing sandstone grains), BQ (replacing siderite).	
8	MDk	Sandstone: fine-coarse grained; trace rutile(?) grains.	EDQ, siderite, minor ankerite, BQ, rutile(?) (floating in BQ).	BQ spatially associated with siderite.
9	MDk	Conglomerate: quartz and chert grains up to 2.5 cm.		
10	MDk	Siltstone: reddish brown, very fine grained, contains tracks and burrows.	EDQ, siderite, BQ.	BQ spatially associated with siderite.
11	MDk	Sandstone: light gray to white weathering, fine to coarse grained, minor conglomerate pebbles.	EDQ, minor ankerite, BQ.	Minor quartz + carbonate + chlorite fractures and late ankerite veinlets.
12	MDk	Sandstone: light green, fine grained, thin lens, minor disseminated pyrite.	EDQ, ankerite, BQ.	Late ankerite micro-veinlets.
13	MDk	Sandstone: light red weathering, light gray colored, fine grained, brecciated, porous-leached sandstone with minor K-, Al-, and Si-clay(?) patches.	EDQ, trace ankerite or siderite, BQ.	Mineralizing fluids flowed through sandstone; fractures of quartz + epidote(???) + sulfides.
14	MDk	Sandstone: light red weathering, light gray colored, fine grained, porous-leached.	EDQ, trace BQ(?)	Mineralizing fluids flowed through sandstone.
15	MDk	Sandstone: light red weathering, light gray colored, fine grained.	EDQ.	Thin veins of BQ + sphalerite + galena.
16	Dn	Sandstone: brown weathering, fine grained, minor Al- and Si-clay grains, porous-leached.	EDQ, bright orange unknown carbonate, BQ, minor green unknown cement.	
17	MDk	Sandstone: red-brown weathering, fine-medium grained, thin bedded, porous-leached with grains of MCQ (55%), chert (30%), polycrystalline quartz (10%), and other (5%). Brittle deformation.	Abundant EDQ, ankerite, minor BQ; some carbonate cement replacing chert grains.	Early ankerite veins cut by late BQ veins.

Appendix 1. Summary of field, petrographic, energy dispersive spectroscopy (EDS), and cathodoluminescence data for clastic and lesser carbonate rocks and mineralization in the Kady area—*Continued.*

Sample number	Unit	Field description and petrographic observations	Cements (listed in paragenetic order)	Veins (minerals listed in paragenetic order)
18	MDk	Sandstone: gray, fine grained, massive bedded, quartz and small black chert grains, rutile, Al- and Si-clay(?) patches, minor disseminated pyrite.	EDQ.	Mineralizing fluids flowed through sandstone.
18.5	MDk	Siltstone: brown weathering, very fine grained, porous-leached sandstone interbedded with shale.	Ankerite.	Pyrite + chalcopyrite + calcite veins.
19	MDk	Siltstone: brown weathering, interbedded with shale.	Ankerite.	
20	MDk	Sandstone: brown, fine-medium grained, abundant carbonate cement, thin bedded.	Minor EDQ, ankerite (replacing quartz and chert grains, ± altered to goethite).	Ankerite replacing quartz and chert grains, late ankerite micro-veinlets.
21	MDk	Sandstone: light gray, medium grained, massive to crossbedded, porous-leached, entirely quartz cemented, slicks on fracture planes.	EDQ.	
22	Min-MDk	Sandstone: breccia of rounded sandstone fragments cemented by rock flour and BQ, cut by late BQ veins. Sandstone is fine-medium grained, porous-leached.	EDQ, BQ.	BQ + sphalerite + pyrite in fracture.
23	Min-MDk	Sandstone: massive, cut by numerous sulfide-bearing quartz veins.		
23.5	Min	Mineralized breccia: chalcedonic quartz and sphalerite breccia.		Chalcedonic quartz and sphalerite.
24	Dn	Sandstone: medium gray, fine grained, interbedded with green, chloritic, foliated shale, area has lesser interbedded sandy carbonates and green, maroon and black shale. Grains composed of quartz, plagioclase (4%), white mica (8-10%), chlorite (after biotite?), chert (flattened, partially dissolved).	EDQ(?), calcite (with trace Fe).	Abundant carbonate and minor quartz veining in the area.
25a	MDk	Sandstone: light gray, fine grained, large-scale crossbeds, massive bedded, very porous leached, slightly foliated, partial chert dissolution, grains of MCQ, chert, lithics, plagioclase (2-3%), white mica, trace zircon.	EDQ.	Micro-veinlets of BQ parallel to foliation adjacent to vein B.
25b	Min	Vein B: growth zoned quartz-galena-calcite veins cut sandstone 25a peripheral to main quartz-chalcopyrite-pyrite zone.		Growth-zoned quartz (blue, tan, yellow)+ galena with late calcite.
26	Min	Mineralized vein-breccia zone:		Vein-breccia zone of quartz + chalcopyrite + pyrite, secondary azurite and malachite.
27	MDk	Sandstone: fine-medium grained, large crossbed sets, porous-leached.	EDQ, minor ankerite, BQ.	Minor gray quartz veinlets.
28	MDk	Sandstone: light gray, fine-medium grained, porous-leached.	EDQ, trace BQ(?)	Mineralizing fluids flowed through rock.
29	?	Sandstone and siltstone: brown to maroon, sandstone medium grained, siltstone very fine grained, interbedded shale, minor carbonate lenses, manganese-oxide coatings, rutile(?) grains.	EDQ, ankerite (± goethite altered), siderite, (BQ and FeMnO(OH) replacing ankerite and siderite).	Abundant BQ + chalcopyrite veins.
30	MDk	Sandstone: brown, fine grained, carbonate rich.	EDQ, abundant ankerite, BQ.	Thin vein of gray quartz; BQ in diffuse vein(?)
31	Min-MDk	Sandstone: light gray, fine-medium grained, bleached, light red iron staining, porous-leached, reflective quartz surfaces, Al- and Si-clay patches, galena cement.	EDQ, abundant BQ + disseminated galena, neon green unknown cement.	Mineralizing fluids passed through rock, cut by gray and BQ veins.

Appendix 1. Summary of field, petrographic, energy dispersive spectroscopy (EDS), and cathodoluminescence data for clastic and lesser carbonate rocks and mineralization in the Kady area—*Continued.*

Sample number	Unit	Field description and petrographic observations	Cements (listed in paragenetic order)	Veins (minerals listed in paragenetic order)
32	MDk	Siltstone: maroon and black, fine grained, interbedded with shale.	Minor EDQ, abundant ankerite, BQ.	Early veins of BQ + siderite (vein rim)+ ankerite (center); late gray quartz veinlets.
33	MDk	Shale: greenish-brown to black paper shale, highly foliated.		
34	MDk	Sandstone: grayish-green weathering, fine-medium grained, iron-stained, porous-leached, crossbedded sandstone with fining-upward sets, minor conglomerate lag beds to 3 cm, interbedded with gray shale; disseminated pyrite, chlorite in sandstone.	EDQ, goethite after carbonate, trace bright neon green unknown cement.	BQ-carbonate veinlets, may contain trace disseminated sphalerite + galena(?)
35	MDk	Sandstone: light gray weathering, medium gray color, medium grained, massive, jointed, porous-leached sandstone with patches and disseminated pyrite (partially altered to goethite).	EDQ, zoned ankerite to siderite(?), pyrite, BQ; minor carbonate replacement of sandstone grains.	Mineralizing fluids flowed through sandstone, outcrop cut by numerous quartz ± carbonate veins.
36	Dn	Sandstone: light greenish brown, fine grained, massive, ± crossbedded, partially carbonate cemented, porous-leached.	EDQ, minor ankerite (± goethite altered).	Late stylolites filled with carbonate.
37	Dn	Sandstone: gray-green weathering, fine grained, porous-leached, minor pyrite patches, crossbed sets to 1 m, sandstone breaks into thin planar pieces.	EDQ, trace goethite after Fe-carbonate.	
38	Dhf	Sandstone: brown weathering, fine grained, micaceous, porous-leached, iron stained, interbedded with black shale.	EDQ, ankerite (± goethite altered).	Calcite + ankerite (± minor goethite altered) veins, and BQ veins.
39	Dhf	Siltstone and shale: dark grayish green, interbedded with minor sandstone, fissile to thin bedded, fractured, iron stained.		
40	Mk?	Concretions: similar to those from the Kayak Shale near the Ivotuk airstrip, and elsewhere in the Killik River and Howard Pass quadrangles.	Central cracks filled with siderite, calcite and pyrite.	
41	MDk	Silty carbonate: dark reddish-brown weathering, with silver-blue weathering phosphatic fossils, minor lens, grains of quartz (<30%).	Phosphatic fossils in mixed siderite, unknown green and yellow cements.	
42	MDk	Sandstone: light gray, fine-medium grained, porous-leached, uniform grain size, minor slickenslides, cut by cleavage fractures.	EDQ, abundant BQ.	
43	Dn	Sandstone: light gray-brown weathering, fine-medium grained, porous-leached, thin bedded, poikilitic carbonate cement, disseminated pyrite altering to goethite.	Minor EDQ, ankerite (minor replacement of sandstone grains, ± goethite altered), BQ (replacing goethite), bright green unknown cement.	
44a	MDk	Sandstone: dark brown, fine grained, abundant goethite (after poikilitic carbonate cement), disseminated pyrite.	Minor EDQ, goethite after poikilitic Fe-carbonate, BQ.	BQ veins, ± cut by micro-veinlets of ankerite.
44b	MDk	Sandstone: dark brown, medium-coarse grained, abundant goethite (after carbonate) cement, disseminated pyrite.	EDQ, abundant goethite after siderite/ankerite (spatially associated with BQ; replacing sandstone grains), BQ; unusual bright orange carbonate replacing(?) goethite and BQ.	Late BQ + chlorite + siderite veins, late ankerite in stylolites.

Appendix 1. Summary of field, petrographic, energy dispersive spectroscopy (EDS), and cathodoluminescence data for clastic and lesser carbonate rocks and mineralization in the Kady area—*Continued.*

Sample number	Unit	Field description and petrographic observations	Cements (listed in paragenetic order)	Veins (minerals listed in paragenetic order)
45	MDk	Coal and sandstone: light gray, fine-grained, planar to crossbedded, carbonaceous sandstone interbedded with coal.	EDQ + coal or carbonaceous plant material.	
46	Dn	Sandstone: light brown, fine grained, slightly porous-leached.	EDQ, ankerite, BQ.	Numerous zoned siderite + ankerite + calcite veins and veinlets.
47	Dn	Sandstone: light brown, fine grained, crossbedded, minor mud-chip conglomerates, porous-leached, disseminated pyrite, grains of MCQ (50%), chert (42%), white mica (<1%), cherty argillite lithics (7%), small K-, Al-, and Si-clay or mica patches (1%), trace epidote. Numerous mineralized quartz + calcite veins with green, 2-6 mm carbonate-removal halos, chert more deformed and irregularly shaped within alteration halo, detrital white mica grains pseudomorphed by recrystallized white mica.	EDQ, ankerite (± goethite altered), pyrite; carbonate cement removed adjacent to and chemically zoned away from quartz vein.	Growth-zoned quartz vein with early BQ and chalcopyrite to late white quartz to late calcite in center; small BQ veinlets along vein margin.
48a	Fault	Fault gouge: breccia composed of angular crystalline calcite fragments floating in a matrix of Al- and Si-clay.	Al- and Si-clay, calcite, minor BQ.	
48b	Min-Dn	Sandstone: light greenish brown, fine grained, abundant carbonate cement.	EDQ, ankerite, minor BQ; calcite(?) replacing sandstone grains.	
48c	Dn	Sandstone breccia: light greenish-brown, fine-grained, porous-leached sandstone with rutile grains.	EDQ, calcite, very minor BQ.	Early ankerite veins cut by vein of quartz (margin) and calcite (center); chalcopyrite, pyrite & galena associated with ankerite veins.
49	Min	Veins: folded.		Quartz + chalcopyrite + trace galena + late calcite veins.
50	Dn	Sandstone: light greenish brown, fine grained, porous-leached; outcrop cut by veins.	EDQ, ankerite (± goethite altered), BQ.	Veins of quartz pinch out/terminate into sphalerite and calcite.
51	MDk?	Sandstone: light brown, massive to thin bedded.	EDQ, carbonate.	
52	MDk?	Sandstone and siltstone: maroon and green, fine grained, interbedded.		
53	Dn	Sandstone: light brown, medium grained, massive; poikilitic carbonate lenses and concretions.	Minor EDQ, ankerite (± minor goethite alteration), BQ, trace pyrite; ankerite in concretion has replaced chert and MCQ grains. EDQ rims on sandstone grains are not present in center of concretion.	
54	MDk-Dn?	Conglomerate: gray/tan, carbonate cemented.	EDQ, carbonate.	
55	MDk?	Shale: dark grayish green, interbedded with sandstone.		
56	Dn	Sandstone: light brown, poikilitic carbonate cement.	EDQ, carbonate.	
57	MDk?	Siltstone: maroon and green, fine grained, MnO tarnish, possibly burrowed, abundant zoned carbonate cement (unusual; most carbonate cement at Kady is not zoned).	Minor EDQ, distinctive zoned rhombohedral ankerite, calcite & siderite.	

Appendix 1. Summary of field, petrographic, energy dispersive spectroscopy (EDS), and cathodoluminescence data for clastic and lesser carbonate rocks and mineralization in the Kady area—*Continued.*

Sample number	Unit	Field description and petrographic observations	Cements (listed in paragenetic order)	Veins (minerals listed in paragenetic order)
58	MDk?	Sandstone: brown, fine grained, very thin bedded, trough crossbedded, abundant carbonate cement, brecciated.	EDQ, ankerite, siderite (± goethite altered), BQ.	Sandstone brecciated, breccia cemented by calcite.
59	MDk	Conglomerate and sandstone: light gray, medium to very coarse grained, contains clasts of quartz, black chert and minor distinctive bright green chert; cycles of conglomerate-massive sandstone-crossbedded sandstone.	EDQ, clay(?), minor goethite(?) after Fe-carbonate, BQ.	Outcrop is fractured/brecciated with quartz.
60	Dn	Sandstone: brown, fine grained, carbonate cemented, poikilitic carbonate concretions.	EDQ, ankerite (± goethite altered), 1% pyrite.	
61	Dnl	Sandy carbonate: brown, fine-grained, bluish-silver and maroon, intra-formational lithoclast (limestone) conglomerate with manganese tarnish within sandy carbonate bed, carbonate concretions, small 1-2 cm brachiopods.	Calcite(?)/ankerite(?)	Calcite vein with trace ankerite along edge.
62	Dn	Sandstone: brown, fine grained, poikilitic carbonate cement, black shale partings/ mud chips, crossbedded, minor plant debris.	EDQ, abundant ankerite (± minor goethite alteration), BQ.	
63	Dn	Sandstone/siltstone: medium green, fine grained, very micaceous, mica gives rock planar breakage habit, very porous leached grains.	EDQ, trace BQ.	
64	MDk?	Sandstone: fine-medium grained, interbedded with maroon shale.	EDQ, unknown light orange carbonate cement, BQ.	Early vein of botryoidal goethite (after Fe-carbonate?), cut by late BQ veins.
65	MDk-Dn?	Sandstone: maroonish gray, bedding sets to 0.7 m, planar to sweeping crossbeds, carbonate cemented.		
66	MDk	Sandstone: maroon to yellow weathering, fine grained, massive to crossbedded.	Ankerite.	
67a	MDk	Sandstone: light gray weathering, massive.	EDQ, siderite (± goethite altered).	
67b	MDk	Siltstone: brownish-gray weathering, extremely fine-grained, quartz siltstone being replaced by zoned, rhomb-shaped crystals of siderite.	Quartz, siderite.	
68	MDk	Siltstone: light brownish-gray to maroon; disseminated pyrite. Siltstone associated with maroon shales, siderite-cemented sandstones, minor coal, iron-stones, manganese-staining, and Fe-concretions with pyritized plant material in them.	Minor EDQ(?), ankerite, minor siderite.	
69	MDk	Sandstone: maroon, fine grained, K-, Al-, and Si-clay or very fine-grained white mica, slightly porous-leached.	EDQ, ankerite(?) (± goethite altered), BQ.	
70	MDk	Sandstone: grayish brown, coarse grained, mostly quartz and altered chert grains.	EDQ(?), siderite (± goethite altered); siderite replacing sandstone grains.	
71a	MDk	Concretion: sandy micritic carbonate with pyritized plant stem.	Siderite.	Pyrite.
71b	MDk	Sandstone: light gray, fine-medium grained, light reddish-tan iron staining, black lichen-covered outcrops, grains of rutile, unknown P- and Si-bearing mineral (fluoresces), very porous leached.	EDQ, trace BQ.	Mineralizing fluids passed through sandstone; veins of quartz + chalcopyrite.
72	Min-Dn	*Gossan C: gossanous Zn-carbonates.*		Banded, secondary Zn (Cd, Ca, ±Fe)CO3.

Appendix 1. Summary of field, petrographic, energy dispersive spectroscopy (EDS), and cathodoluminescence data for clastic and lesser carbonate rocks and mineralization in the Kady area—*Continued.*

Sample number	Unit	Field description and petrographic observations	Cements (listed in paragenetic order)	Veins (minerals listed in paragenetic order)
73	Min-Dn	Sandstone breccia and gossan C: sandstone exhibits at least two stages of brecciation.		Sandstone breccia cemented by quartz + sphalerite + minor galena, cut by calcite veins.
74	MDk	Sandstone: brown, fine and coarse grained, iron stained, disseminated pyrite, cut by en echelon, quartz-filled fractures.	EDQ, ankerite(?) (± trace goethite alteration), pyrite (1-2%), trace BQ.	Outcrop cut by thin quartz + carbonate veins.
75	Min-MDk	Sandstone: light gray, fine grained, very porous leached, rutile.	EDQ, trace ankerite, trace siderite, rutile(?)	Siderite vein, cut by abundant, late, sheeted micro-veinlets of gray quartz and BQ with sulfide mineralization.
76	MDk	Graded sandstone breccia S: fine grained, light gray, Al- and Si-clay patches, 1% rutile as grains/cement(?), porous-leached sandstone. Breccia is inversely graded with clasts to 2.5 cm.	EDQ, BQ.	Milky quartz cemented breccia + trace pyrite.
77	MDk	Sandstone: light grayish brown, medium grained, 15- to 60-cm-thick planar beds, disseminated pyrite altering to goethite, slightly porous-leached.	EDQ, pyrite, trace BQ.	
78	Min-MDk	Sandstone: light brownish-gray weathering, medium-grained, very porous leached sandstone, cut by a large mineralized quartz-sphalerite dominant vein-breccia zone and numerous smaller quartz veins.	EDQ, trace BQ.	Gray quartz micro-veinlets and vein of growth-zoned, grayish-BQ to white quartz with sulfide mineralization, cut by late fractures of BQ or cerussite(?).
79	Dn	Sandstone: light brown, fine grained.	EDQ, calcite, goethite after siderite(?), BQ.	Outcrop cut by quartz veins.
80	MDk	Sandstone: light tan gray, fine grained, Al- and Si-clay patches, rutile, porous-leached.	EDQ, goethite after Fe-carbonate, BQ.	Minor gray quartz veinlet.
81	MDk	Sandstone: fine grained, trace disseminated pyrite, trough crossbedded.	EDQ, ankerite (± altered to goethite).	BQ + ankerite(?) veins.
82	MDk	Shale: maroon, nearby green shale, occurs between MDk gray quartz sandstone above and Dn brown carbonate-cemented sandstone below.		
83a	MDk	Sandstone: white and green mottled, fine grained, porous-leached, 30-cm-thick bed within maroon shale, chlorite slicks along bedding.	EDQ, ankerite, siderite, trace BQ(?)	Gray-blue quartz vein.
83b	MDk	Sandstone: green and white mottled, fine grained, porous-leached, 30-cm-thick bed within maroon shale, chlorite slicks along bedding.	EDQ, minor ankerite, siderite, minor chlorite(?)	Vein of BQ (rim) + calcite (center).
84	MDk	Sandstone: light gray, faint iron staining, medium grained, massive, thick bedded, abundant white mica.	EDQ.	Minor quartz veining.
85	MDk	Sandstone: maroonish-gray weathering, fine-medium grained, ± iron-stained, trough(?) crossbedded, massive to thin bedded, porous-leached, grains of MCQ (50%), chert (50%), rutile, white mica.	EDQ, goethite after Fe-carbonate; rims of chert grains partially replaced by carbonate.	Gray quartz veins, fractured.
86a	MDk	Sandstone: coarse grained.	Phosphate mineral, goethite after siderite(?) cement (notably no EDQ).	
86b	MDk	Sandstone: medium grained, porous-leached.	EDQ, trace BQ(?).	Vein of siderite.

Appendix 1. Summary of field, petrographic, energy dispersive spectroscopy (EDS), and cathodoluminescence data for clastic and lesser carbonate rocks and mineralization in the Kady area—*Continued.*

Sample number	Unit	Field description and petrographic observations	Cements (listed in paragenetic order)	Veins (minerals listed in paragenetic order)
87	MDk	Sandstone: brown, fine grained, abundant, irregularly-zoned carbonate cement, vugs of carbonate, angular sandstone grains, interbedded with maroon, gray and green shale.	Zoned calcite to siderite (notably no EDQ).	
88	MDk	Sandstone: dark brown, medium-coarse grained, angular clastic grains.	Sparse EDQ on a few grains, abundant siderite.	Gray-blue quartz veins.
89	MDk	Sandstone: light gray, fine grained, minor light red iron staining, very porous leached, Al- and Si-clay patches.	EDQ, minor siderite (± minor goethite alteration), BQ.	Gray-BQ veins + sulfides, mineralizing fluids flowed through sandstone.
90	MDk	Sandstone: brown weathering, fine grained, thin bedded, very porous leached, K-, Al-, and Si-clay or white mica (after feldspar?).	EDQ, minor goethite after siderite(?)	Abundant small gray quartz veins.
91	MDk	Sandstone: light gray, fine grained, thin bedded.	EDQ, minor siderite, possible grayish BQ(?), minor neon, teal green, unknown cement.	Large BQ vein that is cut by sheeted BQ veinlets.
92	MDk	Sandstone: light gray, fine-medium grained, massive to crossbedded, porous-leached; grains of MCQ, chert, lithics, rutile, apatite.	EDQ, rutile(?), trace BQ.	Micro-veinlets of gray-blue(?) quartz.
93	Min-MDk	Sandstone: light gray, massive to crossbedded, porous-leached.		Gray quartz + galena + pyrite + chalcopyrite, with secondary neon blue cerussite.
94	MDk	Sandstone: light gray, fine grained, crossbedded, disseminated pyrite, plant material, porous-leached, Al- and Si-clay and K-, Al-, Si-clay or white mica.	EDQ, trace goethite after Fe-carbonate, abundant BQ.	Mineralizing fluids flowed through sandstone.
95	Dhf	Siltstone and shale: dark greenish black, fine grained, finely interbedded, porous-leached; chlorite, rutile(?) grains; mixed with fine-grained sandstone.	EDQ, goethite after Fe-carbonate, pyrite.	Quartz veins with trace chalcopyrite(?)
96	Dhf	Sandstone: dark brownish gray, fine grained, crossbedded, black shale partings, compact, very porous leached.	EDQ, ankerite (± trace goethite? alteration).	
97	Dn	Sandstone: brown weathering, fine grained, trough crossbedded, abundant disseminated pyrite patches, very porous leached, grains of MCQ, chert, lithics, albite, chlorite (after biotite--one zircon grain with metamict halo), white mica, Al- and Si-clay patches, chlorite, rutile, carbonaceous plant fragments.	EDQ, siderite(?), trace BQ.	
98	MDk	Sandstone: light brownish gray, medium grained, thin to trough crossbedded (sets as thick as 0.7 m), grains of MCQ, chert, lithics, white mica.	EDQ, ankerite (± goethite alteration); ankerite replaced several chert grains.	Mineralizing fluids flowed through sandstone; thin quartz vein.
99	MDk	Sandstone: light red iron stained, light gray colored, fine grained, porous-leached, grains of MCQ, chert, white mica, lithics, plagioclase, trace chlorite (after biotite), minor rutile, abundant K-, Al-, and Si-clay or white mica (after feldspar?), plant fragments.	EDQ, rutile(?)	Mineralizing fluids flowed through sandstone; BQ veins, chlorite in one vein in thin section.
100	Min-MDk	Sandstone and shale: light gray sandstone and shale, light red iron staining. sandstone is brecciated and cut by mineralized veins that tend to occur along shale-rich layers.		Numerous veins including a 1-m-wide sphalerite dominant vein with quartz, chalcopyrite and lesser galena.

Appendix 1. Summary of field, petrographic, energy dispersive spectroscopy (EDS), and cathodoluminescence data for clastic and lesser carbonate rocks and mineralization in the Kady area—*Continued.*

Sample number	Unit	Field description and petrographic observations	Cements (listed in paragenetic order)	Veins (minerals listed in paragenetic order)
101	MDk	Sandstone: light gray, fine grained, very porous leached, minor rutile, disseminated pyrite.	EDQ, pyrite.	
102	Dn	Sandstone: light brownish gray, fine grained, thin crossbedded, very porous leached, grains of quartz, chert, lithics, plagioclase, white mica, and patches of very fine-grained white mica.	EDQ, siderite (± goethite alteration), BQ.	
103	Dn	Sandstone: light brown, fine grained, massive to crossbedded, very porous leached, grains of MCQ, chert, plagioclase, lithics, chlorite (after biotite), minor white mica, and trace apatite, rutile, minor Al- and Si-clay patches (after feldspar?).	Abundant EDQ, minor goethite after Fe-carbonate, pyrite, trace BQ; carbonate partially replaced sandstone grains.	Minor quartz veining.
104	Dn	Sandstone: light brown weathering, fine grained, bleached, very porous leached, rutile.	EDQ, thin goethite grain coatings.	Outcrop cut by quartz veins.
105	MDk	Sandstone: light gray, massive, crossbedded, trough crossbedded, plant material along bedding planes, very porous leached, rutile.	EDQ, BQ.	Quartz-veined joints.
106	Min-MDk	Sandstone in fault: light brown weathering, medium grained, very porous leached; rutile grains.	EDQ, trace BQ + rutile(?) (up to 1%).	Mineralizing fluids flowed through sandstone. Vein-breccia zones up to 30 cm wide, with quartz + sphalerite + galena.
107	Min-MDk	Sandstone in fault: brown weathering, iron stained, fine grained, slightly porous-leached; chlorite(?) grains.	EDQ, siderite, BQ.	BQ veins.
108	Min	Vein:		Growth-zoned quartz (blue, grayish-blue, and dull to bright yellow) with sulfides and neon blue cerussite.
109	Min-MDk	Sandstone: brown weathering, abundant disseminated pyrite, grains of MCQ, chert, and brown lithics; cut by numerous mineralized veins.	EDQ, pyrite cement, pyrite has partially replaced all grain types.	Quartz + chalcopyrite + sphalerite + galena veins cut abundant disseminated pyrite.
110	Min-MDk	Sandstone and vein: growth-zoned quartz vein, chlorite; sandstone is bleached, brecciated, contains disseminated pyrite.		Growth-zoned quartz: gray-blue (early) to tan (late).
111	MDk	Siltstone and shale: brown weathering, very fine grained, abundant white mica; 2.5-cm-thick sets of crossbeds.	EDQ, calcite (with minor iron).	Calcite vein.
112	Dn?	Sandstone: light brown, fine grained, abundant black shale rip-up clasts, ripple marks(?), small-scale crossbeds, porous-leached.	EDQ, calcite, goethite after Fe-carbonate, BQ.	
113	Min	Vein:		Growth-zoned, gray-blue, tan, yellow quartz vein with chalcopyrite + sphalerite + galena.
114	MDk	Sandstone: light gray, fine-medium grained, light yellow and red iron staining, massive trough crossbeds, porous-leached; rutile(?) grains.	EDQ, possible late gray quartz(?)	Mineralizing fluids flowed through sandstone; many quartz veins (see sample 113).
115	Min	Vein: vein in sandstone breccia.		Quartz vein with altered pyrite, chalcopyrite.
116	Min-MDk	Sandstone: light gray weathering, light red iron staining, porous-leached, massive, trough crossbedded, minor conglomerate beds.		Mineralizing fluids flowed through sandstone.

Appendix 1. Summary of field, petrographic, energy dispersive spectroscopy (EDS), and cathodoluminescence data for clastic and lesser carbonate rocks and mineralization in the Kady area—*Continued.*

Sample number	Unit	Field description and petrographic observations	Cements (listed in paragenetic order)	Veins (minerals listed in paragenetic order)
117	Dn	Sandstone: gray-green, fine grained, trough crossbedded, disseminated pyrite patches, porous-leached; grains of MCQ, chert, lithics, white mica, abundant plant material.	EDQ, Zn-bearing goethite (after poikilitic carbonate cement), pyrite, BQ, teal green unknown cement.	Mineralizing fluids flowed through sandstone.

Geologic Studies in Alaska by the
U.S. Geological Survey, 1997
U.S. Geological Survey Professional Paper 1614

Chemical and Isotopic Data for Rocks and Ores from the Upper Triassic Greens Creek and Woewodski Island Volcanogenic Massive Sulfide Deposits, Southeastern Alaska

By Rainer J. Newberry *and* David A. Brew

Abstract

Comparison of chemical and isotopic data from samples of drill core and underground exposures at the volcanogenic massive sulfide (VMS) deposit at the Greens Creek mine on Admiralty Island and from samples of drill core at VMS prospects on Woewodski Island in the Duncan Canal area about 200 km to the south indicates that the ores and host rocks at both places have similar compositions. This evidence confirms that these two localities are within the regional VMS belt of Late Triassic age that has been inferred to extend from the Windy-Craggy deposit in British Columbia southeast to Zarembo Island, about 20 km southeast of Woewodski Island. Sparse but consistent fossil evidence indicates the belt's Late Triassic age. Although there are some felsic volcanic rocks near the Woewodski Island prospects, this VMS belt is distinguished by the overwhelming dominance of compositionally similar metabasalts. Specifically, the major- and trace-element chemical data indicate basaltic compositions for Greens Creek stratigraphic footwall rocks and sedimentary compositions for the stratigraphic hanging-wall rocks. The near absence of bimodal volcanism and the rare-earth-element data indicate that the tectonic environment was not extensional, but was instead arc related. The corresponding data for the Woewodski Island rocks give similar results. Although the Woewodski Island metavolcanic rocks are not as deformed or altered as those at Greens Creek, we confidently assign them to the same volcanogenic massive sulfide belt on the basis of lithology, trace-element and rare-earth-element composition, and age.

Introduction

The deposit at the Greens Creek mine is the largest known of many volcanogenic massive sulfide (VMS) deposits in southeastern Alaska (fig. 1). It and the other Late Triassic deposits shown on figure 1 are part of a regional metallogenic belt that extends to the northwest into British Columbia, where it includes the Windy-Craggy deposit. This belt occurs in rocks assigned to the Alexander terrane by Berg and others (1978), but Brew and Ford (1994) and Brew (1996) interpret them instead to be equivalent to the Wrangellia terrane rocks exposed adjacent to the Alexander terrane. The Devonian(?) VMS deposits shown on figure 1 are in what Brew and Ford (1994) and Brew (1996) call the Behm Canal structural zone; their host rocks may actually be as old as Late Proterozoic and as young as late Paleozoic. The Late Proterozoic-early Paleozoic VMS deposits shown on figure 1 are all in the Alexander terrane.

Worldwide, VMS deposits of a given age, like the Late Triassic deposits that are the focus of this report, occur in clusters within larger belts. Thus, the presence of one major deposit signals the likelihood for others. Both the evaluation of undiscovered mineral resources and the strategies for exploration and development of Greens Creek-like deposits in southeastern Alaska depend on understanding the origin of the Greens Creek deposit.

Published models for the Greens Creek deposit include: (1) proximal VMS, ores related to felsic volcanics and phreatoclastic breccias (MacIntyre, 1986); (2) distal VMS, ores related to buildup in felsic tuff-like rocks (Dunbier and others, 1979); (3) sediment-hosted sulfide, with ores related to syn-sedimentary breccias and feeder veins (Dreschler and Dunbier, 1981); and (4) proximal VMS, with ores related to altered and deformed mafic volcanic rocks (Crafford, 1989). Given the degree of chemical and mineralogical alteration typically associated with the formation of VMS deposits (Date and others, 1983) and the highly sheared and foliated character of the rocks at Greens Creek, macroscopic and microscopic observations of color, texture, and mineralogy are insufficient to identify the rock protoliths.

The contrasting interpretations and uncertainties regarding the origin of the Greens Creek deposit prompted this study of the major- and minor-element compositions of the rocks. We also studied the composition of the rocks that enclose VMS

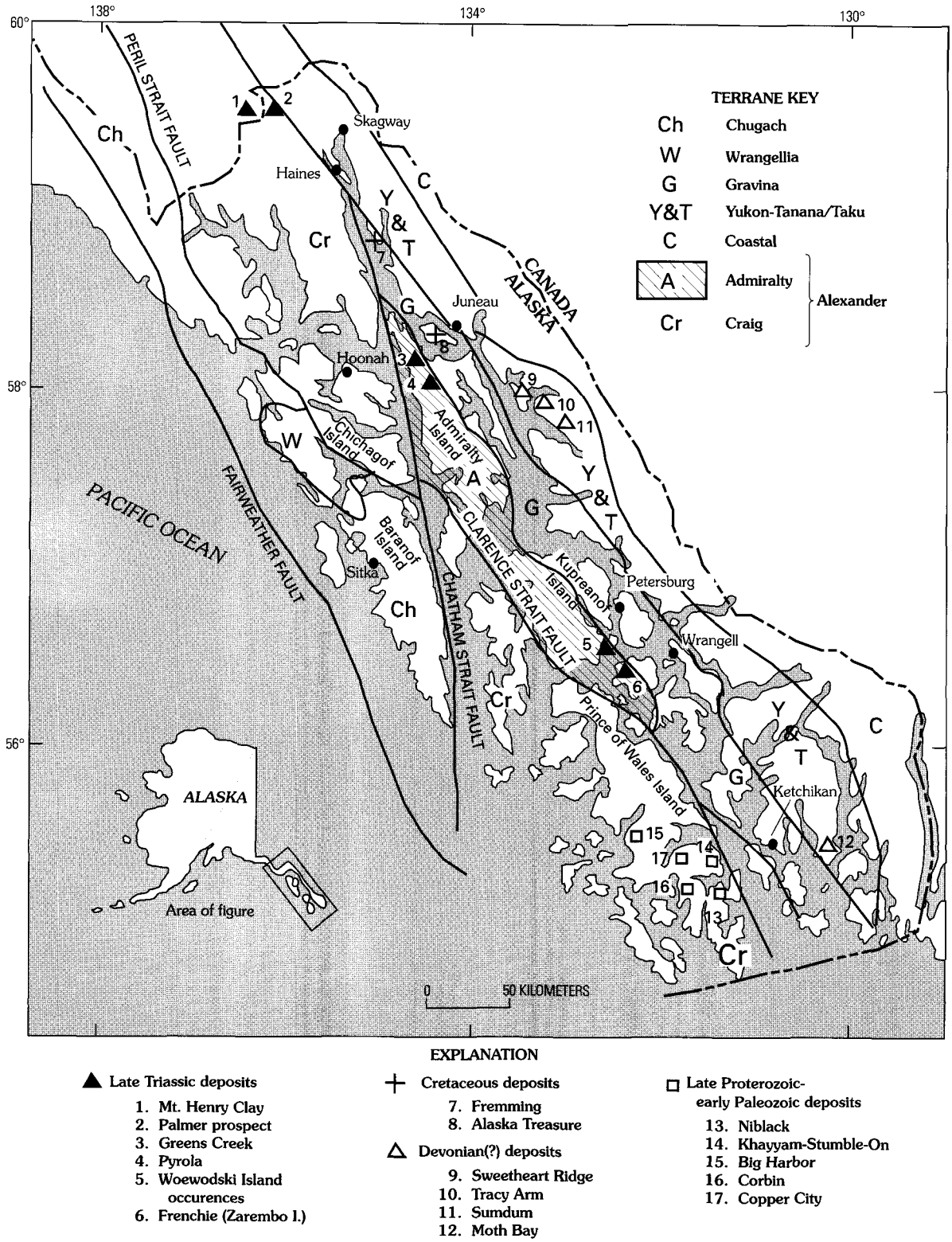

Figure 1. Location map showing major VMS (volcanogenic massive sulfide) deposits and prospects in southeastern Alaska and generalized lithotectonic terrane boundaries. Modified from and Newberry and others (1997).

prospects on Woewodski Island, in the Duncan Canal area (indicated by no. 5 on fig. 1); these prospects have been interpreted to be of the same Late Triassic age as the Greens Creek deposit (Berg, 1981; Berg and Grybeck, 1980). Finally, we studied the lead isotopes of ores from both Greens Creek and Woewodski Island and also from several other VMS prospects in southeastern Alaska in order to further clarify the ages of the deposits.

A preliminary version of this report (Newberry and Brew, 1997) contains additional data and is referred to where we have truncated its data to present it in revised form in this article.

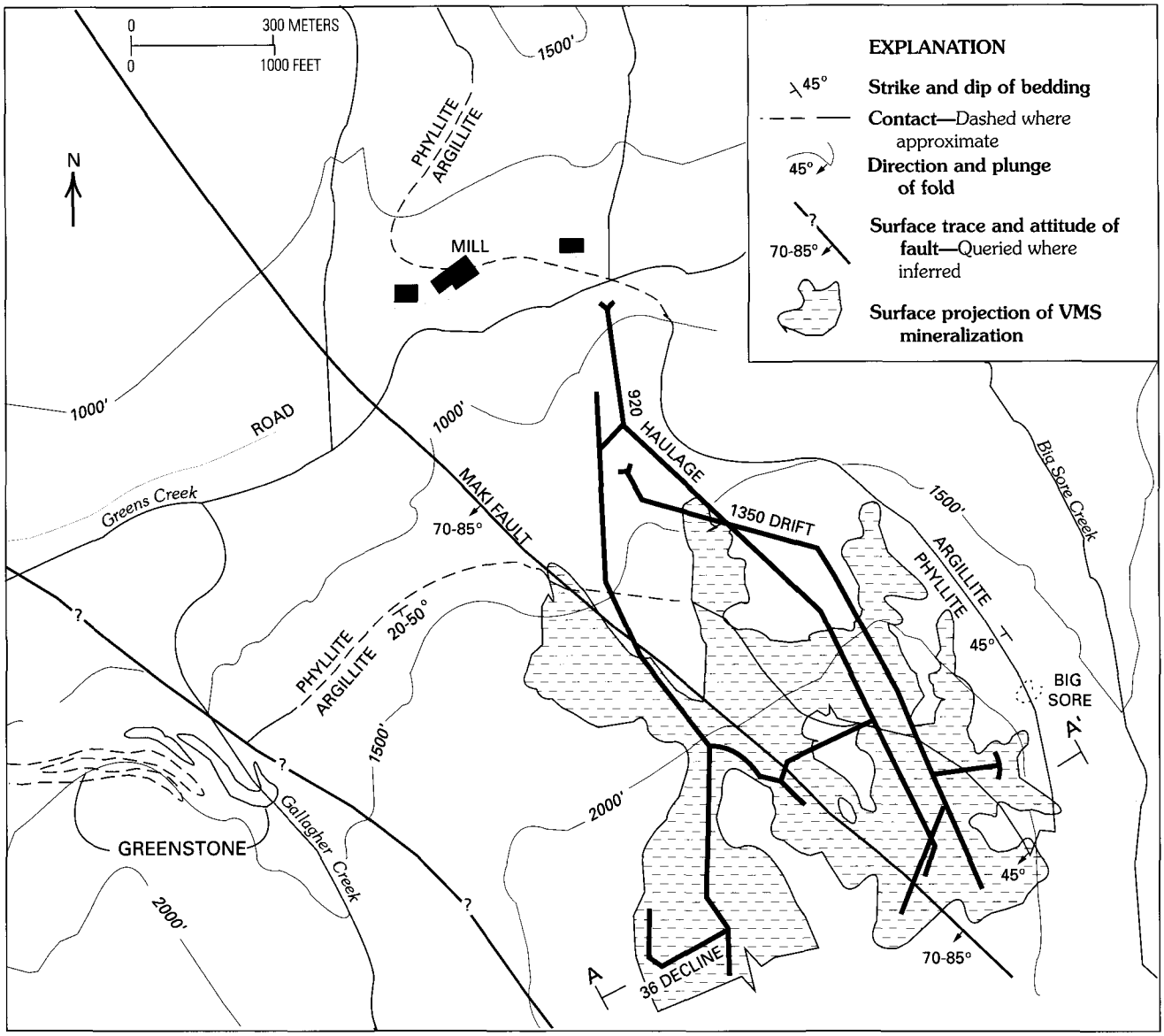

Figure 2. Generalized surface geology and surface projection of mineralized area at the Greens Creek deposit, southeastern Alaska. From Crafford (1989) and Newberry and others (1997).

General Geology of the Greens Creek Deposit

Massive sulfide at the Greens Creek deposit is discontinuously distributed along the contact between a structural hanging wall of thinly laminated quartz-mica-carbonate phyllite and a structural footwall of black graphitic meta-argillite (fig. 2). *Halobia* present in carbonate-rich black argillite clasts contained within pyritic massive sulfide ore indicate a Late Triassic maximum age for the deposit (N.J. Silberling, written commun., 1988, 1989, 1990; Crafford, 1989). Regional structural relationships and locally preserved graded bedding suggest that the stratigraphy at the mine is inverted and that the structural hanging-wall rocks originally underlay the VMS deposit. These stratigraphic footwall rocks are very fine grained (<0.2 mm typically), are strongly foliated, and have been described both as "mudstones," "tuffites," and "exhalites" with an upward-increasing felsic volcanic component (Dunbier and others, 1979) and as sedimentary rocks (Nokleberg and others, 1987). However, at least four folding events are documented at the mine (Crafford, 1989), and their cumulative effect has been to largely obliterate original stratigraphic footwall rock textures.

Given the inverted stratigraphic interpretation, the overall original stratigraphy of the Greens Creek mine is an upward progression from greater than 100 m of chloritic phyllite (chlorite > carbonate > quartz > sericite), to 0 to 70 m of sericitic phyllite (sericite > quartz > carbonate, referred to later as "quartz-carbonate-mica phyllite"), to local siliceous pyritic phyllite, to 0 to 20 m of breccia, to massive sulfide, to (overlying) graphitic calc-argillite and limestone (Newberry and others, 1990). The thickness and silica content of sericitic phyllite increases dramatically in areas proximal to ore. The thicknesses of the breccia unit that is stratigraphically just below the ore horizon are greatest approximately 50 to 300 m laterally away from major sulfide thicknesses (Crafford, 1989). Carbonate-altered quartz-mariposite rocks are variably present near the ore horizon, but are distal to massive sulfide ore. Table 1 summarizes these stratigraphic and structural relations and

Table 1. Generalized original stratigraphic section at the Greens Creek deposit, giving the single-letter abbreviations used in tables and figures.

Estimated thickness	Major rock type(s)	Other rock type(s)	Single-letter symbol	Notes
?	Graphitic calc-argillite	----------	h	Aka hanging-wall argillite, aka black argillite; aka black [siliceous] argillite or calcareous argillite, aka siliceous argillite; hard and siliceous within 3 to 6 m of ore.
		Graphite-rich quartz-mica-carbonate rock transitional to argillaceous limestone-------	h	
	Massive sulfide			Carbonate-altered quartz-mariposite rocks variably present near ore horizon--but distal to ore, they may be altered ultramafic rocks (serpentinite); some black argillite may be interleaved with ore; *Halobia* occur in carbonate-rich black argillite clasts in pyritic massive sulfide ore.
		Mariposite rocks----------	m	
		Serpentinite----------	p	
0-20 m	Breccia----------	----------	x	Aka siliceous breccia; thicknesses greatest 50-300 m away from largest sulfide thicknesses.
Locally beneath ore	Siliceous pyritic phyllite ----------	----------	q	Occurs below most Cu-rich part of ore body.
		Chalcopyrite-quartz-pyrite-sericite rock-----	q	
Locally beneath ore	Graphitic phyllite (=visible graphite)------	----------	r	Rare
0-70 m	Sericitic phyllite-------- (=sericite>quartz> carbonate)	----------	s	Aka quartz-carbonate-mica phyllite, aka "footwall phyllite," aka muscovite phyllite, aka quartz phyllite, aka muscovite phyllite, aka muscovite-dolomite phyllite; thickness and silica content increases proximal to ore, carbonate content may be >10%, more silicic and pyritic closer to ore; some black argillite may be interleaved.
		Also contains ankerite, dolomite, calcite, white mica, chlorite, Ti oxides; mariposite, mariposite-bearing phyllite, mariposite rock, mariposite phyllite, mariposite-dolomite phyllite----------	m	
		Quartz phyllite or pyrite-muscovite phyllite or siliceous phyllite----------	q	
>100 m	*Chloritic phyllite* (= chlorite>carbonate> quartz>sericite----------	----------	c	
		Dolomitic phyllite----------	c	
		Chlorite-calcareous phyllite----------	c	
		Greenstone----------	g	
		Gabbro, diabase, metagabbro----------	g	
Other	Felsic sill, keratophyre--	----------	k	Aka quartz-albite rock.

also provides a key to link the stratigraphy to the samples (and their single-letter symbols) used in our interpretations.

Mafic rocks with recognizable igneous textures are found approximately 2 km north and 1 km west of the Greens Creek mine (beyond the limits of fig. 2). These rocks include massive porphyritic basalt, hornblende clinopyroxenite, and serpentinite. The structural relationship between these rocks and the rocks of the Greens Creek mine is unclear. It is also unclear whether the ultramafic rocks are cumulates related to basaltic volcanism or are unrelated, structurally emplaced bodies.

The structural hanging wall (i.e., stratigraphic footwall), quartz-carbonate-mica phyllite contains variable amounts of ankerite, dolomite, calcite, white mica, chlorite, mariposite, pyrite, and titanium oxides. These rocks were referred to as the "footwall phyllite" by Newberry and others (1997). The carbonate content of these phyllosilicate-rich rocks often exceeds 10 percent by volume, and the rocks typically become progressively more silicic and pyritic with increasing proximity to massive sulfide mineralization (Newberry and others, 1990). A local unit that is stratigraphically beneath the most Cu-rich part of the orebody is a rock consisting of quartz, pyrite, sericite, and minor chalcopyrite referred to as "siliceous pyritic phyllite." An additional, and rare, rock type in the stratigraphic footwall package contains visible graphite and is referred to as "graphitic phyllite;" we interpret the organic carbon in this rock to indicate a sedimentary origin. Reflected light petrography indicates that most of the black color in the stratigraphic footwall rocks is, however, due instead to very fine grained sulfide minerals. The siliceous pyritic phyllite and the graphitic phyllite are below the footwall breccia mentioned previously.

Stratigraphic hanging-wall graphitic argillite, referred to variously as "black argillite," "black graphitic meta-argillite," or "graphitic calc-argillite," is graphite-rich quartz-mica-carbonate-graphite rock that is commonly transitional to argillaceous limestone (Newberry and others, 1990). Within about 3 to 6 m of massive sulfide, the black argillite is hard and siliceous. Black argillite is in places (structurally?) interleaved with massive sulfide and stratigraphic footwall phyllite.

General Geology of Woewodski Island

Rock exposures on Woewodski Island, 30 km south of Petersburg, Alaska (figs. 1, 3), are limited almost exclusively to beaches and stream cuts. Based on similarities to known fossiliferous Triassic rocks only a few kilometers to the northwest, most of the metavolcanic rocks on Woewodski Island have been interpreted to be of Late Triassic age (Berg, 1981; Berg and Grybeck, 1980; Brew, 1997a, 1997b) and some of indeterminate Mesozoic age. However, Cretaceous rocks of the Gravina assemblage are present just east of Woewodski Island, and it is not entirely clear where the contact between Triassic and Cretaceous rocks is located. Lithologies on Woewodski Island include black slate; greenstone of probable basaltic composition; basaltic tuff; limestone; and cherty, sulfide-bearing rocks. VMS mineralization has been identified at the Helen S. prospect, and prospects have been drilled near the center of the island (fig. 3). Due to the limited exposures, the ages and character of the ores and host rocks are not well constrained.

Analytical Methods

Seventy-one samples were selected for major- and minor-element analysis during detailed diamond drill core logging and underground and surface mapping in the Greens Creek deposit area. Ten samples from drill core of VMS prospects on central Woewodski Island were also analyzed. Outcrop samples were clean, fresh, 0.5- to 2.0-kg, composite chip samples. Drill core was sampled by sawing complete 0.2- to 3.0-m sections lengthwise, and the entire half of the core was ground for analysis. All samples were analyzed for major elements using standard fused-pellet X-ray fluorescence (XRF) techniques, for FeO by titration, and for minor and trace elements by energy-dispersive X-ray fluorescence in U.S. Geological Survey laboratories. Some of the same samples were checked by wavelength-dispersive XRF analyses at the University of Alaska-Fairbanks. All analytical methods are essentially those described by Arbogast (1996). CIPW norms were calculated from the major-element analyses using the "Petcal" program (R.D. Koch, written commun., 1980). In addition, 23 samples from Greens Creek were analyzed for rare earth and additional trace elements by standard neutron activation techniques (Arbogast, 1996). Galena-rich samples were analyzed (Richard Hurst, Chempet Research Corporation, Moorpark, Calif., written commun., 1995) for Pb isotopic ratios using standard extraction and analytical techniques, including correction for thermal fractionation (Cameron and others, 1969).

Results

Locations and brief descriptions of rocks from the Greens Creek mine area analyzed for this study are given in table 2. This table also contains (in the column marked by an "*") the rock-type single-letter abbreviations that are employed as symbols on the compositional diagrams (figs. 4–13) and on the interpreted protolith diagrams, which are based on the major- and minor-element compositions. Table 1 explains these symbols and also links the samples to the stratigraphic package at Greens Creek. Major-oxide analyses (table 3) and minor-element analyses (tables 4 and 5) are given for selected samples from both the Greens Creek area and Woewodski Island. CIPW normative analyses are given in Newberry and Brew (1997, their table 3). Lead isotopic analyses for selected VMS deposits of southeastern Alaska are given in table 6.

Interpretation

Compositional Characteristics and Protoliths of Rocks from the Greens Creek Deposit and Vicinity

Major-element analyses of rocks from the Greens Creek mine area indicate broadly basaltic compositions (table 3) for the bulk of stratigraphic footwall rocks. However, extremely high LOI (loss on ignition = sum of $H_2O + CO_2 + S$) values (Newberry and Brew, 1997, their table 2) and variably high normative corundum (Newberry and Brew, 1997, their table 3) indicate that these stratigraphic footwall rocks are either sedimentary or very strongly altered. Manganese oxide, which is commonly associated with hydrothermal alteration, is also present at high concentrations in some samples (table 3). Because LOI and MnO show a positive correlation (fig. 4*A*) for a variety of lithologies, it is likely that MnO, H_2O, CO_2, and S were introduced together, and the rocks have experienced hydrothermal alteration. Because the rocks have such high LOI's, it is best to compare oxide concentrations normalized on an anhydrous basis.

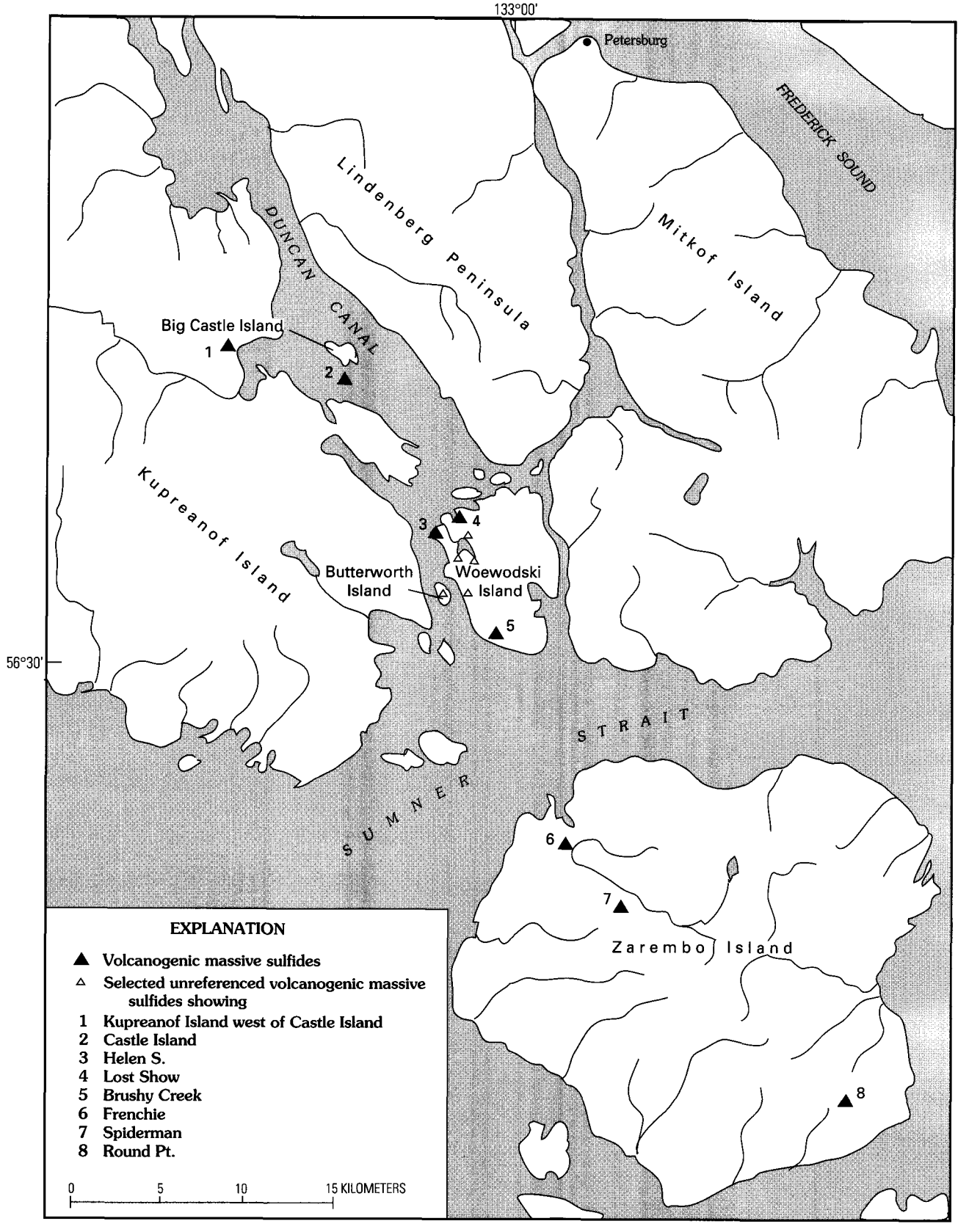

Figure 3. Locations of VMS (volcanogenic massive sulfide) showings in the Duncan Canal–Zarembo Island area, including Woewodski Island, southeastern Alaska. From Berg and Grybeck (1980) and Newberry and others (1997).

Of the various major oxides, TiO_2 is among the most immobile during chemical alteration (Winchester and Floyd, 1977), and it is notable that the bulk of stratigraphic footwall rocks have TiO_2 and also SiO_2 contents compatible with mafic and ultramafic protoliths (BVSP, 1981) (fig. 4*B*). Obvious sedimentary rocks, i.e., the stratigraphic hanging-wall argillites ("h") and stratigraphic footwall graphitic phyllites ("r"), have much higher SiO_2 contents, but TiO_2 concentrations are elevated relative to

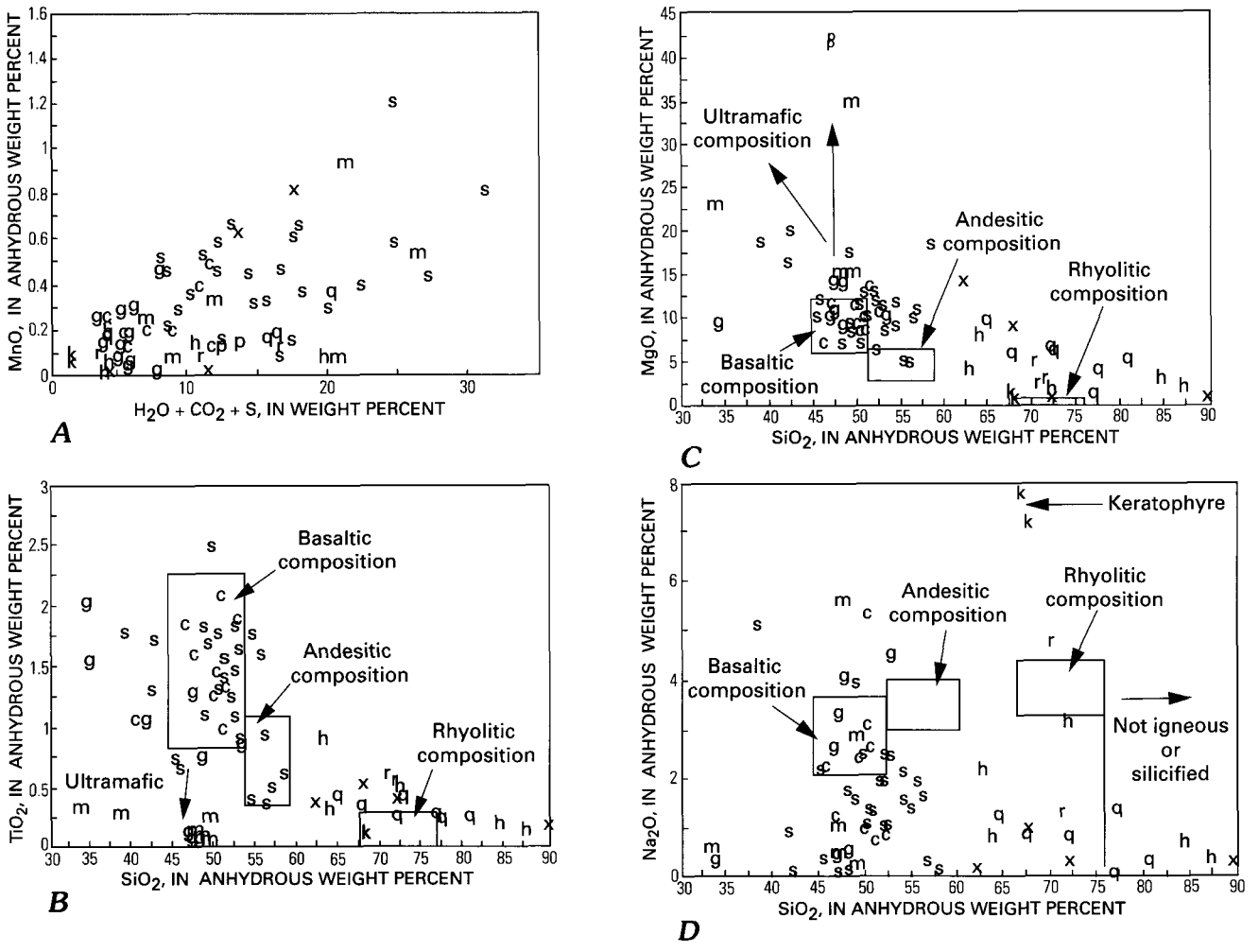

Figure 4. Major-element characteristics of rocks from the Greens Creek deposit and vicinity. Sample/rock type symbols plotted are as follows: Hanging-wall rocks: h, hanging-wall argillite; Footwall rocks: r, graphitic phyllite; q, quartzitic phyllite; c, chloritic phyllite/greenstone; s, muscovite chlorite phyllite; m, mariposite rock; x, siliceous breccia; g, gabbro; p, serpentine. Other: k, felsic sill. *A*, Anhydrous weight percent MnO plotted vs. sum of $H_2O + CO_2 + S$, showing correlation between the two. *B*, Anhydrous weight percent TiO_2 plotted vs. SiO_2, showing that most stratigraphic footwall rocks have compositions consistent with mafic and ultramafic igneous rocks. *C*, Anhydrous weight percent MgO plotted vs. SiO_2, showing that stratigraphic footwall rocks have compositions consistent with mafic and ultramafic igneous rocks. *D*, Anhydrous weight percent Na_2O plotted vs. SiO_2, showing major depletion in Na for most of the stratigraphic footwall rocks relative to normal igenous rocks and extreme enrichment in the sample of keratophyre ("k"). Compositional fields shown are from Streckeisen and LeMaitre (1979).

rhyolite (fig. 4*B*). Only a few of the samples have SiO_2 and TiO_2 contents appropriate for felsic igneous rocks (fig. 4*B*). The relatively close correspondence of the SiO_2 and TiO_2 is interesting and difficult to explain because SiO_2 is generally judged to be mobile, and TiO_2 immobile, during chemical alteration.

MgO contents of the greenstones and chloritic phyllites ("c") , serpentinites ("p"), gabbros ("g"), and mariposite-bearing phyllites ("m") are similarly appropriate for mafic and ultramafic rocks (fig. 4*C*). Many of the muscovite phyllites ("s") also show SiO_2, TiO_2, and MgO contents appropriate for basaltic rocks (figs. 4*B*, 4*C*). Na_2O concentrations, however, are extremely erratic (fig. 4*D*) and reflect the extreme mobility of Na^+ during hydrothermal alteration. Most of the samples in the data set are strongly to somewhat depleted in Na_2O relative to unaltered igneous and sedimentary rocks (Taylor and McLennan, 1985) (fig. 4*C*); two samples from a felsic sill(?) from the mine area ("k") have extremely high Na_2O and keratophyric compositions. Similarly, most of the samples have less than 3.0 percent K_2O and, despite the apparent abundance of fine-grained white mica in the muscovite phyllites, are significantly depleted in K_2O relative to felsic igneous rocks (table 3). Depletion in alkalis, especially Na_2O, is characteristic of alteration developed under some, dominantly felsic-rock-hosted, VMS deposits (e.g., Date and Watanabe, 1979; Date and others, 1983; Hashiguchi and others, 1983).

The CIPW Norms for the samples (Newberry and Brew, 1997, their table 3) show variably high corundum and quartz (Newberry and Brew, 1997, their fig. 6a). Some greenstones and chloritic phyllites have near-zero values for normative corundum and quartz; other footwall phyllites and metagabbros ("c," "g") have variably high corundum and low normative quartz, whereas the sedimentary rocks ("h," "r") have high normative quartz and variable corundum (Newberry and Brew, 1997, their fig. 6a). High normative corundum values in altered igneous

Table 2. Locations and descriptions of Greens Creek (gc) and Woewodski Island (RN) samples.

[Abbreviations in "*" column explained in table 1. Abbreviations are used as symbols on some figures, and sample numbers are used in REE (rare-earth-element) plots. deg, degrees; min, minutes; sec, seconds; meta-hbl, meta-hornblende; musc, muscovite; grnst, greenstone; phyl, phyllite]

Sample no.	Description	*	Location	Latitude (W.)			Longitude (N.)			Most likely protolith
				deg	min	sec	deg	min	sec	
gc78b	siliceous breccia	x	920 Adit, 1st x-cut	58	4	55	134	38	0	silicified breccia
gc80d	pyrite dolomite muscovite quartz phyllite	q	1350 Adit: x-cut to ore	58	4	47	134	37	47	altered sediment?
gc80i	pyrite dolomite muscovite quartz phyllite	q	1350 Adit: x-cut to ore	58	4	47	134	37	47	altered rock
gc80k	pyritic quartz muscovite phyllite	s	1350 Adit: x-cut to ore	58	4	47	134	37	47	altered basalt
gc80m	pyrite dolomite muscovite quartz phyllite	q	1350 Adit: x-cut to ore	58	4	47	134	37	47	altered basalt?
gc80pq	pyritic quartz muscovite phyllite	s	1350 Adit: x-cut to ore	58	4	47	134	37	47	altered basalt
gc81a	graphitic phyllite	r	1350 Adit	58	4	47	134	37	47	C-rich mudstone
gc82a	chlorite dolomite phyllite	c	Greens Creek Road	58	4	54	134	38	37	basalt
gc82c	dolomite muscovite quartz phyllite	q	Greens Creek Road	58	4	54	134	38	37	altered sediment(?)
gc83b	dark-gray quartz phyllite	q	Greens Creek Road	58	4	49	134	38	50	silicified sediment
gc83c	typical muscovite phyllite	s	Greens Creek Road	58	4	49	134	38	50	altered basalt
gc84b	metagabbro	g	Greens Creek Road	58	4	44	134	39	32	gabbro
gc84c	mariposite rock	m	Greens Creek Road	58	4	44	134	39	32	altered mafic rock
gc85b	greenstone	c	Greens Creek Road	58	4	35	134	41	50	basalt
gc89a	black argillite	h	Greens Creek Road	58	5	13	134	43	40	carbonaceous mudstone
gc90a	black siliceous argillite	h	Greens Creek Road	58	5	33	134	44	0	siliceous mudstone
gc93a	siliceous breccia	x	Greens Creek Road	58	5	54	134	44	21	conglomerate(?)
gc94a	mariposite muscovite dolomite phyllite	m	Greens Creek Road	58	5	58	134	44	24	altered ultramafic rock
gc94b	mariposite muscovite dolomite phyllite	m	Greens Creek Road	58	5	58	134	44	24	altered mafic rock
gc95a	graphitic phyllite	r	Greens Creek Road	58	6	5	134	44	22	C-rich mudstone
gc101a	metagabbro	g	Mariposite Ridge	58	6	12	134	40	40	gabbro
gc102a	metagabbro	g	Mariposite Ridge	58	6	16	134	40	36	gabbro
gc103a	metagabbro	g	Mariposite Ridge	58	6	28	134	41	9	gabbro
gc121b	gray muscovite phyllite	s	920 Adit "serp"	58	4	55	134	37	55	altered basalt
gc122a	greenstone	c	GC 511 90-91'	58	4	30	134	38	0	basalt
gc122b	quartz albite rock	k	GC 511 129.5'	58	4	30	134	38	0	keratophyre
gc122d	quartz albite rock	k	GC 511 169.5'	58	4	30	134	38	0	keratophyre
gc122e	meta-diabase	g	GC 511 203'	58	4	30	134	38	0	altered diabase
gc122f	greenstone	c	GC 511 273'	58	4	30	134	38	0	basalt
gc284b	calcareous argillite	h	920 Adit	58	4	55	134	38	0	calcareous mudstone
gc284c	tan muscovite dolomite phyllite	s	920 Adit	58	4	55	134	38	0	altered basalt
gc284d	tan muscovite dolomite phyllite	s	920 Adit	58	4	55	134	38	0	altered basalt
gc284e	chlorite calcareous phyllite	c	920 Adit	58	4	55	134	38	0	basalt
gc284f	siliceous argillite	h	920 Adit	58	4	55	134	38	0	siliceous shale

rocks result from removal of Na_2O, K_2O, and CaO as Al_2O_3 is essentially immobile under most circumstances (Fyfe and others, 1978); the classification of such rocks based on the abundance of alkali elements is consequently misleading. The normative compositions, however, are consistent with mafic-ultramafic protoliths for the less-altered greenstones, chloritic

Table 2. Locations and descriptions of Greens Creek (gc) and Woewodski Island (RN) samples—*Continued.*

Sample no.	Description	*	Location	Latitude (W.)			Longitude (N.)			Most likely protolith
				deg	min	sec	deg	min	sec	
gc285a	mariposite phyllite	m	1350 Adit	58	4	47	134	37	47	altered mafic rock
gc285b	siliceous argillite	h	1350 Adit	58	4	47	134	37	47	siliceous shale
gc285g	mariposite phyllite	m	1350 Adit	58	4	47	134	37	47	altered mafic rock
gc286a	meta-hbl gabbro	g	Mariposite Ridge	58	6	10	134	39	40	hornblende gabbro
gc286b	greenstone	c	Mariposite Ridge	58	6	10	134	39	40	basalt
gc286c	metagabbro	g	Mariposite Ridge	58	6	10	134	39	40	gabbro
gc286d	greenstone	c	Mariposite Ridge	58	6	10	134	39	40	basalt
gc286e	serpentinite	p	Mariposite Ridge	58	6	10	134	39	40	ultramafic rock
gc286f	greenstone	c	Mariposite Ridge	58	6	10	134	39	40	basalt
gc287a	mariposite dolomite phyllite	m	MPR-1 258-261'	58	6	3	134	39	21	altered mafic rock
gc287b	greenish-gray muscovite phyllite	s	MPR-1 40-41'	58	6	3	134	39	21	altered basalt
gc287c	tan muscovite dolomite phyllite	s	MPR-1 166-168'	58	6	3	134	39	21	altered basalt
gc288a	gray-tan muscovite dolomite phyllite	s	PS 25 198-199'	58	4	42	134	37	13	altered basalt
gc288b	gray-tan muscovite dolomite phyllite	s	PS 25 223-224'	58	4	42	134	37	13	altered basalt
gc288c	gray musc phyllite	s	PS-25 46-47'	58	4	42	134	37	13	altered basalt
gc288d	gray musc phyllite	s	PS 25 129-130'	58	4	42	134	37	13	altered basalt
gc288e	gray-tan phyllite	s	PS 25 274-275'	58	4	42	134	37	13	altered basalt
gc288f	pyrite muscovite phyl	q	PS 25 372-374'	58	4	42	134	37	13	silicified rock
gc289a	tan muscovite phyllite	s	PS-5 20-25'	58	4	42	134	37	13	altered basalt
gc289b	muscovite phyllite	s	PS-5 135-139'	58	4	42	134	37	13	altered basalt
gc289c	gray-tan phyllite	s	PS-5 295-300'	58	4	42	134	37	13	altered basalt
gc289d	graphitic phyllite	r	PS-5 80-81'	58	4	42	134	37	13	C-rich sediment
gc289e	gray-tan phyllite	s	PS-5 85-86'	58	4	42	134	37	13	altered basalt
gc289f	gray-tan phyllite	s	PS-5 558-560'	58	4	42	134	37	13	altered basalt
gc289g	breccia	x	PS-5 440-442'	58	4	42	134	37	13	silicified breccia
gc289h	greenish-gray muscovite phyllite	s	PS-5 631-635'	58	4	42	134	37	13	altered basalt
gc289i	breccia	x	PS-5 366-369'	58	4	42	134	37	13	silicified breccia
gc289j	gray siliceous phyllite	q	PS-5 696-698'	58	4	42	134	37	13	silicified rock
gc290a	gray muscovite phyllite	s	GC-139 955-957'	58	4	27	134	37	2	altered basalt
gc291a	serpentinite	p	PS-83 978-980'	58	4	23	134	38	51	ultramafic rock
gc293a	greenish-tan phyllite	s	GC-11 32-34'	58	4	48	134	37	23	altered basalt
gc293b	chlorite phyllite	c	GC-11 89-90'	58	4	48	134	37	23	basalt
gc293d	grayish-tan phyllite	s	GC-11 240-242'	58	4	48	134	37	23	altered basalt
gc294a	greenish-tan phyllite	s	GC-67 8-10'	58	4	36	134	37	9	altered basalt
gc294b	gray musc phyllite	s	GC-67 78-80'	58	4	36	134	37	9	altered basalt
gc294c	tan-gray phyllite	s	GC-67 101-102'	58	4	36	134	37	9	altered basalt
gc294d	dark-gray phyllite	s	GC-67 156-157'	58	4	36	134	37	9	altered basalt
RN116a	massive greenstone	g	-	56	34	32	133	3	19	-
RN116d	pyritic greenschist	a	-	56	34	32	133	3	19	-
RN116g	tuffaceous greenschist	t	-	56	34	32	133	3	19	-
RN118a	massive greenstone	g	-	56	34	25	133	3	10	-
RN118b	masssive greenstone	g	-	56	34	25	133	3	10	-
RN118d	cherty ironstone	-	-	56	34	25	133	3	10	-
RN119c	tuffaceous greenschist	t	-	56	34	27	133	3	0	-
RN120a	diabase(?)	g	-	56	34	23	133	2	55	-
RN121a	amygdaloidal grnst	g	-	56	34	25	133	3	30	-
RN123a	tuffaceous greenschist	t	-	56	34	19	133	3	19	-

phyllites, and gabbros; with non-igneous protoliths for the sedimentary rocks; and with a variety of apparent protoliths for the muscovite phyllites (Newberry and Brew, 1997, their fig. 6b).

Major oxide compositions are plotted in terms of the three components: alkalies $Na_2O + K_2O$ (A), calcium oxide CaO (C), and magnesium oxide MgO (F) (fig. 5). These plots help clarify

Table 3. Major-oxide compositions for selected Greens Creek (gc) and Woewodski Island (RN) samples.

[Abbreviations in column "*" are explained in table 1.Abbreviations are used as symbols on some figures, and sample numbers are used in REE (rare-earth-element) plots. Almost all samples with LOI greater than 10.0 have been removed from the complete data set (Newberry and Brew, 1997, their table 2) to make this selected set; the exceptions are samples that are plotted on the REE diagrams. Leader (-) indicates not analyzed. LOI, loss on ignition to 925°C; Tot, total of anhydrous oxide components; Sum, oxide total + S + CO_2 + H_2O]

Sample no.	*	SiO_2	Al_2O_3	Fe_2O_3	FeO	MgO	CaO	Na_2O	K_2O	TiO_2	P_2O_5	MnO	LOI	Tot	S	H_2O	CO_2	Sum
gc78b	x	85.7	4.12	2.70	0.16	0.60	0.80	0.20	1.00	0.22	0.08	0.02	2.49	95.6	2.76	0.63	1.76	100.8
gc80d	q	57.1	8.74	3.60	4.76	4.90	2.32	0.65	1.64	0.32	0.16	0.17	10.60	84.4	4.7	1.03	10.6	100.7
gc80i	q	60.4	6.41	0.10	9.10	5.40	0.46	0.65	0.74	0.24	0.08	0.19	12.17	83.8	5.68	1.08	9.74	100.3
gc80k	s	37.8	7.73	0.20	13.65	9.40	1.08	1.40	0.18	0.92	0.16	0.44	19.91	73.0	10.2	1.2	16	100.4
gc80m	q	51.7	8.04	0.40	9.33	7.60	0.26	0.95	0.72	0.36	0.14	0.37	15.23	79.9	7.44	1.47	11.4	100.2
gc80pq	s	22.0	11.1	0.22	12.72	11.30	7.50	0.65	1.48	0.90	0.16	0.81	16.39	68.8	10.6	2.2	18.9	100.5
gc81a	r	63.6	12.8	0.60	4.11	2.50	1.24	1.10	2.36	0.50	0.20	0.08	7.05	89.1	4.26	1.79	5.25	100.4
gc82a	c	47.4	14.0	3.20	7.39	10.90	8.08	2.30	0.92	1.22	0.12	0.26	3.14	95.8	0.01	3.64	0.08	99.5
gc82c	q	69.3	10.7	1.30	5.26	5.80	0.22	0.70	1.74	0.44	0.16	0.18	3.55	95.8	0.32	3.68	0.1	99.9
gc83b	q	76.3	5.60	0.80	4.00	4.90	1.50	0.20	0.44	0.28	0.32	0.19	3.50	94.5	1.35	2.6	1.91	100.4
gc83c	s	45.6	13.8	2.80	11.70	11.50	0.76	1.24	0.24	1.40	0.44	0.36	7.32	89.8	3.76	6.45	0.26	100.3
gc84b	g	51.2	13.4	1.50	7.55	9.80	7.40	4.30	0.12	0.86	0.12	0.26	2.47	96.5	0.01	3.35	0.01	99.9
gc84c	m	44.8	19.6	0.86	7.23	13.90	0.46	5.20	0.70	0.10	0.04	0.25	6.24	93.1	0.32	5.91	0.21	99.6
gc85b	c	47.8	17.4	2.40	8.06	8.00	3.30	5.00	0.84	0.94	0.44	0.13	4.00	94.3	0.01	4.36	0.51	99.2
gc89a	h	56.2	14.8	1.90	4.40	3.40	2.54	1.90	3.04	0.82	0.34	0.14	5.50	89.5	2.2	2.9	5.83	100.4
gc90a	h	82.9	6.08	0.25	2.11	2.60	0.48	0.55	1.14	0.22	0.06	1.80	1.65	98.2	0.01	1.7	0.65	100.6
gc93a	x	63.9	8.91	0.06	3.15	0.55	5.24	0.20	2.36	0.39	3.76	0.03	6.25	88.6	5.35	1.25	4.9	100.1
gc94b	m	44.8	20.3	0.26	6.00	13.60	1.88	2.60	1.40	0.24	0.02	0.08	7.67	91.2	0.01	6.96	1.86	100.0
gc95a	r	68.0	14.1	1.50	3.73	2.10	0.44	4.50	1.08	0.60	0.30	0.10	2.49	96.5	0.17	1.78	2.4	100.8
gc101a	g	45.4	21.6	1.02	2.21	8.60	11.5	3.80	0.03	0.08	0.01	0.05	5.46	94.3	0.01	5.18	0.2	99.7
gc102a	g	44.5	21.1	0.50	3.72	10.10	10.3	3.10	0.60	0.10	0.01	0.07	5.68	94.1	0.01	5.51	0.17	99.8
gc103a	g	44.5	19.4	0.70	3.03	9.70	14.9	2.50	0.03	0.14	0.01	0.09	5.12	95.0	0.01	4.71	0.14	99.9
gc121b	s	53.2	11.0	1.55	7.62	16.6	0.56	0.10	0.01	0.56	0.03	0.22	7.35	91.5	-	6.76	0.94	99.2
gc122a	c	48.9	10.1	1.92	6.98	12.9	9.7	0.69	2.86	1.28	0.25	0.19	2.91	95.8	-	3.25	0.84	99.9
gc122b	k	66.3	17.7	0.53	2.07	1.02	1.1	7.57	1.68	0.13	0.03	0.09	1.57	98.2	-	0.89	0.74	99.9
gc122d	k	67	17.9	0.84	1.34	0.54	1.7	7.00	1.81	0.13	0.02	0.06	1.16	98.3	-	0.71	0.6	99.7
gc122e	g	44.4	8.59	1.95	7.02	13.5	16.4	0.43	0.44	1.24	0.06	0.19	4.75	94.2	-	2.84	3.05	100.1
gc122f	c	43.5	10.6	2.08	8.49	10.7	12.9	1.14	1.58	1.49	0.2	0.2	5.98	92.9	-	3.06	3.34	99.3
gc284f	h	69.1	14.0	1.95	2.65	1.43	0.47	2.92	2.41	0.50	0.16	0.06	4.20[1]	99.85	-	-	-	-
gc285b	h	83.6	3.65	1.90	1.33	1.47	3.08	0.22	0.52	0.17	0.03	0.01	4.25[1]	100.2	-	-	-	-
gc286a	g	32.4	12.4	2.20	20.0	8.89	13.10	0.37	0.18	1.92	2.12	0.29	4.41[1]	99.18	-	-	-	-
gc286b	c	45.3	15.3	2.10	8.75	8.41	6.12	0.89	2.54	1.33	0.19	0.20	8.63[1]	99.76	-	-	-	-
gc286c	g	45.8	5.97	2.60	4.81	13.30	19.80	0.53	0.97	0.72	0.16	0.14	5.19[1]	99.99	-	-	-	-
gc286d	c	48.2	14.5	3.40	10.8	7.97	5.52	2.90	0.01	1.99	0.21	0.22	3.91[1]	99.63	-	-	-	-
gc287b	s	47.9	16.1	3.30	8.60	5.74	3.01	2.30	3.06	1.00	0.50	0.52	6.94[1]	98.97	-	-	-	-
gc287c	s	47.9	13.0	6.30	5.14	4.05	3.00	1.63	3.12	0.81	0.42	0.45	9.63[1]	95.45	-	-	-	-
gc288f	q	70.9	7.09	0.10	9.30	1.07	1.19	0.01	2.12	0.29	0.12	0.03	6.22[1]	98.44	-	-	-	-
gc289f	s	49.8	15.5	2.60	7.00	8.21	2.51	1.96	2.00	1.63	0.17	0.47	6.98[1]	98.83	-	-	-	-
gc289j	q	74.3	10.1	0.20	3.20	3.66	0.52	1.23	2.44	0.26	0.06	0.15	2.93[1]	99.05	-	-	-	-
gc290a	s	35.8	16.2	1.00	10.4	16.80	2.15	0.10	0.20	1.45	0.02	0.33	9.16[1]	93.61	-	-	-	-

Table 3. Major-oxide compositions for selected Greens Creek (gc) and Woewodski Island (RN) samples—*Continued.*

Sample no.	*	SiO_2	Al_2O_3	Fe_2O_3	FeO	MgO	CaO	Na_2O	K_2O	TiO_2	P_2O_5	MnO	LOI	Tot	S	H_2O	CO_2	Sum
gc293a	s	47.8	13.1	1.30	12.4	10.40	2.22	0.92	1.03	1.68	0.33	0.46	6.76[1]	98.38	-	-	-	-
gc293b	c	46.6	12.6	2.30	9.64	9.43	4.25	0.73	1.40	1.69	0.17	0.39	9.63[1]	98.83	-	-	-	-
gc294a	s	46.2	14.8	0.60	15.1	9.20	0.37	1.21	1.50	1.28	0.16	0.29	8.54[1]	99.25	-	-	-	-
gc294b	s	45.3	10.8	2.00	8.60	10.20	5.94	1.67	0.35	1.28	0.19	0.67	9.08[1]	96.08	-	-	-	-
gc294c	s	44.1	12.3	2.50	9.30	10.00	5.00	2.16	0.25	1.57	0.19	0.59	8.45[1]	96.41	-	-	-	-
RN116a	g	43.6	13.2	11.6[2]	-	6.1	8.95	2.32	1.83	1.46	0.14	0.22	7.9[1]	-	-	-	-	97.3
RN116d	a	47.6	13.7	14.5[2]	-	2.23	2.64	0.15	2.15	1.91	0.17	0.69	12.9[1]	-	-	-	-	98.6
RN116g	t	45.3	15.7	10.4[2]	-	3.32	5.35	0.15	1.22	1.93	0.17	0.23	15.4[1]	-	-	-	-	99.2
RN118a	g	42.7	15.0	13.7[2]	-	6.85	10.4	1.66	0.57	1.85	0.16	0.21	6.3[1]	-	-	-	-	99.4
RN118b	g	51.1	14.4	9.38[2]	-	7.18	7.54	4.04	0.64	0.49	0.09	0.16	4.8[1]	-	-	-	-	99.8
RN118d	-	33.3	7.33	30.9[2]	-	1.49	1.39	0.1	0.01	0.89	0.06	5.26	19.2[1]	-	-	-	-	99.9
RN119c	t	45.4	16.9	14.8[2]	-	2.33	1.11	0.1	2.61	1.26	0.32	1.13	13.2[1]	-	-	-	-	99.2
RN120a	g	47.4	14.5	11.6[2]	-	7.26	10.3	3.1	0.65	1.36	0.11	0.19	3.8[1]	-	-	-	-	100.3
RN121a	g	44.9	14.3	10.7[2]	-	6.75	11.1	2.85	1.13	1.25	0.11	0.16	4.9[1]	-	-	-	-	98.1
RN123a	t	47.7	14.3	13.2[2]	-	3.0	3.2	0.1	1.39	1.39	0.13	0.46	14.2[1]	-	-	-	-	99.1

1 Total is sum of anhydrous oxide components + LOI.
2 Total iron as Fe_2O_3.

Table 4. *Trace-element concentrations (in parts per million) of selected samples from Greens Creek (gc) and Woewodski Island (RN) by wavelength-dispersive X-ray fluorescence analysis.*

[Abbreviations in column "*" are explained in table 1. Abbreviations are used as symbols on some figures, and sample numbers are used in REE (rare-earth-element) plots. Leader (-) indicates not analyzed]

Sample no.	*	Nb	Rb	Sr	Zr	Y	Ni	Cr	Ba	Ce	La	Cu	Zn
gc78b	x	<10	12	14	34	10	25	48	5000	34	58	10	820
gc80d	q	<10	20	46	92	16	12	11	780	28	10	10	90
gc80i	q	<10	5	24	44	<10	20	14	560	10	10	10	100
gc80k	s	<10	5	74	58	<10	46	91	680	29	10	10	320
gc80m	q	<10	5	60	58	10	28	68	2550	46	30	10	120
gc80pq	s	<10	28	215	76	46	50	129	5000	34	82	68	1500
gc81a	r	14	34	76	122	24	10	12	3450	48	48	10	40
gc82a	c	<10	5	112	68	20	88	355	830	34	24	24	455
gc82c	q	<10	20	5	68	12	15	24	1100	44	10	10	100
gc83b	q	<10	5	36	38	<10	14	29	435	34	10	10	66
gc83c	s	<10	5	16	82	18	46	94	355	30	10	10	196
gc84b	g	14	5	285	82	16	234	610	205	22	10	24	100
gc84c	m	<10	5	5	16	<10	380	345	840	24	24	130	1500
gc85b	c	14	5	325	52	18	63	134	210	54	26	70	98
gc89a	h	16	74	60	140	32	22	28	3350	48	44	82	315
gc90a	h	<10	14	22	48	<10	30	14	1100	40	24	24	66
gc93a	x	14	46	136	62	44	102	355	2850	50	36	26	96
gc94a	m	<10	5	78	10	<10	2500	4150	48	26	22	188	36
gc94b	m	<10	20	36	14	<10	300	920	1850	20	10	48	36
gc95a	r	12	12	16	104	18	12	17	590	42	10	54	90
gc101a	g	<10	5	24	12	<10	240	980	118	64	22	10	10
gc102a	g	<10	5	24	10	<10	260	620	225	30	10	10	32
gc103a	g	<10	5	5	<10	<10	250	1600	68	24	10	10	24
gc121b	s	<10	5	42	60	10	410	750	34	<30	<30	5	690
gc122a	c	10	68	142	50	18	100	830	1900	<30	<30	5	130
gc122b	k	16	56	160	120	12	<10	10	1700	40	<30	34	56
gc122d	k	12	62	790	118	10	<105	10	1400	<30	<30	26	52
gc122e	g	<10	12	560	68	16	130	500	400	<30	<30	88	70
gc122f	c	<10	42	540	66	19	72	330	1600	<30	<30	72	68
gc284b	h	10	14	126	74	26	11	124	-	-	-	-	-
gc284c	s	<10	22	60	78	16	98	114	-	-	-	-	-
gc284d	s	<10	20	86	82	20	72	104	-	-	-	-	-
gc284e	c	12	54	90	104	32	90	142	-	-	-	-	-
gc284f	h	16	42	30	110	26	10	30	-	-	-	-	-
gc285a	m	16	34	166	62	12	600	1650	-	-	-	-	-
gc285b	h	12	16	54	50	16	10	54	-	-	-	-	-
gc285g	m	12	88	70	28	12	405	530	-	-	-	-	-
gc286a	g	<10	5	620	46	10	60	92	-	-	-	-	-
gc286b	c	18	56	72	88	30	92	365	-	-	-	-	-
gc286c	g	16	30	255	34	14	88	250	-	-	-	-	-
gc286d	c	22	5	150	126	48	76	140	-	-	-	-	-
gc286e	p	10	5	12	16	<10	2150	2600	-	-	-	-	-
gc286f	c	20	20	122	98	24	325	980	-	-	-	-	-
gc287a	m	14	38	130	24	10	530	1450	-	-	-	-	-
gc287b	s	10	50	270	92	30	45	132	-	-	-	-	-
gc287c	s	18	54	265	86	28	50	246	-	-	-	-	-
gc288a	s	16	42	26	98	32	50	108	-	-	-	-	-
gc288b	s	16	38	18	40	18	106	330	-	-	-	-	-
gc288c	s	18	34	34	142	34	44	134	-	-	-	-	-
gc288d	s	14	16	230	38	18	150	780	-	-	-	-	-
gc288e	s	20	34	134	58	38	116	650	-	-	-	-	-

the nature of the rock protoliths. The rocks with sedimentary protoliths (stratigraphic hanging-wall argillite, "h;" and stratigraphic footwall graphitic phyllite, "r") plot with argillaceous and carbonate rocks. Some of the rocks of apparent mafic-ultramafic parentage ("g," "c") plot in fields appropriate to basaltic rocks (fig. 5); however, the majority do not. If the

Table 4. Trace-element concentrations (in parts per million) of selected samples from Greens Creek (gc) and Woewodski Island (RN) by wavelength-dispersive X-ray fluorescence analysis—*Continued.*

Sample no.	*	Nb	Rb	Sr	Zr	Y	Ni	Cr	Ba	Ce	La	Cu	Zn
gc288f	q	12	14	42	54	18	11	40	-	-	-	-	-
gc289a	s	14	18	106	66	28	98	194	-	-	-	-	-
gc289b	s	14	28	186	82	22	50	66	-	-	-	-	-
gc289c	s	16	16	128	96	66	38	150	-	-	-	-	-
gc289d	r	18	40	86	76	30	26	18	-	-	-	-	-
gc289e	s	15	48	132	52	42	164	850	-	-	-	-	-
gc289f	s	20	34	46	104	32	54	205	-	-	-	-	-
gc289g	x	10	5	190	44	34	146	340	-	-	-	-	-
gc289h	s	18	18	148	100	32	56	205	-	-	-	-	-
gc289i	x	14	18	160	58	32	46	176	-	-	-	-	-
gc289j	q	<10	62	24	100	<10	10	24	-	-	-	-	-
gc290a	s	28	135	102	280	30	126	176	-	-	-	-	-
gc291a	p	<10	5	40	12	<10	2100	1350	-	-	-	-	-
gc293a	s	18	24	38	82	50	50	62	-	-	-	-	-
gc293b	c	14	24	74	108	32	58	158	-	-	-	-	-
gc293d	s	12	40	24	80	32	32	64	-	-	-	-	-
gc294a	s	18	24	20	84	38	64	320	-	-	-	-	-
gc294b	s	14	5	92	90	34	38	98	-	-	-	-	-
gc294c	s	20	5	96	106	42	46	146	-	-	-	-	-
gc294d	s	21	5	20	86	26	240	630	-	-	-	-	-
RN116a	g	14	32	144	94	26	-	-	-	-	-	-	-
RN116d	a	12	46	44	124	33	-	-	-	-	-	-	-
RN116g	t	17	24	73	114	28	-	-	-	-	-	-	-
RN118a	g	12	12	225	114	28	-	-	-	-	-	-	-
RN118b	g	8	15	184	52	18	-	-	-	-	-	-	-
RN118d	-	12	8	15	53	18	-	-	-	-	-	-	-
RN119c	t	13	44	57	88	24	-	-	-	-	-	-	-
RN120a	g	12	20	270	87	27	-	-	-	-	-	-	-
RN121a	g	10	23	180	74	20	-	-	-	-	-	-	-
RN123a	t	14	24	44	88	25	-	-	-	-	-	-	-

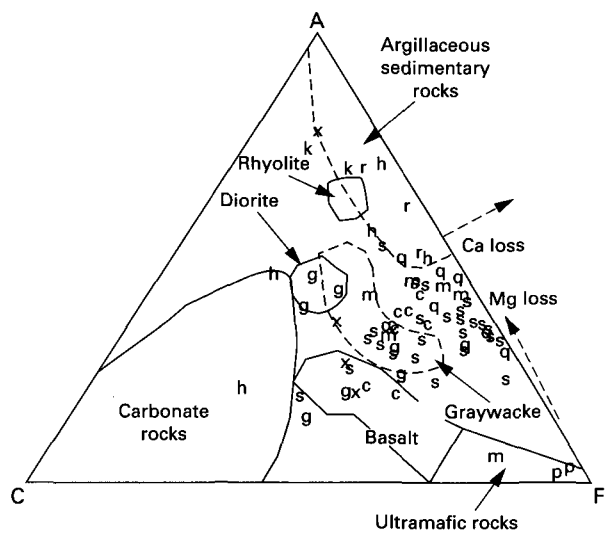

Figure 5. Major-element compositions of rocks from the Greens Creek deposit and vicinity rocks on the ACF diagram (alkalies $Na_2O + K_2O$ (A), calcium oxide CaO (C), and magnesium oxide MgO (F); after Winkler, 1979), showing compositional relationships among rock types. Sample/rock type symbols are as follows: Hanging-wall rocks: h, hanging-wall argillite; Footwall rocks: r, graphitic phyllite; q, pyritic muscovite quartz phyllite; c, chloritic phyllite and greenstones; s, muscovite phyllite; m, mariposite rock; x, siliceous breccia; g, gabbro; p, serpentine. Other: k, felsic sill. Note that stratigraphic hanging-wall rocks fall in well-defined fields of sedimentary rocks, whereas stratigraphic footwall rocks do not. Field boundaries from Winkler (1979).

phyllites were originally unaltered sedimentary rocks, then they would have most likely been graywackes. However, less than a third of the analyses plot in the field of typical graywackes (fig. 5). One possible explanation is that the phyllites were derived from mafic rocks (including possibly mafic tuffs) that experienced various degrees of Na_2O (fig. 4), and especially CaO, loss during hydrothermal alteration.

Trace-element compositions most clearly suggest the mafic-ultramafic parentage for most of the Greens Creek stratigraphic footwall phyllites ("s," "c"). Notably, all these stratigraphic footwall rocks, (except the stratigraphic footwall graphitic ("r") and siliceous-pyritic ("q") phyllites) contain higher concentrations of Cr and Ni than do the rocks of sedimentary parentage (fig. 6). We interpret the low abundance of Cr and Ni in the graphitic phyllites ("r") and in the local siliceous-pyritic phyllite ("q") unit as due to sedimentary parentage and extreme degree of hydrothermal leaching, respectively. Mariposite-bearing phyllites ("m"), serpentinites ("p"), and gabbroic-appearing ("g") rocks show concentrations appropriate to ultramafic rocks; chloritic phyllites and greenstones

Table 5. Trace-element concentrations (in parts per million) for Greens Creek samples by neutron activation analysis.

[Abbreviations in column "*" are explained in table 1. Abbreviations are used as symbols on some figures, and sample numbers are used in REE (rare-earth-element) plots]

Sample no.	*	Ba	Sr	Co	Ni	Cr	Cs	Hf	Rb	Sb	Ta	Th	U
gc78b	x	4570	43.1	7.37	27.9	48.6	0.93	0.84	26.2	15.2	0.158	1.03	0.97
gc80d	q	707	35	12.8	12.8	11.7	1.2	2.39	31.7	1.31	0.157	2.06	1.35
gc80i	q	515	49	18.5	23.7	15.6	0.78	1.09	15.4	1.8	0.126	1.14	0.58
gc80k	s	561	95.9	24.2	53.1	90.9	0.59	1.39	4.7	6.94	0.204	0.44	0.7
gc80m	q	2400	67.6	12.8	44.8	110	1.08	1.49	14.2	1.6	0.258	2.05	0.79
gc80pq	s	8760	171	21.4	63.1	111	1.9	1.66	33.5	7.34	0.272	1.13	1.13
gc81a	r	3530	68.4	10.2	6.42	14.5	2.18	3.36	44.5	2.01	0.239	2.69	1.63
gc82a	c	704	213	34	75.3	276	0.29	1.83	16.8	1.08	0.257	0.24	0.09
gc82c	q	1060	6	13.1	25.2	25.9	0.69	1.9	35.5	0.69	0.268	2.37	0.87
gc83b	q	404	59.2	9.91	26.7	29.1	0.27	0.97	9.08	0.56	0.146	1.32	1.76
gc83c	s	295	7	34.5	40.7	94.1	0.18	2.35	7.29	1.22	0.338	0.85	0.74
gc84b	g	155	346	38.6	241	550	0.07	2.04	6.57	2.89	0.417	1.04	0.43
gc84c	m	794	3	37.8	379	272	0.45	0.22	15.2	1.16	0.072	0.21	0.08
gc85b	c	176	330	24	61.5	109	0.26	3.21	14.5	0.49	0.727	3.41	1.48
gc89a	h	3230	75	8.1	23.5	57.5	4.41	3.14	79.8	1.3	0.613	4.33	4.29
gc90a	h	1020	22	12.4	37	14.5	1.21	1.39	24.4	0.62	0.255	1.96	0.77
gc93a	x	2490	169	15.9	134	235	3.72	1.62	49.8	21.6	0.307	2.49	4.73
gc94a	m	5.9	5	145	3550	2790	0.08	0.06	1.92	1.36	0.01	0.44	0.09
gc9gc4b	m	1910	57	41	306	796	2.4	0.24	34.8	0.52	0.009	0.11	0.16
gc95a	r	492	10	14	14.4	16.5	1.18	3.04	19.7	0.48	0.369	2.69	1.21
gc101a	g	58	8	25.4	186	1010	0.05	0.07	1.3	0.82	0.004	0.02	0.04
gc102a	g	165	24	36.7	252	767	0.24	0.13	12	0.37	0.014	0.04	0.12
103a	g	35.2	4	29.9	229	1760	0.1	0.18	2.02	1.29	0.005	0.05	0.02

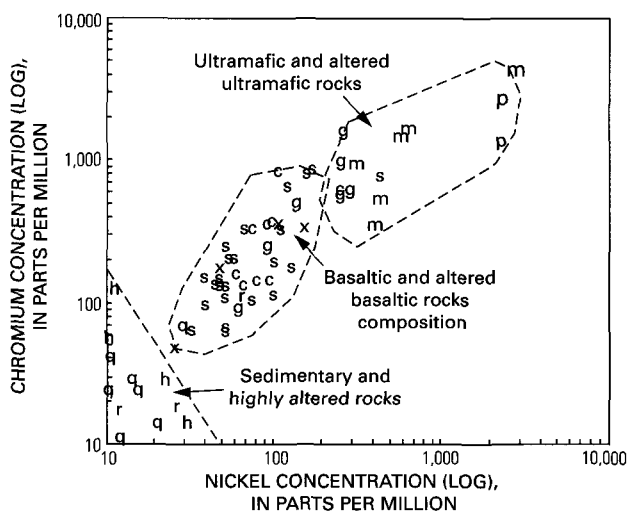

Figure 6. Ni versus Cr for rocks of the Greens Creek deposit and vicinity. Analyses by wavelength-dispersive X-ray fluorescence method. Sample/rock type symbols plotted are as follows: Hanging-wall rocks: h, hanging-wall calcareous argillite; footwall rocks: r, graphitic phyllite; q, quartzitic phyllite; c, chloritic phyllite/greenstone; s, muscovite chlorite phyllite; m, mariposite rock; x, siliceous breccia; g, gabbro; p, serpentine. Other: k, felsic sill. Field boundaries are based on data in BVSP (1981).

("c"), and muscovite phyllites ("s," i.e., non-graphitic stratigraphic footwall rocks) have Cr-Ni ratios appropriate to basaltic rocks (fig. 6). The positive correlation of Ni and Cr concentrations for the bulk of stratigraphic footwall rocks contrasts sharply with the lack of a correlation between Ni and Cr in the metasedimentary rocks; we interpret both the absolute concentrations and element correlations to indicate that the bulk of footwall rocks were mafic volcanic rocks and not sediments derived from such rocks.

Because standard igenous rock chemical classification schemes are based on the mobile elements Na_2O, K_2O, and CaO, and because these elements are tremendously mobile in VMS environments (Date and others, 1983), chemical classification is more reliably based on "immobile" elements (Winchester and Floyd, 1977). These elements, which include Ti, Zr, Y, Nb, and the rare earth elements, are much less susceptible to chemical transport during hydrothermal alteration than most major elements. Furthermore, we consider elemental ratios more reliable than elemental concentrations in most cases, because immobile-element ratios remain constant despite loss of mobile components or addition of new components (e.g., water, carbonate, sulfide). A SiO_2 vs. Zr/ TiO_2 diagram (fig. 7*A*) shows that, with the exception of graphitic ("r") and siliceous ("q") phyllites, all the stratigraphic footwall rocks at Greens Creek have compositions consistent with basalt and andesite. The bulk of the footwall phyllites plot in a field defined as subalkalic basalt (fig. 7*A*).

Concentration of SiO_2 is used in most igneous-rock classification schemes, but silica is clearly a mobile constituent in VMS deposits (Date and others, 1983) and at Greens Creek in particular. Abundant quartz veining in stratigraphic footwall rocks indicates that silica concentrations, which are in the range for andesite to rhyolite (fig. 7*A*) may be of secondary origin.

Table 5. Trace-element concentrations (in parts per million) for Greens Creek samples by neutron activation analysis—*Continued.*

Sample no.	Zn	Zr	Sc	La	Ce	Nd	Sm	Eu	Gd	Tb	Tm	Yb	Lu
gc78b	782	24.3	8.01	7.21	14.8	8.65	1.95	0.73	1.77	0.26	0.17	1.08	0.15
gc80d	89.3	85.2	11.6	9.44	21.1	12	2.98	0.62	3.17	0.52	0.35	2.25	0.35
gc80i	88.8	36.2	9.77	1.63	3.52	2.27	0.72	0.13	0.92	0.17	0.16	1.02	0.16
gc80k	303	43	21.9	1.93	5.8	4	0.99	0.16	0.9	0.12	0.11	0.67	0.14
gc80m	104	66	11.9	13	27.5	14.8	2.67	0.37	2.18	0.3	0.21	1.39	0.22
gc80pq	2260	92.4	26.7	8.22	17.4	9.79	2.83	0.79	3.63	0.63	0.41	2.63	0.38
gc81a	39.1	136	14.6	13.6	30.3	17	4.19	0.85	4.7	0.72	0.48	3.03	0.46
gc82a	303	100	40	6.18	14.6	9.42	3.22	1.19	4.32	0.77	0.48	3.04	0.43
gc82c	83.6	82.3	13.9	9.4	23.3	11.8	2.98	0.5	3.18	0.49	0.32	2.03	0.31
gc83b	105	50.4	8.7	7.78	16.4	9.56	2.23	0.37	2.26	0.34	0.2	1.3	0.2
gc83c	180	121	33.9	7.11	17.2	11.7	3.56	0.69	4.38	0.73	0.43	2.74	0.39
gc84b	107	77.6	35.3	7.38	18.2	12.2	3.38	1.05	3.72	0.58	0.3	1.73	0.26
gc84c	7350	17	6.92	1.51	3.44	1.81	0.47	0.21	0.49	0.07	0.05	0.23	0.04
gc85b	71.7	125	26.4	19.4	44.2	20.8	4.46	1.2	3.87	0.61	0.37	2.34	0.36
gc89a	253	132	21.9	19.5	39.8	22.1	4.86	1.23	4.92	0.8	0.46	2.93	0.42
gc90a	51.8	56.3	7.89	11.1	19.5	12.3	2.7	0.55	2.64	0.36	0.23	1.5	0.25
gc93a	112	64.7	16.2	15.3	26.8	17.5	4.36	1.53	5.12	0.88	0.61	3.95	0.59
gc94a	21.2	5.5	7.96	0.15	0.48	0.28	0.09	0.03	0.12	0.02	0.02	0.14	0.02
gc9gc4b	45.2	8.3	42.1	0.74	1.4	0.96	0.35	0.1	0.52	0.1	0.07	0.43	0.07
gc95a	71.8	122	13.2	9.93	22.3	12.7	3	0.79	3.19	0.56	0.4	2.71	0.41
gc101a	14	8.6	17.7	0.29	0.76	0.61	0.21	0.18	0.29	0.06	0.03	0.19	0.03
gc102a	31.4	4.8	12.5	0.58	1.4	0.98	0.32	0.23	0.41	0.07	0.04	0.26	0.04
103a	87.2	7	25	0.5	1.71	1.33	0.45	0.28	0.6	0.1	0.06	0.43	0.06

Table 6. Pb isotopic data for galenas from Triassic and Cretaceous VMS prospects of southeastern Alaska.

[Lat, latitude; Long, longitude]

Name	Host age	Location		$^{206}Pb/^{204}Pb$	$^{207}Pb/^{204}Pb$	$^{208}Pb/^{204}Pb$
		Lat (N.)	Long (W.)			
Greens Creek	Triassic	58°4′	134°37′	18.635	15.5828	38.239
Woewodski	Triassic	56°34′	133°3′	18.672	15.559	37.954
Fremming	Cretaceous	58°52′	135°5′	18.404	15.466	37.708
Alaska Treasure	Cretaceous	58°15′	134°43′	18.425	15.497	37.924
Alaska Treasure	Cretaceous	58°15′	134°43′	18.412	15.475	37.692

Classification based entirely on immobile element ratios (fig. 7*B*) indicates that, by such a scheme, none of the stratigraphic footwall rocks have protoliths more felsic than andesite or trachyandesite. Unfortunately, several of the samples of footwall phyllite ("r," "q," "c," "s") contained Y or Nb below lower detection limits (table 4), so they could not be plotted. However, all these same samples contained Zr/ TiO_2 ratios below 0.03 (fig. 7*A*), indicating a possible dacite or rhyodacite, but not rhyolite, parentage. Because most of the samples have immobile element ratios compatible with basalt, it suggests that their protoliths were basaltic (e.g., the rocks we have continued to call by their field names "graphitic phyllite" ("r") and even stratigraphic hanging-wall "black argillite" (h)). This is clearly a difficult interpretation and one that has bothered us throughout this study. Either these rocks had unusual sedimentary parents or they have been chemically and mechanically modified to the point that their original protoliths are undecipherable. The quartzose phyllites ("q") are equally problematic—they have experienced such intense hydrothermal alteration that it is unclear whether they represent silicified mafic rocks or silicified sediments—but, in any case, they definitely lack the immobile-trace-element characteristics of felsic volcanic rocks (fig. 7).

Immobile trace elements are also employed in characterization of the tectonic environment of basaltic rocks. The Zr-Ti-Y diagram (fig. 8) of Pearce and Cann (1973) yields ambiguous results with these rocks: the least altered mafic rocks (greenstone and chloritic phyllite) plot in a field ("B") compatible with calc-alkalic arc, tholeiitic arc, or mid-ocean-ridge basalt (MORB). Notably, the majority of the least altered rocks plot outside of the field of "within plate" (extensional setting) basalt. A non-extensional setting is also compatible with the absence of felsic volcanic rocks in the stratigraphic sequence. Compositionally bimodal felsic plus mafic suites are characteristic of extensional settings, as in the Ambler VMS district of the central

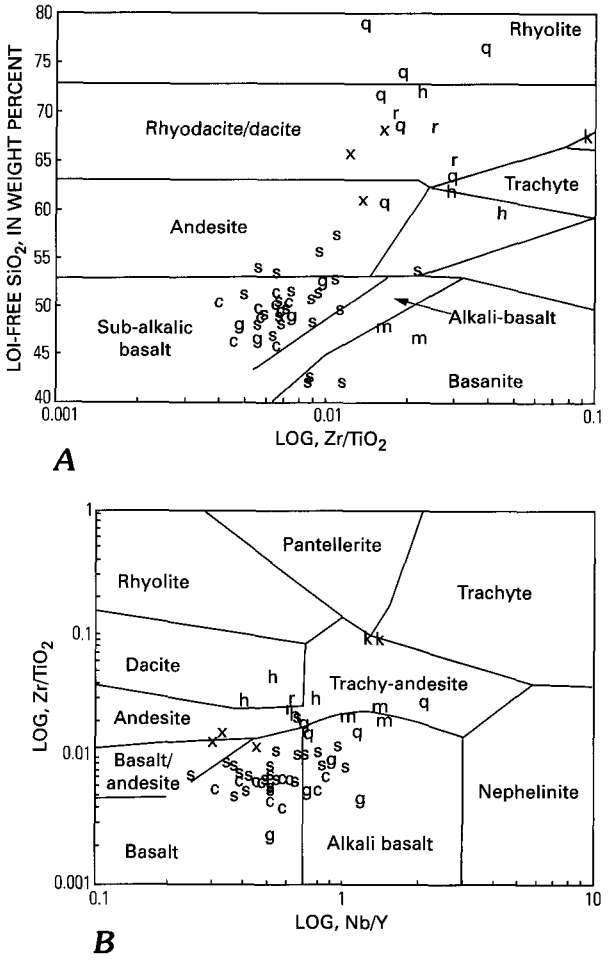

Figure 7. Trace-element characteristics of rocks from the Greens Creek deposit and vicinity. Analyses by wavelength-dispersive X-ray fluorescence method. Sample/rock type symbols plotted are as follows: Hanging-wall rocks: h, hanging-wall argillite; Footwall rocks: r, graphitic phyllite; q, quartzitic phyllite; c, chloritic phyllite/greenstone; s, muscovite-chlorite phyllite; m, mariposite rock; x, siliceous breccia; g, gabbro. Other: k, felsic sill. *A*, SiO_2 plotted (calculated on an LOI-free basis) vs. Zr/TiO_2 diagram of Winchester and Floyd (1977). *B*, Zr/TiO_2 plotted vs. Nb/Y on the diagram of Winchester and Floyd (1977).

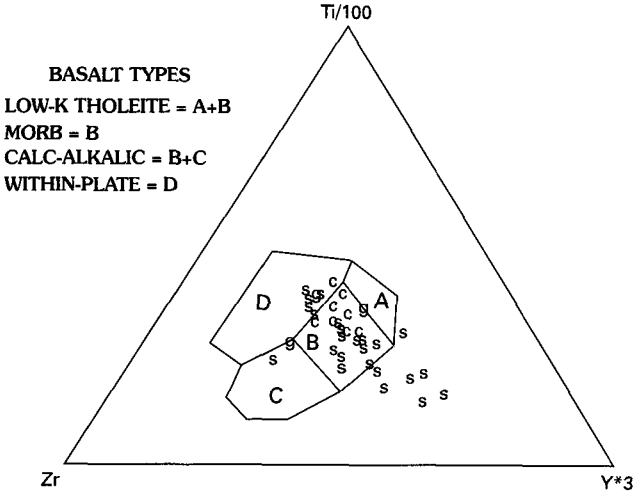

Figure 8. Basalt tectonic environment diagram of Pearce and Cann (1973) with data from those Greens Creek samples that exhibit Ni-Cr compositional evidence (fig. 6) for a basaltic protolith. Sample/rock type symbols plotted are as follows: Footwall rocks: c, chloritic phyllite/greenstone; s, muscovite chlorite phyllite; m, mariposite rock; g, gabbro. MORB, mid-ocean-ridge basalt. Increased scatter of muscovite-chlorite phyllite data is most likely due to slight trace element mobility during hydrothermal alteration.

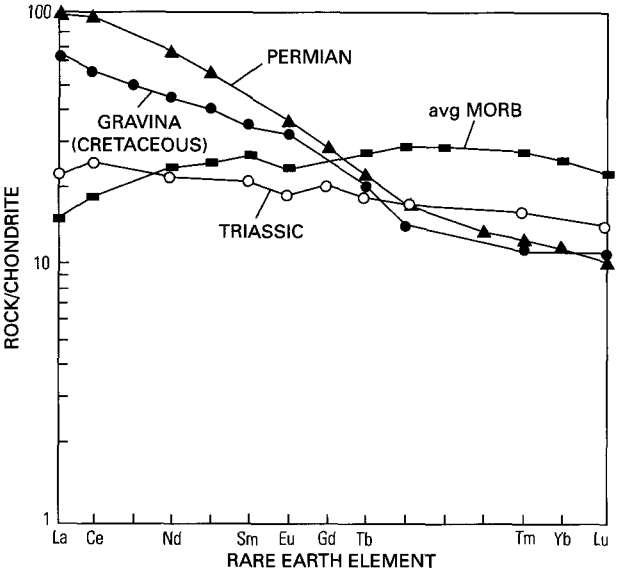

Figure 9. Chondrite-normalized average REE plots for basaltic rocks of northern southeastern Alaska compared to typical mid-ocean-ridge basalt (MORB). Data for Alaskan rocks from Davis and Plafker (1980), MacIntyre (1986), McClelland and others (1991), and Gehrels and Barker (1993). Average MORB from BVSP (1981).

Brooks Range and the Bonnifield VMS district of the central Alaska Range (Gilbert and Bundtzen, 1979; Schmidt, 1988; Newberry and others, 1997). Sericitic phyllites ("s") have compositions that plot in and around the least altered mafic rocks ("c"), which lie in the MORB field (fig. 8) . Such an association is consistent with a greater degree of hydrothermal alteration of the sericitic phyllites (e.g., fig. 4) and the fact that even the most immobile elements exhibit some mobility during extreme hydrothermal alteration (Winchester and Floyd, 1977).

Rare earth element (REE) concentrations are also employed to assess basalt tectonic environments. Existing REE data (Davis and Plafker, 1980; MacIntyre, 1986; McClelland and others, 1991; Gehrels and Barker, 1993) for well-characterized mafic metavolcanic rocks of northern southeastern Alaska show that units of different ages have contrasting patterns (fig. 9). In particular, the known Triassic basalts are different from MORB in that they lack light-REE depletion (fig. 9) but are different from older and younger basalts in generally lacking light-REE enrichment. Within-plate (extensional) basalts invariably display light-REE enrichment, and arc-related basalts commonly exhibit relatively flat patterns (Henderson, 1984), like those exhibited by the Triassic basalts of southeastern Alaska. A.B. Ford and D.A. Brew (written commun., 1998) suggest that most of the compositional features of the Triassic basalts, including REE concentrations, are like those of flood basalts.

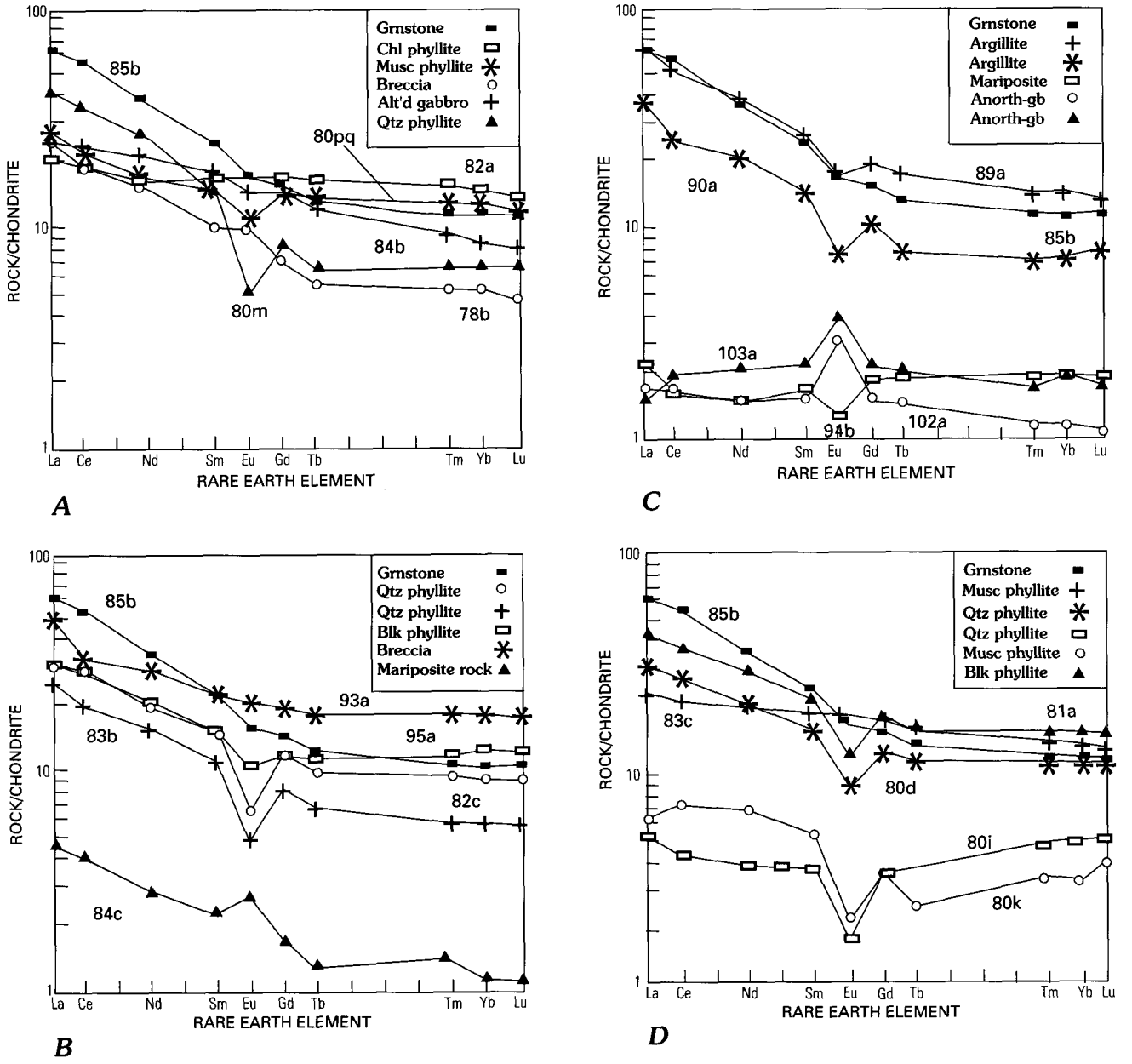

Figure 10. *A, B, C,* and *D.* Chondrite-normalized REE plots for rocks from the Greens Creek deposit and vicinity. Numbers (93a, for example) are abbreviated from the complete sample numbers shown in table 5. Line abbreviations: grnstone, greenstone; chl phyllite, chlorite phyllite; musc phyllite. muscovite phyllite; alt'd gabbro, altered gabbro; qtz phyllite, quartz phyllite; blk phyllite, black phyllite; anorth-gb, anorthitic gabbro. Sample 85b is plotted on all four diagrams as a reference line.

The pattern of REE concentration data in rocks from the Greens-Creek-area rocks most closely resembles that of typical southeastern Alaska Triassic basalts (fig. 10), even though the range of concentrations differs. Most of the rocks identified by other trace and major elements as having mafic protoliths ("c"), such as sample 85b, exhibit relatively flat to slightly light REE-enriched patterns (fig. 10*A*). Rocks identified as having gabbroic parentage ("g") and mariposite-rich phyllites ("m", altered ultramafic rocks?) also exhibit flat patterns but with low REE abundances or positive Eu anomalies (figs. 10*B*, 10*C*) that are characteristic of mafic-ultramafic cumulate rocks (Henderson, 1984). The two breccia samples analyzed for REE's exhibit flat patterns similar to Triassic basalt (figs. 10*A*, 10*B*), suggesting that these two samples are also of basaltic parentage. Finally, all the other rocks analyzed—including graphitic (sedimentary protolith) rocks from both hanging wall and footwall—have patterns almost identical to the mafic or ultramafic protolith rocks, except that they display distinctly low relative Eu concentrations (fig. 10). In igneous rocks, Eu is present largely in feldspar, whereas the other (smaller) REE's are present largely in minor minerals (e.g., apatite). Feldspars are destroyed—and their Eu released—during both extreme hydrothermal alteration and normal weathering. Consequently, an interpretation of the REE patterns compatible with other trace- and major-element data is that the rocks surrounding the Greens Creek deposit have mafic/ultramafic protoliths. Further, the graphitic rocks are metasedimentary rocks derived from weathering of mafic

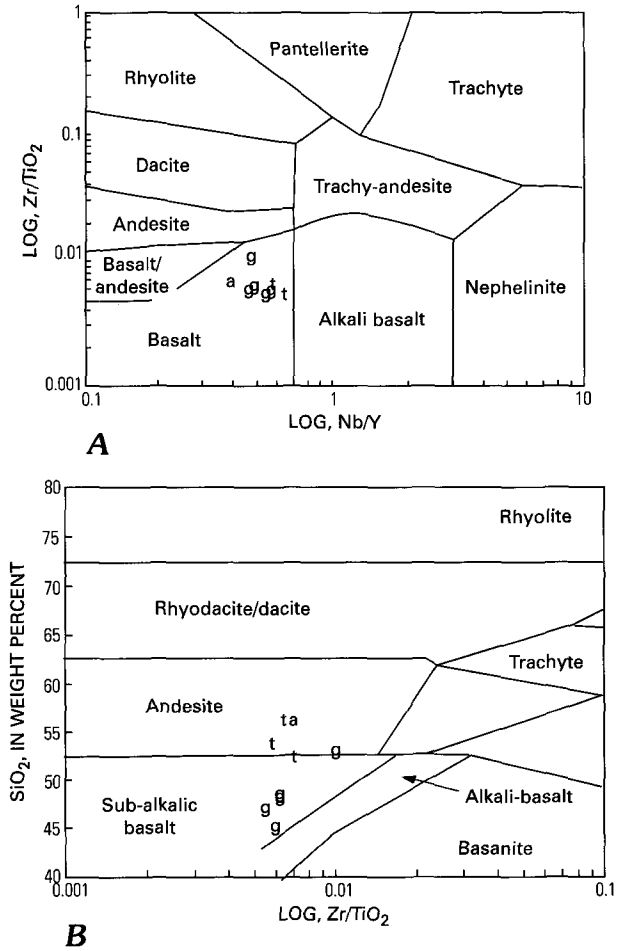

Figure 11. *Classification of metavolcanic rocks on Woewodski* Island using discrimination diagrams of Winchester and Floyd (1977). Symbols are as follows: g, greenstone; a, argillite; t, tuffaceous greenschist. SiO_2 is plotted on a LOI-free basis. *A*, Classification based on immobile-element ratios; *B*, Classification based on silica and Zr/TiO_2.

rocks, and silica-pyrite-rich rocks are extremely altered mafic or sedimentary rocks. Most notably, all the rocks sampled lack the heavy REE enrichment characteristic of felsic igneous rocks.

Woewodski Island Metavolcanic Rocks—Character and Contrast with other Triassic Rocks, Including Those of the Greens Creek Deposit

Metavolcanic rocks sampled from the vicinity of VMS prospects on Woewodski island were identified in the field as massive greenstone/diabase and as andesitic(?) tuff (table 2). Major-element compositions (Newberry and Brew, 1997, their fig. 15) are compatible with basaltic protoliths for the greenstones and indicate that the tuffaceous rocks are either not andesitic or are hydrothermally altered (table 3). In particular, the tuffaceous rocks exhibit very high LOI's (Newberry and Brew, 1997, their fig. 15a) and very low Na_2O (Newberry and Brew, 1997, their fig. 15c). These rocks therefore may be very altered; nevertheless, the SiO_2 and MgO contents are compatible with andesitic protoliths, but the TiO_2 contents are more typical of basaltic rocks (Newberry and Brew, 1997; their fig. 15).

Despite significant major-element compositional differences, immobile element ratios (fig. 11*A*) for the massive and tuffaceous rocks are essentially identical and indicate basaltic protoliths. Classification based on silica and Zr/TiO_2 suggests that the tuffaceous rocks are andesitic (fig. 11*B*). These apparently contradictory classifications can be reconciled if the tuffaceous rocks are recognized as strongly altered basaltic tuffs, with addition of silica, losses in MgO and Na_2O, and large LOI.

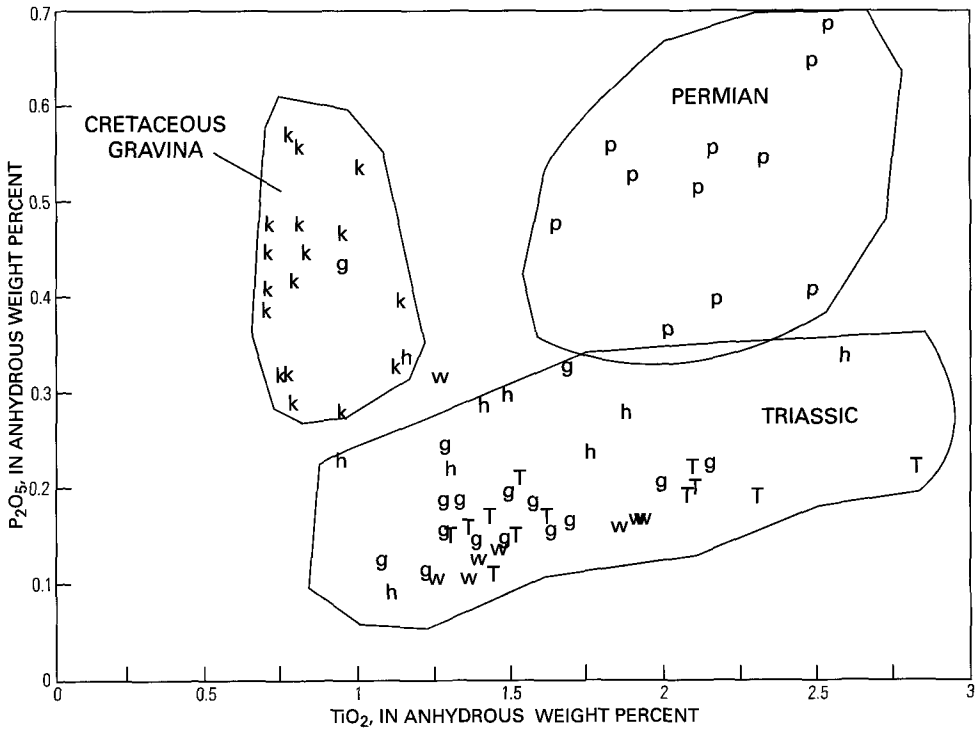

Figure 12. *Anhydrous weight percent* P_2O_5 plotted vs. TiO_2 for metavolcanic rocks of northern southeastern Alaska, showing discrete compositional ranges for rocks of different ages. Symbols are as follows: T, Wrangellia Triassic; W, Woewodski Island; G, Greens Creek; H, Mt. Henry Clay; P, Permian; K, Gravina belt. Metavolcanic rocks from Woewodski Island (W) clearly fall in the range defined by Triassic basalts. Modified from Newberry and others (1995) with data from Ford and Brew (1993) and from this study.

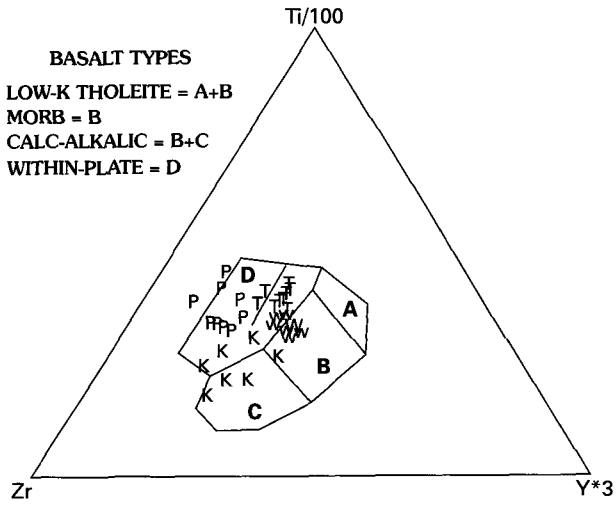

Figure 13. Basalt tectonic environment diagram of Pearce and Cann (1973) compared to data from Woewodski Island metavolcanic rocks and other metavolcanic rocks of northern southeastern Alaska. Symbols are as follows: T, Wrangellia Triassic; W, Woewodski Island; P, Permian; K, Gravina belt. Data from Davis and Plafker (1980), McClelland and others (1991), Gehrels and Barker (1993), and from this study.

Concentrations of the relatively immobile oxides P_2O_5 and TiO_2 suggest that the Woewodski Island metavolcanic rocks are basaltic and similar to those of known rocks of Triassic age (fig. 12). Newberry and others (1995) showed that metavolcanic rocks in northern southeastern Alaska could be distinguished based on concentrations of these elements. Although Woewodski Island lies near the contact between Alexander terrane and the Gravina belt (fig. 1), and although the Woewodski metavolcanic rocks are not as deformed or altered as those at Greens Creek, we confidently group them together on the basis of their chemistry, general lithologic similarity, and age.

Trace-element data also suggest similarities between the rocks of the Greens Creek area and those on Woewodski Island (fig. 13). Permian metabasalts and volcanic rocks of the dominantly Cretaceous Gravina belt plot as "within-plate" and calc-alkalic, respectively, whereas those of Woewodski Island plot in field "B," as do the least altered metabasaltic rocks from Greens Creek (fig. 8). However, other Triassic basalts from the Juneau-Haines area (Ford and Brew, 1993) contain relatively lower Y concentrations and do not plot with Woewodski Island data. It is unclear whether this apparent difference is statistically or geologically significant. The Juneau-Haines-area basalts are from what is clearly Wrangellia terrane (Ford and Brew, 1993) that has oceanic or transitional

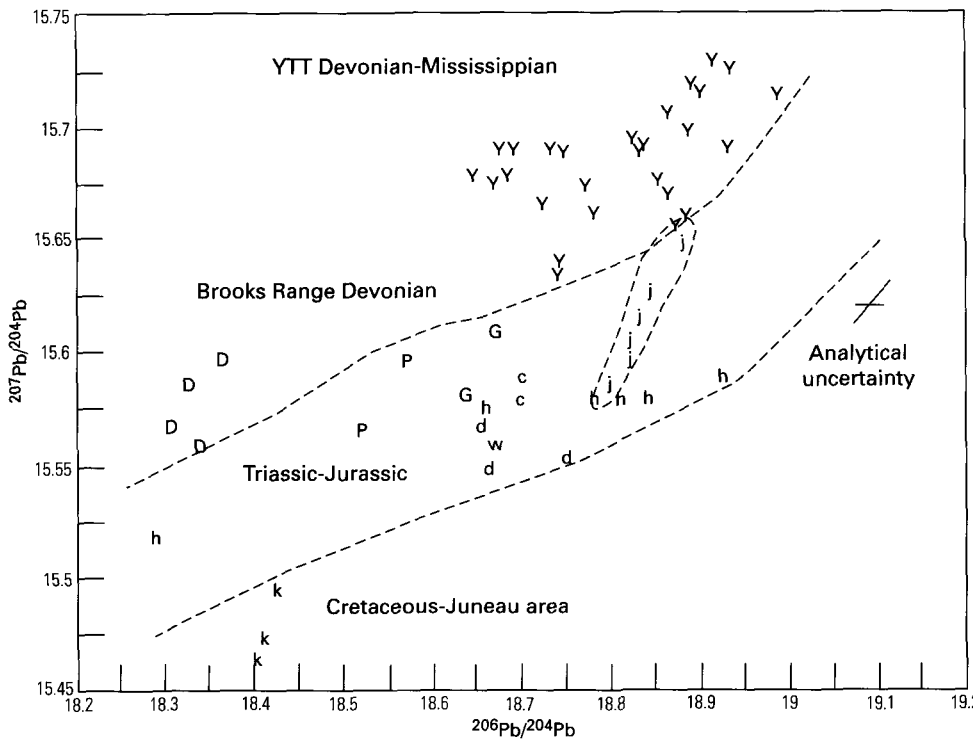

Figure 14. Common Pb isotopic data for galena from selected VMS deposits and prospects of Alaska and adjacent parts of Canada. Dashed-line age boundaries and dotted-line Eskay Creek sample group limit from Newberry and others (1997). Symbols are as follows: Y, Yukon-Tanana terrane (YTT); D, Brooks Range; H, Mt. Henry Clay; P, Pyrola; G, Greens Creek; C, Windy-Craggy; D, Duncan Canal; W, Woewodski Island; J, Eskay Creek; K, Juneau area. Data from Godwin and others (1988), Gaccetta and Church (1989), S.A. Church (written commun., 1996), Childe (1997), and from this study.

crust as substrate to the Triassic basalts, whereas the volcanic rocks on Woewodski and at Greens Creek are from what Ford and Brew (1993) have tentatively interpreted to be Wrangellia-terrane-equivalent rocks that were erupted through a significant thickness of Alexander terrane crust.

Age of VMS Deposits in the Greens Creek–Zarembo Island Belt

Berg and Grybeck (1980) and Berg (1981) inferred that the VMS occurrences on Woewodski and Zarembo Islands were Late Triassic, based on Late Triassic fossils associated with VMS prospects nearby on Kupreanof Island. However, given the absence of local radiometric or fossil evidence and the presence of VMS prospects of other ages in southeastern Alaska (fig.1), this inference remains untested.

Our compositional data for metavolcanic rocks of Woewodski Island show them to be indistinguishable from Triassic basaltic rocks of the Greens Creek mine area. In addition, Pb isotopic data (table 6; fig. 14) for galenas from VMS ores indicates that the Woewodski Island VMS is most likely of Greens Creek age. Newberry and others (1997) have shown that Alaskan VMS deposits exhibit common Pb isotopic ratios that vary with age of the deposit. Our data (table 6) indicate that Woewodski Island and Greens Creek possess nearly identical common Pb isotopic ratios, both of which fall into the range of data for Triassic-Jurassic deposits of southeastern Alaska and nearby Canada. Additionally, prospects in Cretaceous Gravina group rocks of the Juneau area exhibit common Pb isotopic ratios that are significantly different from those of the Triassic-Jurassic deposits. Thus, it is almost certain that the VMS prospects on Woewodski Island and elsewhere in the Duncan Canal area are of the same age and origin as the Greens Creek deposit.

Conclusions

Major- and trace-element data for rocks at Greens Creek and on Woewodski Island indicate the stratigraphic footwall rocks have primarily basaltic and altered basaltic protoliths. There is no evidence for significant associated felsic volcanism at either area. Immobile-trace-element and rare-earth-element data suggest that the basaltic rocks are of immature arc affinity and do not represent an extensional environment. At Greens Creek, most of the phyllitic rocks that were stratigraphically beneath the ore are not of sedimentary parentage, and the geologic environment was not likely to have been a spreading center. Major- and minor-element and Pb isotopic similarities between rocks at Woewodski Island and at Greens Creek confirm previous suggestions that they are part of the same geologic/metallogenic belt.

References Cited

Arbogast, B.F., ed., 1996, Analytical methods manual for the Mineral Resources Program—U.S. Geological Survey: U.S. Geological Survey Open-File Report 96-525, 248 p.

Berg, H.C., 1981, Upper Triassic volcanogenic massive-sulfide metallogenic province identified in southeastern Alaska, *in* Albert, N.R.D., and Hudson, T., eds., The United States Geological Survey in Alaska: Accomplishments During 1979: U.S. Geological Survey Circular 823-B, p. B104 - B108.

Berg, H.C., and Grybeck, D., 1980, Upper Triassic volcanogenic Zn-Pb-Ag(-Cu-Au)-barite mineral deposits near Petersburg, Alaska: U.S. Geological Survey Open-File Report 80-527, 11 p.

Berg, H.C., Jones, D.L., and Coney, P.J., 1978, Pre-Cenozoic tectonostratigraphic terranes of southeastern Alaska and adjacent areas: U.S. Geological Survey Open-File Report 78-1085, scale 1:1,000,000, 2 sheets.

Brew, D.A., 1996, Geologic map of the Craig, Dixon Entrance, and parts of the Ketchikan and Prince Rupert quadrangles, southeastern Alaska: U.S. Geological Survey Miscellaneous Field Investigations Series Map MF-2319, 2 sheets, scale: 1:250,000, 53 p. pamphlet.

Brew, D.A., 1997a, Reconnaissance geologic map of the Petersburg C-3 quadrangle, southeastern Alaska: U.S. Geological Survey Open-File Report 97-156-I, scale 1:63,360, one sheet, 18 p. pamphlet.

Brew, D.A., 1997b, Reconnaissance geologic map of the Petersburg C-4 quadrangle, southeastern Alaska: U.S. Geological Survey Open-File Report 97-156-J, scale 1:63,360, one sheet, 21 p. pamphlet.

Brew, D.A., and Ford, A.B., 1994, The Coast Mountains plutonic-metamorphic complex between Skagway, Alaska, and Fraser, British Columbia—Geologic sketch and road log: U.S. Geological Survey Open-File Report 94-268, 25 p.

BVSP [Basaltic Volcanism Study Project], 1981, Basaltic volcanism on the terrestrial planets: New York, Pergamon Press, 1286 p.

Cameron, A.E., Smith, D.H., and Walker, R.L., 1969, Mass spectrometric analysis of nanogram quantities of lead: Analytical Chemistry, v. 41, p. 525-526.

Childe, F.C., 1997, Timing and tectonic setting of volcanogenic massive sulfide deposits in British Columbia: Constraints from U-Pb geochronology, radiogenic isotopes, and geochemistry: Vancouver, University of British Columbia, unpub. Ph.D. thesis, 270 p.

Crafford, T.C., 1989, The Greens Creek Ag-Au-Pb-Zn massive sulfide deposit, Admiralty Island, southeast Alaska [abs.]: Juneau, Alaska Miners Association Conference, April, 1989, p. 27-29.

Date, J., and Watanabe, Y., 1979, Alteration around Fukazawa Kuroko deposits, Akita Prefecture, with special reference to zonal distribution of alteration in hanging-wall rocks: Mining Geology, v. 29, p. 351-361. [In Japanese with abstract in English.]

Date, J., Watanabe, Y., and Saeki, Y., 1983, Zonal alteration around the Fukazawa Kuroko deposits, Akita Prefecture, northern Japan: Economic Geology Monograph 5, p. 365-386.

Davis, A., and Plafker, G., 1980, Comparative geochemistry and petrology of Triassic basaltic rocks from the Taku terrane on the Chilkat Peninsula and Wrangellia: Canadian Journal of Earth Sciences, v. 22, p. 183-194.

Dreschsler, J.S., and Dunbier, J., 1981, The Greens Creek ore deposit, Admiralty Island, Alaska [abs.]: Canadian Mining and Metallurgical Bulletin, v. 74, no. 833, p. 57.

Dunbier, J., Snow, G.G., and Butler, T.A., 1979, The Greens Creek project, Admiralty Island, Alaska [abs.]: Alaska Geological Society Symposium, Program and Abstracts, p. 40.

Ford, A.B., and Brew, D.A., 1993, Geochemical character of upper Paleozoic and Triassic greenstone and related metavolcanic rocks of the Wrangellia terrane in northern southeastern Alaska, *in* Dusel-Bacon, C., and Till, A.B., eds., Geologic Studies in Alaska by the U.S. Geological Survey, 1992: U.S. Geological Survey Bulletin 2068, p. 197-217.

Fyfe, W.S., Price, N.J., and Thompson, A.B., 1978, *Fluids in the Earth's* crust: Amsterdam, Elsevier, 247 p.

Gaccetta, J.D., and Church, S.E, 1989, Lead isotope data base for sulfide occurrences from Alaska: U.S. Geological Survey Open-File Report 89-688, 60 p.

Gehrels, G.E., and Barker, F., 1993, Reconnaissance geochemistry of Permian and Triassic basalts of Taku and Wrangellia terranes, southeastern Alaska, *in* Dusel-Bacon, C., and Till, A.B., eds., Geologic Studies in Alaska by the U.S. Geological Survey, 1992: U.S. Geological Survey Bulletin 2068, p. 218-227.

Gilbert, W.G., and Bundtzen, T.K., 1979, Mid-Paleozoic tectonics, volcanism, and mineralization in the north-central Alaska Range: Journal of the Alaska Geological Society, v.1, p. F1-F22.

Godwin, C.I., Gabites, J.E., and Andrew, A., 1988, Leadtable: A galena lead isotope database for the Canadian Cordillera, with a guide to its use by explorationists: British Colimbia Ministry of Energy, Mines, and Petroleum Resources, Mineral Resources Division, Geological Survey Branch, Paper 1988-4, 188 p.

Hashiguchi, H., Yamada, R., and Inoue, T., 1983, Practical application of low Na_2O anomalies in footwall acid lava for delimiting promising areas around the Kosaka and Fukazawa Kuroko deposits, Akita Prefecture, Japan: Economic Geology Monograph 5, p. 387-394.

Henderson, P., ed., 1984, Rare earth element geochemistry: Amsterdam, Elsevier, 510 p.

MacIntyre, D.G., 1986, The geochemistry of basalts hosting massive sulphide deposits, Alexander terrane northwest British Columbia: British Columbia Ministry of Energy, Mines, and Petroleum Resources, Geological Fieldwork 1985, Paper 1986-1, p. 197-210.

McClelland, W.C., Gehrels, G.E., Samson, S.D., and Patchett, P.J., 1991, Protolith relations of the Gravina belt and Yukon-Tanana terrane in central southeastern Alaska: Journal of Geology, v. 100, p. 107-123.

Newberry, R.J., and Brew, D.A., 1997, The Upper Triassic Greens Creek VMS (volcanogenic massive sulfide) deposit and Woewodski Island VMS prospects, southeastern Alaska: Chemical and isotopic data for rocks and ores demonstrate similarity of these deposits and their host rocks: U.S. Geological Survey Open-File Report 97-539, 49 p.

Newberry, R.J., Brew, D.A., and Crafford, T.C., 1990, Genesis of the Greens Creek volcanogenic massive sulfide deposit, S.E. Alaska: A geochemical study: Geological Association of Canada, Program with Abstracts, v. 15, p. A96.

Newberry, R.J., Crafford, T.C., Newkirk, S.R., Young, L.E., Nelson, S.W., and Duke, N.A., 1997, Volcanogenic massive sulfide deposits of Alaska, *in* Goldfarb, R.J., and Miller, L.D., eds., Mineral Deposits of Alaska: Economic Geology Monograph 9, p. 120-150.

Newberry, R.J., McCoy, D.T., and Brew, D.A., 1995, Pluton-hosted gold ores in Alaska: Igneous vs. metamorphic origins: Resource Geology Special Issue 18, p. 57-100.

Nokleberg, W.J., Bundtzen, T.K., Berg, H.C., Brew, D.A., Grybeck, D., Robinson, M.S., Smith, T.E., and Yeend, W., 1987, Significant metalliferous lode deposits and placer districts of Alaska: U.S. Geological Survey Bulletin 1786, 104 p.

Pearce, J.A., and Cann, J.R., 1973, Tectonic setting of volcanic rocks determined using trace element analyses: Earth and Planetary Science Letters, v. 19, p. 290-300.

Schmidt, J.M., 1988, Mineral and whole rock compositions of seawater-dominated hydrothermal alteration at the Arctic VMS prospect, Alaska: Economic Geology, v. 83, p. 822-842.

Streckeisen, A.L., and LeMaitre, R.W., 1979, A chemical approximation to the modal QAPF classification of the igneous rocks: Neues Jahrbuch für Mineralogie Abhandlung, v. 136, p. 169-206.

Taylor, R.S., and McLennan, S.M., 1985, The continental crust: Its composition and evolution: Oxford, Blackwell, 321 p.

Winchester, J.A., and Floyd, P.A., 1977, Geochemical discrimination of different magma series and their differentiation products using immobile elements: Chemical Geology, v. 20, p. 325-343.

Winkler, H.G.F., 1979, Petrogenesis of metamorphic rocks (5th ed.): New York, Springer-Verlag, 348 p.

Reviewers: D.A. Singer, J.M. Schmidt.

Geologic Studies in Alaska by the
U.S. Geological Survey, 1997
U.S. Geological Survey Professional Paper 1614

Core Lithofacies Analysis and Fluvio-Tidal Environments in the AK 94 CBM-1 Well, Near Wasilla, Alaska

By Romeo M. Flores, Mark D. Myers, Gary D. Stricker, *and* Julie A. Houle

Abstract

The AK 94 CBM-1 well penetrated and cored, from 108 to 378 m, the Tyonek Formation (Miocene-Pliocene) near Wasilla, Alaska. Based on core and well-log descriptions, the Tyonek Formation consists of two major lithofacies types: fluvial dominated and tidallike. The upper (97 m thick) and lower (107 m thick) parts of the core consist of fluvial-dominated lithofacies occasionally interbedded with thin intervals of tidallike lithofacies, whereas the middle part (67 m thick) of the core predominantly contains tidallike lithofacies. Coal beds are mainly associated with the fluvial-dominated lithofacies where they were deposited in freshwater mires developed mainly on abandoned fluvial channel belts and subordinately on distal flood plains. In contrast, only thin coal lenses are present within the tidallike lithofacies, where they are associated with paleosols, well-drained mires, and freshwater lakes.

Sedimentary and biogenic structures suggest that the tidallike lithofacies formed in intertidal to subtidal environments. The most compelling evidence for this interpretation is the common occurrence of lenticular and flaserlike beds; foresets with reactivation surfaces; and rhythmic, mud-draped, bipolar ripple laminae. In addition, associated trace fossils of possibly *Thalassinoides*, *Chondrites*, *Teichicnus*, *Gyrolithes*, *Planolites*, and *Paleophycus*, as well as synaeresis cracks, support a tidal influence. These sedimentary structures are interbedded with heavily bioturbated units, suggesting subaqueous deposition. Alternatively, the only subaqueous fluvial setting that could produce most of these sedimentary structures is in a freshwater lacustrine setting with ebb and flow processes. Some of these tidallike deposits contain the freshwater lacustrine alga *Pediastrum* reported by Nichols (1998).

The alternating fluvial-dominated and tidallike lithofacies are similar to lithofacies found in the Tyonek Formation in the Chuitna drainage basin by Flores and others (1994, 1997). The discovery of these Tyonek tidallike lithofacies in the Chuitna River drainage basin and near Wasilla in the Upper Cook Inlet suggests that brackish water processes may have deposited part of the Tertiary coal-bearing deposits. Previous interpretations have limited these rocks to a nonmarine origin. If our interpretation of these rocks is correct, it requires their reevaluation and suggests that the generally accepted paleogeographic reconstructions of the Tertiary Cook Inlet Basin may need revision with respect to the location and distribution of marine-influenced sedimentation. However, if these rocks were deposited in freshwater lakes, the depositional processes that created these tidallike sedimentary structures need to be better documented.

Introduction

The Cook Inlet Basin (fig. 1) contains the second largest (the largest is the North Slope) amount of hypothetical coal resources in Alaska (Stricker, 1991). These coal resources are contained in the Oligocene to Pliocene Kenai Group (fig. 2) (Calderwood and Fackler, 1972), which is as much as 7,617 m thick in the offshore Cook Inlet Basin. The hypothetical coal resources of the basin exceed 1.5 trillion short tons of which 500 billion short tons are found onshore (Stricker, 1991; Smith, 1995).

The coal-bearing Kenai Group includes, from bottom to top, the Hemlock Conglomerate, and the Tyonek, Beluga, and Sterling Formations (fig. 2). These formations consist of interbedded conglomerate, sandstone, siltstone, mudstone, coal, and carbonaceous shale. Coals are mainly found in the Tyonek, Beluga, and Sterling Formations; however, the thickest coals are found in the Tyonek and Beluga.

The depositional environment of the Kenai Group has generally been interpreted as a nonmarine continental setting (Hite, 1976; Hayes and others, 1976). More specifically, the Beluga and Sterling Formations were interpreted as deposits of braided and meandering streams. Flores and Stricker (1993), and Flores and others (1994, 1997) reinterpreted the Beluga and Sterling Formations to be mixed anastomosed, meandering, and braided streams. In this setting, the thick and thin coal beds accumulated in raised mires and low-lying swamps, respectively. The Tyonek Formation has generally been interpreted as braided-stream deposits (McGee, 1972; Adkison and others, 1975; Dickinson and Campbell, 1978; Dickinson and others, 1995). However, tidallike deposits of the Tyonek in the Chuitna River drainage basin (fig. 1) were reported by Flores and others (1994, 1997).

The purpose of this paper is to report additional evidence for tidallike deposits in the Tyonek Formation near Wasilla (fig.

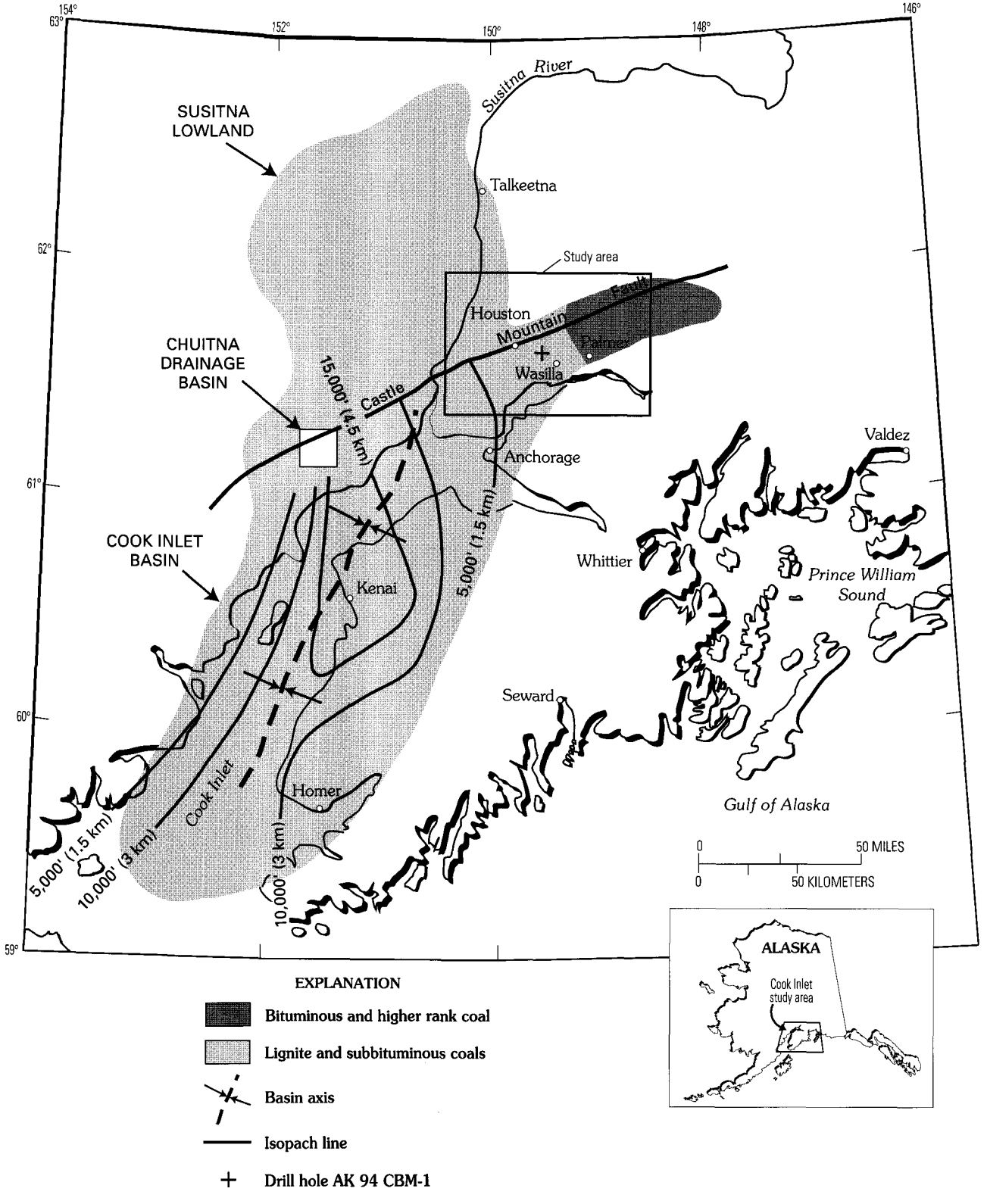

Figure 1. Offshore and onshore Cook Inlet Basin in south-central Alaska. Modified from Smith (1995).

1), which is about 161 km northeast of the Chuitna River drainage basin. These deposits were described from cores of the AK 94 CBM-1 well that was drilled for a coal-bed methane prospect by the Alaska Department of Natural Resources (Smith, 1995). This paper includes detailed lithofacies analysis, sedimentology, and interpretation of the depositional environments, which were not previously performed by Smith (1995).

Geologic Setting

The AK 94 CBM-1 well was drilled in 1994 at a location about 4.2 km northwest of Wasilla on the northeast margin of the Cook Inlet Basin (fig. 3). The northeast margin of the basin forms a northeast-trending trough bounded by the Castle

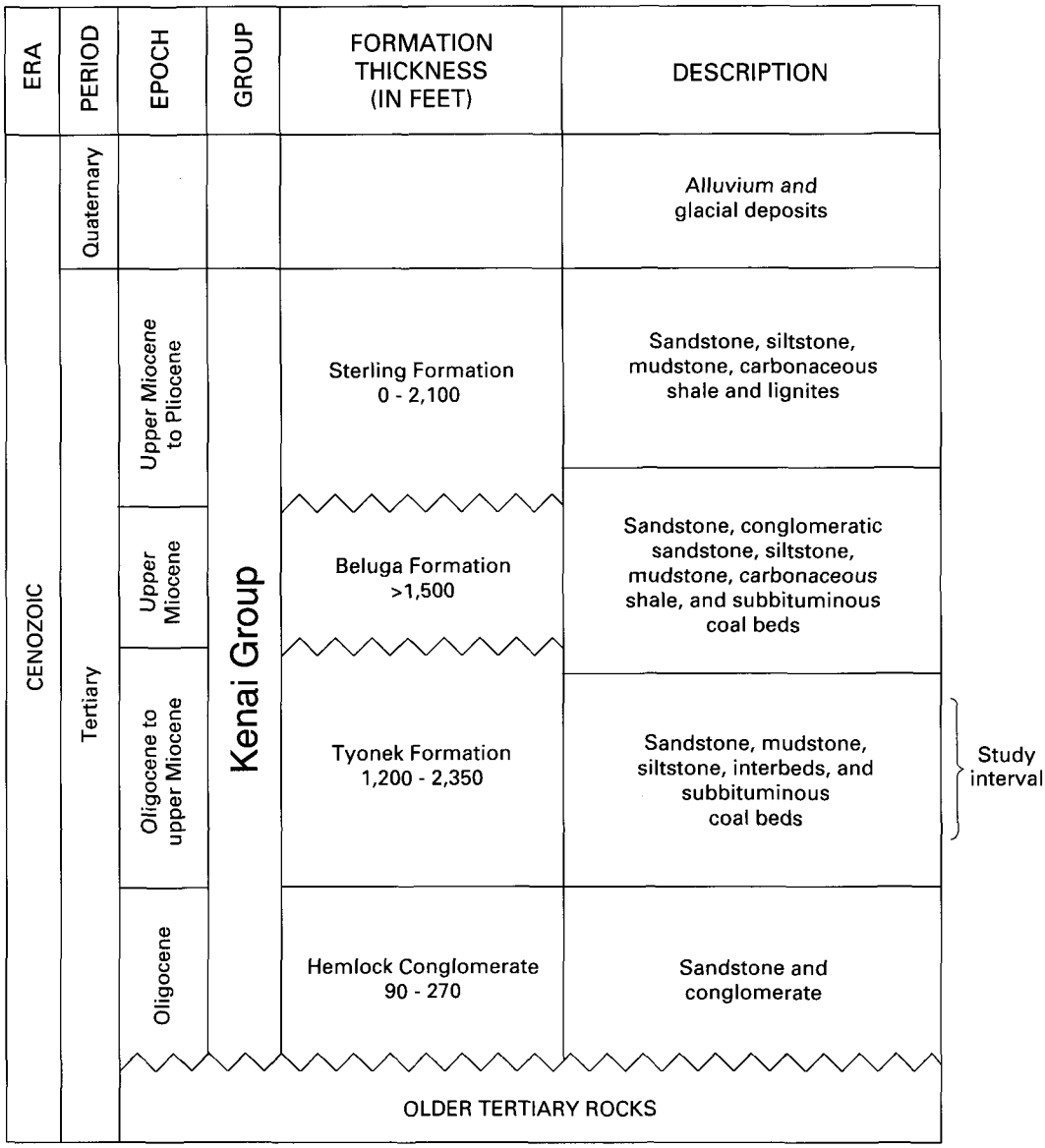

Figure 2. A general stratigraphic column showing the coal-bearing formations of the Kenai Group and the study interval in the Tyonek Formation in the upper Cook Inlet.

Mountain fault and Talkeetna Mountains on the north and the Chugach Mountains on the south (fig. 3). The western part of the trough, which is 40.2 km wide and 121 km long, contains the Tyonek Formation; in this area, it is more than 1,219 m thick and contains a cumulative thickness of greater than 30.5 m of coal beds at depths from 152 to 1,828 m (Smith, 1995). Smith (1995) reported that these coals are high-volatile bituminous with vitrinite reflectance (R_o) values ranging from 0.6 to 1.2 percent (fig. 3).

Johnsson and others (1993) reported that coals in the Kenai Group in the northern Cook Inlet Basin range from 0.2 to 0.9 percent R_o in depths from 30.5 to 2,742 m. Post-depositional uplift of the northern margin of the basin exposed older rocks (Paleocene to Oligocene) with high thermal maturity. For example, Paleocene to Eocene rocks, which contain high-volatile bituminous and anthracite coals, are exposed in the Matanuska Valley (Anonymous, 1990). Coal mines in this area have emitted methane gas, which caused outbursts and explosions in 1937 and 1957 (Barnes and Payne, 1956; Smith, 1995).

The high-thermal-maturity Tertiary coals, particularly in the northern margin of the Cook Inlet Basin, have been targeted for coal-bed methane exploration. Smith and Clough (1993) identified the Wasilla area as a prospect because of its proximity to infrastructure, including gas pipelines. This led to the drilling of the AK 94 CBM-1 well by the Department of Natural Resources, State of Alaska, to test for the presence of coal-bed methane in the Tyonek Formation (Smith, 1995). This test well will serve as an important guide to future coal-bed gas measurements and resource estimates of Tertiary coal-bearing rocks in the Cook Inlet Basin.

Previous Work Performed on the AK 94 CBM-1 Well

The AK 94 CBM-1 well was drilled to a total depth of 379 m, and a continuous core of the Tyonek Formation was

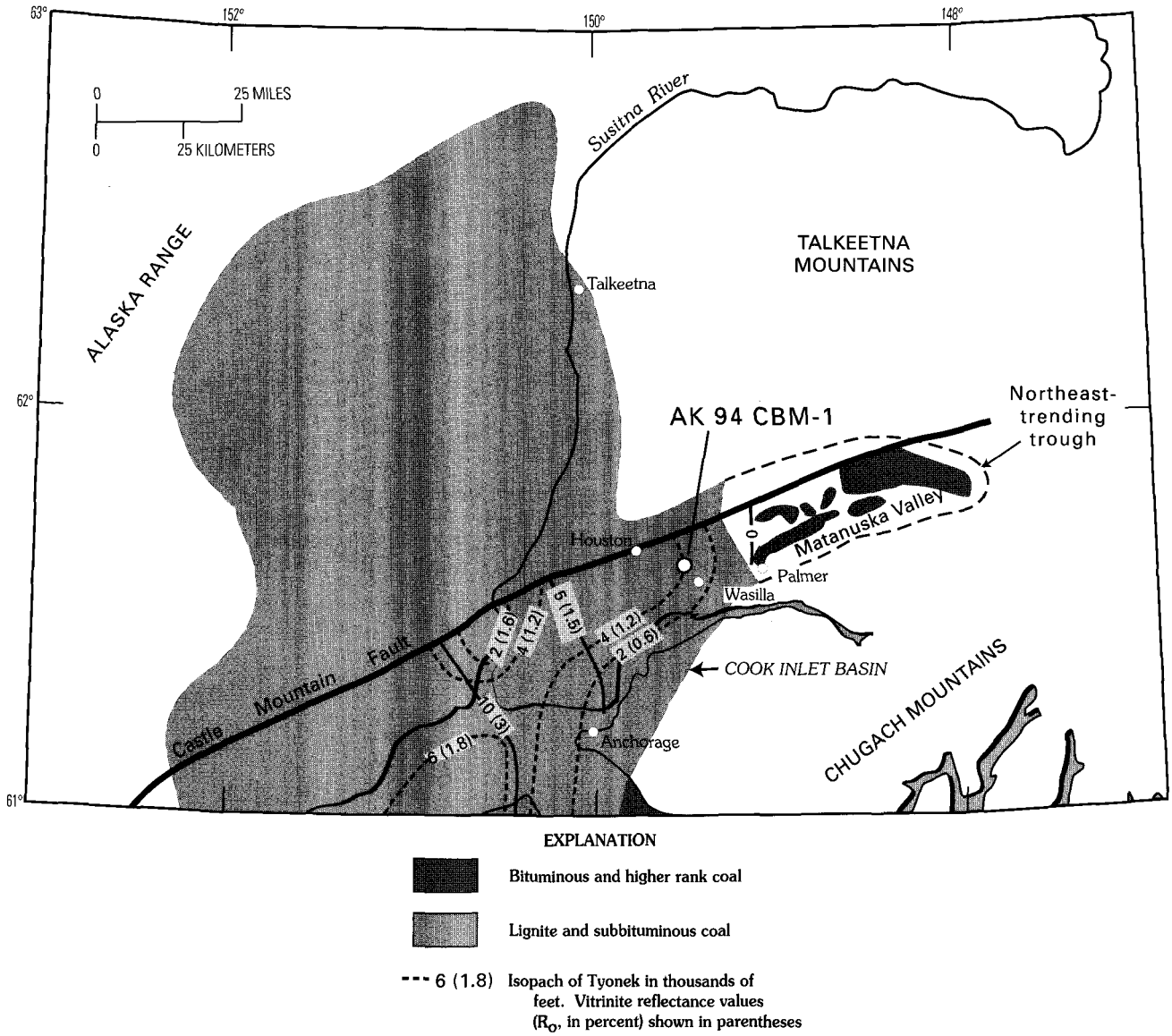

Figure 3. Upper Cook Inlet Basin showing location of the AK 94 CBM-1 well; coal rank in the Matanuska Valley; and coal rank, R_o, and thickness of the Tyonek Formation. Modified from Smith (1995).

recovered from 108 to 379 m (Smith, 1995). The depths from 0 to 108 m were cased; however, rock samples indicate that the interval is composed of Quaternary glacial conglomerate. A suite of geophysical logs (e.g., gamma ray, density, spontaneous potential, and resistivity) was also run to evaluate the Tyonek rocks. The drilling project was mainly designed by Smith (1995) to collect samples from Tyonek coal beds that were greater than 0.6 m thick for proximate and geochemical analyses, and gas desorption. Thus, only coal beds that are less than 0.3 m thick were left in the core for detailed description. Smith (1995) noted that the coal beds are thick (as thick as 2.9 m) at depth and their cumulative thickness is about 12.5 m.

Out of the total of 18 coal beds drilled in the Tyonek Formation, 13 beds were sampled for gas content. Proximate analysis of these coals indicates an as-received moisture content of 4.8 to 9.02 percent, volatile matter of 5.57 to 22.85 percent, fixed carbon of 23.03 to 48.71 percent, and ash yield from 5.57 to 44.74 percent. In general, moisture and fixed carbon increased with depth. Gas content ranges from 63 ft^3/short ton at standard temperature and pressure (STP) for coal beds at a shallow depth (152 m) to 245 standard ft^3/short ton at STP for coal beds at a great depth (366 m). Carbon isotopes of the coal-bed gases range from –49.3 to –43.3 ‰ (per mil) $\delta^{13}C$, with slightly heavier isotope values at depth, indicating both a thermogenic and biogenic origin of the coal-bed gas. Composition of this gas is 90 percent methane with minor amounts of CO_2 and N_2. Vitrinite reflectance values range from 0.47 to 0.58 percent and generally increases with depth (Smith, 1995).

Lithostratigraphy of the AK 94 CBM-1 Core

Smith (1995) described the general lithology of the AK 94 CBM-1 core, from 379 to 108 m depth, as consisting of interbedded coal, mudstone, siltstone, sandstone, and conglomerate. Our detailed description of this 271-m-thick interval of 7.6-cm-diameter core included thickness, lithology, color, grain size,

sorting, mineral composition, nature of contact, sedimentary structures, trace fossil content, and biological constituents (figs. 4*A*–4*C*).

In order to summarize the lithofacies association of the core, the Tyonek interval is divided into lower, middle, and upper parts based on the grain size, abundance, and thickness of diagnostic lithologic types. The lower part (fig. 4*A*), from 379 to 272 m, is 107 m thick and consists of abundant conglomeratic sandstones and thick (0.3–2.9 m) coals and carbonaceous shales. The middle part (fig. 4*B*), from 272 to 205 m, is 67 m thick and is composed of abundant mudstone, siltstone, fine-grained sandstone, and sparse, thin (8.9 cm to 0.3 m) coal and carbonaceous shale. The upper part (fig. 4*C*), from 205 to 108 m, is 97 m thick and comprises abundant medium- to coarse-grained sandstones and thin to thick (1–3.5 ft or 0.3–1 m) coal and carbonaceous shale.

The gamma-ray curve measures the natural radioactivity of rock types caused by absorption of thorium by clay minerals, potassium content of clay minerals (mainly illite), and uranium fixed by associated organic matter (Doveton, 1994). In general, low levels of radioactivity are observed in sandstone and siltstone, which is attributed to the amount of clay minerals, potassium feldspar, mica, and heavy minerals. Coal displays much lower gamma radiation compared to these rock types and is readily identifiable by the gamma-ray log curve. Density and resistivity curves were also used to identify the coal beds. Responses of both gamma-ray and spontaneous-potential logs are indirectly related to sediment grain size and may be used as a vertical grain-size profile (Galloway, 1968; Selley, 1978).

A comparison of the gamma-ray and spontaneous-potential logs of the conglomerates and sandstones have significantly different patterns (see fig. 4*A*). The gamma-ray log curve displays serrated cylindrical and bell shapes (rightward excursions). However, the spontaneous-potential log curve shows smooth cylindrical to combined smooth and serrated bell shapes (leftward excursions). The better definition of the spontaneous potential is probably due to changes in grain size of the sandstone. The cylindrical-shaped curve suggests uniform vertical grain size of the sandstone and the bell-shaped curve indicates fining upward.

Lower Part of the Core

The lower part (379–272 m) of the Tyonek interval (see fig. 4*A*) is dominated by medium- to coarse-grained sandstone and conglomerate, which make up as much as 60 percent of the total rock volume. The sandstones occur as fining-upward beds that are from 0.6 to 4.6 m thick and display erosional bases (fig. 5). The sandstones are light gray and show a "salt-and-pepper" texture (Krynine, 1950); light minerals consist mainly of quartz. The dark color is due to the presence of chert and other rock fragments (e.g., metamorphic and volcanic). Sedimentary structures consist of trough crossbeds that are 7.6 cm to 0.3 m in height (fig. 5). These structures are interbedded by a few planar crossbeds (0.3 m in height) with steep foresets (fig. 5). Asymmetrical and climbing ripple laminations (7.6-cm- to 0.6-m-thick units) cap the trough and planar crossbedded units (fig. 6).

The conglomerates, which make up less than 5 percent of the total rock volume, have erosional bases and occur as 7.6-cm- to 0.6- m-thick beds (figs. 4*A* and 5). They are gray and composed of rounded to subrounded pebbles and cobbles of quartz, black chert, and volcanic rock fragments. They are commonly framework supported, and a few are matrix supported. The framework-supported conglomerates exhibit clast imbrication.

Forty percent of the lower part of the Tyonek interval (fig. 4*A*) consists of interbedded, very fine to fine-grained sandstone, siltstone, mudstone, coal, and carbonaceous shale (fig. 7). Sandstones have sharp basal contacts, are gray in color, and vary from 0.3 to 1.5 m thick. They are mainly ripple laminated, lenticular and flaserlike bedded (with bipolar ripple laminae), and are vertically burrowed by nondescript trace fossils. Siltstones are gray, a few centimeters to 0.4 m thick, ripple laminated, burrowed, and are commonly interbedded with the sandstones. Mudstones are dark gray to black, depending on the amount of macerated plant content, and vary from 0.3 to 8.2 m thick. They are massive to crudely laminated, vertically and horizontally burrowed, and contain whole shells of bivalve mollusks or pelecypods. These bivalves are articulated, 3.8 cm wide and 6.3 cm long, and resemble a unionid clam in shape. Root marks, defined by vertical branchlike tubules lined by carbonaceous matter, are common in the sandstones, siltstones, and mudstones. Coal beds vary from 15.2 to 2.9 m in thickness (fig. 4*A*). They contains vitrinite bands indicating woody composition. They are commonly interbedded with carbonaceous shales, which vary from a few centimeters to 0.3 m thick. Carbonaceous shales are fissile and contain a mixture of mud and macerated plant fragments. Root marks are a common bioturbation feature in the carbonaceous shale.

Middle Part of the Core

The middle part (272–205 m) of the Tyonek interval (fig. 4*B*) is dominated by abundant fine-grained sandstones (fig. 8), which make up as much as 55 percent of the total rock volume. Sandstones display sharp to erosional bases and uniform grain size from bottom to top; they are from 0.3 to 7.9 m thick and are light gray and show a "salt-and-pepper" texture. Sedimentary structures consist mainly of foresets that range from 23 to 25 cm in height and are separated by clay-draped reactivation surfaces. Trough crossbeds, 8–15 cm in height, are common, but planar crossbeds, as much as 15 cm in height, and convolutions are rare. Lenticular bedding (0.25–0.64 cm thick) and flaserlike ripple laminations are very common (fig. 8*A*). Ripple sets in the flaserlike laminations are bipolar and draped by burrowed mudstones (fig. 8*B*). The sandstones are heavily bioturbated, and the accompanying sedimentary structures have been partly to completely destroyed. Vertical burrows in the form of escape and branching structures are very common. Escape structures are 1.3 cm high and 2.5 cm wide, and the branching vertical burrows (e.g., *Thalassinoides*-like) are 5–8 cm wide and 1.5 m long (fig. 9). The branching burrows were open and passively infilled by overlying sand (fig. 9). Plant bioturbation in the form of root marks is rare.

The gamma-ray and spontaneous-potential logs of the sandstones have significantly different patterns (fig. 4*B*). The gamma-ray log curve displays mainly a serrated bell shape (rightward excursions). However, the spontaneous-potential log curve shows combined smooth and serrated bell shapes and funnel

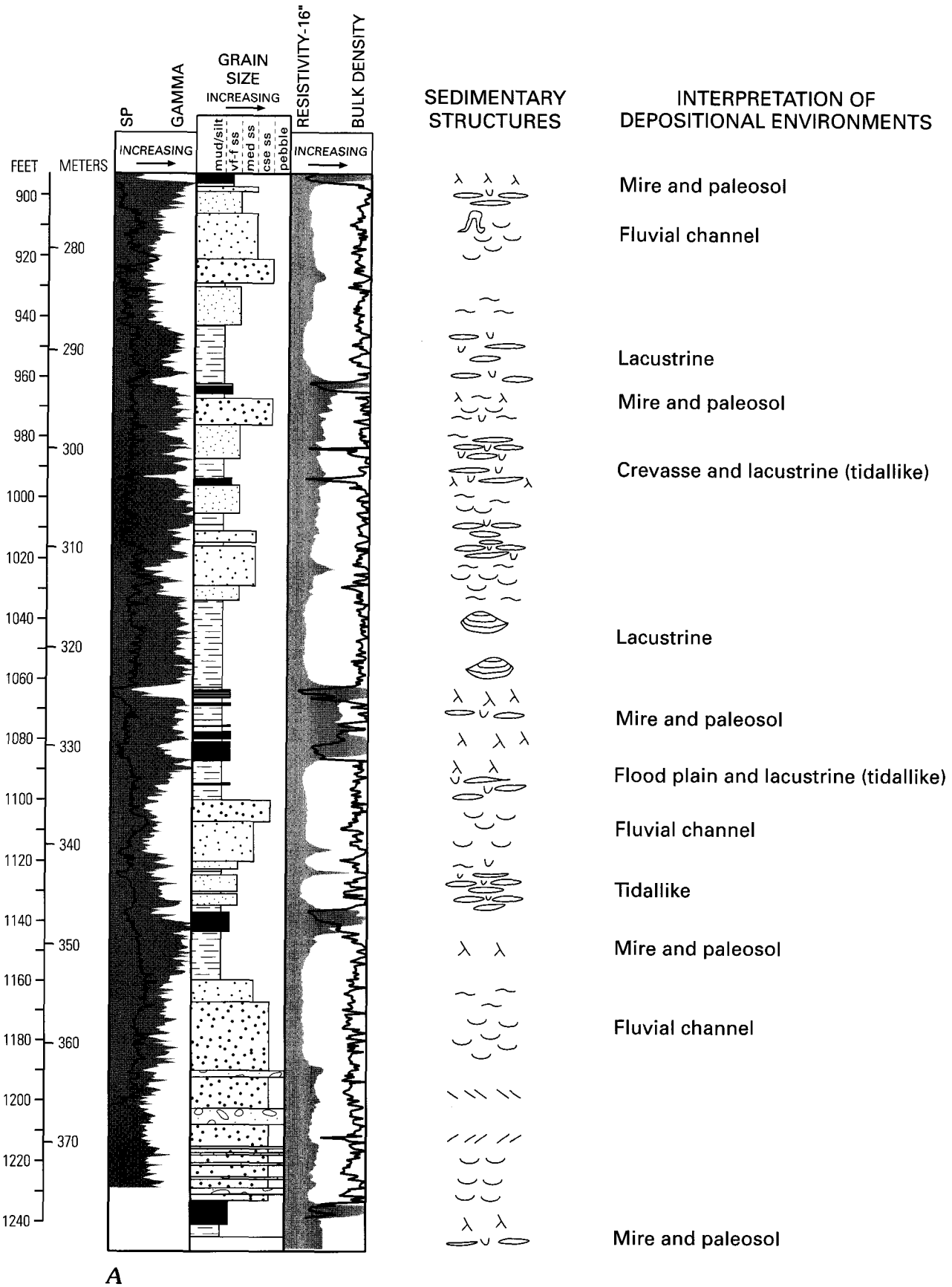

Figure 4*A*. Lithostratigraphy, geophysical logs, and lithofacies variation of the lower part (379–272 m) of the AK 94 CBM-1 core.

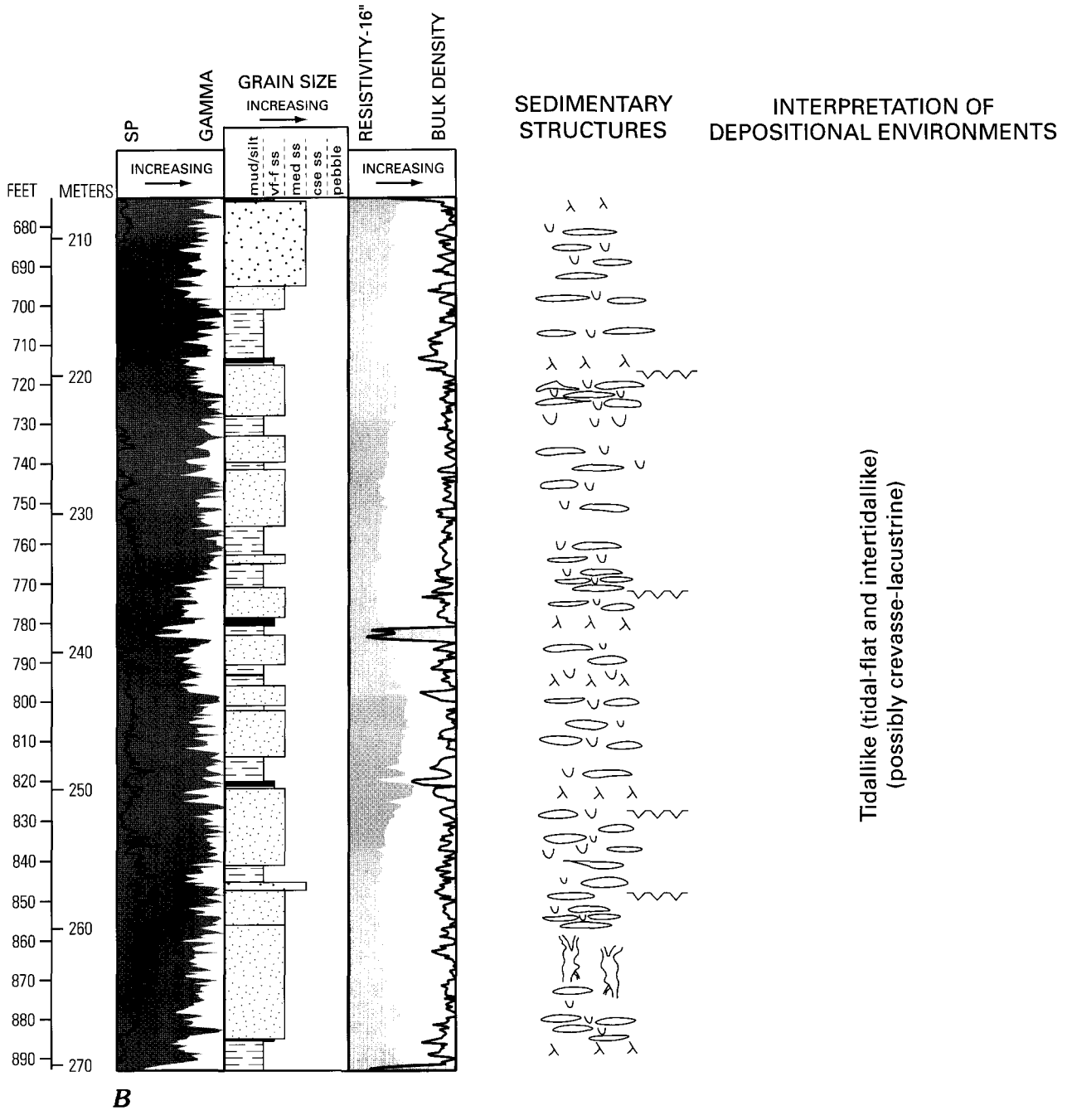

Figure 4*B*. Lithostratigraphy, geophysical logs, and lithofacies variation of the middle part (272–205 m) of the AK 94 CBM-1 core.

shapes (leftward excursions). The spontaneous-potential log curve is probably due to fining-upward grain size of the sandstone. The funnel shape curve of the spontaneous potential curve suggests coarsening-upward vertical grain size of the sandstone.

Forty-five percent of the total rock volume of the middle part of the Tyonek interval (fig. 4*B*) is composed of siltstone, mudstone, carbonaceous mudstone, and coal (fig. 10). The siltstones and mudstones are light to dark gray and are commonly intercalated, making up units as much as 2.7 m thick. These units are commonly lenticular and (or) flaser bedded with lenses of siltstones draped by mudstones. Wispy lenses or "starved ripples" in siltstones are also common. Siltstone lenses are as much as 0.6 cm thick and are vertically burrowed by trace fossils—the burrows include small oval burrows of possibly *Chondrites* and *Teichicnus* (Pemberton and Wightman, 1992; Beynon and Pemberton, 1992) at 264.3–264.4 m. Possible trace fossils of *Planolites* and *Paleophycus* (Pemberton and Wightman, 1992; Beynon and Pemberton, 1992) are found at 264.5 m. A *Thalassinoides*-like (Pemberton and Wightman, 1992; Beynon and Pemberton, 1992) trace fossil (fig. 9) is found at 263.4–262.9 m. The mudstones are heavily bioturbated vertically by wormlike or spiroform burrows (possibly *Gyrolithes*) that are 1 mm in diameter and 1.3 cm long. These burrowed horizons are commonly associated with mud and synaeresis cracks. Discrete units of black,

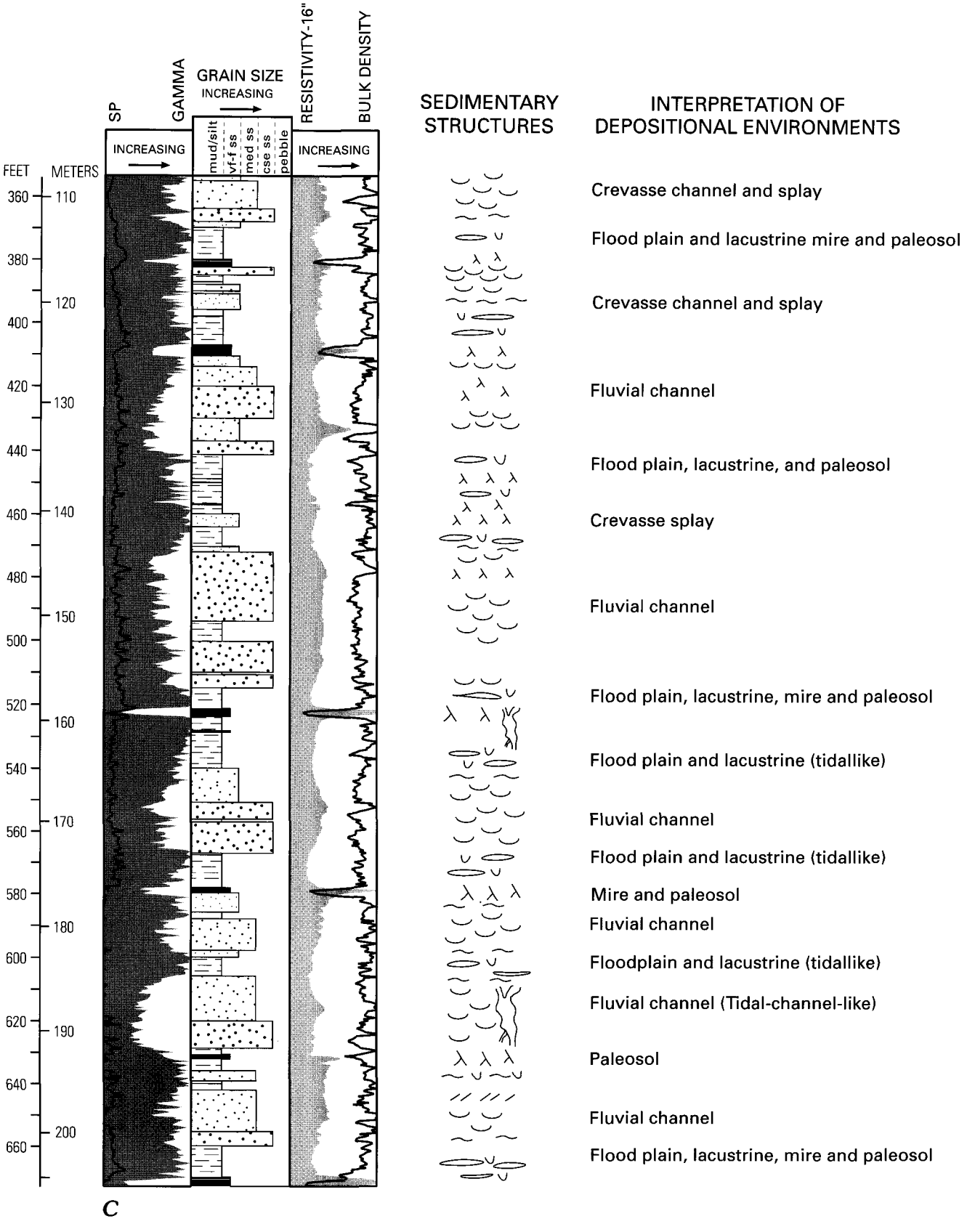

Figure 4*C*. Lithostratigraphy, geophysical logs, and lithofacies variation of the upper part (205–108 m) of the AK 94 CBM-1 core.

carbonaceous mudstones are as much as 0.6 m thick and are bioturbated by plant rootlets associated with yellow mottles. These mudstone units are interbedded with thin, vitrain-rich, coaly layers that are as much as 8.2 cm thick.

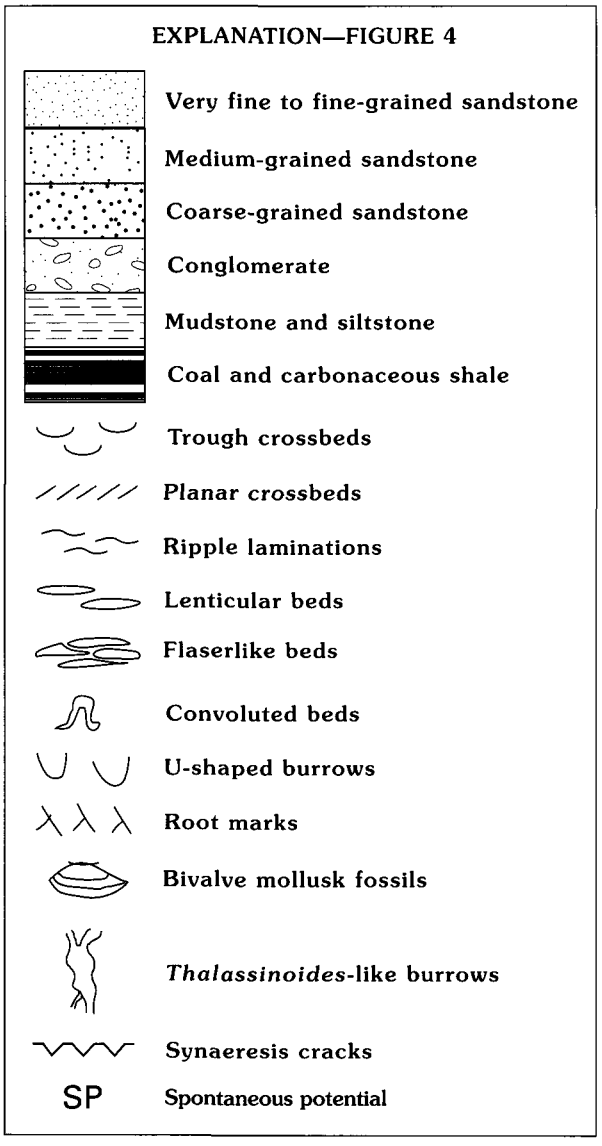

Upper Part of the Core

The upper part (205–108 m) of the Tyonek interval (fig. 4*C*) is dominated by fine- to coarse-grained sandstones, which make up about 55 percent of the total rock volume, and commonly by thin coal beds. The sandstones occur as fining-upward beds that are from 4.6 to 9.1 m thick and display sharp to erosional bases (fig. 11). The sandstones are light gray and show a "salt-and-pepper" texture. Sedimentary structures commonly consist of trough crossbeds that are as much as 0.3 m in height (fig. 11). Massive beds as much as 1.8 m thick are commonly interbedded with the trough crossbeds. Planar crossbeds (as much as 1.5 cm in height) and slump structures are sparse. Asymmetrical and climbing ripple laminations in units as much as 0.6 m thick cap the fining-upward sandstones. Bioturbation by trace fossils and plants is common. Trace-fossil burrows are vertical (fig. 11) and branchlike or *Thalassinoides*-like and are as much as 10 cm in diameter and 0.5 m long. Carbonaceous plant root marks are common in the upper part of the fining-upward sandstones. The root marks are both younger and older than the vertical burrows.

The gamma-ray log curve (fig. 4*C*) displays serrated-bell and cylindrical shapes (rightward excursions). The spontaneous-potential log curve shows combined smooth- and serrated-bell and cylindrical shapes and funnel shape (leftward excursions). The spontaneous-potential log curve is probably due to uniform vertical and fining-upward grain size of the sandstones. These vertical grain-size variations of the sandstones are reflected by the gamma-ray log curves. The funnel shape curve of the spontaneous potential curve suggests coarsening-upward vertical grain size of the sandstones.

Forty-five percent of the upper part of the Tyonek interval (fig. 4*C*) consists of siltstone, mudstone, coal and carbonaceous shale (fig 12). Siltstones are light gray, a few centimeters to 1.4 m thick, contain very fine grained sandstone lenses (lenticular bed), and are rippled, rooted, and burrowed (fig. 11). Mudstones are gray to black, depending on the amount of carbonaceous matter content, and vary from 0.3 to 2.7 m thick (fig 12). They are massive to crudely laminated, rippled (lenticular beds and "starved ripples"), rooted, and vertically burrowed. Vertical burrows in the mudstones are 0.6 to 2.5 cm in diameter, more than 8 cm long, and sand-infilled. Carbonaceous root marks penetrate these branchlike vertical burrows. Coal and carbonaceous shales are interbedded, forming units as thick as 0.9 m. Coals are brightly banded, indicating woody composition. Carbonaceous shales are commonly rooted (fig. 12).

LOWER PART OF THE CORE

Lithofacies Associations and Sequences

Lithofacies associations of the Tyonek Formation may be recognized as a depositionally related group of lithofacies that occur together. Lithofacies sequences of the Tyonek Formation are recognized as a series of lithofacies that pass vertically from one lithofacies to another.

Three thick, fining-upward sandstone units occur as lithofacies sequences in the lower part of the Tyonek interval (fig. 4*A*), from bottom to top, 376–353 m, 344–334 m, and 287–273 m. These 12- to 23-m-thick sandstones consist of stacked, multiple scoured units, each of which fines upward. The fining-upward sandstones at 376–353 m are associated with erosionally based conglomerates that are either singular or stacked units. This lithofacies association is mainly found at 374.6–362.7 m, where the conglomerates occur. In addition, pebble floats are associated with erosionally based sandstones in the middle part of the succession. The fining-upward sandstones at 287–272 m are associated with some conglomerates that mark erosional bases below the sandstones.

The fining-upward sandstone lithofacies sequences are interbedded, from bottom to top, with lithofacies associations consisting of coal, carbonaceous shale, sandstone, siltstone, and mudstone at 379–376 m, 353–344 m, 334–287 m, and 273–272 m. The lithofacies association at 379–376 m consists mainly of coal and carbonaceous shale underlain by mudstone and siltstone, which are rooted, burrowed, lenticular bedded, and rippled. The lithofacies association at 353–344 m includes, from bottom to top, a rooted mudstone capped by vitrinite lenses, coal

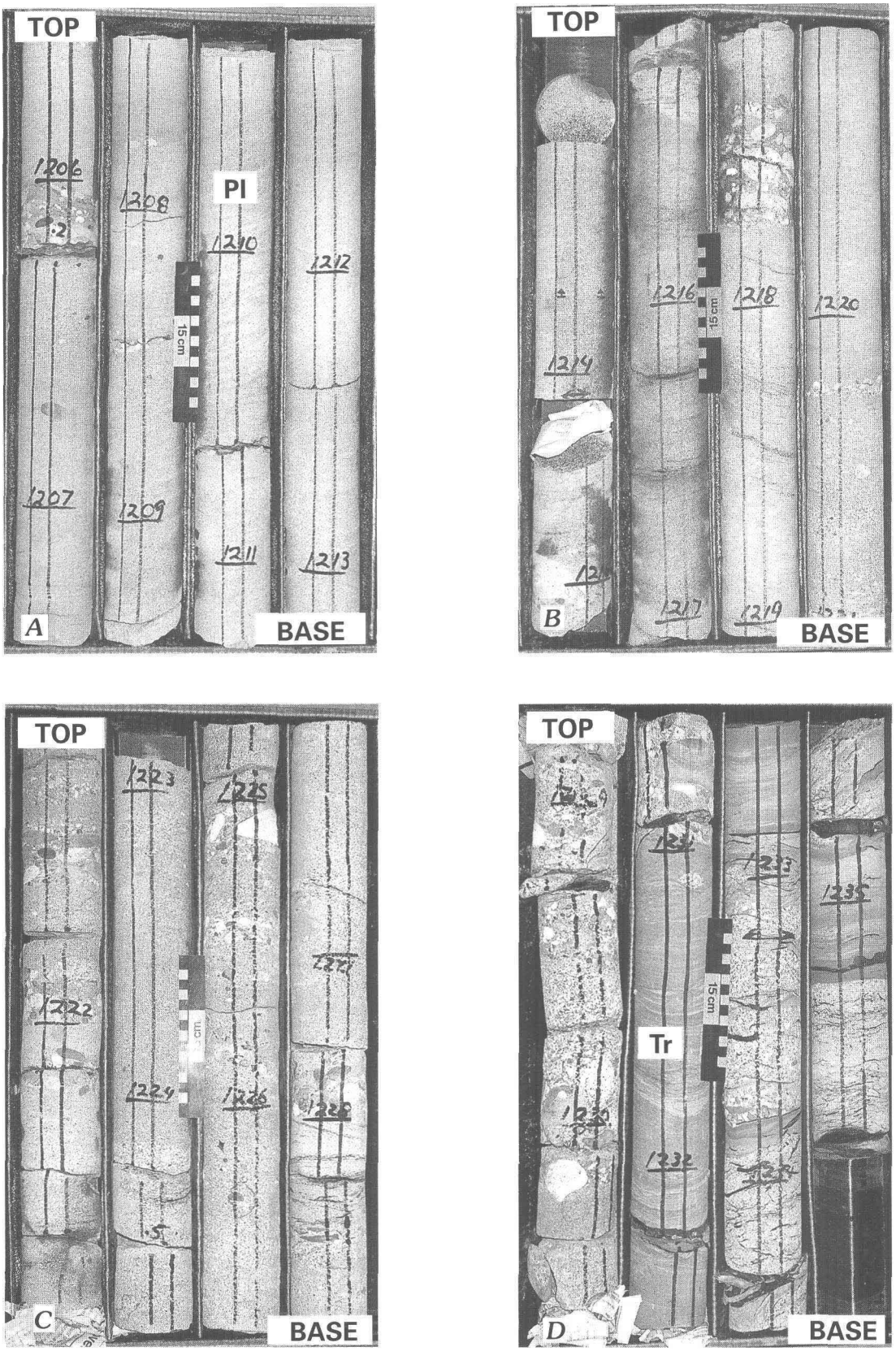

Figure 5. Stacked, erosionally based, fining-upward sandstones interbedded with conglomerates from 376.4 to 367.4 m in the lower part of the core (photos *A*, from 376.3 to 369.9 m; *B*, from 369.9 to 372.2 m; *C*, from 372.2 to 374.6 m; and *D*, from 374.6 to 376.8 m). Trough (Tr) and planar (PI) crossbeds in the fining-upward sandstones from 375.6–375.0 m and 371.8 to 367.7 m, respectively. Numbers on core show depth in feet. To convert from feet to meters multiply by 0.304 (note centimeter scale on photo).

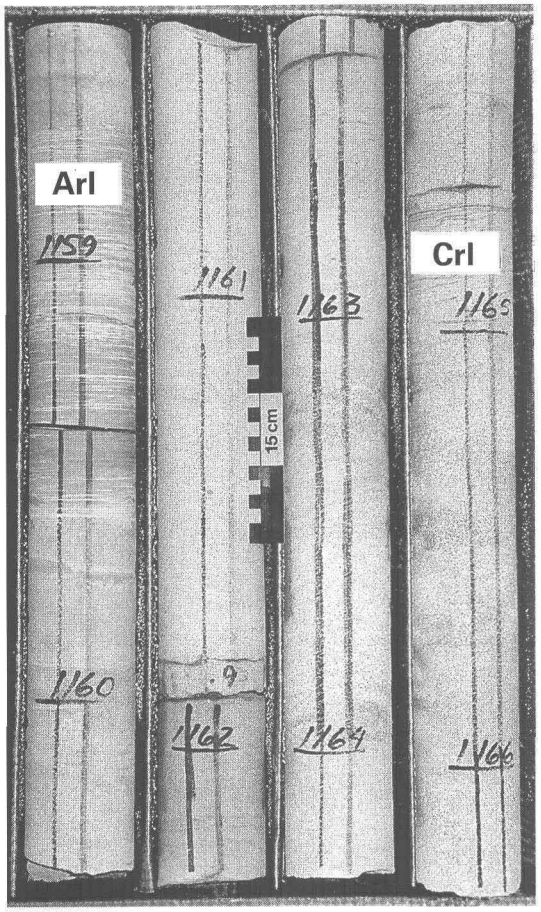

Figure 6. Climbing ripple laminations (Crl) interbedded with asymmetrical ripple laminations (Arl) that cap the stacked, fining-upward sandstones from 355.2 to 353.1 m in the lower part of the core. Numbers on core show depth in feet. To convert from feet to meters multiply by 0.304 (note centimeter scale on photo).

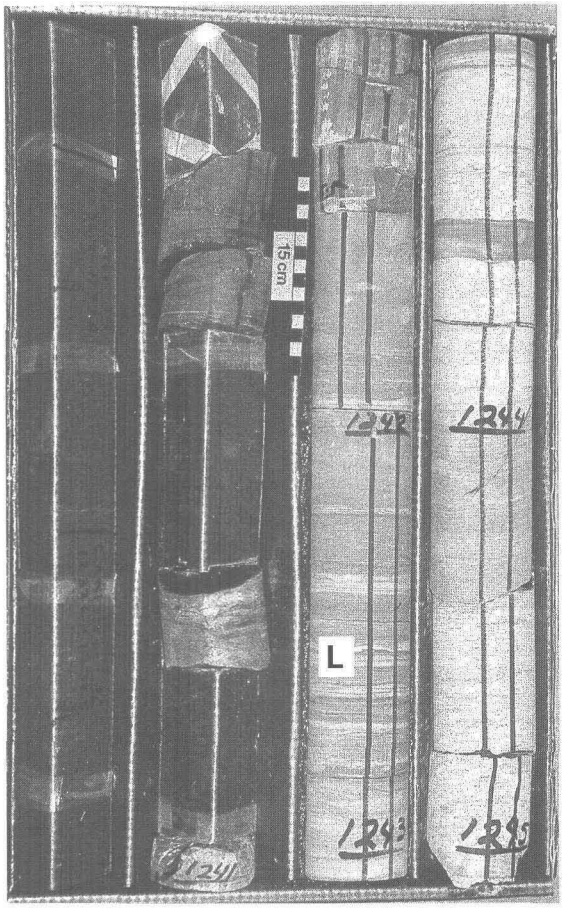

Figure 7. Interbedded coal, carbonaceous mudstone, siltstone, and sandstone from 379.3 to 377.1 m in the lower part of the core. A part of the coal bed is missing and was sampled for analysis (378–377). L, lenticular bedding. Numbers on core show depth in feet. To convert from feet to meters multiply by 0.304 (note centimeter scale on photo).

and carbonaceous shale, and interbedded burrowed mudstone; tonstein; fining-upward, rippled-burrowed sandstone; and siltstone. The lithofacies association at 334–287 m consists of coal and rooted carbonaceous shale interbedded with lenticular-bedded, mud-draped (flaserlike) sandstone, siltstone, and mudstone in the lower part. A massive mudstone containing bivalve mollusks interbedded with a multi-erosional, 7.3-m-thick, fining-upward sandstone occurs in the middle part. A lithofacies association of coal and carbonaceous shale interbedded with mudstone and stacked, multi-erosional, 1.5- to 3.3-m-thick, fining-upward sandstone occurs in the upper part. The lithofacies association at 273–272 m consists mainly of coal and carbonaceous shale. A mudstone at 260.4 m (below a coal) analyzed by Nichols (1998) for palynomorphs yielded the freshwater alga *Pediastrum* and common conifer pollen.

Interpretation

The thick, fining-upward sandstone sequences are interpreted as deposits of major fluvial channels. The stacked, multiple scoured units represent deposits of shallow (thin) to deep (thick) subchannels. The thin, erosionally based conglomerates are interpreted as channel-floor and gravel-bar deposits similar to braided streams (Webb, 1994). Pebbles in the sandstone reflect debris-flow deposits. The lithofacies association of sandstone and conglomerate suggests that the major fluvial channels were braided, consisting of subchannels that were aerially separated by gravel bars (Best and Bristow, 1993). The fining-upward sandstones floored by conglomerates indicate channel-fill during waxing to waning channel flows (Allen, 1965).

The coal and carbonaceous shale lithofacies associations are interpreted as mire deposits in freshwater environments as indicated by the alga *Pediastrum*. The massive mudstones containing bivalve mollusks or pelecypods suggest deposition in a subaqueous, probably freshwater, lacustrine environment. The lithofacies association of mudstone with lenticular-bedded, mud-draped sandstone, siltstone, and mudstone reflects deposition either in a wave-influenced flood plain crevasse and lacustrine environment, or tidallike environment. The thin, fining-upward sandstone lithofacies sequence is interpreted as deposits

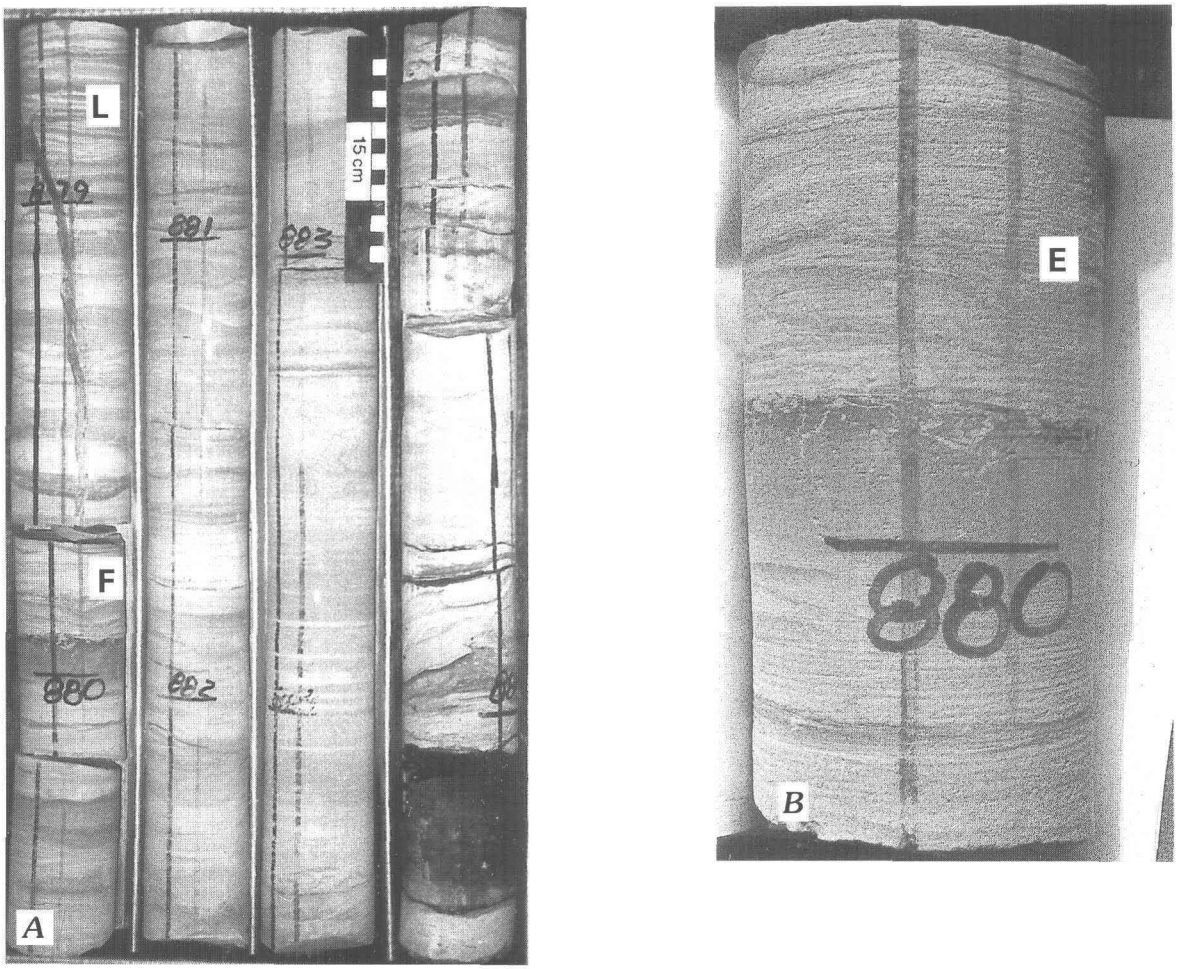

Figure 8. *A*, Siltstones, mudstones, and silty sandstones containing lenticular (L) and flaserlike (F) beds underlain by a thin coal and carbonaceous shale lithofacies from 270.1 to 267. 9 m. *B*, Flaserlike beds with bipolar ripple sets draped by burrowed mudstone lenses and a mudstone exhibiting synaeresis or shrinkage cracks (SC). E, escape structure. Numbers on core show depth in feet. To convert from feet to meters multiply by 0.304 (note centimeter scale on photo).

of minor, sinuous or meandering fluvial channels that drained the mires, flood plains, and lacustrine environments (Miall, 1996). They also served as minor drainages that were laterally contemporaneous to the major braided fluvial channels in the alluvial plain.

MIDDLE PART OF THE CORE

Lithofacies Associations and Sequences

The lithofacies association in the middle part of the core consists mainly of erosionally based, thick, heavily bioturbated, fine-grained sandstones at 272–242 m (fig. 4*B*). The fine-grained sandstones are mainly lenticular, wispy, and flaserlike bedded and contain subordinate crossbed foresets with clay-draped reactivation surfaces and opposed foresets in ripple laminae. These sedimentary structures are partly destroyed by "tidallike" burrows and U-shaped escape burrows. The fine-grained sandstones are associated with minor siltstones and mudstones that are commonly lenticular and flaserlike bedded. Lithofacies association of minor amounts of rooted carbonaceous mudstones with the siltstones and mudstones are at 250–249 m and 243–242.8 m.

The lithofacies association from 242–205 m of the middle part of the core is mainly composed of sharp-based, thin, heavily bioturbated, fine-grained sandstones. These are commonly lenticular and flaserlike bedded with the mud-drapes being burrowed. These sedimentary structures are locally rhythmic and are commonly destroyed by vertical burrows and root marks. Root marks are in the form of yellow mottles. The fine-grained sandstones are commonly associated with thin to thick siltstones and mudstones. The siltstones and mudstones in this lithofacies association are characterized by lenticular, wispy, and flaserlike beds that are almost destroyed by vertical burrows and root marks. The root marks and mottled structures are associated with thin coal and carbonaceous mudstones. A rooted carbonaceous mudstone analyzed for palynomorphs by Nichols (1998) yield abundant pine and hemlock pollen.

Interpretation

The lithofacies association in the middle part of the core is very similar to that described as tidallike deposits by Flores and others (1997) in core from the Chuitna drainage. The thin to thick, erosional- to sharp-based, fine-grained sandstone

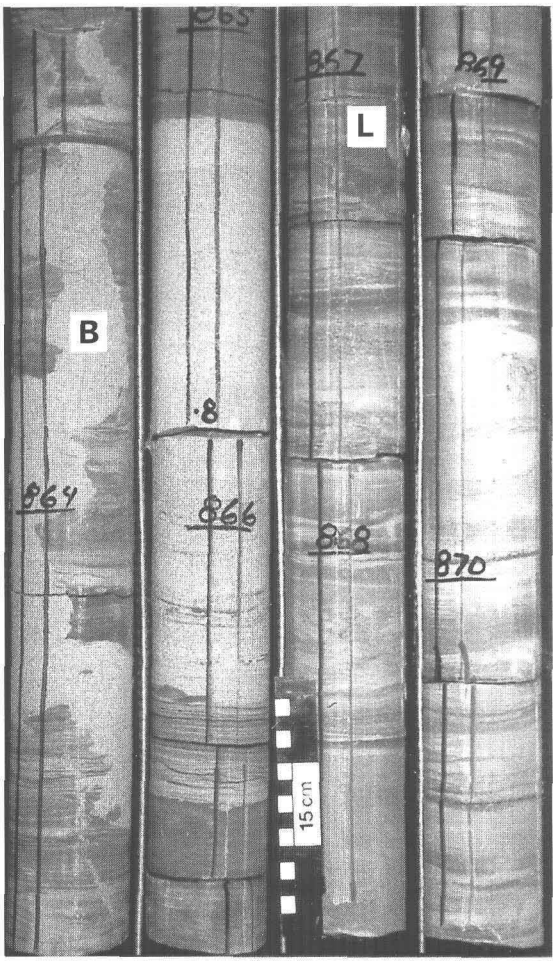

Figure 9. Siltstones, mudstones and silty sandstones displaying lenticular beds (L) and a *Thalassinoides*-like burrow (B) from 265.4 to 262.9 m. Numbers on core show depth in feet. To convert from feet to meters multiply by 0.304 (note centimeter scale on photo).

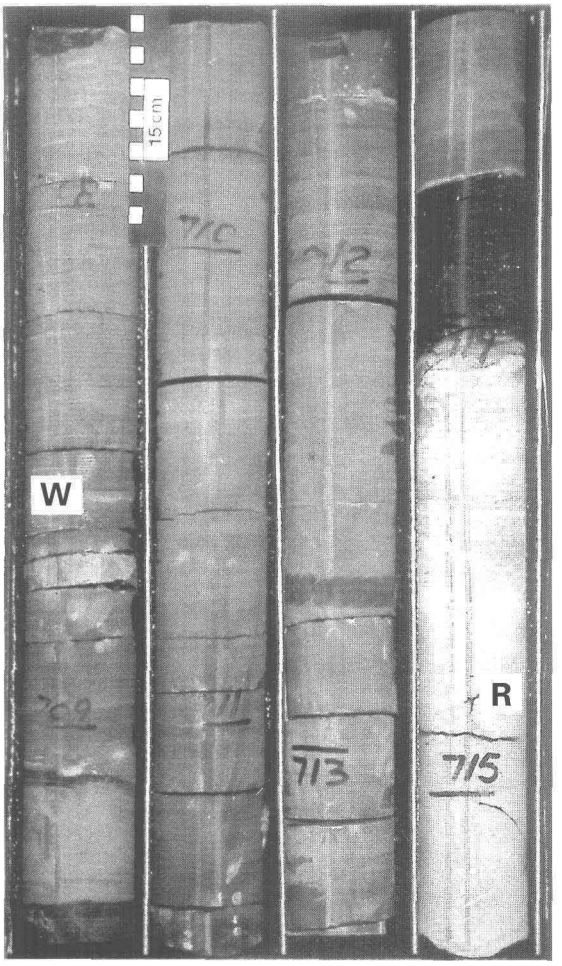

Figure 10. Mudstones, siltstones, carbonaceous shales, and coals from 217.8 to 215.7 m in the middle part of core. W, wispy structure. R, root mark. Numbers on core show depth in feet. To convert from feet to meters multiply by 0.304 (note centimeter scale on photo).

lithofacies are interpreted by Flores and others (1997) as deposits in tidal-channel to tidal-flat-like environments similar to sediments described by Evans (1975), Visser (1980), Reinson (1989), Nio and Yang (1991), Flores and Johnson (1995), and Flores and Sykes (1996). The *Thalassinoides*-like burrows suggest that these lithofacies associations were influenced by brackish or marine water. However, MacKenzie (1975) suggested that the same burrows may have been generated by some species of clams. If this is correct, we suggest that these clams may be similar to the unionid bivalve mollusks found in the mudstones in the lower part of the core, interpreted to be deposited in a large flood-plain freshwater lake. The tidallike deposits may have been deposited in crevasse splays and reworked by burrowing animals as well as ebb-and-flow processes. The presence of burrowed lenticular and flaserlike beds in the sandstone and siltstone, and in the wispy beds, indicates intertidal-subtidal-like environments (Reineck and Wunderlich 1968). The opposed bipolar ripple laminae and development of reactivation surfaces probably reflects successive tidallike ebb and flow. The possible trace fossils *Thalassinoides*, *Chondrites*, *Teichicnus*, *Gyrolithes*, *Planolites*, and *Paleophycus* reflect brackish-marine influence and may support tidallike deposition of the associated rocks (Pemberton and Wightman, 1992; Beynon and Pemberton, 1992). Furthermore, the presence of synaeresis or shrinkage cracks support the idea of large fluctuations in salinity (Burst, 1965). The rooted and mottled mudstone lithofacies are interpreted as paleosols or millisols (Retallack, 1988). The coal and carbonaceous mudstone lithofacies associated with the paleosols suggest deposition either in low-lying or well-drained mires. Retallack (1988) recognized this coal and carbonaceous mudstone lithofacies as a form of paleosol or histosol.

Upper Part of the Core

Lithofacies Associations and Sequences

The upper part of the core from 205–108 m is dominated by lithofacies sequences of erosional-based, fining-upward (medium to fine) sandstone (fig. 4*C*). The sandstone commonly displays branching *Thalassinoides*-like vertical burrows. The thick, fining-upward sandstones are found at 201–125 m. At these depths, the sandstones are commonly associated with

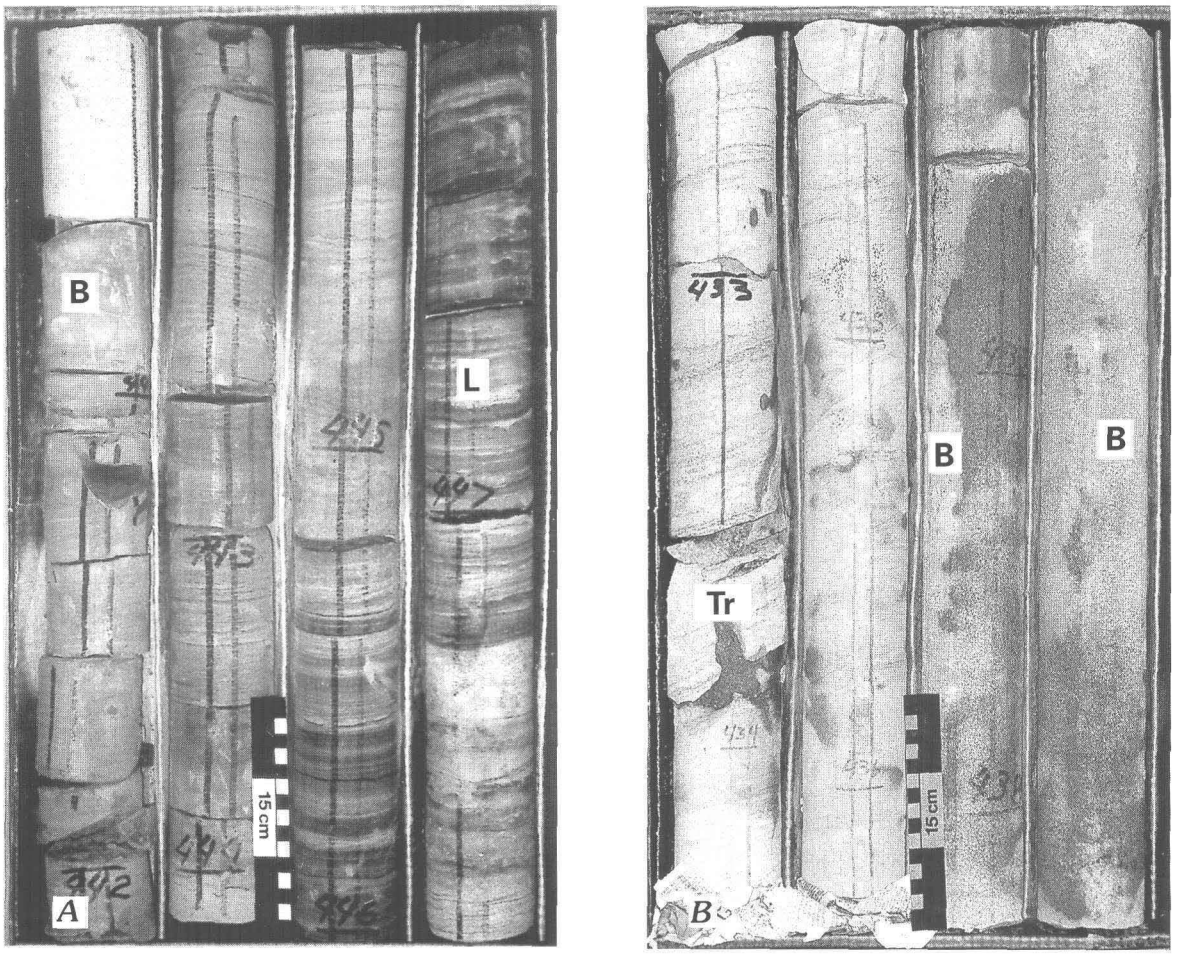

Figure 11. *A*, Burrowed mudstones and siltstones from 149.6–134.5 m, and *B*, sandstones containing trough crossbeds (Tr) and burrows (B) from 134.5–132.1 m. Numbers on core show depth in feet. To convert from feet to meters multiply by 0.304 (note centimeter scale on photo).

coarsening-upward lithofacies sequences of rippled ("starved") mudstones and burrowed, lenticular, flaser-bedded siltstones, and sandstones. In addition, thick coals and carbonaceous shales are interbedded with these lithofacies associations. Mudstones at 174.6 m and 202 m (above coals), analyzed by Nichols (1998) for palynomorphs, yielded the freshwater alga *Pediastrum* and common conifer pollen. Thin fining-upward sandstone lithofacies sequences are found at 120–117 m. Thin coal and rooted carbonaceous shales and mudstones cap the fining-upward sandstone lithofacies sequences. These lithofacies sequences are underlain by coarsening-upward lithofacies sequences of burrowed mudstones, and rippled siltstones and sandstones.

Interpretation

The thin to thick, fining-upward sandstone lithofacies sequences are interpreted as fluvial channels. Because these channels exhibit *Thalassinoides*-like burrows, it suggests reworking of the fluvial sediments by either crustaceanlike organisms typical of tidal-flat-like settings (Reineck, 1967) or some species of pelecypods (MacKenzie, 1975). The tidal influence may be indicated by the lenticular and flaser-bedded units. The coarsening-upward lithofacies sequences of mudstones, siltstones, and sandstones represent fluvial aggradational complexes (e.g., crevasse channels and splays) in subaqueous floodplain or freshwater lacustrine environments. Thus, the fluvial channels overlying these coarsening-upward lithofacies sequences may represent crevasse channels that were reoccupied by flow-through systems. The coal and carbonaceous shales and rooted mudstones are interpreted as mire and paleosol deposits on abandoned deposits of these flow-through channel systems. These mires were inundated by freshwater lakes, as indicated by the presence of the freshwater alga *Pediastrum*.

Summary and Conclusions

The Tyonek interval in the AK 94 CBM-1 well contains interbedded fluvial-dominated and tidallike lithofacies. The fluvial-dominated lithofacies are found in the lower and upper parts of the core. The tidallike lithofacies are found in the middle part of the core; however, tidallike lithofacies are associated with the fluvial-dominated lithofacies. These alternating fluvial-dominated and tidallike lithofacies are similar to lithofacies found in the Tyonek Formation in the Chuitna drainage basin described by Flores and others (1994, 1997).

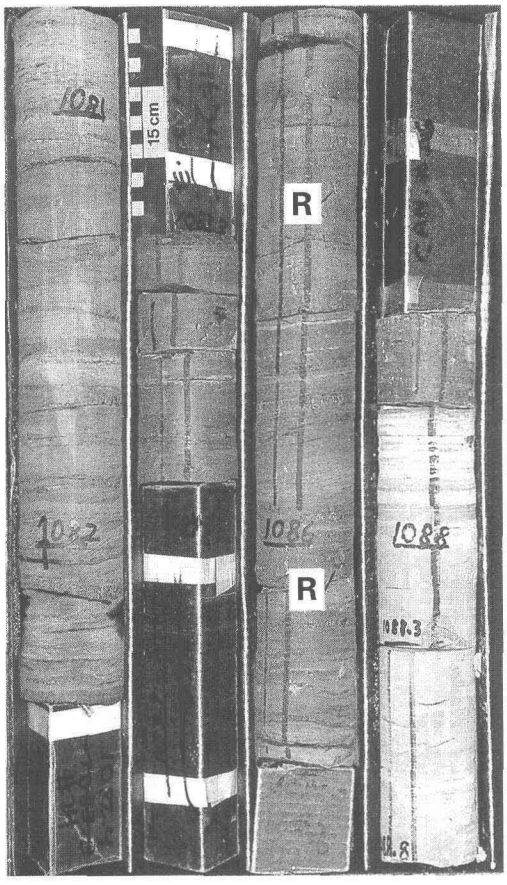

Figure 12. Siltstones and mudstones interbedded with carbonaceous shales and coals (removed for analysis) from 329.4 to 331.9 m. Mudstones are mainly rooted (R). *Numbers on core show depth in feet.* To convert from feet to meters multiply by 0.304 (note centimeter scale on photo).

The coal beds are mainly associated with the fluvial-dominated lithofacies. Here, the coal beds formed in freshwater mires developed mainly on abandoned fluvial channel belts and, subordinately, on distal flood plains. Paleosols and well-drained mires, forming only thin coal lenses, are associated with the tidallike lithofacies. The tidallike lithofacies are interpreted to form in intertidal-subtidal-like environments. Perhaps the most compelling characteristics of these tidallike lithofacies are the lenticular and flaserlike beds; foresets with reactivation surfaces; and rhythmic, mud-draped, bipolar ripple laminae. Associated trace fossils (*Thalassinoides*-like, *Chondrites*, *Teichicnus*, *Gyrolithes*, *Planolites*, and *Paleophycus*) and synaeresis cracks with these lithofacies support a brackish-marine influence (Burst, 1965; Pemberton and Wightman, 1992; Beynon and Pemberton, 1992). Subaqueous deposition is suggested by sedimentary structures that are laced with heavy bioturbation. The only subaqueous fluvial setting that is equivalent to a tidallike setting in which most of these sedimentary structures may be formed is possibly in a freshwater lacustrine setting with ebb-and-flow processes, possibly driven by wind storms.

The discovery of these Tyonek tidallike lithofacies near Wasilla and in the Chuitna River drainage basin (Flores and others, 1994, 1997) in the upper Cook Inlet suggests that the processes that formed them are more prevalent and widespread than originally thought. Another interpretation could be that tidallike processes in freshwater lakes in fluvial-dominated environments, particularly in the Cook Inlet Basin, have been overlooked. It is an enigma that these lithofacies have not been found associated with fluvial-dominated lithofacies of the Kenai Group during previous studies. The generally accepted paleogeographic reconstructions of the Tertiary Cook Inlet Basin may need to be revised with respect to the paleogeography and distribution of brackish-marine-influenced sedimentation. Thus, based on this study and previous work by Flores and others (1994, 1997), the estuarine and marine environments that existed during deposition of the Tyonek are probably found in the southern and central part of the Cook Inlet Basin.

Acknowledgments

This investigation is a cooperative work between the Alaska Department of Natural Resources, Oil and Gas Division and the U.S. Geological Survey. Lisa R. Bader and Allan M. Ochs of the U.S. Geological Survey assisted in drafting figures, and their work is appreciated. Assistance by Dr. John W. Reeder, Curator of the Alaska Geologic Materials Center, is appreciated for permission to describe the cores in their facilities. Appreciation is extended to Bo Henk of the University of Alberta and on sabbatical from ARCO, Anchorage, for identifying the trace fossils of the cores. Dr. Robert Blodgett of the University Oregon identified the unionid bivalve fossil.

References Cited

Adkison, W.L., Kelley, J.S., and Newman, K.R., 1975, Lithology and palynology of Tertiary rocks exposed near Capps Glacier and along Chuitna River, Tyonek quadrangle, southern Alaska: U.S. Geological Survey Open-File Report 75-21, 58 p., 1 plate.

Allen, J.R.L., 1965, Fining upward cycles in alluvial successions: Liverpool and Manchester Geological Journal, v. 4, p. 229–246.

Anonymous, 1990, Alaska's high-rank coals: Department of Natural Resources, Division of Geological and Geophysical Surveys, Information Circular 33, 36 p.

Barnes, F.F., and Payne, T.G., 1956, The Wishbone Hill district, Matanuska coal field, Alaska: U.S. Geological Survey Bulletin 1016, 88 p.

Best, J.L., and Bristow, C.S., 1993, Braided rivers: Geological Society Special Publication, 367 p.

Beynon, B.M., and Pemberton, S.G., 1992, Ichnological signature of a brackish water deposits: An example from the Lower Cretaceous Grand Rapids Formation, Cold Lake Oil Sands area, Alberta, *in* Pemberton, S.G., ed., Applications of Ichnology to Petroleum Exploration, A Core Workshop. SEPM (Society for Sedimentary Geology), p. 199–221.

Burst, J.F., 1965, Subaqueously formed shrinkage cracks in clay: Journal of Sedimentary Petrology, v. 35, p. 348–353.

Calderwood, K.W., and Fackler, W.C., 1972, Proposed stratigraphic nomenclature for Kenai Group, Cook Inlet basin, Alaska: American Association of Petroleum Geologists Bulletin, v. 56, p. 739–754.

Dickinson, K.A., and Campbell, J.A., 1978, Sedimentary facies in Tertiary rocks in the Tyonek quadrangle, *in* Geological Survey Research 1978: U.S. Geological Survey Professional Paper 1100, p. 84.

Dickinson, K.A., Campbell, J.A., and Dula, W.F., Jr.,1995, Geology, geochemistry, and uranium favorability of Tertiary continental sedimentary rocks in the northwestern part of the Cook Inlet area, Alaska: U.S. Geological Survey Bulletin 2098, p. B1–B37.

Doveton, J.H., 1994, Geologic log interpretation: Society of Economic Paleontologists and Mineralogists Short Course Notes No. 29, 169 p.

Evans, G., 1975, Intertidal flat deposits of the Wash, western margin of the North Sea, *in* Ginsburg, R.N., ed., Tidal Deposits—A Casebook of Recent Examples and Fossil Counterparts: New York, Springer-Verlag, p. 13–20.

Flores, R.M., and Johnson, S.Y., 1995, Sedimentology and lithofacies of the Eocene Skookumchuck Formation in the Centralia coal mine, southwest Washington, *in* Fritsche, A.E., ed., Cenozoic Paleogeography of the Western United States—II: Pacific Section, SEPM (Society for Sedimentary Geology), Book 75, p. 274–290.

Flores, R.M., and Stricker, G.D., 1993, Responses of coal splitting and associated drainage pattern to syntectonism in the Paleocene and Eocene Chickaloon Formation, Matanuska coalfield, Alaska, *in* Rao, P.D., and Walsh E., eds., Focus on Alaska's Coal 1993: Mineral Industry Research Laboratory, University of Alaska, p. 190–226.

Flores, R.M., Stricker, G.D., and Roberts, S.B., 1994, Miocene coal-bearing strata of the Tyonek Formation: Braided-stream deposits in the Chuit Creek–Chuitna River drainage basin, southern Alaska, *in* Till, A.B., and Moore, T.E., eds., Geologic Studies in Alaska by the U.S. Geological Survey, 1993: U.S. Geological Survey Bulletin 2107, p. 95–114.

Flores, R.M., Stricker, G.D., and Stiles, R.B., 1997, Tidal influence on deposition and quality of coals in the Miocene Tyonek Formation, Beluga coal field, upper Cook Inlet, Alaska, *in* Dumoulin, J.A., and Gray, J.E., eds., Geologic Studies in Alaska by the U.S. Geological Survey, 1995: U.S. Geological Survey Professional Paper 1574, p. 137–156.

Flores, R.M., and Sykes, R., 1996, Depositional controls on coal distribution and quality in the Eocene Brunner coal measures, Buller coalfield, South Island, New Zealand: International Journal of Coal Geology, v. 29, p. 291–336.

Galloway, W.E., 1968, Depositional systems of the lower Wilcox Group, north-central Gulf Coast Basin: Gulf Coast Association of Geological Society Transaction, v. 18, p. 275–289.

Hayes, J.B., Harms, J.C., and Wilson, T.W., 1976, Contrasts between braided and meandering stream deposits, Beluga and Sterling Formations (Tertiary), Cook Inlet, Alaska, *in* Miller, T.P., ed., Recent and Ancient Sedimentary Environments in Alaska: Anchorage, Alaska Geological Society Symposium Proceedings, p. J1–J27.

Hite, D.M., 1976, Some sedimentary aspects of the Kenai Group, Cook Inlet, Alaska, *in* Miller, T.P., ed., Recent and Ancient Sedimentary Environments in Alaska: Alaska Geological Society Symposium Proceedings: Anchorage, Alaska, p. I1–I22.

Johnsson, M.J., Howell, D.G., and Bird, K.J., 1993, Thermal maturity patterns in Alaska: Implications for tectonic evolution and hydrocarbon potential: American Association of Petroleum Geologists Bulletin, v. 77, p. 1874–1903.

Krynine, P.D., 1950, Petrology, stratigraphy and origin of the Triassic sedimentary rocks of Connecticut: Connecticut Geology and Natural History Survey, 239 p.

MacKenzie, D.B., 1975, Tidal sand flat deposits in Lower Cretaceous Dakota Group near Denver, Colorado, *in* Ginsburg, R.N., ed., Tidal Deposits—A Casebook of Recent Examples and Fossil Counterparts: New York, Springer-Verlag, p. 117–125.

McGee, D.C., 1972, Coal reserves, Beluga and Chuitna Rivers and Capps Glacier areas Alaska: Alaska Geological and Geophysical Surveys, 5 p., 3 plates.

Miall, A.D., 1996, The geology of fluvial deposits: sedimentary facies, basin analysis, and petroleum geology: New York, Springer-Verlag, 582 p.

Nichols, D.J., 1998, Report on samples from Tyonek Formation facies possibly deposited under marine influence: U.S. Geological Survey Administrative Report, 2 p.

Nio, S.D., and Yang, C., 1991, Diagnostic attributes of clastic tidal deposits—A review, *in* Smith, D.G., Reinson, G.E., Zaitlin, B.A., and Rahmani, R.A., eds., Clastic Tidal Sedimentology: Canadian Society of Petroleum Geology Memoir 16, p. 3–28.

Pemberton, S.G., and Wightman, D.M., 1992, Ichnological characteristics of brackish waster deposits, *in* Pemberton, S.G., ed., Applications of Ichnology to Petroleum Exploration, A Core Workshop: SEPM (Society for Sedimentary Geology), p. 141–167.

Reineck, H.E., 1967, Layered sediments of tidal flats, beaches, and shelf bottoms of the North Sea, *in* Lauff. G.H., ed., Estuaries: American Association of Advancement of Sciences, p. 191–206.

Reineck, H.E., and Wunderlich, F., 1968, Classification and origin of flaser and lenticular bedding: Sedimentology, v. 11, p. 99–104.

Reinson, G.E., 1989, Tide-influenced channel deposits in the Lower Cretaceous Glauconitic Member, southern Alberta, *in* Reinson, G.E., ed., Modern and Ancient Examples of Clastic Tidal Deposits—A Core and Peel Workshop: Calgary, Canadian Society of Petroleum Geologists, Second International Research Symposium on Clastic Tidal Deposits, Calgary, p. 98–104.

Retallack, G.J., 1988, Field recognition of paleosols, *in* Reinhardt, J., and Sigleo, W.R., eds., Paleosols and Weathering Through Geologic Time: Principles and Applications: Geological Society of America Special Paper 216, p. 1–20.

Selley, R.C., 1978, Ancient sedimentary environments: Ithaca, New York, Cornell University Press, 287 p.

Smith, T.N., 1995, Coalbed methane potential for Alaska and drilling results for the Upper Cook Inlet Basin: Intergas '95, May 15–19, 1995, Tuscaloosa, Alabama, University of Alabama, p. 1–21.

Smith, T.N., and Clough, J.G., 1993, Coalbed methane potential for Alaska: 1993 American Association of Petroleum Geologists Annual Convention Program Abstracts, p. 184.

Stricker, G.D., 1991, Economic Alaskan coal deposits, *in* Gluskoter, H.J., Rice D.D., and Taylor, R.B., eds., The Geology of North America: Economic Geology, U.S., v. P-2, p. 591–602.

Visser, M.J., 1980, Neap-spring cycles reflected in Holocene subtidal large-scale bedform deposits: A preliminary note: Geology, v. 8, p. 543–546.

Webb, E.K., 1994, Simulating the three-dimensional distribution of sediment units in braided stream deposits: Journal of Sedimentary Research, B64, p. 219–231.

Reviewers: P. Warwick, C. Keighin.

Geologic Studies in Alaska by the
U.S. Geological Survey, 1997
U.S. Geological Survey Professional Paper 1614

Lower Paleozoic Deep-Water Facies of the Medfra Area, Central Alaska[1]

By Julie A. Dumoulin, Dwight C. Bradley, Anita G. Harris, *and* John E. Repetski

Abstract

Deep-water facies, chiefly hemipelagic deposits and turbidites, of Cambrian through Devonian age are widely exposed in the Medfra and Mt. McKinley quadrangles. These strata include the upper part of the Telsitna Formation (Middle-Upper Ordovician) and the Paradise Fork Formation (Lower Silurian–Lower Devonian) in the Nixon Fork terrane, the East Fork Hills Formation (Upper Cambrian–Lower Devonian) in the East Fork subterrane of the Minchumina terrane, and the chert and argillite unit (Ordovician) and the argillite and quartzite unit (Silurian-Devonian? and possibly older) in the Telida subterrane of the Minchumina terrane.

In the western part of the study area (Medfra quadrangle), both hemipelagic deposits and turbidites are largely calcareous and were derived from the Nixon Fork carbonate platform. Eastern exposures (Mt. McKinley quadrangle; eastern part of the Telida subterrane) contain much less carbonate; hemipelagic strata are mostly chert, and turbidites contain abundant rounded quartz and lesser plagioclase and potassium feldspar. Deep-water facies in the Medfra quadrangle correlate well with rocks of the Dillinger terrane exposed to the south (McGrath quadrangle), but coeval strata in the Mt. McKinley quadrangle are compositionally similar to rocks to the northeast (Livengood quadrangle). Petrographic data thus suggest that the Telida subterrane as presently defined is an artificial construct made up of two distinct sequences of disparate provenance.

Restoration of 90 and 150 km of dextral strike-slip on the Iditarod and Farewell faults, respectively, aligns the deep-water strata of the Minchumina and Dillinger terranes in a position east of the Nixon Fork carbonate platform. This restoration supports the interpretation that lower Paleozoic rocks in the Nixon Fork and Dillinger terranes, and in the western part of the Minchumina terrane (East Fork subterrane and western part of the Telida subterrane), formed along a single continental margin. Rocks in the eastern part of the Telida subterrane are compositionally distinct from those to the west and may have had a different origin and history.

Introduction

Lower Paleozoic rocks deposited in deep-water, off-platform settings occur widely throughout central Alaska. In this paper we describe the lithofacies, biostratigraphy, depositional environments, and regional correlation of Upper Cambrian through Lower Devonian deep-water strata exposed in parts of the Medfra and Mt. McKinley 1:250,000 quadrangles (figs. 1, 2). These rocks have been variously correlated but have received little detailed study. They were assigned to the Nixon Fork and Minchumina terranes by Patton and others (1994) but were included in the White Mountain sequence of the Farewell terrane by Decker and others (1994).

The terminology used for lower Paleozoic rocks in central Alaska is confusing and contentious. Deep-water strata in the McGrath and Lime Hills quadrangles south of the Medfra area, considered part of the White Mountain sequence by Decker and others (1994), have also been called the Dillinger terrane (Jones and others, 1981; Silberling and others, 1994) or sequence (Gilbert and Bundtzen, 1984). Coeval platform facies in this area, called Nixon Fork terrane or sequence by other authors (Silberling and others, 1994; Gilbert and Bundtzen, 1984), are included by Decker and others (1994) in their White Mountain sequence. We agree with Decker and others (1994) that lower Paleozoic strata in their Farewell terrane probably formed along a single continental margin but find their terminology for subdivisions of the Farewell awkward and inadequate. In this paper we follow the terrane terminology of Silberling and others (1994) except where noted and refer to lower Paleozoic deep-water facies in the McGrath and Lime Hills quadrangles as the "Dillinger terrane" (fig. 1). We use terrane, however, in the older sense of the word to indicate a belt of related rocks and not as redefined (e.g., Jones and others, 1981) to require fault boundaries and imply "exotic" origins for these belts.

Our lithologic and biostratigraphic data indicate that lower Paleozoic deep-water facies of the Medfra quadrangle correlate relatively well with deep-water facies of the Dillinger terrane

[1] During field work in 1998, we discovered a previously unreported belt of Silurian-Devonian deep-water facies in the northeastern corner of the Medfra quadrangle. These rocks are described in Dumoulin, J.A., Bradley, D.C., and Harris, A.G., in press, Paleozoic strata of the Dyckman Mountain area, northeastern Medfra quadrangle, Alaska, *in* Kelley, K.D., and Gough, L.P., eds., Geologic Studies in Alaska by the U.S. Geological Survey, 1998: U.S. Geological Survey Professional Paper 1615.

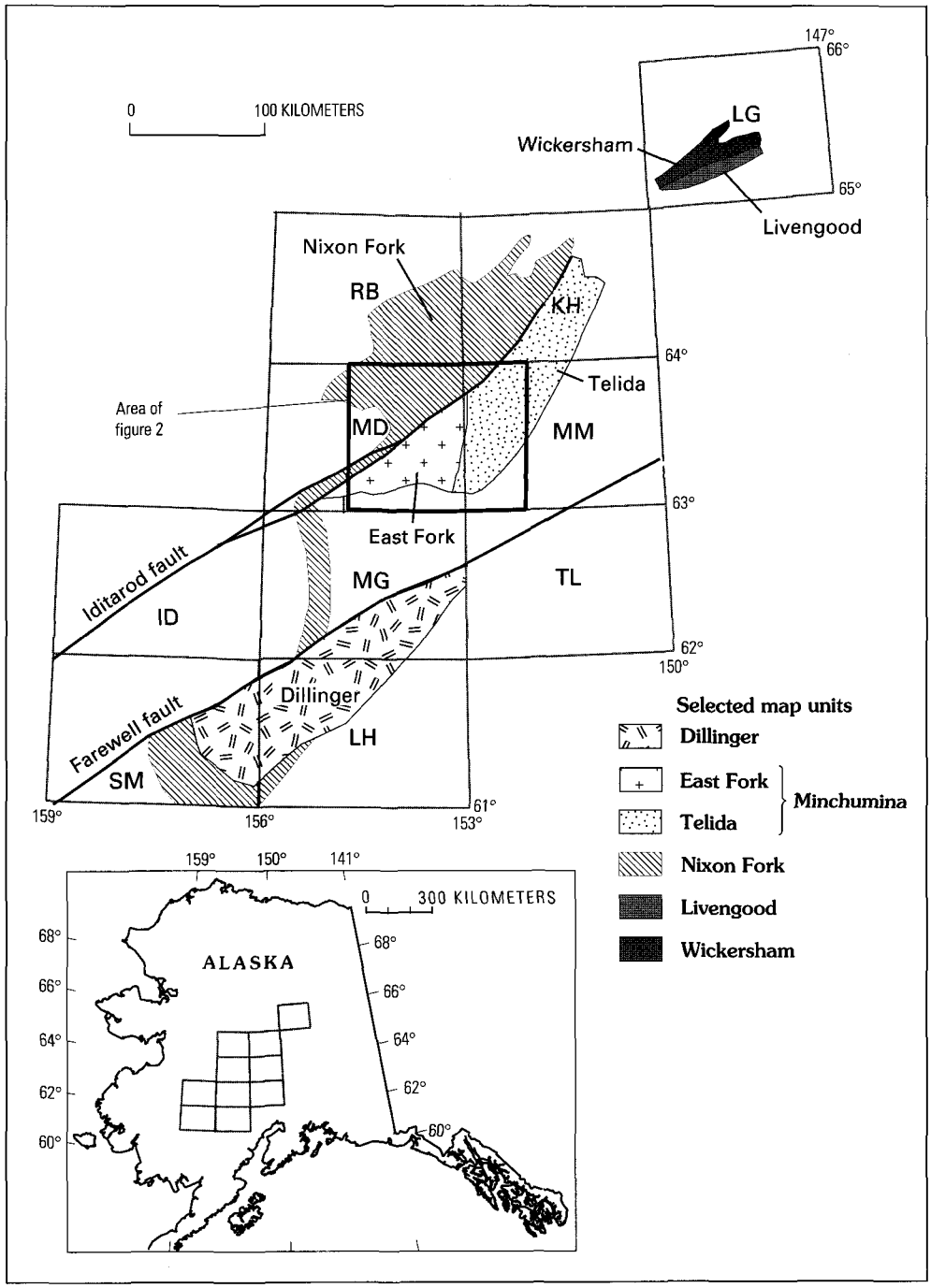

Figure 1. Location of quadrangles and selected tectonostratigraphic terranes and subterranes mentioned in text; East Fork and Telida are subterranes of Minchumina terrane. Dillinger and Nixon Fork south of lat 63°N. modified from Decker and others (1994) and Silberling and others (1994); East Fork, Nixon Fork north of lat 63°N., and Telida from Patton and others (1994); Livengood and Wickersham from Silberling and others (1994). The Farewell terrane of Decker and others (1994) includes the Nixon Fork, Minchumina, and Dillinger terranes shown here. Quadrangles: ID, Iditarod; KH, Kantishna River; LG, Livengood, LH, Lime Hills; MD, Medfra; MG, McGrath; MM, Mt. McKinley; RB, Ruby; SM, Sleetmute; TL, Talkeetna.

exposed to the south (McGrath quadrangle). Coeval deep-water strata in the Mt. McKinley quadrangle have stronger lithologic similarities to rocks of the Wickersham and Livengood terranes to the northeast (Livengood quadrangle).

Previous Work and Methods

Lower Paleozoic deep-water strata in the Medfra quadrangle were briefly described by Patton and others (1980) and Dutro

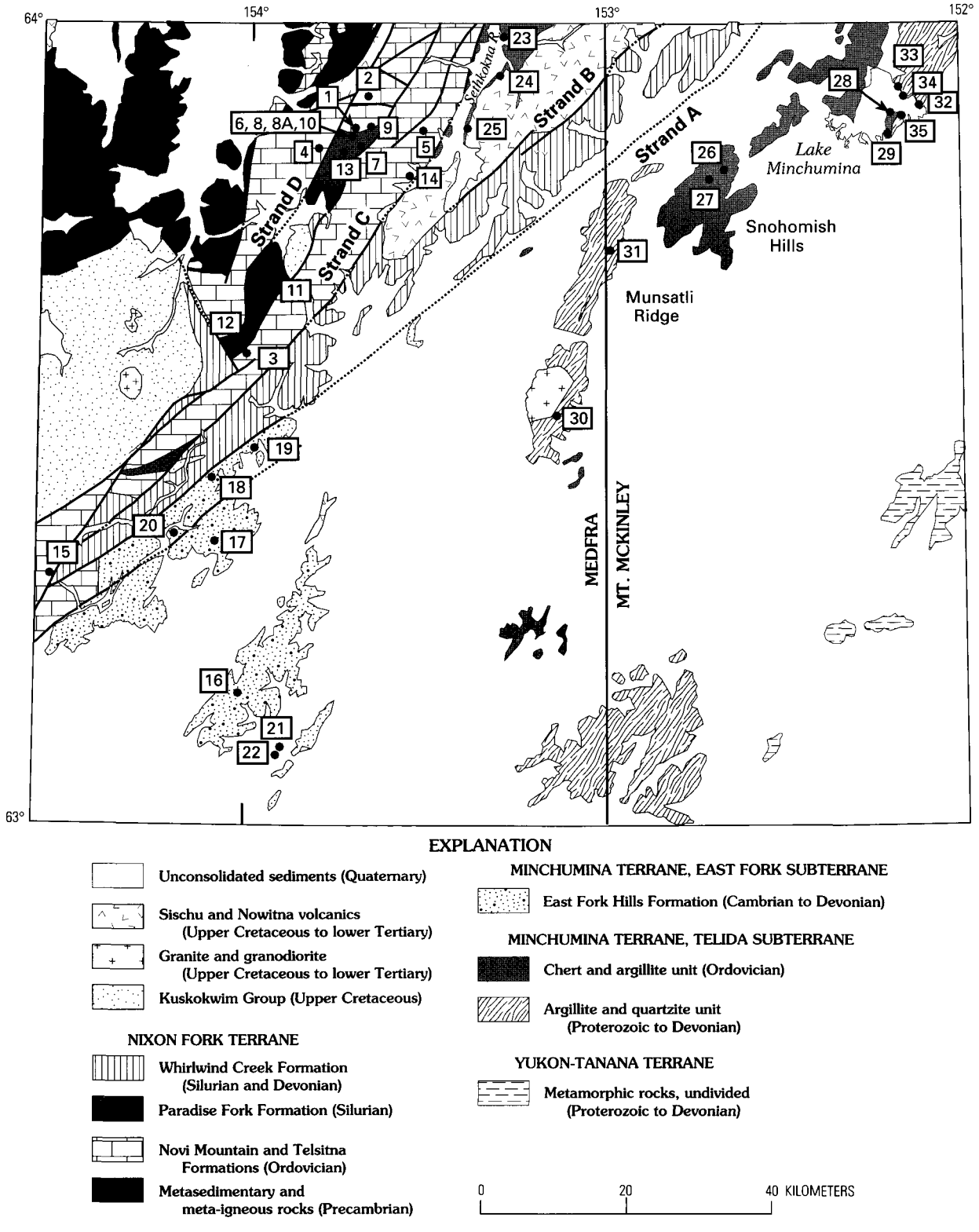

Figure 2. Location of lithologic and fossil collections and structural data from study area in Medfra (MD) and Mt. McKinley (MM) quadrangles. Geologic mapping from Patton and others (1980) (MD) and Wilson and others (1998) (MM). Letters A, B, C, and D refer to strands of the Iditarod fault system mentioned in text. Outcrops between Iditarod fault strands B and C shown here as chert and argillite unit were mapped as Pzc by Patton and others (1980). Novi Mountain and Telsitna Formations as shown include outcrops of Whirlwind Creek Formation too small to show at scale of map. Newly recognized deep-water facies mentioned in footnote on first page of this article are located between localities 25 and 31 in belt shown as Whirlwind Creek Formation.

and Patton (1982); sparse lithologic and fossil data from correlative rocks in the Mt. McKinley and Kantishna River quadrangles were reported by Chapman and others (1975), Chapman and Yeend (1981), Chapman and others (1981), and Patton and others (1994).

We examined lower Paleozoic rocks in the Medfra area at 36 localities. Microlithofacies were established through field observations and study of about 80 thin sections. Conodont age and biofacies determinations are based on 14 new collections and 13 older, unpublished collections reexamined for this paper (table 1). Interpretations of depositional environments follow models in Wilson (1975), Cook and others (1983), and Scholle and others (1983).

Lithofacies, Age, and Depositional Environment

Deep-water strata described here belong to three formations (Dutro and Patton, 1982) and several unnamed map units (Patton and others, 1980; Chapman and Yeend, 1981) that have been grouped into two terranes (Patton and others, 1994). We follow below the terrane terminology of Patton and others (1994) unless otherwise noted.

Nixon Fork Terrane

Precambrian through Mesozoic strata of the Nixon Fork terrane form a southwest-trending belt in the eastern and central Medfra quadrangle (fig. 1). Some 5,500 m of Ordovician through Devonian rocks in this terrane comprise a chiefly platform carbonate succession interrupted by an interval of deeper water facies. Four formations are recognized (Dutro and Patton, 1982); deep-water strata occur in the uppermost part of the Telsitna Formation (Ordovician) and throughout the Paradise Fork Formation (Silurian and Lower Devonian). The Novi Mountain Formation (Lower Ordovician) and the Whirlwind Creek Formation (Upper Silurian and Devonian) consist exclusively of shallow-water facies. In this report, we focus on deep-water facies within the lower Paleozoic succession. The Nixon Fork terrane is cut by a series of northeast-striking faults (Patton and others, 1980); details of stratigraphy, lithofacies, and thermal history differ across these faults, as will be detailed below.

Telsitna Formation

The Telsitna Formation consists of about 2,000 m of limestone and lesser dolostone (Dutro and Patton, 1982) deposited largely in supratidal to shallow subtidal settings (Measures and others, 1992). In a section just south of the type section (fig. 2, loc. 1), the uppermost part of the Telsitna is light-gray-weathering, dark-brownish-gray micrite, partly dolomitized, in 10- to 30-cm-thick beds. Stringers and nodules of tan, gray, or black chert, generally a few centimeters thick, parallel bedding. Bioherms a few meters across, made up of corals and (or) stromatoporoids, are locally abundant. These beds contain conodonts of probable Late Ordovician age deposited in a warm, shallow-water setting (table 1, loc. 1; fig. 3*A*). Lithologically similar strata comprise the upper part of the type section, 4.5 km to the north (fig. 2, loc. 2). Conodonts near the top of this section are early Late Ordovician (middle Edenian–early Maysvillian) and indicate a tropical, shallow-water environment (table 1, loc. 2). Corals and brachiopods in the uppermost beds in this section are also of Maysvillian age (Dutro and Patton, 1982).

Distinctly different facies, however, characterize the uppermost Telsitna Formation in an elongate fault block southeast of the type section (fig. 2, loc. 3). In this area, several hundred meters of dark-gray-weathering, grayish-black micrite, in platy to irregular beds a few millimeters to 20 cm thick, forms the top of the Telsitna. Subordinate silt- to sand-sized clasts are disseminated throughout this micrite and are locally concentrated into graded layers a few millimeters thick. Clasts include peloids, calcitized radiolarians, and calcareous and siliceous sponge spicules (some radiolarians and spicules are pyritized) (figs. 3*B*, 3*C*). A few samples contain fragments of pelmatozoans, brachiopods, ostracodes, trilobites, and possible algae. These beds produced three conodont collections; the most diagnostic samples are very latest Ordovician (table 1, loc. 3; figs. 4*M*–4*AA*). All collections are distal winnows deposited in a deep-shelf to basinal setting.

Conodonts indicative of a deep-water depositional environment were also recovered from the upper part of the Telsitna Formation in fault blocks west and east of the type area (table 1, locs. 4, 5). Strata at both localities are fine-grained, brownish-gray, locally bioclastic limestone. The western collection (loc. 4) is late Middle Ordovician; the eastern faunule (loc. 5) is correlative or slightly younger.

Lithologic and paleontologic data thus demonstrate that different sections of the uppermost Telsitna Formation are not precisely coeval and formed in distinctly different depositional environments. Upper Ordovician strata in and south of the type section (table 1, locs. 1 and 2) accumulated in a shallow-water, inner-shelf or platform setting. The slightly younger section at locality 3 consists of hemipelagic sediment derived from a carbonate platform but deposited in a slope or basin environment. Sections at localities 4 and 5 appear intermediate between these two extremes and probably formed in an outer-shelf or outer-platform setting.

Telsitna Formation conodonts from locality 3 have notably higher color alteration indices (CAI's) than do those from the type area (4.5 vs. 2 and 3.5). Similarly sharp contrasts in conodont CAI's from correlative strata occur in other parts of the Nixon Fork terrane (Savage and others, 1995; A.G. Harris and J.E. Repetski, unpub. data, 1997). CAI contrasts—along with the differences in lithofacies, age, and depositional environment documented above—suggest that discrete fault blocks in the Medfra quadrangle preserve fragments of the Nixon Fork platform with divergent depositional and thermal histories. These differences are not confined to Upper Ordovician rocks, as will be seen below.

Paradise Fork Formation

The Paradise Fork Formation is a sequence of dark-gray, thin-bedded limestone and black shale that forms a southwest-trending, 40-km-long synform through the northeastern part of

Table 1. Conodont data for localities shown on figure 2.

[Localities discussed in text but not sampled for conodonts not listed below. Letters in field number refer to collector: AD, J.A. Dumoulin; ADw, D.C. Bradley; APa, W.W. Patton, Jr. and (or) J.T. Dutro, Jr. Abbreviations: CAI, color alteration index; indets., indeterminate bar, blade, platform, and coniform fragments]

Locality no., (terrane or subterrane; unit)	Quadrangle latitude/ longitude	Conodont fauna and CAI [field no.; USGS collection no.]	Age	Biofacies	Remarks
1 (Nixon Fork; Telsitna Fm.)	Medfra D-2 63°51.90' 153°43.18'	3 belodinids of probable Late Ordovician morphotype 7 *Panderodus gracilis* (Branson & Mehl) 1 unassigned coniform CAI=2 [97AD14B; 11504-CO]	Middle-Late Ordovician, probably Late Ordovician on the basis of the belodinid morphotype.	Indeterminate (too few conodonts); probably, warm, shallow-water depositional environment.	Medium-gray-weathering, light-gray, fine-grained dolostone containing abundant colonial corals. Sample weight 8.8 kg.
2 (Nixon Fork; Telsitna Fm.)	Medfra D-2 63°54.50' 153°40.50'	1 belodinid 1 *Culumbodina occidentalis* Sweet 1 *Drepanoistodus* sp. indet. 1 *Panderodus* sp. 4 indet. coniform fragments CAI=3.5 [79APa99a; 11524-CO]	Age is middle Edenian-early Maysvillian (early-middle Late Ordovician), probably early Maysvillian because corals and brachiopods from this interval indicate a Maysvillian age.	Indeterminate (too few conodonts). Conodonts are indicative of a tropical shallow-water depositional setting. *C. occidentalis* is the most biostratigraphically diagnostic element and a component of the western North American Midcontinent province.	Thick-bedded limestone at ~5,700 ft. above base of type section.
3 (Nixon Fork; Telsitna Fm.)	Medfra C-3 63°35.89' 154°01.76'	1 ozarkodinid P element (fig. 4V) 36 *Panderodus* sp. *Paroistodus*? n. sp. A of Nowlan and others, 1988 28 M & 46 S elements (figs. 4O-S) *Periodon grandis* (Ethington)? 1 Pa, 1 M & 2 Sc elements (figs. 4W-Y) 4 *Pseudooneotodus mitratus* (Moskalenko) (figs. 4M, N) 13 indet. fragments 6 *Strachanognathus parvus* Rhodes (figs. 4T, U) CAI=4.5 [97AD34A; 11510-CO)	Age is late Middle-middle Late Ordovician, probably Late Ordovician on the basis of the morphology of the ozarkodinid P element.	Paroistodid-panderodid biofacies: faunule represents a distal (deep shelf to basinal) winnow. Cosmopolitan and (or) cool-water faunule.	Dark-gray-weathering, grayish-black micrite in irregular 20-cm beds; contains graded laminae of peloids and bioclasts (chiefly calcitized radiolarians and calcareous and pyritized sponge spicules, lesser pelmatozoan and brachiopod fragments). Sample weight 10.4 kg.

Table 1. Conodont data for localities shown on figure 2---*Continued.*

Locality no., (terrane or subterrane; unit)	Quadrangle latitude/ longitude	Conodont fauna and CAI [field no.; USGS collection no.]	Age	Biofacies	Remarks
3 (cont.) (Nixon Fork; Telsitna Fm.)	Medfra C-3 63°35.89' 154°01.80'	1 Pb *Ozarkodina hassi* (Pollock, Rexroad & Nicoll)? (fig. 4AA) 12 juvenile *Panderodus* spp. 4 M elements *Paroistodus* sp. 1 unassigned multidenticulate Sc element 5 indet. fragments 3 scolecodont fragments 2 *Ptiloncodus simplex* Harris (not a conodont; fig. 4Z) CAI=4.5. [97ADw124A;11515-CO]	Age is very latest Late Ordovician	Indeterminate; because all conodonts are extremely small, the faunule undoubtedly represents a distal winnow. The entire fauna (ostracodes, trilobite fragments [including spines], and probable radiolarians) suggests a slope or basin depositional setting.	Subcrop of dark micrite, beds 2-10 cm thick; contains graded laminae of peloids and bioclasts (chiefly calcitized radiolarians and calcareous and siliceous sponge spicules, lesser ostracodes and pelmatozoan fragments). A few hundred meters west of 97AD34. Heavy-mineral concentrate includes ferruginous hollow spines, spine steinkerns, phosphatized tubes, and lesser phosphatized ostracode carapaces (mostly smooth forms), phosphatic brachiopod fragments, composite small phosphatic grains, possible minor radiolarians, and rare trilobite fragments. Sample weight 7.5 kg.
		2 *Dapsilodus* sp. 1 M *Paroistodus* sp. indet. *Ozarkodina sesquipedalis* Nowlan & McCracken 1 Pa (fragment), 1 Pb & 1 Sb elements 2 *Panderodus* sp. 7 indet. fragments CAI=4.5 [76APa58; 8680-CO]	Age is very latest Ordovician	Indeterminate (too few conodonts). The only other reported occurrence of *O. sesquipedalis* is 50-74 m below the Ordovician-Silurian boundary in two sections in the Mackenzie Mountains, Northwest Territories (Nowlan and others, 1988); these sections are Selwyn basin margin facies near the platform edge. The conodonts are more typical of outer shelf facies, however, and were probably hydraulically transported basinward.	Dark-gray to black, very fine grained, thin-bedded to platy limestone. Same general locality as 97AD34 and 97ADw124. Sample weight 2 kg.

Table 1. Conodont data for localities shown on figure 2—*Continued.*

Locality no., (terrane or subterrane; unit)	Quadrangle latitude/ longitude	Conodont fauna and CAI [field no.; USGS collection no.]	Age	Biofacies	Remarks
4 (Nixon Fork; Telsitna Fm.)	Medfra D-2 63°50.42' 153°49.33'	1 *Belodina compressa* (Branson & Mehl) 1 juvenile *Belodina* sp. 2 *Paroistodus* sp. 2 *Drepanoistodus* sp. 10 *Panderodus unicostatus* (Branson & Mehl) 2 *Paroistodus* sp. *Periodon aculeatus* Hadding 3 Pa, 4 M, 1 Sb & 4 Sc element fragments 1 *Staufferella* sp. 1 *Strachanognathus parvus* Rhodes 6 unassigned coniform fragments and juveniles CAI=3.5 [76APa34A; 8660-CO]	Age is late Middle Ordovician; *B. compressa* Zone (late Blackriveran, late early Caradocian)	Mixed biofacies but chiefly pelagic realm cosmopolitan (e.g., *Periodon, Dapsilodus, Strachanognathus*)), pandemic (*Panderodus*), and rare tropical cosmopolitan (*Belodina*) taxa. Rock probably represents outer shelf or off-shelf depositional setting.	Light-gray to brownish-gray, thin-bedded, fine-grained limestone. Sample weight 2 kg.
4 (Nixon Fork; Whirlwind Creek Fm.?)	Medfra D-2 63°52.11' 153°50.32'	*Ozarkodina confluens* (Branson & Mehl) 6 Pa, 1 Pb, 1 M, 1 Sa, 1 Sb & 1 Sc elements digyrate apparatus (oulodid?) 2 Pb element fragments 17 indet. fragments CAI=2.5-3 [97ADw143B; 12599-SD]	Ludlovian-Pridolian (Late Silurian and probably not early Ludlovian)	Indeterminate (too few conodonts); *O. confluens* as well as the amphiporids suggest at least partial restriction.	*Amphipora*-bearing dolostone and dolomicrite rubble. Patton and others (1980) mapped these rocks as Od, but the conodonts indicate Whirlwind Creek Formation. 2 km northwest of, and apparently overlying, 76APA34A. Sample weight 9.5 kg.
5 (Nixon Fork; Telsitna Fm.)	Medfra D-2 63°51.50' 153°31.33'	8 *Belodina? repens* Moskalenko s.f. 5 juvenile belodinids 2 M elements *Drepanoistodus* sp. 13 *Panderodus* sp. 6 *Plectodina? tunguskaensis* (Moskalenko) 1 unassigned Pb element CAI=3.5 [76APa39; 8679-CO]	Age is late Middle-Late Ordovician, possibly Late Ordovician	Indeterminate; likely a distal winnow into deeper water facies. The species association is chiefly Siberian-Alaskan with minor pandemics.	Massive-bedded, brownish-gray, fine-grained to finely crystalline limestone containing gastropods, trilobites, and cephalopods of probable Ordovician age. Sample weight 2 kg.

Table 1. Conodont data for localities shown on figure 2—*Continued.*

Locality no., (terrane or subterrane; unit)	Quadrangle latitude/ longitude	Conodont fauna and CAI [field no.; USGS collection no.]	Age	Biofacies	Remarks
6 (Nixon Fork; Paradise Fork Fm.)	Medfra D-2 63°51.80' 153°43.08'	120 *Panderodus unicostatus* (Branson & Mehl) *Ozarkodina excavata* (Branson & Mehl) 1 Pa, 1 Pb & 2 Sc elements *Pterospathodus procerus* (Walliser) (figs. 4NN-PP) 7 Pa & 2 Pb elements 5 indet. fragments CAI=2.5 [97ADw103; 12598-SD]	*Pt. celloni* Zone into *K. ranuliformis* Zone (= late Llandoverian-very early Wenlockian; = middle Early Silurian)	Panderodid biofacies: postmortem transport from or within a mid shelf or slope depositional setting.	Dark-gray, finely laminated, fissile micrite. Overlies 97AD14 (loc. 1) and underlies 97AD13C (loc. 8); near base of formation. Same general locality as 77APa112 (table 2). Heavy-mineral concentrate includes pyritized sponge spicules. Sample weight 7.9 kg.
7 (Nixon Fork; Paradise Fork Fm.)	Medfra D-2 63°50.92' 153°41.33'	1 incomplete, robust, hyaline, coniform-like Sc element of Middle Ordovician-Silurian morphotype CAI=2 or 3 [97AD8B]	Middle Ordovician-Silurian	Indeterminate (too few conodonts).	Light-gray-weathering, grayish-black, fine-grained limestone in beds 2-5 cm thick, with graded laminae of silt- to sand-sized micritic clasts. Upper part of unit. Heavy-mineral concentrate includes minor schistose (chloritic-muscovitic) lithoclasts. Sample weight 9.7 kg.
8 (Nixon Fork; Paradise Fork Fm.)	Medfra D-2 63°51.67' 153°43.08'	*Kockelella patula* Walliser 1 Pa, 1 Pb & 1 Sb elements (figs. 4QQ-SS) 2 unassigned Sc (2 morphotypes) elements 4 indet. fragments CAI=2 [97AD13; 12594-SD]	*K. patula* Zone (= *K. ranuliformis* + *K. amsdeni* Zones of Barrick and Klapper, 1976). *K. patula* has been found with *Cyrtograptus rigidus* Zone graptolites in the Carnic Alps (Jaeger, 1975). Kleffner (1995), on the basis of graphic correlation, indicates the range of *K. patula* is within the *C. lundgreni* Zone which, according to him, occupies most of the middle Wenlockian.	Indeterminate (too few conodonts); the kockelellids were derived from a shelf or platform depositional environment. *K. patula* is common in Europe but rare in North America.	Medium-gray-weathering, grayish-black, finely laminated micrite with minor calcitized radiolarians. Several hundred meters stratigraphically above 97ADw103 (loc. 6). Heavy-mineral concentrate includes minor schistose (chloritic-muscovitic) lithoclasts. Sample weight 9.7 kg.

Table 1. Conodont data for localities shown on figure 2—*Continued.*

Locality no., (terrane or subterrane; unit)	Quadrangle latitude/ longitude	Conodont fauna and CAI [field no.; USGS collection no.]	Age	Biofacies	Remarks
8A (Nixon Fork; Paradise Fork Fm.)	Medfra D-2 63°51.50' 153°42.50'	7 juvenile *Dapsilodus* sp. indet. elements 1 juvenile Sb? element *Oulodus*? sp. indet. 1 Pa element fragment *Ozarkodina excavata* (Branson & Mehl)? 1 *Panderodus unicostatus* (Branson & Mehl) element 1 juvenile Pa element *Polygnathus* sp. indet. of late Emsian or younger Devonian morphotype 1 *Pseudooneotodus bicornis* Drygant element CAI=2-2.5 [98ADw206; 12616-SD]	Conodonts in this sample represent two ages: late Llandoverian to at least latest Ludlovian (*Ps. bicornis*) and late Emsian or even younger Devonian (juvenile polygnathid). *Ps. bicornis* has recently been shown to range at least into the *Oz. remscheidensis* Zone in Sardinia (Corradini and others, 1998); until the Sardininian report the species had not been reported above the Wenlockian (Kleffner, 1995). About 20% of the slabs in 98ADw206 contained the graptolite *Monograptus uniformis* of early Lochkovian age (table 2). We interpret this sample as a mix of Llandoverian-Ludlovian, early Lochkovian, and late Emsian (or younger Devonian) weakly laminated limestones.	Indeterminate (too few conodonts); those that are present are mainly extremely small coniform elements that indicate a distal winnow. The conodonts and graptolites from this collection indicate mixed ages, making the sample ineligible for biofacies analysis.	Dark gray, weakly laminated calcisiltstone with rare micrite clasts and small fossil fragments. Sample weight 8.1 kg. Heavy-mineral concentrate includes minor metacarbonate rock fragments (talc-actinolite-tremolite) and rare phosphatic brachiopod fragments.
11 (Nixon Fork; Paradise Fork Fm.)	Medfra C-2 63°40.33' 153°57.52'	*Kockelella* sp. indet. or another Silurian digyrate apparatus 3 Pb, 3 M & 2 Sb elements CAI=2.5-3 [77APa130; 9145-CO]	Silurian, late Llandoverian into late Ludlovian	Indeterminate (too few conodonts). Normal-marine depositional setting.	Brownish-gray limestone. Sample weight 2.5 kg.
12 (Nixon Fork; Paradise Fork Fm.)	Medfra C-3 63°37' 154°00.75'	3 *Panderodus* sp. 10 indet. coniform fragments CAI=4.5 [77APa134; 9146-CO]	Middle Ordovician-Silurian (other coniform elements are not Devonian morphotypes)	Indeterminate (too few conodonts).	Light-brownish-gray limestone. Sample weight 2.7 kg.

Table 1. Conodont data for localities shown on figure 2—*Continued.*

Locality no., (terrane or subterrane; unit)	Quadrangle latitude/ longitude	Conodont fauna and CAI [field no.; USGS collection no.]	Age	Biofacies	Remarks
13 (Nixon Fork; Whirlwind Creek Fm.)	Medfra D-2 63°50.23' 153°44.47'	BARREN [97AD12]			Thick-bedded to massive, light-gray, vuggy dolostone, locally cherty, with molds of brachiopods(?), underlies *Amphipora*-bearing dolostone. Mapped by Patton and others (1980) as Paradise Fork Formation [Sls] but represents shallow-water facies. Lies just above Sls. Sample weight 9.1 kg.
	Medfra D-2 63°50.08' 153°45.30'	1 *Dapsilodus* sp. element 2 Sb elements of "*Ligonodina*" *confluens confluens* of Jeppsson (1972) *Ozarkodina confluens* (Branson & Mehl) (at least 3 morphotypes) 19 Pa, 7 Pb, & 2 Sb elements *Ozarkodina excavata* (Branson & Mehl) 1 Sa and 1 Sb elements 4 *Panderodus unicostatus* (Branson & Mehl) elements CAI=2.5 [98ADw211; 12617-SD]	Late Silurian; within *A. ploeckensis* Zone to very high in the *Oz. remscheidensis* Zone (middle Gorstian [=within early Ludlovian] to within the late Pridolian)	Ozarkodinid biofacies; these conodonts were deposited in the shallow part of the ozarkodinid biofacies, as *Oz. confluens* is chiefly a shallow-water species.	Thick-bedded, finely crystalline dolostone; 1 km west of, and at a stratigraphic level close to, 97AD12. Sample weight 10.3 kg.
14 (Nixon Fork; Whirlwind Creek Fm.)	Medfra D-2 63°48.80' 153°33.27'	1 Pb element fragment *Oulodus* sp. indet. *Ozarkodina remscheidensis* (Ziegler) 8 Pa elements (mostly incomplete) *Ozarkodina confluens* (Branson & Mehl) or *Pandorinellina optima* (Moskalenko) 7 Pa elements (mostly incomplete) *Ozarkodina* spp. indet. 2 Pa, 3 Pb (2 morphotypes), 4 M, 2 Sa, 10 Sb & 5 Sc elements 99 chiefly incomplete *Panderodus* spp. elements 174 indet. fragments CAI=4	Age is late Ludlovian-Pridolian (Late but not earliest Late Silurian) or late Lochkovian (late early Early Devonian); probably the Silurian range because of the variety of *O. remscheidensis* morphotypes and because the 7 Pa elements attributed to either *O. confluens* (a Late Silurian species) or *Pa. optima* (a late Lochkovian species) are more like *O. confluens.*	Panderodid biofacies; the panderodids and the type of ozarkodinids indicate a shallow-water depositional setting. The abundant but chiefly broken conodonts indicate a high-energy setting.	Skeletal packstone in 3-20 cm beds; about 2-3 m of section here. Mapped by Patton and others (1980) as Telsitna Ridge Formation [Od], but the conodonts suggest this sample is from the Whirlwind Creek Formation. Strata appear to overlie Od. Sample weight 9.9 kg.

Table 1. Conodont data for localities shown on figure 2—*Continued.*

Locality no., (terrane or subterrane; unit)	Quadrangle latitude/ longitude	Conodont fauna and CAI [field no.; USGS collection no.]	Age	Biofacies	Remarks
15 (Nixon Fork; Whirlwind Creek Fm.)	Medfra B-4 63°18.67' 154°34.17'	*Oulodus* n. sp. 2 Pa, 1 Pb, 4 Sa, 2 Sb & 2 Sc elements (distinctive oulodid with outer lower margin of cusp extended as prong on the Pa, Sa & Sb elements) *Ozarkodina confluens* (Branson & Mehl)? 1 Pa, 2 Pb, 3 M, 1 Sa & 6 Sc elements 4 indet. fragments CAI=3.5 [79APa82B; 11994-SD]	Wenlockian-middle Pridolian (late Early-Late, but not latest, Silurian.)	Oulodid-ozarkodinid biofacies: shallow-water, relatively high energy depositional setting.	Limestone in thrust sheet at Limestone Hill, mapped as Telsitna Formation [Od] by Patton and others (1980). Sample weight 6.0 kg.
16 (East Fork; East Fork Hills Fm.)	Medfra A-3 63°09.25' 154°02.29'	2 *Cordylodus proavus* Müller 1 *Hirsutodontus hirsutus* Miller 2 indet. coniform elements CAI=5 [97AD30B; 11508-CO]	Age is latest Late Cambrian (*Co. proavus* Zone through succeeding *Co. intermedius* Zone)	Indeterminate (too few conodonts).	Subcrop of medium-gray-weathering, medium-gray, fine-grained limestone in beds 0.5 to 5 cm thick with grayish-orange dolomitic layers, parallel- and cross-laminated. Minor quartz and plagioclase silt. Type section of East Fork Hills Formation. Heavy-mineral concentrate includes muscovite, lithoclasts, and rare phosphatic brachiopod fragments. Sample weight 7.5 kg.
		3 indet. coniform elements CAI=4.5 [D8-26]	Age is latest Cambrian-Devonian	Indeterminate (too few conodonts).	Schistose limestone. Same general locality as 97AD30B. Sample weight 2.9 kg.

Table 1. Conodont data for localities shown on figure 2—*Continued.*

Locality no., (terrane or subterrane; unit)	Quadrangle latitude/ longitude	Conodont fauna and CAI [field no.; USGS collection no.]	Age	Biofacies	Remarks
17 (East Fork; East Fork Hills Fm.)	Medfra B-3 63°21.10' 154°06.44'	Many conodonts are deformed. 31 *Cordylodus proavus* Müller (fig. 4D) 9 *Eoconodontus notchpeakensis* (Miller) (fig. 4E) 22 *Hirsutodontus hirsutus* Miller (figs. 4A-C) 57 *Teridontus nakamurai* (Nogami) (fig. 4F) 109 indet. and unassigned fragments CAI=5-5.5 [97AD32C; 11509-CO]	Age is latest Late Cambrian *(Co. proavus* Zone through succeeding *Co. intermedius* Zone)	Cordylodid biofacies: fauna includes chiefly open-marine pandemic forms (cordylodids, teridontids, and eoconodontids) and minor tropical cosmopolites (*H. hirsutus*). Outer shelf or deeper depositional setting.	Good outcrop of gray- and yellow-weathering, very fine grained limestone in mm to 8-cm beds with parallel- and cross-laminations and climbing ripples. Silty laminae contain dolomite, quartz, plagioclase, white mica, and metamorphic lithic clasts. Sample weight 9.3 kg.
		1 *Cordylodus proavus* Müller 1 *Teridontus nakamurai* (Nogami) CAI=about 5 [P5-27; 8841-CO]	Age is latest Cambrian-very early Early Ordovician	Indeterminate (too few conodonts); conodonts are pandemics but would not likely occur in restricted shallow-water marine deposits.	Silty limestone. Same general locality as 97AD32C. Sample weight 2.8 kg.
18 (East Fork; East Fork Hills Fm.)	Medfra B-3 63°25.99' 154°07.40'	*Ansella* sp. indet. 1 Pa, 1 M, 1 Sb & 1 Sc elements 2 *Belodina* sp. 3 *Drepanoistodus* sp. *Erraticodon balticus* Dzik 1 Pa, 2 M, 2 Sb & 1 Sc elements 13 *Panderodus* sp. 2 *Paroistodus? mutatus* (Rhodes) *Periodon aculeatus* Hadding 25 Pa, 8 Pb, 51 M, 7 Sa, 26 Sb & 27 Sc elements 33 *Protopanderodus* cf. *P. varicostatus* (Sweet & Bergström) *Pygodus anserinus* Lamont & Lindström 3 P & 20 S elements 1 *Spinodus ramosus* (Hadding) 57 indet. fragments CAI=4.5 [97AD29C; 11507-CO]	*Pygodus anserinus* Zone (middle Middle Ordovician)	Periodontid-protopanderodid biofacies: slope to basinal depositional setting.	Medium-gray-weathering, dark-gray, fine-grained limestone in 2- to 5-cm beds that are delineated by orange silty laminae; interbedded with tan-weathering, dark-gray to black cherty argillite. Limestone contains 5-15% bioclasts, mostly radiolarians (some calcitized) and lesser pelmatozoan fragments. Heavy-mineral concentrate includes phosphatized grains and bioclasts and phosphatic brachiopod fragments. Sample weight 9.7 kg.

Table 1. Conodont data for localities shown on figure 2—*Continued.*

Locality no., (terrane or subterrane; unit)	Quadrangle latitude/ longitude	Conodont fauna and CAI [field no.; USGS collection no.]	Age	Biofacies	Remarks
19 (East Fork; East Fork Hills Fm.)	Medfra B-3 63°28.28 153°59.80'	1 *Panderodus* sp. indet. CAI=indet. [97AD28A]	Middle Ordovician-Middle Devonian	Indeterminate (too few conodonts).	Medium-gray-weathering, medium-dark-gray, fine-grained limestone in 1- to 2-cm beds with yellow, dolomitic, peloidal laminae. Sample weight 9.7 kg.
		1 juvenile belodinid 1 juvenile *Panderodus* sp. indet. CAI=6-6.5 [D7-24; 8861-CO]	Age is early, but not earliest, Middle and Late Ordovician	Indeterminate (too few conodonts); postmortem winnow.	Medium-dark-gray limestone. Same general locality as 97AD28A. Sample weight 3.0 kg.
20 (East Fork; East Fork Hills Fm.)	Medfra B-3 63°21' 154°13'	3 small coniform elements of an icriodid(?) or an Early Ordovician coniform apparatus CAI=4.5-5 [78ADu24; 9977-SD]	Ordovician-Devonian	Indeterminate (too few conodonts); distal winnow.	Sample weight 3.2 kg.
21 (East Fork; East Fork Hills Fm.)	Medfra A-2 63°05.77' 153°53.83'	3 coniform elements Late Ordovician-earliest Devonian morphotype 1 P element fragment of Silurian-Devonian morphotype CAI=5.5 [76APa112; 9731-SD]	Silurian-early Early Devonian	Indeterminate (too few conodonts); normal-marine depositional setting.	Dark-gray, laminated, fine-grained limestone.
22 (East Fork; East Fork Hills Fm.)	Medfra A-2 63°05.13' 153°54.45'	1 Pa *Eognathodus* cf. *E. sulcatus* (Philip) 1 Pa *Ozarkodina* sp. indet. CAI=5.5 [78ADu27; 9978-SD]	Pragian (middle Early Devonian)	Indeterminate (too few conodonts); normal-marine depositional setting.	Sample weight 2 kg.

Table 1. Conodont data for localities shown on figure 2—*Continued.*

Locality no., (terrane or subterrane; unit)	Quadrangle latitude/ longitude	Conodont fauna and CAI [field no.; USGS collection no.]	Age	Biofacies	Remarks
23 (Telida; chert and argillite unit)	Medfra D-1 63°59.17' 153°17.67'	2 *Cordylodus intermedius* Furnish (fig. 4G) 6 *Drepanoistodus* cf. *D. pervetus* Nowlan (fig. 4H) 18 unassigned drepanodontiform elements 18 *Laurentoscandodus triangularis* (Furnish) (fig. 4J) 1 New genus & new species? 4 *Oneotodus simplex* Furnish 3 *"Oneotodus"* cf. *"O." variabilis* Lindström 13 *Rossodus manitouensis* Repetski & Ethington (fig. 4I) 3 *Rossodus*? sp. 1 unassigned scandodontiform element 8 *Scolopodus sulcatus* Furnish (fig. 4K) 6 *Variabiloconus bassleri* (Furnish) (fig. 4L) 7 unassigned coniform elements CAI=4 [97ADw116A; 11513-CO]	Age is early Early Ordovician (*Rossodus manitouensis* Zone; early Ibexian). This collection is the same age and contains many of the same conodont species as the oldest samples from the type section of the Novi Mountain Formation in the Medfra D-1 quadrangle.	Laurentoscandodid-rossodid biofacies; tropical, normal-marine shelf or platform depositional setting. Species association includes some North American Midcontinent elements, but tropical cosmopolites and some pandemics predominate.	Distal, thin-bedded, silty limestone turbidites with local black carbonaceous partings. Sample is from 12-cm-thick bed of medium-dark-gray, fine-grained, dolomitic limestone with parallel- and cross-laminations and starved ripples; laminae contain peloids and lesser quartz and plagioclase silt. Pzc map unit of Patton and others (1980). Heavy-mineral concentrate includes schistose grains. Sample weight 8.6 kg.

Table 1. Conodont data for localities shown on figure 2—*Continued.*

Locality no., (terrane or subterrane; unit)	Quadrangle latitude/ longitude	Conodont fauna and CAI [field no.; USGS collection no.]	Age	Biofacies	Remarks
33 (Telida; argillite and quartzite unit)	Mt. McKinley D-5 63°55.08' 152°10'	*Aspelundia expansa* Armstrong 4 Pb and 1 M elements (figs. 4BB-DD) *Aspelundia fluegeli* (Walliser) 3 Pa, 4 Pb, 1 Sb1 & 1 Sb2 elements (figs. 4EE-GG) *Aspelundia* spp. vicarious elements 8 M, 2 Sb & 9 Sc (some of the Sc elements could belong in *Ozarkodina*) (fig. 4HH) 1 fragment *Carniodus*? sp. indet. *Dapsilodus obliquicostatus* (Branson & Mehl) (figs. 4JJ-MM) 4 M & 30 S elements 1 Sb element *Distomodus* sp. indet. (fig. 4II) 1 unassigned oistodontiform element of Ordovician morphotype 1 Pa? element *Ozarkodina*? sp. indet. 31 *Panderodus unicostatus* (Branson & Mehl) 2 *Walliserodus* sp. indet. 1 unassigned Sb element 1 unassigned Sc element of deep-water morphotype 94 indet. fragments CAI=4-4.5 [97AD54C; 12597-SD]	Age is early Early Silurian; middle-late Llandoverian but could be middle Llandoverian. According to Armstrong (1990), *Aspelundia expansa* may not extend above the middle Llandoverian.	Aspelundid-coniform biofacies. Post-mortem transport from or within this biofacies, which represents outer shelf or slope depositional setting according to Armstrong (1990).	Light-olive-gray-weathering, medium-dark- to dark-gray, very fine grained dolomitic micrite with silty laminae rich in calcareous sponge spicules, quartz, and lesser plagioclase. From 20-cm chunk presumed fallen from adjacent cliffs and interbedded with argillite and sandstone. Heavy-mineral concentrate includes phosphatized bioclasts and rare phosphatic brachiopod fragments and phosphatized radiolarians. Sample weight 4.2 kg.

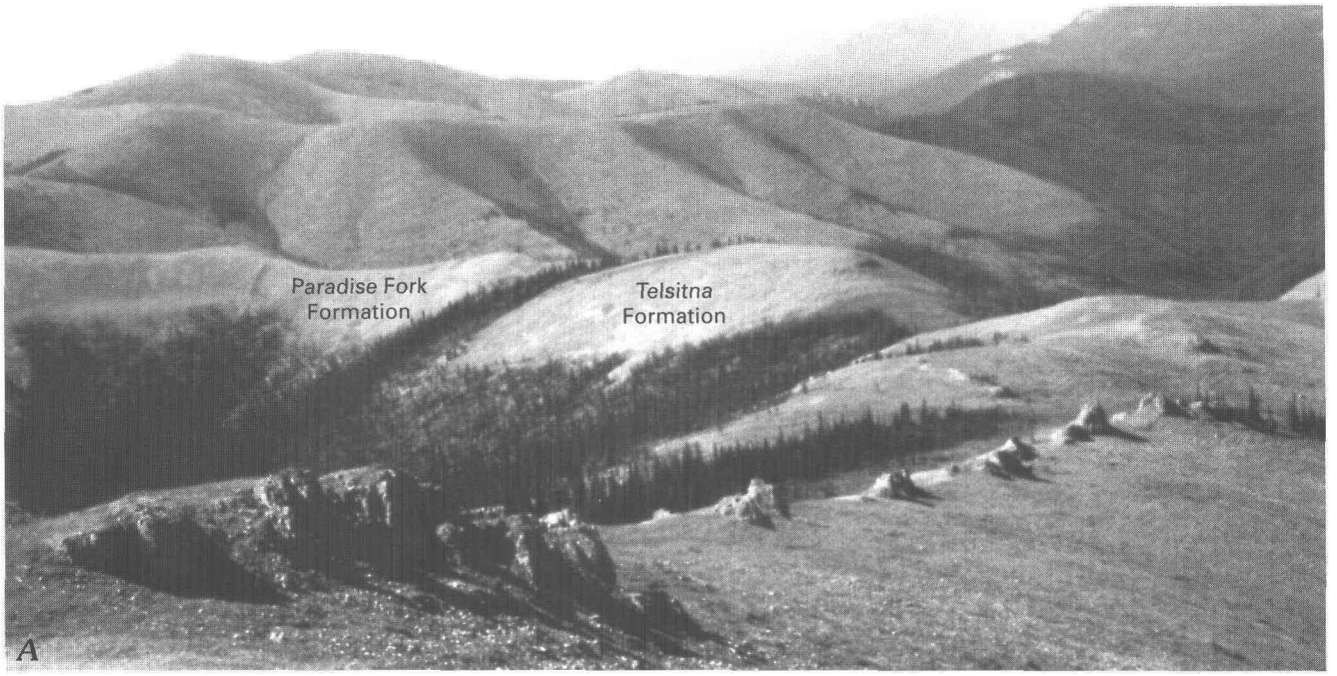

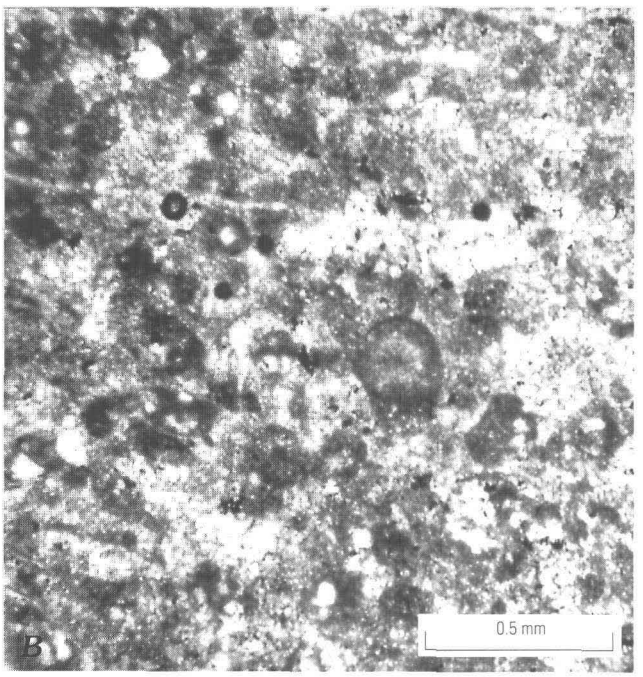

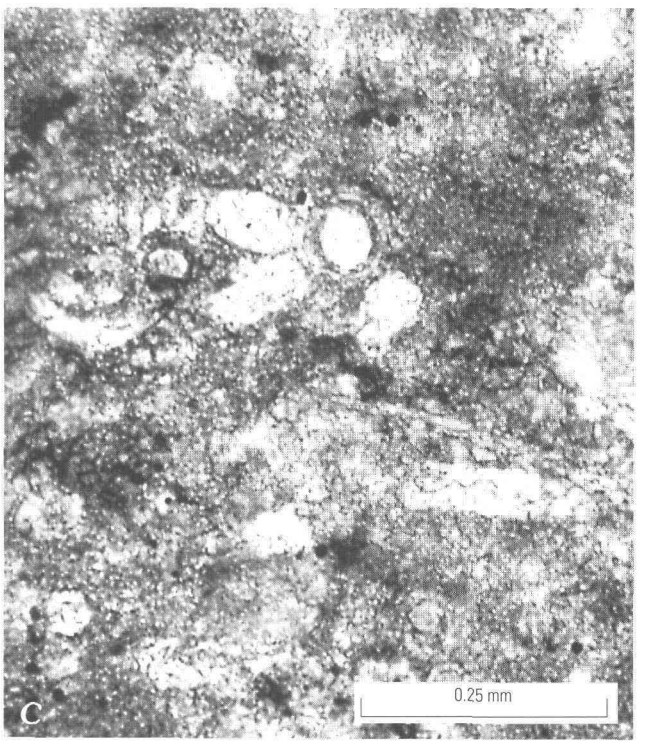

Figure 3. *A,* View to south of shallow-water facies (coralline dolostone) in the upper part of the Telsitna Formation (fig. 2, loc. 1) overlain by deep-water facies (shale and fissile to laminated limestone) in the lower part of the Paradise Fork Formation (fig. 2, locs. 6, 8); Nixon Fork terrane. *B, C,* Sedimentary features of the upper part of the Telsitna Formation (fig. 2, loc. 3). *B,* Lamina rich in peloids and calcitized radiolarians; station 97AD34. *C,* Calcareous sponge spicules in micrite; station 97ADw124.

the Medfra quadrangle (Patton and others, 1980). It is generally poorly exposed, but appears to be at least 1,000 m thick (Dutro and Patton, 1982). Dutro and Patton (1982) assigned a middle Early Silurian age to the Paradise Fork based on graptolites and ostracodes and suggested that the unit was deposited in a relatively deep water setting. Our studies confirm a deep-water depositional environmental for this unit but indicate that it is, in part, as young as Early Devonian.

We examined the Paradise Fork Formation at six partial sections in and near its type locality (fig. 2, locs. 6–10) and reexamined conodont collections from two additional sections (fig. 2 and table 1, locs. 11, 12). The lower part of the Paradise Fork (locs. 6, 8, 9) is grayish-brown-weathering, dark-gray to black, fissile to laminated limestone and limy shale in 3- to 5-cm-thick beds. Limestones are micrite and calcareous siltstone with 5–20 percent calcitized radiolarians and rare calcareous and pyritized

sponge spicules (figs. 5*B*, 5*C*); fine dolomite rhombs and rare quartz silt form the laminae. The upper part of the formation (locs. 7, 10) is chiefly light-gray-weathering, medium-gray to black limestone with tan-weathering dolomitic partings (fig. 5*A*). Beds are 1–15 cm thick (most ≤5 cm), with well-developed parallel- and cross-laminae, and consist of graded alternations of fine- to medium-grained calcareous sandstone, siltstone, and micrite. Sandy layers contain rounded to irregular micrite clasts (40–400 μm) in a sparry matrix (fig. 5*D*); rare bioclasts in these strata include pelmatozoan debris (locally silicified), ostracodes, calcareous sponge spicules, and calcitized radiolarians. Minor metamorphic lithic clasts occur in coarser layers and laminae throughout the formation (table 1, locs. 7, 8, 8A). The uppermost part of the Paradise Fork, known only from a single rubble outcrop (loc. 8A), is dark-gray, weakly laminated calcisiltstone with rare micritic clasts and fossil fragments.

Conodont collections support a middle Early Silurian age for much of the Paradise Fork Formation, but the uppermost part of the unit is at least as young as Early Devonian. Fissile, very finely laminated limestone near the base of the unit, at about the same locality and horizon that produced late Llandoverian to early Wenlockian graptolites (table 2, loc. 6) (Dutro and Patton, 1982), yielded late Llandoverian to very early Wenlockian conodonts that indicate post-mortem transport from or within a mid-shelf or slope depositional setting (table 1, loc. 6; figs. 4*NN*–4*PP*). Laminated limestone a few hundred meters higher in the section contains early to middle Wenlockian conodonts (table 1, loc. 8; figs. 4*QQ*–4*SS*) redeposited from a shelf or platform environment. Dutro and Patton (1982) reported ostracodes of probable Wenlockian age from near the top of the Paradise Fork, and no fossils younger than Wenlockian have been found in outcrop. An isolated rubble outcrop, however, 0.5 km southeast of locality 8 (tables 1 and 2, loc 8A), yielded a mixed fauna that indicates a surprisingly young age for the uppermost part of the Paradise Fork. A single collection of apparently uniform lithology from this locality contained numerous specimens of the early Lochkovian graptolite *Monograptus uniformis*. Conodonts from the same collection are of two ages: late Llandoverian to at least latest Ludlovian and late Emsian or even younger Devonian. This collection most likely represents rubble derived from a relatively condensed section of Wenlockian to Emsian (or possibly even younger Devonian) age.

The Paradise Fork Formation originated as hemipelagic deposits and distal turbidites derived from a carbonate platform. Fine-grained "background" sediment (laminated radiolarian-bearing micrite) predominates in the lower part of the unit. Turbidites (calcareous siltstone and sandstone) are most notable in the upper part of the section and increase upward in thickness and abundance. The uppermost section appears extremely condensed.

In the southern part of its type locality (fig. 2, loc. 13), the Paradise Fork Formation interfingers with shallow-water strata. These rocks are thick- to massive-bedded, light-gray, vuggy dolostone with locally abundant tubular stromatoporoids (*Amphipora* sp.). A sample from locality 13 contained conodonts of early Ludlovian to late Pridolian age; strata here are lithologically similar to, and probably correlative with, the lower part of the Whirlwind Creek Formation of Late Silurian–Early Devonian age (Dutro and Patton, 1982).

Fault blocks adjacent to those containing the Paradise Fork Formation display a different Silurian stratigraphy. Six kilometers west of the Paradise Fork type locality (fig. 2, loc. 4), Ordovician deep-water limestone at the top of the Telsitna Formation is overlain by Upper Silurian amphiporid dolostone; strata equivalent in age and lithology to the lower part of the Paradise Fork are missing. A similar sequence occurs 8 km east of the Paradise Fork type locality (fig. 2 and table 1, loc. 14), where shallow-water skeletal packstone of probable late Late Silurian age overlies deep-water Ordovician facies. Deep-water Silurian rocks are also absent from Nixon Fork sections throughout the southern half of the Medfra quadrangle (Patton and others, 1980). In this area, shallow-water facies of the Whirlwind Creek Formation directly overlie the Telsitna Formation (Dutro and Patton, 1982). The age of the lower part of the Whirlwind Creek is not well constrained. Dutro and Patton (1982) suggested that the basal strata are Ludlovian or younger, but a conodont collection that could be as old as Wenlockian was obtained from locality 15 (table 1).

Deep-water strata of the Paradise Fork Formation are thus quite limited in extent but not in age. They appear to have formed in a small, relatively long lived basin that developed within the Nixon Fork platform. Deep-water facies found in some sections of the upper Telsitna Formation suggest that basinal conditions were locally established by Late (possibly late Middle) Ordovician time. Shallow-water strata precisely coeval with the thick Lower Silurian part of the Paradise Fork Formation have not yet been identified in the Nixon Fork terrane. The condensed, upper part of the Paradise Fork interfingers with shallow-water facies of Late Silurian age.

Minchumina Terrane

The Minchumina terrane lies directly southeast of the Nixon Fork terrane in the Medfra and Mt. McKinley quadrangles and extends some 300 km into the Kantishna River quadrangle (fig. 1). Two subterranes are recognized (Patton and others, 1994). The East Fork subterrane is confined to the Medfra quadrangle and comprises the East Fork Hills Formation (Upper Cambrian through Lower Devonian; age revised herein). The more extensive Telida subterrane consists of sparse, discontinuous exposures of Precambrian(?) and Paleozoic rocks.

East Fork Subterrane

The East Fork Hills Formation is a sequence of laminated, locally dolomitic limestone that forms a northeast-trending belt at least 60 km long and 40 km wide in the southeastern part of the Medfra quadrangle (Patton and others, 1980) (fig. 1). The unit was named by Dutro and Patton (1982), who reported a thickness of several hundred meters, an age (based on sparse conodont collections) of Early Ordovician to Middle Devonian, and a deep-water depositional environment. Exposures of the East Fork Hills Formation are uniformly poor, and relations with other units are obscure. Shallow-water facies of the Nixon Fork

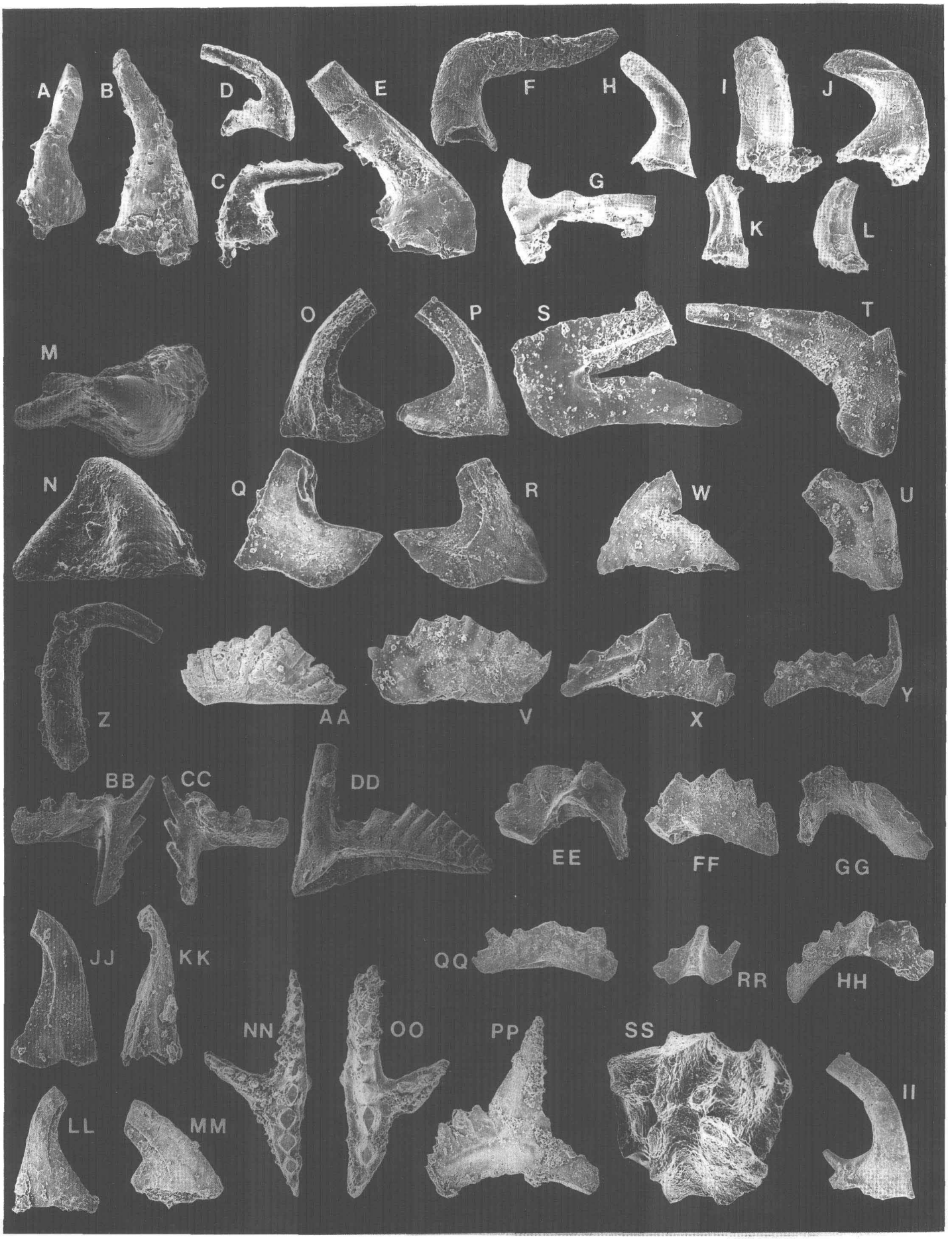
A
B
D
C
E
F
H
G
I
J
K
L
M
O
P
S
T
N
Q
R
W
U
Z
AA
V
X
Y
BB
CC
DD
EE
FF
GG
JJ
KK
QQ
RR
HH
NN
OO
PP
SS
II
LL
MM

Figure 4. Early Paleozoic conodonts from deep-water facies in the Medfra area, central Alaska (scanning electron photomicrographs); figure 4*Z* is not a conodont. Illustrated specimens are reposited in the U.S. National Museum, USNM, Washington, D.C. See table 1 for lithostratigraphic description, faunal analysis, and age assignment of collections and figure 2 for their geographic and geologic position.

A–F, very Late Cambrian, East Fork Hills Formation, USGS colln. 11509-CO (fig. 2, loc. 17), x100 except D x50.
- A–C, *Hirsutodontus hirsutus* Miller, antero-lateral and two lateral views, USNM 497666-68.
- D, *Cordylodus proavus* Müller, outer lateral view, USNM 497669.
- E, *Eoconodontus notchpeakensis* (Miller), outer lateral view, USNM 497670.
- F, *Teridontus nakamurai* (Nogami), outer lateral view, USNM 497671.

G–L, *Rossodus manitouensis* Zone, early Early Ordovician, argillite and quartzite unit, Telida subterrane, USGS colln. 11513-CO (fig. 2, loc. 23), x100.
- G, *Cordylodus intermedius* Furnish, outer lateral view, USNM 497672.
- H, *Drepanoistodus cf. D. pervetus* Nowlan, outer lateral view, USNM 497673.
- I, *Rossodus manitouensis* Repetski and Ethington, antero-lateral view, USNM 497674.
- J, *Laurentoscandodus triangularis* (Furnish), outer lateral view, USNM 497675.
- K, *Scolopodus sulcatus* Furnish, postero-lateral view, USNM 497676.
- L, *Variabiloconus bassleri* (Furnish), inner lateral view, USNM 497677.

M–Y, late Middle-Late Ordovician, upper part of Telsitna Formation, USGS colln. 11510-CO (fig. 2, loc. 3), x100.
- M, N, *Pseudooneotodus mitratus* (Moskalenko), upper and lateral views, USNM 497678.
- O–S, *Paroistodus?* sp. A of Nowlan and others (1988), inner and outer lateral views of two S elements and inner lateral view of M element, USNM 497679-81.
- T, U, *Strachanognathus parvus* Rhodes, outer and inner lateral views, USNM 497683-84.
- V, Ozarkodinid P element, outer lateral view, USNM 497685.
- W–Y, *Periodon grandis* (Ethington)?, M, Pa, and Sb elements, two inner and an outer lateral views, USNM 497686-88.

Z, AA, very latest Late Ordovician, upper part of Telsitna Formation, USGS colln. 11515-CO (fig. 2, loc. 3).
- Z, *Ptiloncodus simplex* Harris, lateral view, x125, USNM 497689. This phosphatic microfossil is known chiefly as discrete elements but does occur in clusters (Tipnis, 1979); its taxonomic affinities remain uncertain. It is rare to common in late Early to Late Ordovician conodont collections in North America.
- AA, *Ozarkodina hassi* (Pollock, Rexroad, and Nicoll)?, Pb element, inner lateral view, x75, USNM 497690.

BB–MM, middle and late Llandoverian, argillite and quartzite unit, Telida subterrane, USGS colln. 12597-SD (fig. 2, loc. 33), x75 except DD x65.
- BB–DD, *Aspelundia expansa* Armstrong, Pb and M elements, inner and outer lateral views of Pb and inner lateral view of M, USNM 497691-92.
- EE–GG, *Aspelundia fleugli* (Walliser), Pb, Pa, and Pb elements, inner, inner, and outer lateral views, USNM 497693-95.
- HH, *Aspelundia* sp. indet. vicarious Sb element, inner lateral view, USNM 497696.
- II, *Distomodus* sp. indet., Sb element, inner lateral view, USNM 497697.
- JJ–MM, *Dapsilodus obliquicostatus* (Branson & Mehl), three S and 1 M (fig. 4MM) elements, two inner and two outer lateral views, USNM 497698-700.

NN–PP, *Pterospathodus celloni* Zone into *K. ranuliformis* Zone, late Llandoverian and very early Wenlockian, lower part of Paradise Fork Formation, USGS colln. 12598-SD (fig. 2, loc. 6), *Pt. procerus* (Walliser), Pa and Pb elements, upper and inner lateral views, x75, USNM 497701-03.

QQ–SS, *Kockelella patula* Zone, lower part of Paradise Fork Formation, USGS colln. 12594-SD (fig. 2, loc. 8), *K. patula* Walliser, Pb, Sb, and Pa elements, inner lateral and upper views, x50, USNM 497704-06.

terrane occur in fault contact to the northwest and deeper water facies of the Telida subterrane are exposed to the east and northeast (Patton and others, 1980) (fig. 2).

Our studies revise the age of the East Fork Hills Formation to Late Cambrian through Early Devonian and indicate that at least three subunits can be distinguished based on lithofacies and conodont faunas. The first subunit makes up the central part of the outcrop belt (fig. 2, locs. 16, 17) and includes the type locality (loc. 16) along the crest of the East Fork Hills. Thin-bedded (0.5 to 8 cm), fine-grained, medium-gray limestone and grayish-orange silty limestone comprise this subunit; beds contain parallel-laminae and small-scale cross-laminae, climbing ripples, and possible flute casts. Limestone layers are chiefly slightly recrystallized micrite. Silty layers are finely crystalline (40–60 μm) dolomite with 1–15 percent detrital grains (mostly quartz, plagioclase feldspar, white mica, and metamorphic lithic clasts). Collections from this subunit produced phosphatic brachiopod fragments and latest Late Cambrian conodonts indicative of an outer-shelf or deeper depositional setting (table 1, locs. 16, 17; figs. 4*A*–4*F*).

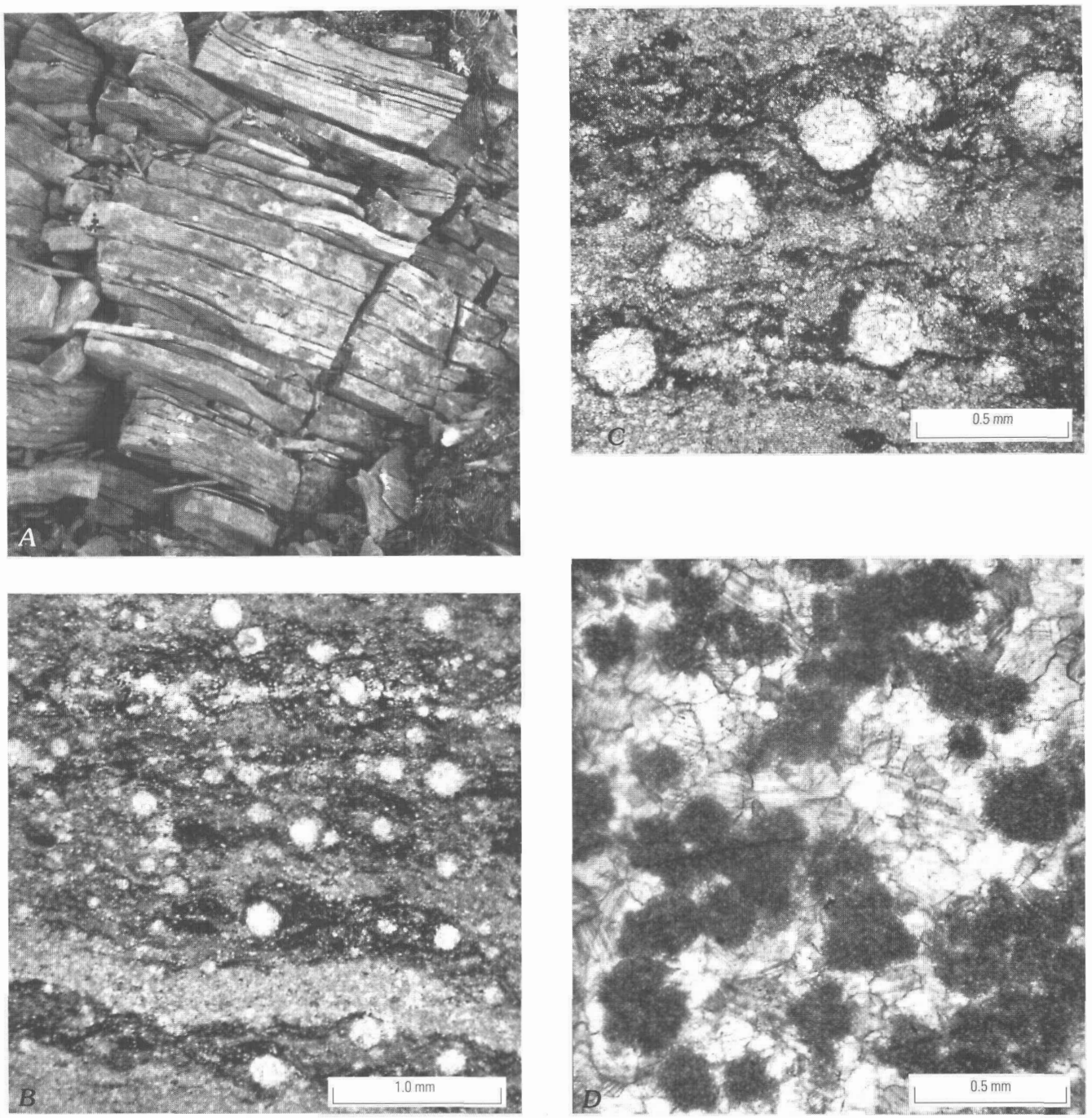

Figure 5. *Sedimentary features of the Paradise Fork Formation, Nixon Fork terrane. A, Thin-bedded, fine-grained, distal carbonate turbidites; upper part of unit (fig. 2, loc. 7). B, C.* Photomicrographs of calcitized radiolarians in micrite matrix; lower part of unit (fig. 2, loc. 8). *D,* Photomicrograph of turbidites shown in *A,* made up of sand- to silt-sized micrite clasts in sparry calcite matrix.

The second subunit forms a fault-bounded block along the northwestern edge of the outcrop belt (fig. 2, locs. 18, 19, 20). It consists chiefly of limestone with subordinate dark chert and siliceous siltstone; basalt rubble occurs at locality 18. Limestone is slightly recrystallized micrite with thin concentrations of peloids and (or) bioclasts, including locally abundant calcitized radiolarians and rare pelmatozoan and brachiopod fragments. Some samples contain thin laminae of chert or dolomite; noncarbonate detritus (<5 percent of most samples) is largely white mica and clasts of silty argillite. Where biostratigraphically diagnostic, conodonts from this subunit are of middle Middle Ordovician age and indicate a slope to basinal setting (table 1, loc. 18).

A distinctive conodont fauna delineates a third subunit of the East Fork Hills Formation in the southeastern part of the outcrop belt. Dark-gray, fine-grained, laminated limestone at two localities contains the youngest conodonts definitively identified from this formation (fig. 2 and table 1, locs. 21, 22). One collection could be as old as Silurian but is no younger than early Early Devonian (Lochkovian); the other is of middle Early Devonian (Pragian) age. Conodonts from both samples denote a normal-marine depositional setting.

Lithofacies, sedimentary structures, and conodont biofacies suggest an outer-shelf or deeper depositional setting for all three subunits of the East Fork Hills Formation. Laminated limestones

Table 2. Other fossil data for localities shown on figure 2.

[Letters in field number refer to collector: CH, R. Chapman and M. Churkin; Dw, D.C. Bradley; Pa, W.W. Patton, Jr.; Rb and Wr, F.R. Weber]

Locality no. (terrane or subterrane; unit)	Quadrangle latitude/ longitude	Fauna [field no.; USGS collection no.]	Age	Source
6 (Nixon Fork; Paradise Fork Fm.)	Medfra D-2 63°51.80′ 153°43.08′	Graptolites: *Monograptus* cf. *M. parapriodon* Boucek, *Paraplectograptus* aff. *P. eiseli* (Manck) [77APa112B]	Early Silurian (late Llandoverian-early Wenlock; probably late Llandoverian, *Monoclimacis crenulata* Zone	Written report from C. Carter to W.W. Patton, Jr., 1978
8A (Nixon Fork; Paradise Fork Fm.)	Medfra D-2 63°51.50′ 153°42.50′	Graptolites: *Monograptus uniformis* Pribyl [98ADw206]	Age is early Early Devonian (Lochkovian; *Monograptus uniformis* Zone)	Written report from S. Finney, California State University (Long Beach), to D. Bradley, 1998
28 (Telida; chert and argillite unit)	Mt. McKinley D-5 63°53.17′ 152°11′	Graptolites: poorly preserved *Orthograptus*(?) cf. *O. quadrimucronatus* (Hall) [79CH89]	Middle Ordovician (approx. *C. tubuliferous* Zone)	Written report from C. Carter to R. Chapman, 1979
29 (Telida; chert and argillite unit)	Mt. McKinley D-5 63°51.5′ 152°12′	Graptolites: *Orthoretiolites hami* Whittington and *Orthograptus* sp. [79CH88]	Middle Ordovician (approx. *C. tubuliferous* Zone)	Written report from C. Carter to R. Chapman, 1979
35 (Telida; argillite and quartzite unit)	Mt. McKinley D-5 63°53′ 152°9.5′	Corals: *Favosites*(?) [59ARb86] (in place) and *Xystriphyllum* sp. [78AWr8] (float—may not be from argillite and quartzite unit)	Silurian or Devonian; *Xystriphyllum* sp. is restricted to latest Silurian (Pridolian)-early Middle Devonian	Written report from W.A. Oliver, Jr., to F.R. Weber, 1997. *Favosites*(?) was originally identified (Oliver and others, 1975; Chapman and others, 1981) as *Saffordophyllum* sp. of Middle-Late Ordovician age

formed as hemipelagic deposits and distal turbidites derived from a carbonate platform. "Common" penecontemporaneous slump structures reported by Patton and others (1980) imply a slope environment for at least some parts of the unit. Radiolarians and periodontid and protopanderodid conodonts in the second subunit indicate that it may have accumulated in somewhat deeper water conditions than did the rest of the East Fork Hills Formation.

Telida Subterrane

Exposures in the Telida subterrane are scarce, discontinuous, and have yielded few fossils, so the detailed stratigraphy of these rocks remains uncertain. Patton and others (1994) recognized four units, in ascending stratigraphic order: (1) pre-Ordovician limestone and phyllite; (2) pre-Ordovician(?) and Ordovician argillite and quartzite; (3) Ordovician (and younger?) chert and argillite; and (4) Middle to Upper Devonian limestone. We report here new lithologic and paleontologic data from the argillite and quartzite unit and the chert and argillite unit in the Medfra and Mt. McKinley quadrangles. Our studies suggest that the chert and argillite unit is older than at least some parts of the argillite and quartzite unit.

Chert and Argillite Unit

The chert and argillite unit includes map units Pzc (lower Paleozoic chert and phyllite of Patton and others, 1980) in the Medfra quadrangle, DOc (Ordovician through Devonian chert)

in the northwestern part of the Mt. McKinley quadrangle (Chapman and Yeend, 1981), and Oc (Ordovician chert and slate unit) in the western Kantishna River quadrangle (Chapman and others, 1975). We examined this unit at six localities in the study area (fig. 2, locs. 23–28).

The westernmost outcrops of the chert and argillite unit occur in a fault block bounded by fragments of the Nixon Fork terrane (figs. 1, 2; locs. 23–25). Discontinuous exposures along the Sethkokna River consist of fine-grained limestone, silty dolostone, argillite, and chert; all lithologies are thin bedded (<0.5–12 cm, most 2–5 cm) with black carbonaceous partings. Carbonate rocks are medium to dark gray, weather olive gray to dark yellowish brown, and are locally graded, with well-developed parallel- and cross-laminae, starved ripples, and load casts (figs. 6*A*, 6*B*). Samples consist of slightly recrystallized calcite and (or) dolomicrite, locally abundant peloids and calcareous sponge spicules, and <5–50 percent detrital quartz, plagioclase, and metamorphic lithoclasts (fig. 6*C*). Chert is dark gray to brown to black and contains siliceous sponge spicules and radiolarian ghosts (fig. 6*D*).

Exposures of the chert and argillite unit in the Mt. McKinley quadrangle are similar to those in the Medfra quadrangle but lack a carbonate component (fig. 2, locs. 26–28). Rubble in the Snohomish Hills is laminated, very light gray to black, spiculitic, radiolarian chert and lesser tan argillite; outcrops at Lake Minchumina are light olive gray silty argillite.

The chert and argillite unit yields fossils of Early and Middle Ordovician age (table 1, loc. 23; table 2, locs. 28, 29). Limestone in the Medfra quadrangle (loc. 23) produced abundant conodonts of early Early Ordovician age (*Rossodus manitouensis* Zone; figs. 4*G*–4*L*); this fauna is the same age as the oldest part of the Novi Mountain Formation in the Nixon Fork terrane and contains many of the same species found in Novi Mountain samples. Argillite contains late Middle Ordovician (Caradocian) graptolites at Lake Minchumina (fig. 2 and table 2, locs. 28, 29) and a less diagnostic fauna of Middle(?) Ordovician age in the southwestern part of the Kantishna River quadrangle, 50 km to the north (Chapman and others, 1981).

Lithofacies, sedimentary structures, and biofacies indicate an off-platform setting for the chert and argillite unit. Calcareous beds are distal turbidites, derived at least in part from the Nixon Fork terrane. Argillite and chert formed as hemipelagic deposits.

Argillite and Quartzite Unit

We examined the argillite and quartzite unit at five localities (fig. 2, locs. 30–34). These rocks are mapped as PzpЄq (Precambrian or lower Paleozoic quartzite, grit, and argillite) in the Medfra quadrangle (Patton and others, 1980), DOs (Ordovician to Devonian shaly rocks) in the northwestern part of the Mt. McKinley quadrangle (Chapman and Yeend, 1981), and Ꞓqs (Cambrian quartzite, metasiltstone, slate, and grit) in the western Kantishna River quadrangle (Chapman and others, 1975).

Along Munsatli Ridge (fig. 2, locs. 30, 31) and on the east side of Lake Minchumina (fig. 2, loc. 32), the argillite and quartzite unit consists chiefly of sandstone, pebbly sandstone, and fine-grained conglomerate in slabby beds 3–10 cm thick. Fresh surfaces are parallel-laminated and range from very pale orange to olive or blue-gray. Some sandstones are graded, and some contain thin argillite interbeds. Sandstone samples are very poorly sorted; most are medium grained but contain notable (5–10 percent) outsized clasts, 4–10 mm in diameter. Clasts are angular to rounded and are chiefly monocrystalline quartz (Qm) with undulous extinction (Qm=60–95 percent, generally >80 percent). Other framework grains include feldspar (both plagioclase and microcline, based on twinning), polycrystalline quartz, metasedimentary lithic clasts, and rare tourmaline. Matrix, mostly finely intergrown quartz and phyllosilicates, makes up <5 to >30 percent of the samples examined. Grain boundaries are generally recrystallized, and some samples are semischists.

More heterogeneous strata also included in the argillite and quartzite unit crop out along the northeastern shore of Lake Minchumina (fig. 2, locs. 33, 34). These rocks consist of strongly cleaved, silty to cherty argillite, phyllite, and chert, intercalated with intervals of sandstone and carbonate that are 20 cm to 1.5 m thick (fig. 7*A*). Finer grained rocks range from reddish brown to silvery gray to black; siliceous sponge spicules and radiolarian ghosts are locally abundant in some cherty layers. Sandstones weather white to orange to brownish gray and are medium to dark gray, very fine to medium grained, poorly sorted, and locally cross-laminated and graded. Some samples are mostly rounded to angular monocrystalline quartz with lesser plagioclase and microcline feldspar and are virtually identical to strata described above from Munsatli Ridge. Others contain a similar suite of quartz and subordinate feldspar as well as 10 to 70 percent carbonate, chiefly dolomite, that occurs as clasts and matrix (figs. 7*B*–7*D*). Clasts are finely crystalline dolomite mosaics and lesser pelmatozoan fragments. Rare carbonate layers are mostly finely crystalline (5–40 μm) dolomite with abundant calcareous sponge spicules, lesser calcitized radiolarians, and minor detrital quartz and feldspar (fig. 7*E*).

No fossils have been obtained from the argillite and quartzite unit along Munsatli Ridge, but several collections constrain the age of the rocks at Lake Minchumina. Fine-grained dolostone from locality 33 (fig. 2; table 1) contains abundant conodonts of Early Silurian (middle-late Llandoverian, possibly middle Llandoverian) age (figs. 4*BB*–4*MM*); the heavy-mineral concentrate from this sample contains rare phosphatic brachiopod fragments and phosphatized radiolarians. The conodont faunule represents postmortem transport from or within the aspelundid-coniform biofacies, which indicates an outer-shelf or slope depositional setting.

Several collections of corals from locality 35 (fig. 2; table 2, loc. 35) are of Silurian or Devonian age (W.A. Oliver, Jr., 1997; written commun. to F. Weber). The most diagnostic form is a ptenophylid coral—*Xystriphyllum* sp., of latest Silurian (Pridolian) to early Middle Devonian age—found in a beach cobble that may not have come from the argillite and quartzite unit (Chapman and others, 1981). A second coral was collected from outcrop. This specimen was originally identified as *Saffordophyllum* sp. of Middle to Late Ordovician age (Oliver and others, 1975; Chapman and others, 1981) but is now identified as *Favosites*? sp. of Silurian or Devonian age (W.A. Oliver, Jr., 1997; written commun. to F. Weber). Two-hole crinoid columnals, indicative of a late Early-early Middle Devonian (Emisian-Eifelian) age, are also reported from beach float found near locality 35 (R.B. Blodgett, Oregon State University, 1997, written commun. to F. Weber).

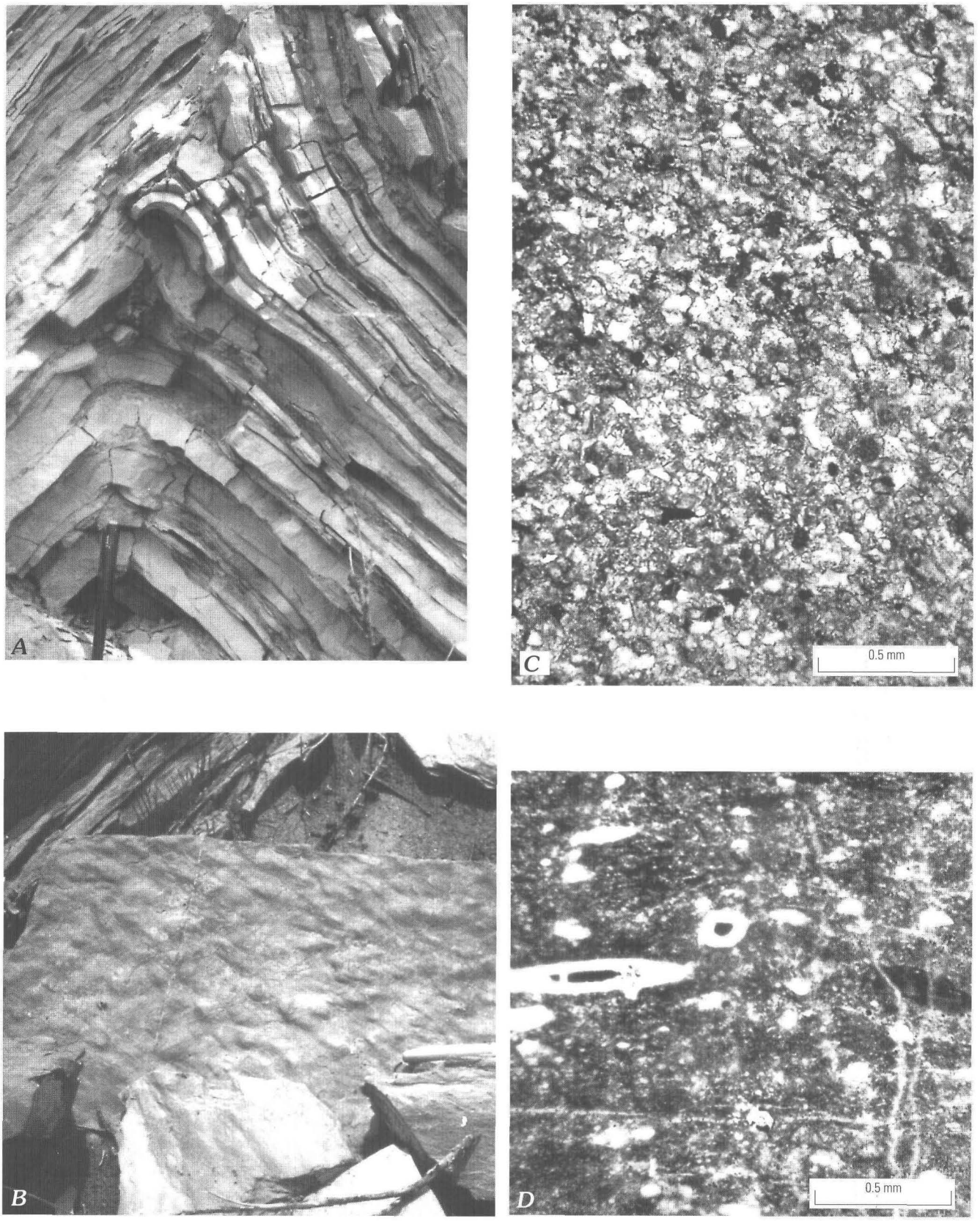

Figure 6. Sedimentary features of the chert and argillite unit, Telida subterrane, Minchumina terrane. *A–C*, Outcrop views and photomicrograph (*C*) of distal, thin-bedded, silty limestone turbidites (fig. 2, loc. 23). Note black carbonaceous partings in *A*, load casts on bed bottom in *B*, and parallel laminae rich in peloids (dark grains) and quartz and lesser plagioclase silt (light grains) in *C*. *D*, Photomicrograph of chert with abundant siliceous sponge spicules; some spicule centers are pyritized (fig. 2, loc. 24).

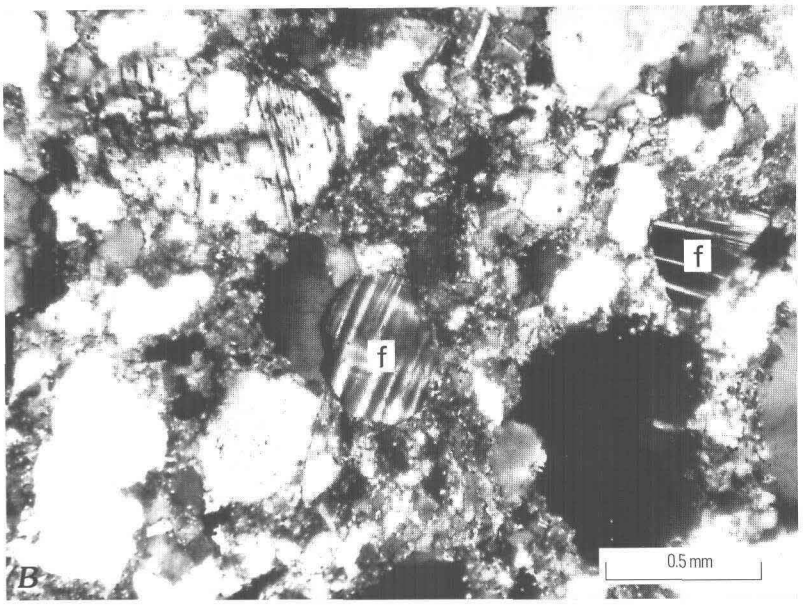

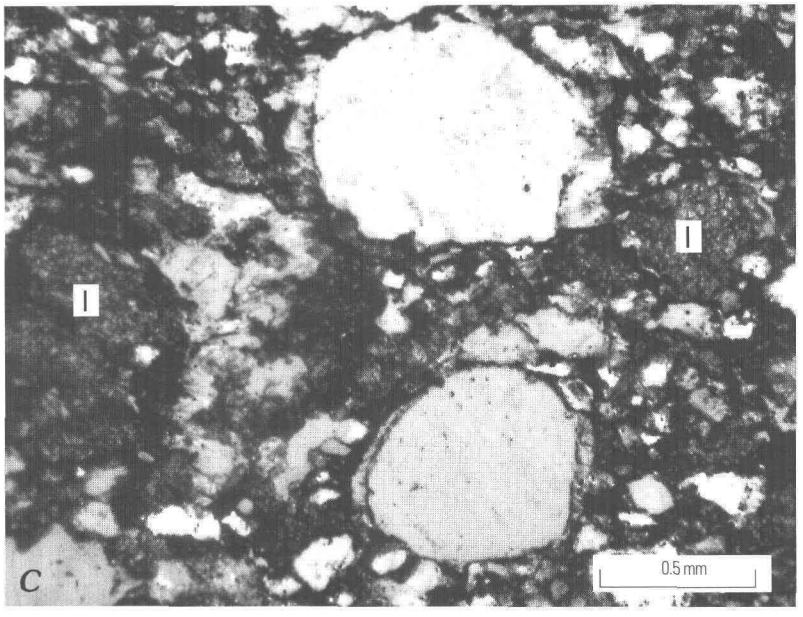

Figure 7 (above and facing page). Sedimentary features of the argillite and quartzite unit, Telida subterrane, Minchumina terrane. Outcrop view (*A*) and photomicrographs (*B–D*; *B*, crossed nicols) of sandstone turbidites, intercalated with argillite and thin carbonate layers (*E*, photomicrograph) (fig. 2, loc. 33). Sandstone contains abundant, rounded quartz, lesser plagioclase and potassium feldspar (f), polycrystalline carbonate lithic clasts (l) and pelmatozoan fragments (p). Carbonate layer shown in *E* is dolomitic micrite with silty laminae rich in calcareous sponge spicules, quartz, and lesser plagioclase.

Like the chert and argillite unit, the argillite and quartzite unit probably represents chiefly turbidites and hemipelagic deposits. Quartz-rich, locally calcareous sandstones are graded, poorly sorted, and were likely deposited as turbidites. They are coarser grained and more abundant than the calcareous turbidites in the chert and argillite unit; they appear to have had a different source and may have accumulated in a less distal position. Fine-grained calcareous, siliceous, and argillaceous strata in the argillite and quartzite unit formed as "background" sedimentation between pulses of turbidite deposition.

Stratigraphy of the Telida Subterrane

Our studies indicate that, at Lake Minchumina, the chert and argillite unit is older than the argillite and quartzite unit. Previous workers considered the chert and argillite unit to be the younger of the two, but assigned all strata at Yutokh Hill (the area between locs. 28, 29, and 35 on fig. 2) to the argillite and quartzite unit (Chapman and others, 1981; Patton and others, 1994). If graptolite-bearing strata on the north and south sides of Yutokh Hill are included in the chert and argillite unit, however, a different stratigraphy results (F. Weber, written commun., 1997). In this interpretation, the argillite and quartzite unit, exposed at the top and on the east side of Yutokh Hill, unconformably overlies the chert and argillite unit (the contact could also be a low-angle thrust fault). Although structure in this area is complex (see further discussion below) our new fossil data, and the reinterpreted age of the in situ coral from Yutokh Hill, suggest that the chert and argillite unit at Lake Minchumina is Ordovician and the argillite and quartzite unit is Silurian and perhaps, in part, Devonian. It is possible, however, that the argillite and quartzite unit includes strata of several ages. Previous workers (Patton and others, 1980; Chapman and others, 1975) correlated this unit with Cambrian-Upper Proterozoic rocks, such as the Wickersham unit in the Livengood quadrangle, on

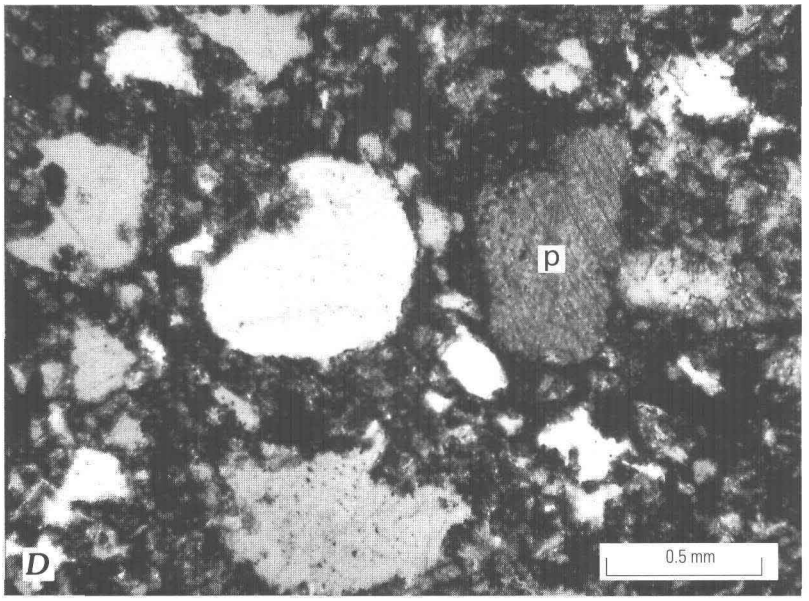

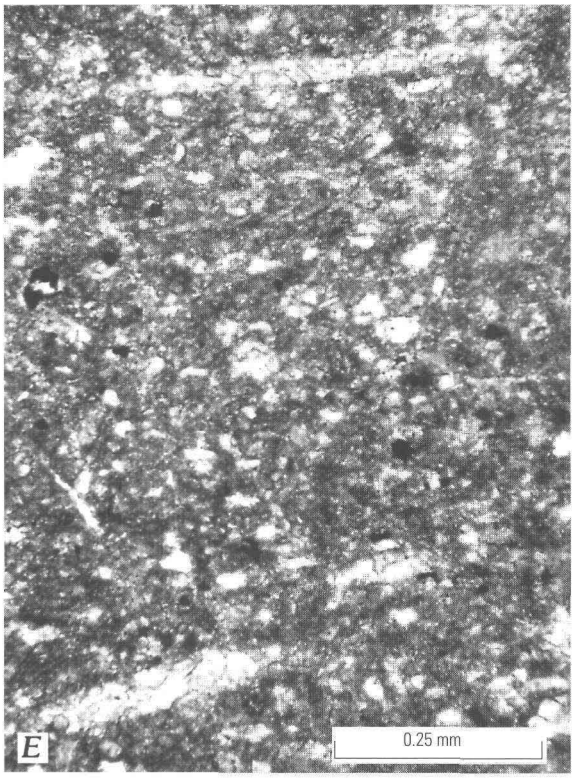

lithologic grounds—grits in the Wickersham are bimodal quartzite with locally abundant potassium and plagioclase feldspar (Weber and others, 1992). The compositional ties that we noted in our study area between calcareous and noncalcareous turbidites in the argillite and quartzite unit need not signify stratigraphic equivalence but could instead indicate erosion and reworking of older material into younger turbidites. Thus, undated, noncalcareous parts of the argillite and quartzite unit (for example, rocks at Munsatli Ridge) could be Cambrian or older and could have provided a source for the coarse quartz and feldspar found in the Silurian turbidites at Lake Minchumina.

Correlation

Lithologic and paleontologic data detailed above constrain correlations between the Nixon Fork and Minchumina terranes and provide a basis for regional comparison of these strata with coeval deep-water facies exposed to the south (Dillinger terrane). In this section, we compare Upper Cambrian to Lower Devonian deep-water sequences in the Nixon Fork, Minchumina, and Dillinger terranes and consider depositional and tectonic factors affecting their correlation.

Stratigraphic Constraints and Implications

The lower Paleozoic stratigraphies of the Nixon Fork, Minchumina, and Dillinger terranes are compared in figure 8. Gaps remain in these stratigraphies (particularly for the Minchumina terrane), but the available data outline several interesting patterns. In the discussion that follows, "Nixon Fork terrane" refers only to rocks in the Medfra quadrangle and not to correlative strata in the McGrath and Lime Hills quadrangles to the south that some workers have included in this terrane.

Nixon Fork Terrane

Deep-water facies in the Nixon Fork terrane accumulated primarily at times when deposition is not recorded in adjacent deep-water sequences. In the Nixon Fork, deep-water sediments formed chiefly during the Late Ordovician, Early Silurian, and Early Devonian, but strata of Late Ordovician age and some intervals in the Early Silurian have not been identified in the Minchumina terrane or in the paleontologically well constrained Dillinger terrane. If these terranes indeed represent parts of a single continental margin, depositional patterns suggest that the shelf edge along this margin stepped back (retreated landward) in Late Ordovician and Early Silurian time. During this period, turbidites and hemipelagic material were trapped near the platform in sequences such as the Paradise Fork Formation and did not reach more distal sequences such as the Dillinger that formed farther from the continental margin.

East Fork Subterrane of the Minchumina Terrane

Well-dated intervals in the East Fork subterrane correlate in part with platform facies of the Nixon Fork terrane, do not match dated intervals in the Telida subterrane, and correlate well with the Dillinger terrane. The general correlation between Nixon Fork and East Fork rocks supports the suggestion that deep-water facies in the East Fork were derived from the Nixon Fork platform. Strata as old as the Late Cambrian part of the East Fork, however, have not been identified in the Nixon Fork terrane in the Medfra quadrangle. The base of the Novi Mountain Formation, the oldest dated unit in the Nixon Fork terrane in this area, is paleontologically well constrained at its type section as early Early Ordovician (*R. manitouensis* Zone) (A.G. Harris and J.E. Repetski, unpub. data, 1997). Not all sections of the Novi

Mountain have been dated, however, and it is possible that, outside its type area, the unit is as old as Late Cambrian. Alternatively, Cambrian strata in the East Fork may have accumulated before the Nixon Fork platform was established and may have derived from a more distant source. Upper Cambrian beds in the East Fork correlate well, biostratigraphically and lithologically, with the Lyman Hills Formation (Bundtzen and others, 1994) in the Dillinger terrane and could have had the same provenance.

Middle Ordovician and Lower Devonian strata in the East Fork subterrane correlate well with, and could have been derived from, the Nixon Fork platform. Ordovician and Devonian East Fork rocks also correlate with parts of the Post River Formation and the Barren Ridge Limestone, respectively, in the Dillinger terrane (fig. 8). However, the Dillinger terrane is characterized by a thick sandstone turbidite unit of Silurian age, the Terra Cotta Mountains Sandstone (Churkin and Carter, 1996). No lithologic or biostratigraphic match for this unit has been found in the East Fork subterrane.

Our biostratigraphic data indicate that strata in the East Fork subterrane accumulated during Late Cambrian, Middle Ordovician, and Early Devonian time. These data could be an artifact of the poor exposures characteristic of this subterrane. It is also possible, however, that carbonate turbidites and associated hemipelagites were generated chiefly at certain times during the long history of the Nixon Fork platform, and the stratigraphy of the East Fork subterrane reflects this discontinuous generation. Episodic transfer of sediment from shelf to basin could be due to tectonic events, eustatic fluctuations, and (or) autocyclic changes in platform sedimentation, among other factors.

Telida Subterrane of the Minchumina Terrane

Lower Ordovician strata in the Telida subterrane have the strongest ties to the Nixon Fork platform of all deep-water rocks in the study area. Conodonts from calcareous turbidites at locality 23 (fig. 2) match those from the lower part of the Novi Mountain Formation species for species (table 1) (A.G. Harris and J.E. Repetski, unpub. data, 1997). These Telida strata also correlate well, biostratigraphically and lithologically, with the lower siltstone member of the Post River Formation in the Dillinger terrane (Churkin and Carter, 1996). Middle Ordovician rocks in the Telida subterrane correlate with broadly dated parts of the Nixon Fork platform and with the middle part of the Graptolite Canyon Member of the Post River Formation. Telida sandstones at Lake Minchumina correlate with, or are just slightly older than, the lower part of the Paradise Fork Formation in the Nixon Fork terrane and correlate well with the upper part of the Post River Formation. Lake Minchumina sandstones are at least in part older than, and differ in composition from, the Terra Cotta Mountains Sandstone in the Dillinger terrane, as will be discussed below.

Compositional Trends

Several notable patterns in the composition of Medfra-area deep-water facies can be discerned. These patterns reflect variations in the proportion of carbonate to noncarbonate detritus, and in the types of noncarbonate detritus, that are found in deep-water strata of the Nixon Fork and Minchumina terranes.

Carbonate Input

Turbidites and hemipelagic strata show similar carbonate-to-noncarbonate ratios in the study area. In the Nixon Fork terrane, the East Fork subterrane, and the westernmost exposures of the Telida subterrane, turbidites consist chiefly of carbonate material and were derived principally from a shallow-water carbonate platform, presumably the Nixon Fork platform. Turbidites in the eastern exposures of the Telida subterrane are much less calcareous and include detritus—such as coarse, rounded quartz grains and microcline—not found in turbidites in the other sequences. Finer grained strata show similar trends. In the Nixon Fork terrane, the East Fork subterrane, and the western Telida subterrane, hemipelagic deposits are chiefly micrite and shale, but in the eastern part of the Telida subterrane these deposits are much less terrigenous and consist predominantly of chert. The chert and argillite unit of the Telida subterrane is lithologically similar to, but somewhat older than, the Livengood Dome chert (Upper Ordovician; Chapman and others, 1980) in the Livengood quadrangle to the northeast (Livengood terrane of Silberling and others, 1994) (fig. 1).

Compositional data thus suggest that strata in the eastern Telida subterrane accumulated farthest from the continental margins, experienced relatively little input from carbonate platforms adjacent to these margins, and received some noncarbonate detritus that did not reach the other deep-water sequences in the study area.

Noncarbonate Components

Noncarbonate detritus occurs sparsely in most parts of the Nixon Fork terrane and the East Fork subterrane but is a significant component in turbidites in the western part of the Telida subterrane. Plagioclase feldspar and metamorphic lithic clasts made up of quartz, chlorite, and (or) white mica are notable minor constituents of Upper Cambrian strata in the East Fork subterrane, Lower Ordovician turbidites in the western Telida subterrane, and Lower Ordovician rocks in the Nixon Fork platform succession; rare metamorphic clasts were also noted in the Silurian-Lower Devonian Paradise Fork Formation. The clasts, and perhaps the feldspar, may have been derived from metamorphosed basement rocks that underlie the Nixon Fork platform succession; these rocks are of early Paleozoic or Precambrian age and include quartz-chlorite-muscovite schist and quartz-plagioclase porphyry (map units Pzp€p and Pzp€v of Patton and others, 1980).

Noncarbonate detritus is a significant component in turbidites of the argillite and quartzite unit in the Telida subterrane. Correlation of these turbidites with the Terra Cotta Mountains Sandstone in the Dillinger terrane has been suggested (T. Bundtzen, Pacific Rim Inc., oral commun., 1997) and is broadly supported by age data from the exposures at Lake Minchumina, although the Minchumina strata are slightly older than the base of the Terra Cotta in its type area (fig. 8) (Churkin and Carter, 1996). Published petrographic descriptions of the Terra Cotta, however, suggest significant compositional differences between the two units. Slate clasts, polycrystalline quartz, and white mica are important constituents of the Terra

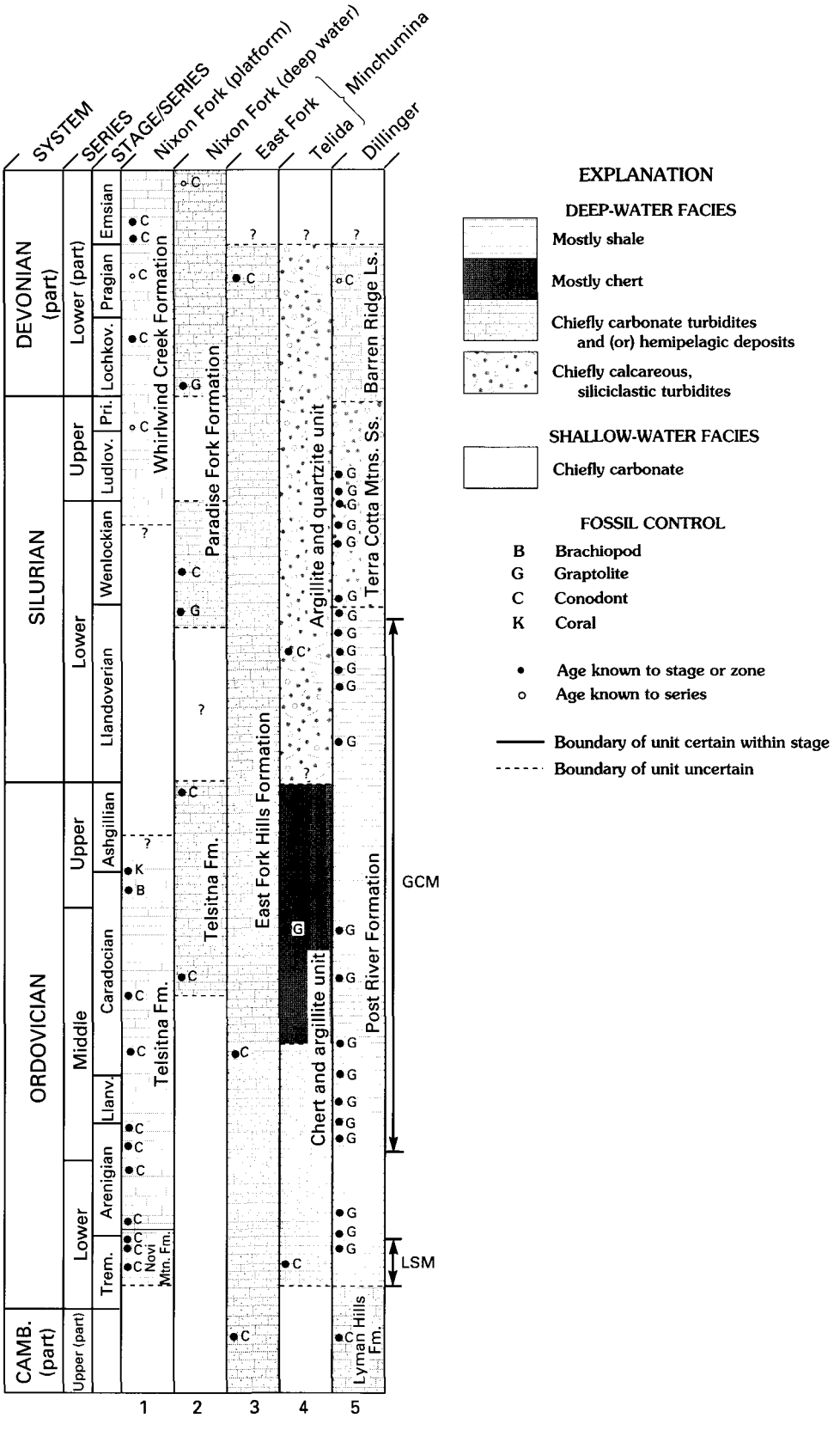

Figure 8. Correlation, lithologies, fossil control, and depositional environments of uppermost Cambrian to Lower Devonian rocks in selected areas of central Alaska. Only fossil groups that most narrowly restrict age of collection or unit are listed. Age of argillite and quartzite unit (column 4) is poorly constrained. Parts of this unit could be older than chert and argillite unit but youngest beds could be as young as Devonian; see text for discussion. Arrows adjacent to column 5 indicate lower siltstone member (LSM) and Graptolite Canyon Member (GCM) of the Post River Formation. Data sources as follows: column 1, Dutro and Patton (1982), A.G. Harris and J.E. Repetski, unpub. data; columns 2–4, this paper; column 5, Bundtzen and others (1994), Churkin and Carter (1996). The former Llandeilian Series is now considered a stage of the Llanvirnian Series (Fortey and others, 1995).

Cotta (Bundtzen and others, 1994; Churkin and Carter, 1996) but are rare or absent in Telida turbidites, whereas the potassium feldspar and rounded, bimodal, monocrystalline quartz that are so notable in the Telida turbidites are not reported from the Terra Cotta.

As noted above, parts of the argillite and quartzite unit in the Telida subterrane could be of Cambrian-Precambrian age and equivalent to the Wickersham unit (and related rocks) in the Livengood area to the north (Wickersham terrane of Silberling and others, 1994) (fig. 1). Erosion of these older Telida rocks could then have provided quartz and feldspar to the Silurian turbidites at Lake Minchumina. If all parts of the argillite and quartzite unit are of Silurian and younger age, grits such as the Wickersham still seem to be a likely source for the quartz and feldspar found in Telida subterrane turbidites. Whatever the age of the turbidites in the argillite and quartzite unit, their composition implies ties to rocks currently exposed to the northeast (Livengood quadrangle) rather than to the south (McGrath quadrangle). Petrographic data thus indicate that the Telida subterrane contains at least two distinct sequences, each derived from a different source, and these sequences need not have had a shared Paleozoic history.

Structure

Paleozoic rocks of the study area have been affected by two principal deformations: an earlier folding about northeast axes, followed by dextral strike-slip on the Iditarod fault system. The focus will be here on aspects of the structure that bear on the palinspastic relations among the strata of interest.

The Iditarod fault is one of the most significant strike-slip faults in Alaska (Grantz, 1966). In the Iditarod quadrangle, the fault cuts a Late Cretaceous to early Tertiary volcano-plutonic complex and separates its two halves—the Iditarod Volcanics and the Beaver Mountains volcanic field—by 88 to 94 km in a dextral sense (Miller and Bundtzen, 1988). Similarly, in the McGrath and Medfra quadrangles, the eastern contact between Cretaceous siliciclastic strata of the Kuskokwim Group and Paleozoic carbonate rocks of the Nixon Fork terrane shows a dextral map separation of about 90 km. Although the Iditarod fault has only one strand of any significance in the Iditarod quadrangle (Miller and Bundtzen, 1988), several splays are mapped in the Medfra quadrangle (Patton and others, 1980). Presumably, dextral displacement across all of the splays sums to at least ~90 km—or even more if some dextral strike-slip preceded deposition of the Kuskokwim Group. There are no piercing points on any of these splays, so map separation cannot be measured; they are presumed to be dextral strike-slip faults because of their continuity and subparallelism with the Iditarod fault in the Iditarod quadrangle.

In the area of figure 2, the Iditarod fault has four main strands, labeled A through D (fig. 9), and several minor ones. Strand A juxtaposes deep-water facies of the Minchumina terrane against shallow-marine carbonate rocks of the Upper Silurian–Devonian Whirlwind Creek Formation. Strand A is presumably the main strand of the Iditarod fault system in this area; horizontal displacement is likely to be several tens of kilometers. Strand B juxtaposes the Whirlwind Creek Formation against the Upper Cretaceous to lower Tertiary Sischu volcanics. There is no direct evidence for the amount of displacement but it is inferred to have a small component of northwest-side-down vertical displacement and perhaps a few to a few tens of kilometers of dextral horizontal displacement. Strand C juxtaposes deep-water facies of the chert and argillite unit, which depositionally underlie the Sischu volcanics, against coeval shallow-marine facies of the Nixon Fork terrane. As noted above, an Early Ordovician conodont fauna in the chert and argillite unit precisely matches the conodont fauna of the age-equivalent Novi Mountain Formation. Significant fault displacement, either strike-slip, thrusting, or both, is needed to explain the current close juxtaposition of environments that must once have been farther apart.

A second regional-scale dextral strike-slip fault, the Farewell, lies to the south of the present study area, but it does bear on the palinspastic relations betweeen the Minchumina and Dillinger terranes. In the McGrath and Lime Hills quadrangles, a Late Silurian to Early Devonian algal barrier reef complex in the Nixon Fork terrane shows a dextral map separation of 145 to 153 km (Blodgett and Clough, 1985).

The Paleozoic rocks that were rearranged along these various strike-slip faults had already been folded. Fold axial traces trend roughly northeast-southwest in both the Nixon Fork and Minchumina terranes. Nixon Fork strata typically are deformed into open to tight folds with wavelengths as long as a few kilometers. On this basis, we suggest that each of the fault-bounded tracts containing Nixon Fork strata were probably not much wider prior to shortening than they are today—perhaps 10–20 percent wider. Shortening across the Minchumina terrane cannot be estimated with confidence but was undoubtedly far greater than in the Nixon Fork. Shoreline exposures at Lake Minchumina disclose the presence of inverted subhorizonal beds and nearly recumbent isoclinal folds (T.M. Kusky, Boston University, unpub. data, 1997) that require extreme amounts of shortening for at least some rocks in the belt. Large amounts of shortening are *not* suggested by the simple map pattern of the Minchumina terrane (fig. 2), but this is strictly an artifact of the mapping conditions: outcrops and helicopter landings are so sparse that entire mountains were assigned to a single unit on the basis of one or two rubble outcrops. It seems likely that the belt of northwest-directed thrust faults mapped in the Livengood quadrangle (Weber and others, 1992) continues along strike into the area of figure 2 and that the structure in the Minchumina terrane is as complex as in the southeastern part of the Livengood quadrangle.

Figure 9 shows the palinspastic distribution of our sample localities. On the Farewell fault, we restored 150 km of dextral map-separation (Blodgett and Clough, 1985). Where the Iditarod fault has a single strand (extreme western part of fig. 9, and beyond), we restored 90 km of dextral map separation (Miller and Bundtzen, 1988). For lack of any concrete evidence, we arbitrarily restored 30, 20, 20, and 20 km of dextral map separation across strands A, B, C, and D, respectively. Regardless of the displacements assigned to the individual strands, the total on all four should sum to 90 km; the relative positions of rocks northwest of strand D and southeast of strand A are the same regardless of the details. Figure 9 does not restore any shortening—only strike-slip. As noted above, shortening was relatively minor in the Nixon Fork terrane but probably quite severe in the

Minchumina terrane. The distance across the Minchumina terrane between the Farewell fault and Iditarod fault systems was undoubtedly wider than at present.

In figure 9, deep-water strata between strands B and C remain isolated from the broader tract of the Minchumina terrane, and there seems no way to bring these tracts together given *only* 90 km of only dextral displacement on strands A through D combined. One possible explanation for this map pattern is that deeper water strata between strands B and C accumulated in an intrashelf basin in the Nixon Fork platform, as implied by the restoration in figure 9. A second possibility is that these deep-water facies record a northwestward Ordovician transgression across the Nixon Fork platform that was followed by southeastward progradation of this platform during Silurian-Devonian time, prior to any shuffling on strike-slip faults. A third possibility is that rocks between strands B and C represent a piece of the Minchumina terrane that was thrust into position from the southeast, prior to any shuffling on strike-slip faults, over shallow-water strata of the Nixon Fork platform that lie between strands A and B. A fourth possibility is that the shallow-water rocks between strands A and B belong to the Minchumina and not the Nixon Fork terrane; in this interpretation, fault strand C, not strand A, marks the boundary between the Nixon Fork and Minchumina terranes (Patton and others, 1984; Patton and others, 1994). These alternatives cannot be evaluated without more information.

Biogeography

The ultimate origin of lower Paleozoic rocks in central Alaska remains contentious. Some authors have suggested that the Nixon Fork, Minchumina, and Dillinger terranes represent

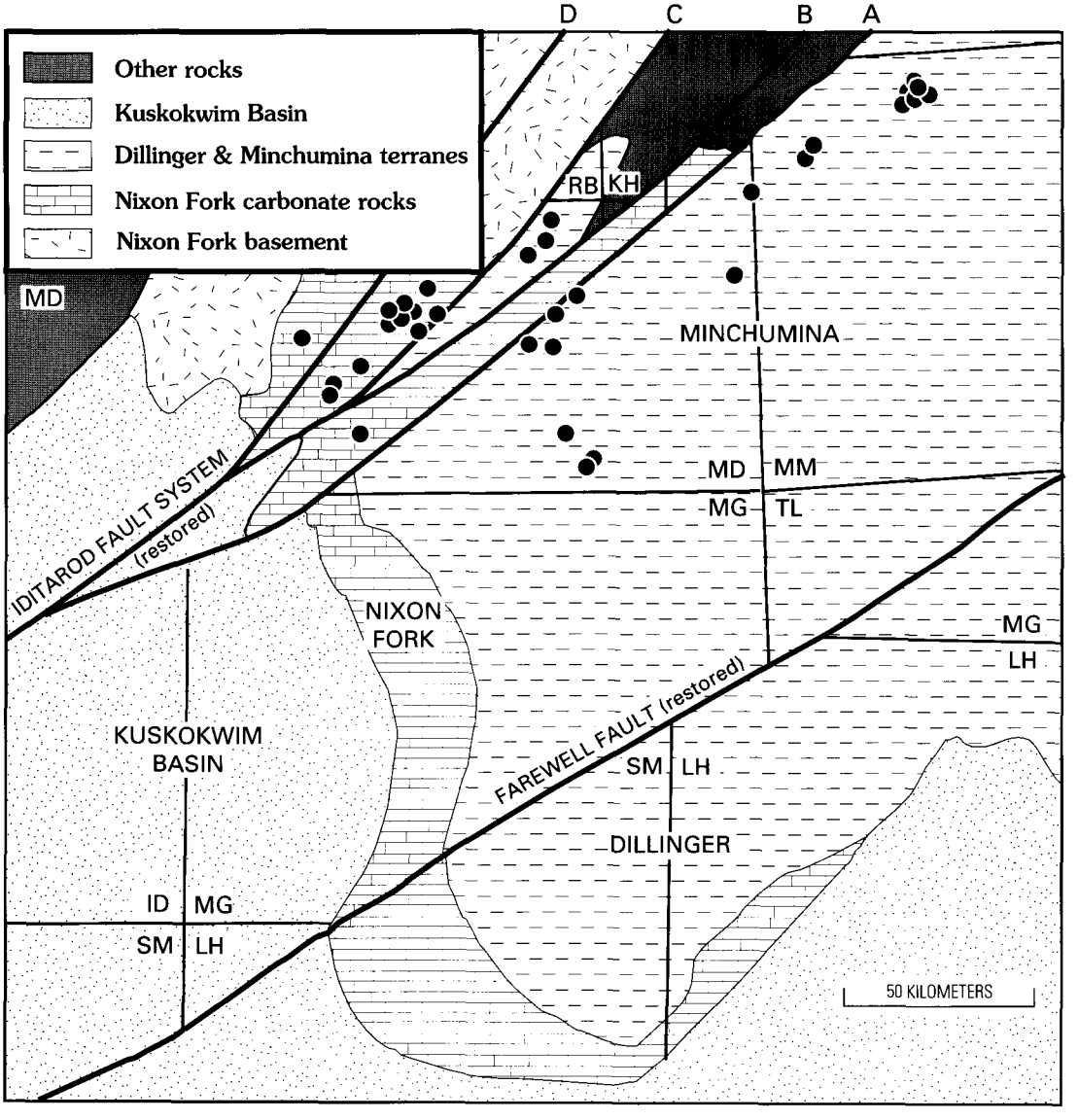

Figure 9. Palinspastic map of study area. Letters A, B, C, and D refer to strands of the Iditarod fault system mentioned in text. Restoration of 90 and 150 km of dextral strike-slip on the Iditarod and Farewell faults, respectively, aligns the deep-water Dillinger and Minchumina terranes in a position east of the Nixon Fork carbonate platform. Terrane affinity of lower Paleozoic rocks between fault strands A and C is uncertain; see text for dicussion. Black dots are locations plotted in figure 2. Fine lines are quadrangle boundaries; quadrangle abbreviations as in figure 1.

displaced fragments of the North American continental margin (Decker and others, 1994), but, more recently, others have interpreted these terranes as a sequence rifted away from the Siberian craton (Blodgett and Brease, 1997).

Biogeographic affinities of lower Paleozoic faunas can constrain the paleogeographic position of central Alaska, but the faunas discussed above are not particularly useful for such analyses. Deep-water conodont faunas, and most conodont faunas of Silurian and Devonian age, are relatively cosmopolitan. With the exception of a faunule from the upper part of the Telsitna Formation in the Nixon Fork terrane (loc. 5, fig. 2; table 1), conodont collections from deep-water facies in the Medfra area consist of tropical cosmopolites, pandemics, and North American Midcontinent species. The collection at locality 5, however, of late Middle-Late Ordovician age, consists chiefly of Siberian-Alaskan province (SAP) elements with minor pandemics.

SAP elements are common in some collections from shallow-water facies of the Nixon Fork terrane, particularly those of late Early-Middle Ordovician age (Dumoulin, Bradley, and others, 1998). They are also noteworthy in some Early, Middle, and Late Ordovician faunas from the western and central Brooks Range and Seward Peninsula of northern Alaska (Dumoulin and Harris, 1994). A full explication of the biogeography of lower Paleozoic rocks in central Alaska is beyond the scope of this paper, but it is worth noting here that Siberian-Alaskan province elements have not been identified from Paleozoic conodont faunas of east-central Alaska or northwestern Canada (Dumoulin, Harris, and de Freitas, 1998; A.G. Harris, unpub. data).

Conclusions

Deep-water facies of Cambrian through Devonian age crop out widely in the eastern Medfra and western Mt. McKinley quadrangles and have been included in several discrete terranes. Calcareous hemipelagic deposits and fine-grained carbonate turbidites comprise the upper part of the Telsitna Formation (Middle-Upper Ordovician) and the Paradise Fork Formation (Lower Silurian–Lower Devonian) in the Nixon Fork terrane, the East Fork Hills Formation (Upper Cambrian–Lower Devonian) in the East Fork subterrane of the Minchumina terrane, and western exposures of the chert and argillite unit (Ordovician) in the Telida subterrane of the Minchumina terrane. These strata were derived largely from the Nixon Fork carbonate platform and correlate well with parts of the Dillinger terrane exposed to the south. The chert and argillite unit (eastern outcrops) and the argillite and quartzite unit (Silurian-Devonian? and possibly older) in the Telida subterrane of the Minchumina terrane consist chiefly of siliceous hemipelagic deposits and quartzofeldspathic turbidites and may correlate with parts of the Wickersham and Livengood terranes to the northeast (Livengood quadrangle). The Telida subterrane as presently defined thus includes two roughly coeval sequences of disparate origin.

Deep-water strata of the Minchumina and Dillinger terranes restore to a position east of the Nixon Fork carbonate platform when 90 and 150 km of dextral strike-slip on the Iditarod and Farewell faults, respectively, are removed. This restoration and our petrographic and paleontologic data suggest that lower Paleozoic rocks in the Nixon Fork and Dillinger terranes, as well as those in the western part of the Minchumina terrane, formed along a single continental margin. Strata in the eastern part of the Minchumina terrane (eastern part of the Telida subterrane) differ in composition and provenance from those to the west and may have had a distinct geologic history.

Acknowledgments

Tom Bundtzen and Grant Abbott accompanied the field party and provided valuable insights about potentially correlative rocks in the Alaska Range and Yukon. Tim Kusky helped with structural studies at Lake Minchumina. Stan Finney identified a key graptolite collection. We thank Jack and Sherry Hayden of Denali West Lodge for logistical support.

References Cited

Armstrong, H.A., 1990, Conodonts from the Upper Ordovician–Lower Silurian carbonate platform of north Greenland: Gronlands Geologiske Undersogelse Bulletin 159, 151 p.

Barrick, J.E., and Klapper, G., 1976, Multielement Silurian (late Llandoverian-Wenlockian) conodonts of the Clarita Formation, Arbuckle Mountains, Oklahoma, and phylogeny of *Kockelella*: Geologica et Palaeontologica, v. 10, p. 59–100.

Blodgett, R.B., and Clough, J.G., 1985, The Nixon Fork Terrane—Part of an *in situ* peninsular extension of the Paleozoic North American continent [abs.]: Geological Society of America, Abstracts with Programs, v. 17, no. 6, p. 342.

Blodgett, R.B., and Brease, P.F., 1997, Emsian (late Early Devonian) brachiopods from Shellabarger Pass, Talkeetna C-6 quadrangle, Denali National Park, Alaska indicate Siberian origin for Farewell terrane [abs.]: Geological Society of America, Abstracts with Programs, v. 29, no. 5, p. 5.

Bundtzen, T.K., Laird, G.M., Blodgett, R.B., Clautice, K.H., and Harris, E.E., 1994, Geology of the Gagaryah River area, Lime Hills C-5 and C-6 quadrangles, southwest Alaska: Alaska Divison of Geological & Geophysical Surveys Public Data File 94-40, 17 p., 1 plate, scale 1:63,360.

Chapman, R.M., Churkin, Michael, Jr., Carter, Claire, and Trexler, J.H., Jr., 1981, Ordovician graptolites and early Paleozoic radiolarians in the Lake Minchumina area date a regional shale and chert belt, *in* Albert, N.R.D., and Hudson, Travis, eds., The U.S. Geological Survey in Alaska: Accomplishments During 1979: U.S. Geological Survey Circular 823-B, p. B32–B34.

Chapman, R.M., Weber, F.R., Churkin, Michael, Jr., and Carter, Claire, 1980, The Livengood Dome Chert: A new Ordovician formation in central Alaska and its relevance to displacement on the Tintina fault, *in* Shorter Contributions to Stratigraphy and Structural Geology, 1979: U.S. Geological Survey Professional Paper 1126-F, p. F1–F13.

Chapman, R.M., and Yeend, Warren, 1981, Geologic reconnaissance of the east half of Kantishna River quadrangle and adjacent areas, *in* Albert, N.R.D., and Hudson, Travis, eds., The U.S. Geological Survey in Alaska: Accomplishments During 1979: U.S. Geological Survey Circular 823-B, p. B30–B32.

Chapman, R.M., Yeend, W.E., and Patton, W.W., Jr., 1975, Prelíminary reconnaissance map of the western half of Kantishna River quadrangle, Alaska: U.S. Geological Survey Open-File Map 75-351, scale 1:250,000.

Churkin, Michael, Jr., and Carter, Claire, 1996, Stratigraphy, structure, and graptolites of an Ordovician and Silurian sequence in the Terra Cotta Mountains, Alaska Range, Alaska: U.S. Geological Survey Professional Paper 1555, 84 p.

Cook, H.E., Hine, A.C., and Mullins, H.T., 1983, Platform margin and deep water carbonates: Society of Economic Paleontologists and Mineralogists Short Course Notes No. 12, 573 p.

Corradini, Carlo, Ferretti, Annalisa, Serpagli, Enrico, and Barca, Sebastiano, 1998, The Ludlow-Pridoli section Genna Ciuerciu, west of Silius: Giornale di Geologia, ser. 3, Special Issue, ECOS VII-Sardinia Guidebook, p. 112–118.

Decker, John, Bergman, S.C., Blodgett, R.B., Box, S.E., Bundtzen, T.K., Clough, J.G., Coonrad, W.L., Gilbert, W.G., Miller, M.L., Murphy, J.M., Robinson, M.S., and Wallace, W.K., 1994, Geology of southwestern Alaska, *in* Plafker, George, and Berg, H.C., eds., The Geology of Alaska: Boulder, Colo., Geological Society of America, The Geology of North America, v. G-1, p. 285–310.

Dumoulin, J.A., Bradley, D.C., Harris, A.G., and Repetski, J.E., 1998, Sedimentology, conodont biogeography, and subsidence history of the Nixon Fork terrane, Medfra quadrangle, Alaska [abs.]: Celle, Germany, III International Conference on Arctic Margins Abstracts, p. 49.

Dumoulin, J.A., and Harris, A.G., 1994, Depositional framework and regional correlation of pre-Carboniferous metacarbonate rocks of the Snowden Mountain area, central Brooks Range, northern Alaska: U.S. Geological Survey Professional Paper 1545, 74 p.

Dumoulin, J.A., Harris, A.G., and de Freitas, T.A., 1998, Facies patterns and conodont biogeography in Arctic Alaska and the Canadian Arctic Islands: Evidence against juxtaposition of these areas during early Paleozoic time [abs.]: Celle, Germany, III International Conference on Arctic Margins Abstracts, p. 50.

Dutro, J.T., Jr., and Patton, W.W., Jr., 1982, New Paleozoic formations in the northern Kuskokwim Mountains, west-central Alaska, *in* Stratigraphic Notes, 1980–1982: U.S. Geological Survey Bulletin 1529-H, p. H13–H22.

Fortey, R.A., Harper, D.A.T., Ingham, J.K., Owen, A.W., and Rushton, A.W.A., 1995, A revision of Ordovician series and stages from the historical type area: Geological Magazine, v. 132, no. 1, p. 15–30.

Gilbert, W.G., and Bundtzen, T.K., 1984, Stratigraphic relationship between Dillinger and Mystic terranes, western Alaska Range, Alaska [abs.]: Geological Society of America Abstracts with Programs, v. 16, no. 5, p. 286.

Grantz, Arthur, 1966, Strike-slip faults in Alaska: U.S. Geological Survey Open-File Report 267, 82 p.

Jaeger, Hermann, 1975, Die Graptolithenführung im Silur/Devon des Cellon-Profils (Karnische Alpen): Carinthia II, p. 111–126.

Jeppsson, Lennart, 1972, Some Silurian conodont apparatuses and possible conodont dimorphism: Geologica et Palaeontologica, no. 6, p. 51–69.

Jones, D.L., Silberling, N.J., Berg, H.C., and Plafker, George, 1981, Map showing tectonostratigraphic terranes in Alaska, columnar sections, and summary description of terranes: U.S. Geological Survey Open-File Report 81-792, 20 p., 2 sheets, scale 1:2,500,000.

Kleffner, M.A., 1995, A conodont- and graptolite-based Silurian chronostratigraphy, *in* Mann, K.O., and Lane, H.R., eds., Graphic Correlation: SEPM Society for Sedimentary Geology Special Publication No. 53, p. 159–176.

Measures, E.A., Rohr, D.M., and Blodgett, R.B., 1992, Depositional environments and some aspects of the fauna of Middle Ordovician rocks of the Telsitna Formation, northern Kuskokwim Mountains, Alaska, *in* Bradley, D.C., and Dusel-Bacon, Cynthia, eds., Geologic Studies in Alaska by the U.S. Geological Survey, 1991: U.S. Geological Survey Bulletin 2041, p. 186–201.

Miller, M.L., and Bundtzen, T.K., 1988, Right-lateral offset solution for the Iditarod-Nixon Fork fault, western Alaska: U.S. Geological Survey Circular 1016, p. 99–103.

Nowlan, G.S., McCracken, A.D., and Chatterton, B.D.E., 1988, Conodonts from Ordovician-Silurian boundary strata, Whittaker Formation, Mackenzie Mountains, Northwest Territories: Geological Survey of Canada Bulletin 373, 99 p.

Oliver, W.A., Jr., Merriam, C.W., and Churkin, Michael, Jr., 1975, Ordovician, Silurian, and Devonian corals of Alaska: U.S. Geological Survey Professional Paper 823-B, p. 13–44.

Patton, W.W., Jr., Box, S.E., Moll-Stalcup, E.J., and Miller, T.P., 1994, Geology of west-central Alaska, *in* Plafker, George, and Berg, H.C., eds., The Geology of Alaska: Boulder, Colo., Geological Society of America, The Geology of North America, v. G-1, p. 241–269.

Patton, W.W., Jr., Moll, E.J., Dutro, J.T., Jr., Silberman, M.L., and Chapman, R.M., 1980, Preliminary geologic map of the Medfra quadrangle, Alaska: U.S. Geological Survey Open-File Report 80-811A, scale 1:250,000.

Patton, W.W., Jr., Moll, E.J., and King, H.D., 1984, The Alaskan Mineral Resources Assessment Program: Guide to information contained in the folio of geologic and mineral-resource maps of the Medfra quadrangle, Alaska: U.S. Geological Survey Circular 928, 11 p.

Savage, N.M., Rohr, D.M., and Blodgett, R.B., 1995, Late Silurian conodonts from the Medfra B-4 quadrangle, west-central Alaska [abs.]: Geological Society of America Abstracts with Programs, v. 27, no. 5, p. 76–77.

Scholle, P.A., Bebout, D.G., and Moore, C.H., 1983, Carbonate depositional environments: American Association of Petroleum Geologists Memoir 33, 708 p.

Silberling, N.J., Jones, D.L., Monger, J.W.H., Coney, P.J., Berg, H.C., and Plafker, George, 1994, Lithotectonic terrane map of Alaska and adjacent parts of Canada, *in* Plafker, George, and Berg, H.C., eds., The Geology of Alaska: Boulder, Colo., Geological Society of America, The Geology of North America, v. G-1, plate 3, 1 sheet, scale 1:2,500,000.

Tipnis, R.S., 1979, Fused clusters of *Ptiloncodus simplex* Harris: An Ordovician phosphatic microfossil, *in* Current Research, Part C: Geological Survey of Canada Paper 79-1C, p. 51–54.

Weber, F.R., Wheeler, K.L., Rinehart, C.D., Chapman, R.M., and Blodgett, R.B., 1992, Geologic map of the Livengood quadrangle, Alaska: U.S. Geological Survey Open-File Report 92-562, 20 p., scale 1:250,000.

Wilson, F.H., Dover, J.H., Bradley, D.C., Weber, F.R., Bundtzen, T.K., and Haeussler, P.J., 1998, Geologic map of central (Interior) Alaska: U.S. Geological Survey Open-File Report 98-133, 3 sheets, scale 1:500,000, 63 p.

Wilson, J.L., 1975, Carbonate facies in geologic history: New York, Springer-Verlag, 471 p.

Reviewers: W.W. Patton, Jr. and F.R. Weber.

Geologic Studies in Alaska by the
U.S. Geological Survey, 1997
U.S. Geological Survey Professional Paper 1614

Alagogshak Volcano: A Pleistocene Andesite-Dacite Stratovolcano in Katmai National Park

By Wes Hildreth, Judy Fierstein, Marvin A. Lanphere, *and* David F. Siems

Abstract

Alagogshak volcano, a newly recognized volcanic-front stratovolcano on the Alaska Peninsula rangecrest, 15 km southwest of Katmai Pass, produced 10–18 km^3 of andesite-dacite eruptive products during several episodes of activity in the middle and late Pleistocene. From a central vent marked by hydrothermal alteration and remnants of a cratered fragmental cone on the present-day drainage divide, glacially incised stacks of lava flows (57–66 percent SiO_2) dip radially and extend 6–10 km in most directions. Lava flows that make up four ridge-capping outliers well west of the volcano may also have erupted there. The medium-K calcalkaline Alagogshak eruptive suite is compositionally varied, probably reflecting independent evolution of different magma batches supplied in several episodes spread intermittently over at least 600,000 years. In contrast, the exclusively Holocene andesite-dacite suite (59–64 percent SiO_2) produced by the Mount Martin cone, which is centered 3 km northeast of Alagogshak, yields far more coherent compositional trends.

Introduction

While studying the volcanoes of the Katmai cluster (fig. 1), we recognized a glacially eroded vent complex of Pleistocene age on the Alaska Peninsula drainage divide, 3 km southwest of the active crater of Mount Martin. Mapping in 1996 and 1997 demonstrated this vent to be the source of most of the glaciated lava flows nearby and showed Mount Martin to be a small, much younger edifice, constructed entirely during the Holocene. This note describes the remnants of what we call the Alagogshak volcano, estimates its original extent and volume, and compares the compositions of its eruptive products with those of nearby Mount Martin.

Glacially Eroded Ediface

Surviving remnants of Alagogshak volcano are mapped in figure 2. The high point today is a rounded ice-capped knob at an elevation of about 6,020 ft (1,835 m) on the rangecrest 12.5 km northeast of Kejulik Pass, 15 km southwest of Katmai Pass, and 95 km southeast of the town of King Salmon (fig. 1). This summit forms the east rim of a glacially gutted vent complex, from which lavas flowed north toward Angle Creek, south into the forks of Kejulik River, and southeast into Alagogshak Creek.

The vent is an area of focused hydrothermal alteration about 800 m wide, now hollowed out as a cirque-amphitheater (fig. 3) occupied by a northwest-draining glacier. Preserved along its south rim (the present rangecrest) are outward-dipping agglutinates, beds of coarse scoria (57–58 percent SiO_2), and poorly sorted layers of phreatomagmatic ejecta rich in dense glassy blocks. Preserved along the north rim of the cirque (fig. 3) are part of the fumarolically acid altered core, a remnant of the old crater rim draped by stratified ejecta that dip both inward and outward, and an effusive lava flow of black glassy dacite (63.7 percent SiO_2) that dips 20° NW. and is as thick as 140 m.

Stacks of lava flows that dip radially away from the vent region are well preserved in four main sectors (fig. 2). In all sectors, the lavas were emplaced onto a ruggedly incised glacial terrain that had more than 1,200 m of local relief, cut entirely into subhorizontal siltstone and sandstone of the Jurassic Naknek Formation (Riehle and others, 1993). To the south, at the head of the east fork of Kejulik River, a set of glaciated benches that steps down from the summit to an elevation as low as 1,500 ft (450 m) consists of a stack of at least seven andesitic lava flows (57–63 percent SiO_2), which range from 10 to 30 m thick. At their present-day distal extremity, canyon-wall remnants of these flows range in elevation from 1,500 ft to as high as 2,300 ft (700 m), indicating that the stack was once at least 250 m thick there and suggesting that intracanyon lava flows formerly extended much farther downstream.

To the southwest, the Kejulik River cleaver is a stack of about 20 andesite-dacite lava flows (fig. 4) that dip gently away from the vent and range from 8 to 40 m thick and from 58 percent to 66 percent SiO_2. The greatest thickness of the stack preserved is 950 ft (300 m). One of the lavas thickens southward as a formerly intracanyon flow as thick as 80 m that today forms a sinuous interfluve along the east wall of the main Kejulik River (fig. 2), where its lowest basal elevation is 1,300 ft (400 m).

To the northwest, two glaciated lava-flow stacks of different ages face each other across the outlet gorge that drains the

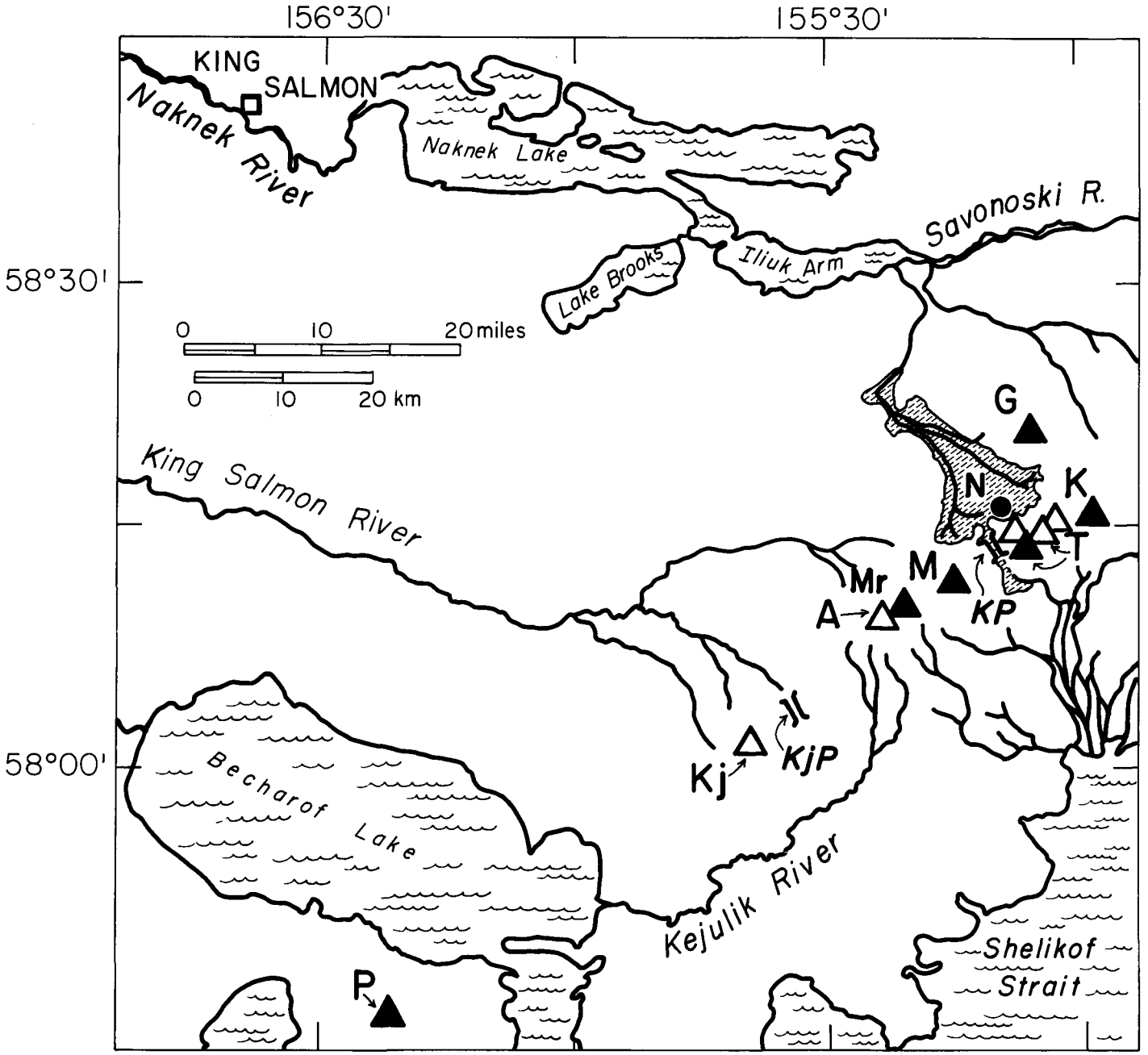

Figure 1. Map showing part of the stratovolcanic chain along the Alaska Peninsula, southeast of the town of King Salmon. Solid triangles indicate cones active during the Holocene; open triangles indicate Pleistocene cones long extinct. The Katmai volcanic cluster includes Alagogshak (A), Martin (Mr), Mageik (M), Griggs (G), Trident (T; three extinct cones and one recently active cone), and Mount Katmai (K). Farther southwest are Kejulik (Kj) and Peulik (P) volcanoes. Solid circle (N) indicates Novarupta, site of the great explosive eruption of 1912, when ignimbrite (shaded valley fill) was emplaced in the Valley of Ten Thousand Smokes (Hildreth, 1983). Low points along the volcanic axis, which here forms the Alaska Peninsula drainage divide, include Katmai Pass (KP) and Kejulik Pass (KjP).

vent-cirque glacier toward Angle Creek. Today, both stacks reach about 6 km from the vent, dipping 5°–10° NNW., but they originally extended many kilometers farther. The western (older) stack is a set of three or four andesite flows (60–63 percent SiO_2), each 50 to 125 m thick, that widely exhibit basal colonnades and thick entablatures of slender glassy columns that suggest ice-contact emplacement. The eastern stack begins with three dacite lava flows (each 64 percent SiO_2), one of which is 200 m thick, glassy, columnar, probably englacial, and descends to a basal elevation as low as 1,900 ft (580 m)—about 90 m lower than the nearby older stack. The dacites are overlain proximally by three or four more andesite-dacite lava flows (58–64 percent SiO_2) that are extensively covered by ice and till but include the thick crater-rim dacite illustrated in figure 3.

To the southeast, a single thick glassy andesite lava flow (61 percent SiO_2) descended steeply from the rangecrest and spread into Alagogshak Creek, where it now forms a glacially scoured plateau. Its base is today as low as 1,500 ft (450 m), but because the flow thickens to more than 100 m at its distal extremity, it must have extended much farther downstream prior to glacial excavation.

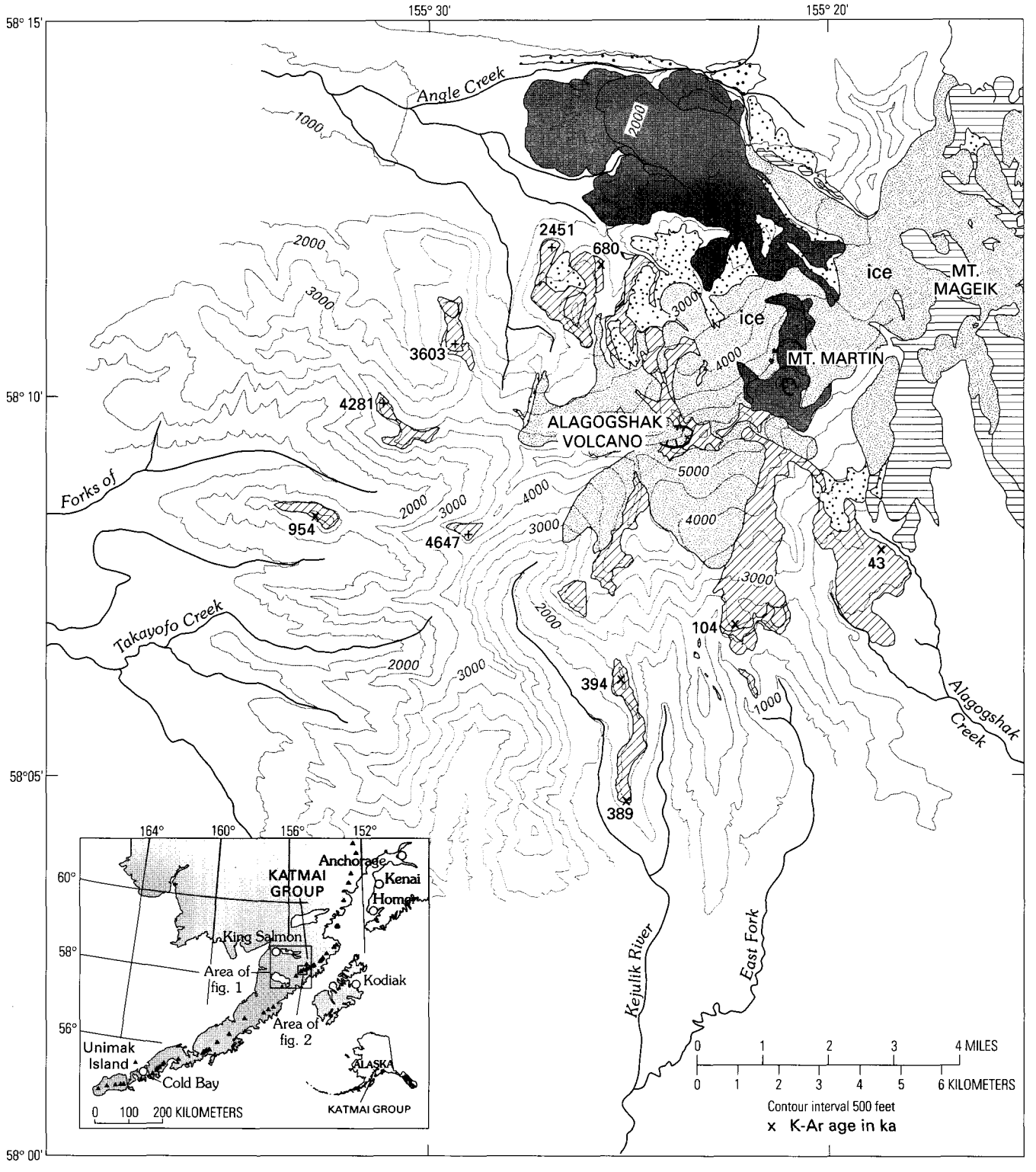

Figure 2. Distribution of Holocene eruptive products of Mount Martin (dark shading) and glacially eroded Pleistocene lavas of Alagogshak volcano (diagonal pattern). Their craters are indicated by hachures. Also shown is the western half of Mount Mageik (horizontal pattern) and various glacial deposits (stippled pattern). Pale shading is glacial ice, and uncolored regional basement is Jurassic Naknek Formation (plus scattered surficial deposits and a few Tertiary intrusive rocks, not indicated). Elevations (+) in feet (1 m=3.28 ft). Locations of samples dated by K-Ar method (table 1, this report; Shew and Lanphere, 1992) are indicated by "X" accompanied by age (in ka). Topographic base simplified from USGS 1:63,360 quadrangles Mt. Katmai A-4 and A-5.

Western Outliers

In addition to the four unequivocal outflow sectors just described, four craggy outliers of ridge-capping andesite 6–10 km west of the Alagogshak vent (fig. 2) may also have erupted there.

The northernmost outlier, at peak 3603 on the divide between tributaries of Angle Creek, consists of three, gently northwest dipping, andesite lava flows (57–61 percent SiO_2), each as thick as 100 m. Thick flow-breccia and glassy columnar zones suggest ice-contact emplacement. The southernmost (and

Figure 3. View northward from south-rim rangecrest across vent area of Alagogshak volcano, glacially gutted to produce an 800-m-wide cirque-amphitheater that opens to the northwest (left). Acid-altered crater-fill forms lower wall beyond ice. Black ridge is part of a 140-m-thick dacitic outflow lava (samples K-2089, 2089A) that dips 20° NW. (left). Knob 5290 at upper right is a crater-rim remnant, across which stratified ejecta drape both inward and outward.

Figure 4. Stack of twelve andesite lava flows (exposed above the ice) along upper part of Kejulik cleaver, at elevation 4,900–5,150 ft, 3 km southwest of the Alagogshak vent. View toward the northeast. As many as eight more flows, stratigraphically lower in the stack, form basal part of the cleaver (behind the camera).

smallest) of the outliers, capping peak 4647 on the divide between Kejulik River and Takayofo Creek, is a single lava flow of silicic andesite (62 percent SiO_2) as thick as 200 m. Between them, on the Takayofo-Angle Creek divide, a third outlier consists of coarse flow-breccia and four lava flows, three of which are atypically mafic (52–53 percent SiO_2) for Alagogshak and unusually rich in big clinopyroxene and plagioclase phenocrysts. Overlying these on the northwestern spur of the outlier (peak 4281), the fourth lava consists of a 100-m-thick flow of ordinary Alagogshak-type andesite (58 percent SiO_2). Finally, the fourth

and westernmost outlier, which caps the ridge dividing two tributaries of Takayofo Creek (fig. 2), consists of a single phenocryst-rich andesite lava flow (61–62 percent SiO_2) as thick as 200 m. Shew and Lanphere (1992) reported a K-Ar age of 954±109 ka for plagioclase separated from this flow.

Basal contacts of the outliers dip gently away from the Alagogshak center, except for the westernmost outlier, which is subhorizontal. As each of the four remnants rests upon Jurassic sedimentary rocks along low-angle contacts that are now perched 300–600 m above the floors of adjacent glacial valleys, it is clear on physiographic grounds that all the outliers are relatively old. No other source vent or dike has been recognized, however, between Alagogshak volcano and the still older Kejulik stratocone, 21 km farther southwest (Riehle and others, 1993; Shew and Lanphere, 1992). Our favored but inconclusive inference is that the lava flows of the outliers, at least most of them, represent eruptive phases of Alagogshak volcano older than the episodes that produced the andesites and dacites in the four more proximal sectors described above.

Geochronology

K-Ar ages were measured for whole-rock samples of andesitic lava flows in three of the proximal sectors described (table 1), employing the multiple-collector mass spectrometer at the U.S. Geological Survey (USGS) in Menlo Park (Stacey and others, 1981) and following the methods described by Hildreth and Lanphere (1994). Plagioclase K-Ar ages were reported previously by Shew and Lanphere (1992) for lava flows in the fourth sector, as well as for the old, westernmost outlier.

In the older stack of andesite lavas in the northwest sector, the basal flow (resting on Jurassic strata) gives an age of 680±20 ka. To the south, the top flow of the stack of seven andesite lavas at the head of the east fork of Kejulik River yields an age of 104±10 ka. To the southeast, the thick plateau-forming andesite lava flow at the head of Alagogshak Creek gives an age of 43±8 ka. All three nonglassy whole-rock samples provided satisfactory yields of radiogenic argon (6–13 percent $^{40}Ar^*$; table 1), permitting high-precision age determinations.

In the southwest sector, plagioclase separated from two of three andesite-dacite lava flows that make up the sinuous remnant of an intracanyon stack along the main fork of Kejulik River provided accordant ages of 394±46 ka and 389±71 ka (Shew and Lanphere, 1992). Finally, Shew and Lanphere (1992) measured an age of 954±109 ka for plagioclase from the crystal-rich andesite that makes up the westernmost outlier (fig. 2).

The apparent longevity of more than 600 k.y. (or 900 k.y. if the westernmost outlier did indeed erupt from the Alagogshak center) is greater than that of many andesite-dacite stratovolcanoes, but it is not extraordinary. In the Cascade arc, for example, high-precision K-Ar measurements in our Menlo Park laboratory indicate that the Adams, Baker, Hood, Lassen, Mazama, and Rainier volcanic centers have erupted intermittently for comparably long periods of time. Owing in part to its modest eruptive volume, however, the longevity of volcanism at Alagogshak seems to require that long periods of repose separated its episodes of eruptive activity.

Eruptive Volume

Much of Alagogshak volcano has been erosively stripped. Rapid rates of erosion have been promoted by Pleistocene expansions of glacial ice that repeatedly covered most of the Alaska Peninsula (Riehle and Detterman, 1993). Areas still covered by products of the Alagogshak center thus sum to less than 20 km^2, less even than the area (33 km^2) covered by the postglacial products of Mount Martin (fig. 2). Distribution of the remnants shown in figure 2 clearly indicates, however, that the area originally covered by Alagogshak lavas was at least 60 km^2 and, if the western outliers and distal intracanyon lava tongues are included, perhaps as much as 90 km^2.

Volume reconstruction is somewhat less certain. Because the central vent of Alagogshak straddles a rangecrest arête of Jurassic sandstone that today extends (at 1,550–1,620 m elevation) for more than 4 km west of its 1,835-m summit, it is obvious that a cone model is inappropriate for the volume calculation. From a modest vent cone perched on a basement high, lavas flowed steeply outward into cirques and valleys to the north, south, and west. Judging by the rim-draping fall and surge

Table 1. Whole-rock potassium-argon ages and analytical data.

[Analysts: potassium by D.F. Siems; argon by F.S. McFarland and J.Y. Saburomaru (Menlo Park, Calif.). Constants: $\lambda_\varepsilon = 0.581 \times 10^{-10}\ y^{-1}$; $\lambda b = 4.962 \times 10^{-10}\ y^{-1}$; $^{40}K/K = 1.167 \times 10^{-4}$ mol/mol]

Sample number	Location (see fig. 2)	Weight percent		Radiogenic ^{40}Ar		Calculated age
		SiO_2	K_2O	10^{-13}mol/g	Percent	
K-2049	Alagogshak Creek: Plateau-forming lava flow, 2,300 ft	61.1	1.644±0.008	1.007	6.0	43±8 ka
K-2135	Kejulik River, East Fork: Top lava of stack at 2,500 ft rim	57.7	1.580±0.004	2.369	9.0	104±10 ka
K-2074	Angle Creek, SE. Fork: Basal lava flow, W. wall of gorge at 2,300 ft	60.0	1.419±0.001	13.90	13.3	680±20 ka

deposits preserved on remnants of the crater walls (fig. 3), the vent cone is unlikely to have been more than 100–200 m higher than the present summit. By comparison, the present-day active crater of Mount Martin is about 225 m deep and the crater of Mount Mageik only about 100 m. Conservatively, then, if we assume original thicknesses of only 500 m for the perched vent region and an *average* of 250 m for the flanking stacks of outflow lavas, we estimate 10–13 km^3 for the Alagogshak edifice—or 13–18 km^3 if all the western outliers are assigned to Alagogshak. This is much larger than our estimate for modern Mount Martin (7 km^3) but far less voluminous than for nearby Mageik (30 km^3) and Griggs (20–25 km^3) volcanoes. No evidence has been found of voluminous tephra that might add appreciably to Alagogshak's eruptive volume, nor would the former existence of much glacially stripped fallout be expected on the basis of the generally low explosivity eruptive products preserved.

Mount Martin

Mount Martin is a small Holocene successor volcano that barely overlaps the northeastern edge of the glaciated Alagogshak edifice. Its inception postdates the last known activity at Alagogshak by about 30,000 years (table 1), and its fumarolically active crater lies 3 km northeast of the ravaged central vent of Alagogshak. Mount Martin consists of a small fragmental cone and, descending 10 km northwestward, a staircase of 10 overlapping coulees of blocky dacite, each 75–100 m thick. Although its summit exceeds 6,100 ft (1,860 m) in elevation, the 2-km-wide cone itself has local relief of only 500 m, owing to its construction (like Alagogshak) upon a high ridge of Jurassic basement rocks. Of the total eruptive volume estimated for Mount Martin (7 km^3), the small cone thus makes up less than 5 percent and the 31-km^2 lava-flow field about 95 percent (fig. 2). Scoriaceous and massive glassy (phreatomagmatically ejected) blocks of the cone are andesitic (58.9–61percent SiO_2), whereas the sequence of coulees is largely dacitic (62.5–64.2 percent SiO_2; table 2). Despite its high ring of active glaciers (fig. 2), erosion of the cone and coulees is insignificant, indicating that Mount Martin is a Holocene volcano in its entirety. The glaciated lava flows adjacent to Martin's western flank are readily distinguishable, chemically and stratigraphically, as having erupted at Alagogshak volcano. The cone of Mount Martin is marked by a persistent steam plume derived from as many as 20 vigorous fumaroles that are precipitating sulfur in the talus northwest of a shallow acid lake on the floor of its 300-m-wide crater.

Composition of Eruptive Products

Nearly all lava flows from Mount Martin and most of the exposed flows surviving at Alagogshak were sampled, as were glassy blocks of juvenile ejecta from the rims of both craters. Major-element determinations by X-ray fluorescence spectroscopy are given in table 2 and illustrated in figure 5. Essentially all samples from both volcanoes are plagioclase-rich two-pyroxene andesites and dacites, all of which also carry Fe-Ti-oxide microphenocrysts, but none of which contain amphibole, biotite,

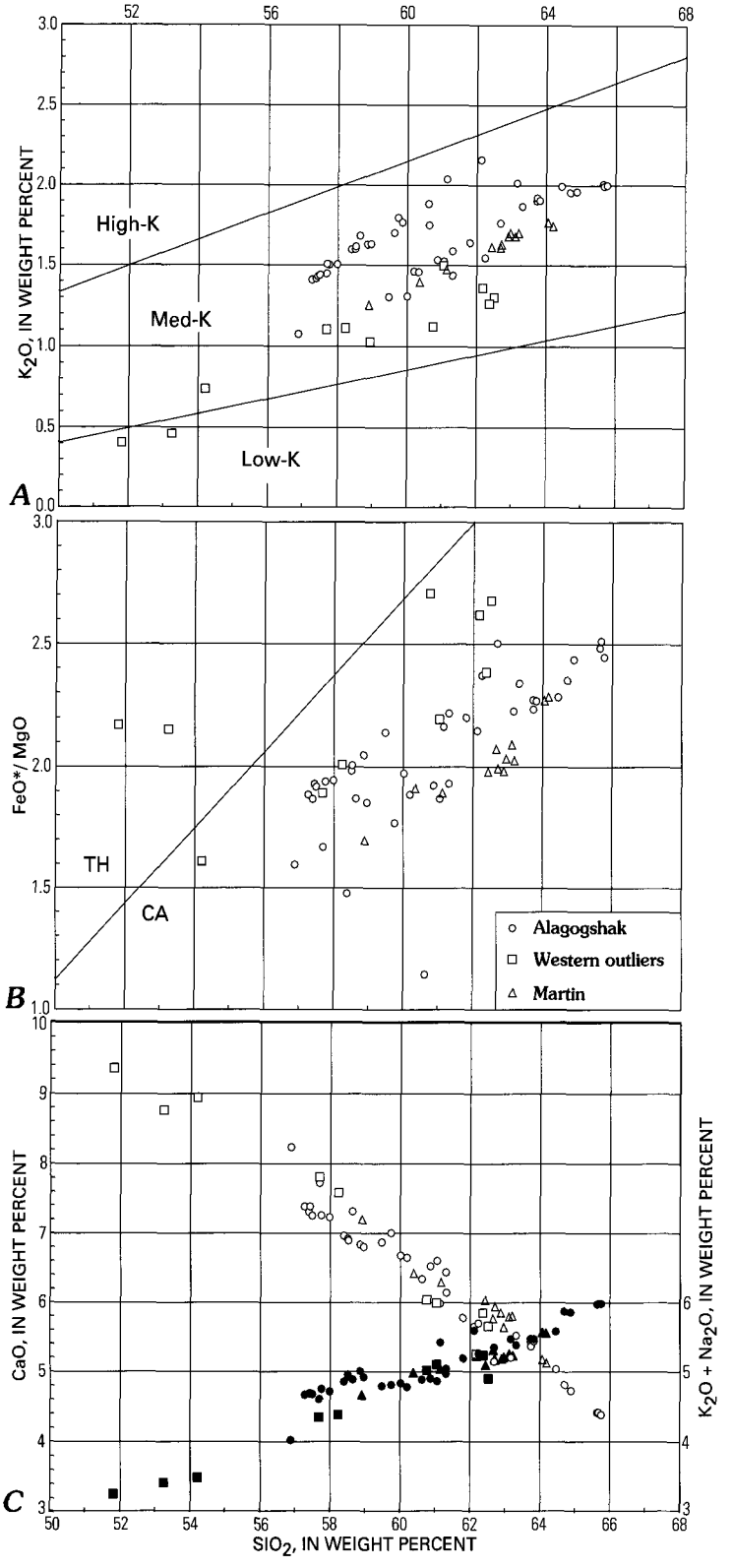

Figure 5. Whole-rock compositional data for Alagogshak and Martin volcanoes and the western outliers: *A*, K_2O vs. SiO_2; *B*, FeO*/MgO vs. SiO_2; *C*, (K_2O + Na_2O) (closed symbols) and CaO (open symbols) vs. SiO_2. TH/CA is conventional boundary between tholeiitic and calcalkaline suites in panel *B*. FeO* is total iron calculated as FeO.

Table 2. *Chemical analyses of eruptive products.*

[The ten major oxides are normalized to H_2O-free totals of 99.6 weight percent (allowing 0.4 weight percent for trace oxides and halogens). Determinations by wavelength-dispersive X-ray fluorescence in USGS laboratory at Lakewood, Colo.; D.F. Siems, analyst. "FeO*" is total iron calculated as FeO. "Original total" is the volatile-free sum of the ten oxides, as analyzed, before normalization, with total iron calculated as Fe_2O_3. LOI, weight percent loss on ignition at 900°C]

Sample no.	SiO_2	TiO_2	Al_2O_3	FeO*	MnO	MgO	CaO	Na_2O	K_2O	P_2O_5	LOI	Original total (dry)
ALOGOGSHAK VOLCANO												
K-2049	61.1	0.70	16.1	6.55	0.13	3.50	6.60	3.33	1.53	0.15	0.13	99.40
2049-i	56.9	0.72	16.7	7.83	0.15	4.90	8.24	2.94	1.08	0.15	0.56	98.66
2074	60.0	0.73	17.1	6.63	0.14	3.36	6.68	3.52	1.31	0.17	0.51	98.58
2075	62.2	0.67	16.5	6.31	0.12	2.66	5.70	3.71	1.55	0.17	0.31	98.81
2076	62.7	0.70	16.4	6.44	0.13	2.57	5.15	3.58	1.76	0.15	0.81	98.43
2077	60.2	0.66	16.4	6.93	0.14	3.67	6.65	3.31	1.46	0.15	0.24	98.72
2078	60.6	0.64	14.7	6.46	0.13	5.65	6.34	3.00	1.88	0.17	1.55	97.77
2079	61.3	0.68	16.6	6.59	0.13	2.97	6.14	3.60	1.44	0.17	0.56	98.41
2080	61.8	0.67	16.3	6.60	0.13	3.00	5.78	3.55	1.64	0.17	0.72	98.49
2081	64.5	0.69	15.4	5.67	0.11	2.48	5.04	3.59	1.99	0.15	0.12	98.85
2082	63.7	0.69	15.6	5.86	0.12	2.62	5.36	3.55	1.92	0.16	0.51	98.39
2083	63.8	0.69	15.6	5.75	0.11	2.54	5.44	3.56	1.90	0.15	0.02	99.23
2087	62.1	0.76	16.0	6.27	0.12	2.92	5.65	3.43	2.16	0.19	-0.03	99.31
2088	58.6	0.73	16.4	7.40	0.14	3.96	7.31	3.20	1.68	0.18	0.02	99.11
2089	63.7	0.69	15.6	5.83	0.11	2.56	5.43	3.57	1.90	0.16	0.00	99.18
2089-A	63.3	0.71	15.7	6.07	0.12	2.60	5.52	3.51	1.87	0.16	0.11	98.92
2099	59.0	0.77	16.7	7.25	0.14	3.91	6.80	3.29	1.63	0.18	0.06	99.03
2100	59.8	0.74	16.2	6.86	0.14	3.88	7.01	3.01	1.80	0.18	1.34	97.60
2102	58.5	0.81	17.1	7.34	0.14	3.70	6.92	3.35	1.60	0.19	0.09	98.99
2103	57.3	0.80	17.2	7.79	0.14	4.13	7.39	3.25	1.41	0.18	0.22	99.04
2104	57.4	0.80	17.4	7.61	0.14	3.94	7.39	3.26	1.43	0.19	0.15	98.86
2105	57.8	0.79	17.1	7.66	0.14	3.95	7.26	3.24	1.50	0.18	0.24	98.76
2106	61.2	0.77	16.1	6.72	0.13	3.11	5.99	3.38	2.04	0.19	1.20	97.74
2107	58.9	0.82	16.9	7.28	0.13	3.55	6.83	3.37	1.63	0.19	0.24	98.77
2108	57.4	0.80	17.3	7.68	0.14	4.11	7.31	3.27	1.42	0.19	0.26	98.99
2109	63.2	0.69	16.3	5.84	0.11	2.62	5.20	3.45	2.02	0.18	0.74	98.32
2110	57.5	0.81	17.3	7.72	0.14	4.02	7.26	3.23	1.44	0.18	0.30	98.93
2111	58.0	0.80	17.1	7.57	0.14	3.89	7.23	3.20	1.51	0.18	0.25	98.67
2112	58.5	0.80	17.0	7.43	0.14	3.71	6.90	3.31	1.62	0.19	0.26	98.87
2120	64.7	0.63	15.7	5.33	0.12	2.27	4.81	3.91	1.95	0.18	0.01	99.27
2121	65.6	0.61	15.5	5.08	0.12	2.05	4.42	3.97	2.01	0.17	0.14	98.96
2122	59.5	0.70	17.1	7.04	0.14	3.29	6.87	3.49	1.30	0.19	0.81	98.55
2123	58.4	0.75	16.2	7.23	0.14	4.90	6.96	3.25	1.60	0.17	0.76	98.63
2124	65.8	0.60	15.6	4.99	0.12	2.04	4.38	3.98	2.00	0.17	0.15	99.01
2125	65.7	0.60	15.7	4.94	0.12	1.97	4.42	3.99	2.00	0.18	0.23	99.13
2135	57.7	0.73	16.3	7.66	0.14	4.58	7.72	3.15	1.45	0.18	0.15	98.54
2140	64.9	0.62	15.8	5.26	0.12	2.16	4.72	3.90	1.96	0.18	0.19	99.00
2141	60.9	0.69	16.4	6.53	0.13	3.39	6.53	3.36	1.53	0.15	0.59	98.91
2142	61.3	0.70	16.1	6.49	0.12	3.36	6.44	3.38	1.59	0.15	0.11	99.07
2259	60.6	0.75	16.6	6.70	0.14	3.24	6.31	3.31	1.75	0.21	0.84	98.27
2260	59.9	0.75	16.7	6.90	0.14	3.44	6.63	3.20	1.77	0.23	0.90	98.34
2261	59.6	0.75	16.6	7.13	0.14	3.46	6.82	3.18	1.70	0.20	0.82	98.45
2262	57.7	0.76	16.7	7.53	0.14	4.32	7.56	3.16	1.51	0.22	0.03	100.00
2263	60.3	0.70	16.9	6.56	0.13	3.21	6.84	3.33	1.46	0.17	0.27	98.77

quartz, or sanidine. Microdioritic blebs and clots, predominantly made up of pyroxene and plagioclase but generally containing a little glass, are common in the products of both centers. Some of the andesites that have less than 59 percent SiO_2 additionally carry a little olivine, as do mafic magmatic inclusions present in some Alagogshak lavas.

Thirteen samples from Mount Martin range from 58.9 percent to 64.2 percent SiO_2 and plot rather tightly (fig. 5) relative to the scattered compositional arrays for 44 samples from the long-lived Alagogshak center (54.2–65.8 percent SiO_2). All samples from both volcanoes fall in the medium-K field (fig. 5A), and both suites define calcalkaline differentiation trends

Table 2. Chemical analyses of eruptive products—*Continued.*

Sample no.	SiO_2	TiO_2	Al_2O_3	FeO*	MnO	MgO	CaO	Na_2O	K_2O	P_2O_5	LOI	Original total (dry)
ALOGOGSHAK VOLCANO—Western outliers, north												
K-2085	61.0	0.69	16.7	6.71	0.14	3.06	5.99	3.60	1.50	0.17	0.25	99.12
2085-i	54.2	0.63	19.9	7.48	0.15	4.65	8.95	2.75	0.74	0.14	0.98	98.45
2086	57.7	0.74	17.1	7.55	0.16	3.99	7.81	3.24	1.10	0.18	0.78	98.22
2253	58.9	0.64	17.2	6.98	0.14	3.67	7.63	3.16	1.03	0.17	0.12	99.53
ALOGOGSHAK VOLCANO—Western outliers, middle												
K-2168	58.2	0.72	17.2	7.47	0.15	3.72	7.58	3.27	1.11	0.18	0.21	99.23
2254	53.2	0.90	18.0	10.20	0.18	4.74	8.76	2.96	0.46	0.19	0.01	99.01
2255	51.8	0.92	18.3	10.66	0.20	4.91	9.36	2.85	0.40	0.16	-0.09	99.12
ALOGOGSHAK VOLCANO—Western outliers, south												
K-2257	62.2	0.73	16.5	6.76	0.14	2.58	5.25	3.86	1.36	0.22	2.72	95.72
2258	62.5	0.71	16.3	6.65	0.14	2.49	5.65	3.59	1.30	0.21	3.34	94.90
ALOGOGSHAK VOLCANO—Western outliers, westernmost												
K-2169	62.4	0.70	17.2	5.60	0.13	2.35	5.84	3.97	1.27	0.21	1.14	98.10
2256	60.8	0.74	17.0	7.07	0.16	2.61	6.04	3.89	1.12	0.21	0.27	98.08
MOUNT MARTIN												
K-2066	63.1	0.67	15.8	5.88	0.12	2.82	5.79	3.58	1.67	0.15	0.16	99.37
2067	62.4	0.66	16.0	6.04	0.12	3.05	6.03	3.48	1.61	0.15	0.04	99.25
2068	62.7	0.66	16.0	5.88	0.12	2.94	5.94	3.53	1.63	0.15	-0.05	99.31
2090	64.2	0.69	15.7	5.63	0.12	2.47	5.13	3.80	1.75	0.15	0.16	98.89
2093	63.2	0.65	15.7	5.83	0.12	2.87	5.79	3.53	1.70	0.15	-0.01	99.17
2094	62.9	0.68	15.7	5.97	0.12	3.01	5.85	3.52	1.67	0.15	0.24	98.85
2095	63.0	0.66	16.1	5.90	0.12	2.90	5.63	3.51	1.69	0.14	0.51	98.72
2096	62.7	0.65	16.1	5.86	0.12	2.93	5.94	3.56	1.62	0.15	0.19	99.00
2097	62.7	0.69	16.1	5.98	0.12	2.89	5.76	3.70	1.61	0.15	0.05	98.97
2098	60.4	0.73	16.5	6.73	0.13	3.52	6.42	3.59	1.39	0.17	-0.03	99.30
2115	61.2	0.72	16.2	6.46	0.13	3.42	6.29	3.56	1.47	0.17	-0.13	99.52
2170	64.1	0.67	15.8	5.59	0.12	2.47	5.17	3.80	1.76	0.15	0.12	99.16
2333	58.9	0.73	16.7	6.99	0.14	4.12	7.20	3.41	1.25	0.16	0.36	98.30

(fig. 5*B*). Alkali-lime intersections at 63–63.5 percent SiO_2 (fig. 5*C*) define calcic suites for both Alagogshak and Martin, similar to the zoned suite ejected at nearby Novarupta in 1912 (Hildreth, 1983).

The rocks of both volcanoes are typically low-Ti arc suites, most having TiO_2 contents of only 0.60–0.82 percent; the two most mafic samples (K-2254, K-2255, both from the middle outlier) have 0.90–0.92 percent TiO_2. Relatively primitive material has not erupted here, as all but one sample represents magma that had evolved to less than 5 percent MgO. Contents of Al_2O_3 are mostly <17.5 percent, although the three samples lowest in SiO_2 (fig. 5; all from the western outliers) have higher Al_2O_3 values of 18.0–19.9 percent.

Relatively mafic magmatic inclusions, generally finer grained than the host lava and typically 1–10 cm across, are common in a few Alagogshak lava flows, are sparse to absent in most, and were not found in products of Mount Martin. The two such inclusions analyzed (samples K-2049-i and K-2085-i) are among the least silicic (56.9 percent; 54.2 percent SiO_2) eruptive products sampled here.

Two subparallel trends are conspicuous for Alagogshak data in the K_2O-SiO_2 panel (fig. 5*A*), one suite having about 0.4 weight percent more K_2O than the other at any given SiO_2 content. The suite higher in K_2O includes (a) near-vent scoria; (b) 11 of 12 samples from the southerly (East Fork) sector; (c) 4 of 10 samples from the southwesterly (Kejulik cleaver) sector; and (d) 5 of 16 samples from the northwesterly (Angle Creek) sector. On the other hand, the trend lower in K_2O includes the southeasterly (Alagogshak Creek) lobe, all lavas of the western outliers, and the entire Holocene suite from Mount Martin, as well as many lavas of the Kejulik cleaver and Angle Creek sectors (fig. 5*A*). No mineralogical difference is recognized between the lavas lower and higher in K_2O, which are interstratified without any consistent age distinction. Lavas lower in K_2O include those dated at 954 ka, 680 ka, 389 ka, and 43 ka, as well as the crater-rim dacite (fig. 3) and all the postglacial products of Mount Martin.

The sample richest in MgO (K-2078; 5.65 percent MgO), which stands out from the rest in figure 5*B* by virtue of its low FeO/MgO ratio, is anomalous also in its relative Al_2O_3 deficiency (14.7 percent Al_2O_3; table 2). The sample is an olivine-bearing, plagioclase-rich, two-pyroxene andesite (60.6 percent SiO_2) belonging to the suite higher in K_2O and does not appear in thin section to be olivine-accumulative. It is from the basal colonnade of a 75-m-thick flow that makes up ridge 2451 at the northwest limit of the Angle Creek sector.

Resting on Jurassic sandstone, this flow is likely to be one of the oldest in the sector.

Conclusions

The simple central-vent Alagogshak stratovolcano produced 10–18 km^3 of eruptive products, mostly andesite-dacite lava flows, in several eruptive episodes spread widely over at least 600,000 years. About two-thirds of the Alagogshak volcano has already been stripped by glacial erosion, even though substantial lava production took place as recently as 43±8 ka. The eruptive focus shifted in the Holocene to Mount Martin, 3 km northeast. In contrast to the coherent compositional arrays for eruptive products of Mount Martin, the variety of compositions erupted at Alagogshak probably reflects independent evolution of successive magma batches that arose at widely separated intervals in its long history.

Like Alagogshak, the adjacent volcanic-front edifice to the southwest, Kejulik volcano (fig. 1), is apparently now extinct (Riehle and others, 1993; Shew and Lanphere, 1992). This leaves a 76-km-long inactive gap along the front between the Holocene cones of Mount Martin and Mount Peulik (fig. 1). So lengthy a gap accentuates the anomaly of the adjacent Katmai cluster (Hildreth, 1983), where the recently active Martin, Mageik, Trident, Griggs, and Katmai stratovolcanoes are all closely spaced along a 25-km reach of the volcanic arc.

Acknowledgments

Michelle Coombs and Dave Tucker contributed substantially to the fieldwork, Tracey Felger to the map preparation, Forrest McFarland to sample preparation, and James Saburomaru to the K-Ar dating. John Paskievitch arranged and anchored the sometimes difficult logistics, and pilot Paul Walters got us where we needed to go (fig. 4). Game McGimsey and Chris Nye provided helpful reviews of the manuscript.

Reviewers: Game McGimsey, Chris Nye.

References Cited

Hildreth, W., 1983, The compositionally zoned eruption of 1912 in the Valley of Ten Thousand Smokes, Katmai National Park, Alaska: Journal of Volcanology and Geothermal Research, v. 18, p. 1–56.

Hildreth, W., and Lanphere, M.A., 1994, Potassium-argon geochronology of a basalt-andesite-dacite arc system: The Mount Adams volcanic field, Cascade Range of southern Washington: Geological Society of America Bulletin, v. 106, p. 1413–1429.

Riehle, J.R., and Detterman, R.L., 1993, Quaternary geologic map of the Mount Katmai quadrangle and adjacent parts of the Naknek and Afognak quadrangles, Alaska: U.S. Geological Survey Miscellaneous Investigations Series Map I-2032, scale 1:250,000.

Riehle, J.R., Detterman, R.L., Yount, M.E., and Miller, J.W., 1993, Geologic map of the Mount Katmai quadrangle and adjacent parts of the Naknek and Afognak quadrangles, Alaska: U.S. Geological Survey Miscellaneous Investigations Series Map I-2204, scale 1:250,000.

Shew, N., and Lanphere, M.A., 1992, Map showing potassium-argon ages from the Mount Katmai and adjacent parts of the Naknek and Afognak quadrangles, Alaska Peninsula, Alaska: U.S. Geological Survey Miscellaneous Field Studies Map MF-2021-E, scale 1:250,000.

Stacey, J.S., Sherrill, N.D., Dalrymple, G.B., Lanphere, M.A., and Carpenter, N.V., 1981, A five-collector system for the simultaneous measurement of argon isotope ratios in a static mass spectrometer: International Journal of Mass Spectrometry & Ion Physics, v. 39, p. 167–180.

Geologic Studies in Alaska by the
U.S. Geological Survey, 1997
U.S. Geological Survey Professional Paper 1614

Gravity Changes During the 26 Years Following the 1964 Alaskan Earthquake

By David F. Barnes

Abstract

The 1964 Alaskan earthquake caused elevation changes that were measured in meters and extended over distances that were measured in hundreds of kilometers. Most of the measured gravity changes showed a Bouguer ratio to the elevation changes and thus suggested addition of mass in the uplift areas and loss of mass in the subsidence areas. However, the gravity increase measured at Anchorage was only 0.04 mGal despite a subsidence of nearly 1 m, which might have caused a free-air change of 0.3 mGal. This small change in gravity was probably the result of elastic expansion and a density decrease that diminished the free-air elevation effect.

Post-earthquake readjustments have caused small elevation changes during the 25 years that followed the earthquake. However, measured gravity changes are much less extensive and suggest that differing tectonic processes are now active in the earthquake area. The first change reported was an uplift of nearly 0.5 m, shown by releveling along the highway southeast of Anchorage. No gravity change has been measured, and the uplift is interpreted to be caused by horizontal elastic compression. Later global positioning system (GPS) measurements showed that this domal uplift extends into the central Kenai Peninsula, where additional measurements are probably needed to confirm the absence of gravity change.

In contrast, there is better evidence for a post-earthquake gravity change at Cordova, where repeated visits have shown a gravity increase of 0.1 mGal during a 25-year period and where tide-gage data show a subsidence of nearly 0.2 m during the same period. The combined data indicate a free-air process with no change in underlying mass and a probable isostatic phase-change response to the broad uplift during the 1964 earthquake. At Middleton Island, on the edge of the continental shelf, a gravity decrease of perhaps 0.2 mGal has been measured, but the large gravimeter drift and data scatter show the need for additional measurements. GPS data and barnacle observations also indicate uplift.

Introduction

The vertical crustal deformation during the 1964 Alaskan earthquake exceeded that measured in any previous earthquake (Krauskopf, 1972) and was sufficient to cause measurable and interpretable gravity changes in at least part of the deformed region (Barnes, 1965). During the 30 years following the earthquake, evidence for further vertical movement and post-earthquake readjustment has gradually accumulated (Brown and others, 1977; Savage and Plafker, 1981; Cohen and others, 1995; Gilpin and Carver, 1994). I have also measured small gravity changes that have accompanied some of this post-earthquake readjustment. However, the gravity changes are much less extensive than the elevation changes, and the relationship between the vertical movement and the gravity changes is not uniform, suggesting that more than one physical process may be active in the post-earthquake readjustment. Furthermore, additional data collected during the summer of 1965 after the preparation of the initial paper (Barnes, 1965) provide supplemental data that support some variation in gravity change and deformation process during the 1964 coseismic event The gravity changes in that event were not as consistent as once reported. Therefore, in this paper, I reexamine some of the 1964 coseismic gravity-change data, in addition to evaluating the post-earthquake gravity-change data.

Interpretation Principles

The limited 1964 earthquake gravity-change data were interpreted by plotting gravity changes as a function of elevation changes and comparing the data with two lines derived from physical principles (fig. 1). The line with the steeper slope (fig.1) represents the free-air gradient of gravity, which is the rate of change of gravity above the Earth's surface with no change in underlying mass; its slope is determined by the distance of the measurement from the Earth's center. The gentler slope represents the Bouguer gradient, which shows how the gradient is modified by considering the additional gravitational attraction of an infinite slab of normal rock density near the Earth's surface. The Bouguer slope provided the best fit for most of the data obtained after the 1964 earthquake. However, the agreement was least satisfactory in the negative-elevation-change or subsidence portion of the graph, for which many of the points were acquired after the initial publication. Later studies have refined the analysis of gravity changes and have considered the gravity-change effects of density variation and specific dislocation models (Whitcomb, 1976; Walsh and Rice, 1979; Savage, 1984)

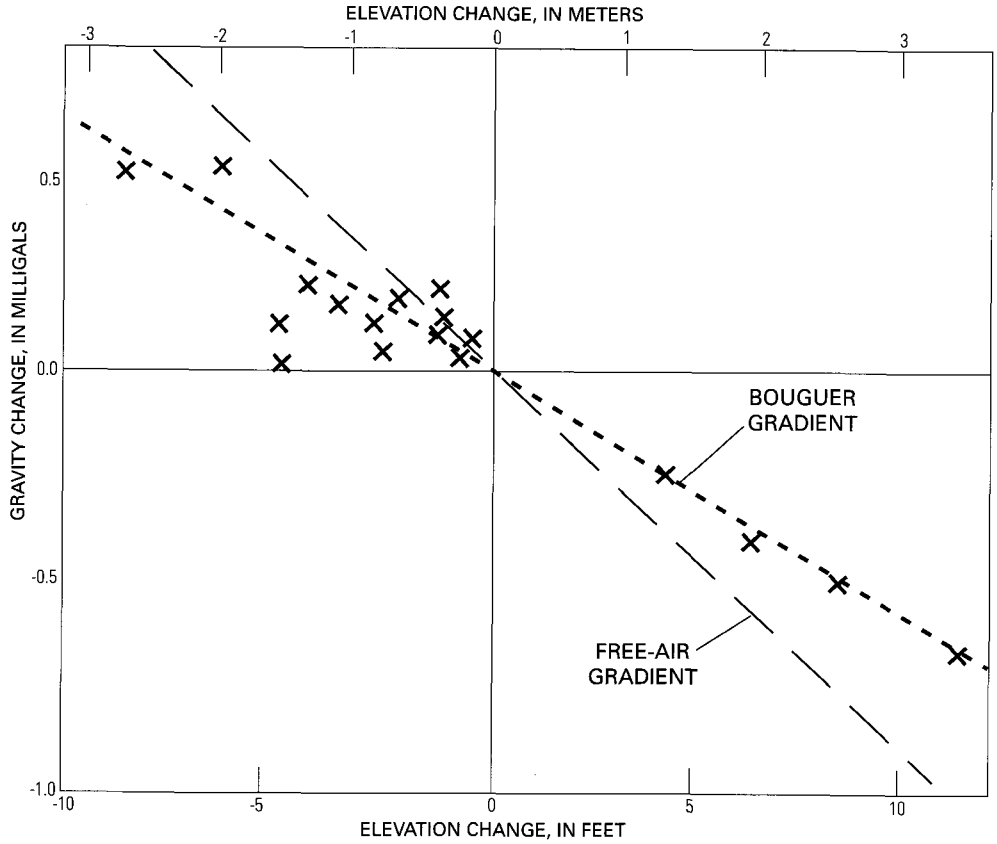

Figure 1. Gravity changes caused by the 1964 Alaskan earthquake calculated from measurements before and after the earthquake and plotted as a function of elevation change. From Barnes (1965) plus additional data collected during the summer of 1965.

Data Collection

Almost all of these Alaskan gravity-change data have been accumulated as an incidental product of the preparation of successive Alaskan State regional gravity maps (Thiel and others, 1958; Woollard and others, 1960; Barnes, 1970, 1977; Barnes and others, 1995). This regional mapping objective thus influenced both the equipment used for this study and the areal distribution of the coverage. Virtually all the data were collected with gravimeters that were primarily designed for quick measurement of gravity differences between exploration stations and previously established base stations. Absolute gravimeters may now provide better methods for measuring temporal gravity changes (Carter and others, 1997), but such equipment was in its infancy at the time of the earthquake. Furthermore the Alaskan earthquake was the first to produce measurable coseismic and postseismic gravity changes. Better studies should be possible for future earthquakes of comparable magnitude.

Measurement of temporal gravity changes requires good control of the accuracy and stability of gravimeter calibrations. The meters used in the Alaskan surveys have been carefully chosen and repeatedly checked. At the start and end of each field season the meters were tested on mountain calibration loops (Barnes and others, 1969) near Anchorage, Fairbanks, and the U.S. Geological Survey (USGS) headquarters in California. Most of the meters have also been intermittently compared with pendulum data along parts of the North America Midcontinent calibration range (Woollard and Rose, 1963), which provided the basic scale for establishing mountain calibration loops.

Base stations initially used during collection of data for the regional maps provide the primary framework for gravity-change studies. These base stations were occupied as often as possible to insure the accuracy of regional coverage. Thus multiple ties are available for many station pairs, and their data scatter provides an estimate of measurement reliability. For convenience and ease of reoccupation, most base stations were located at transportation hubs, airports, and road junctions, where they could be most easily reached after the regional survey had extended to other areas. The standard deviation of base-station ties made during the Alaskan gravity surveys is 0.02 to 0.03 mGal, which is probably the best indicator of data precision. However, the precision of the gravity-change data was also affected by two other factors, the magnitudes of which are difficult to estimate. First, a variety of factors sometimes made reoccupation of the same spot difficult and uncertain. Second, during other ties, the drift of the gravimeter was very large and thus added measurement uncertainty.

Alaskan economic development has been rapid during the more than 30 years since the earthquake, and there have been major changes at many airports and along the primary highways. A good example is provided by the Richardson Highway (fig. 2), which extends northeast from Valdez toward Tonsina. Gravity measurements were made with a LaCoste and Romberg gravimeter at mile posts along this road in 1962, and those

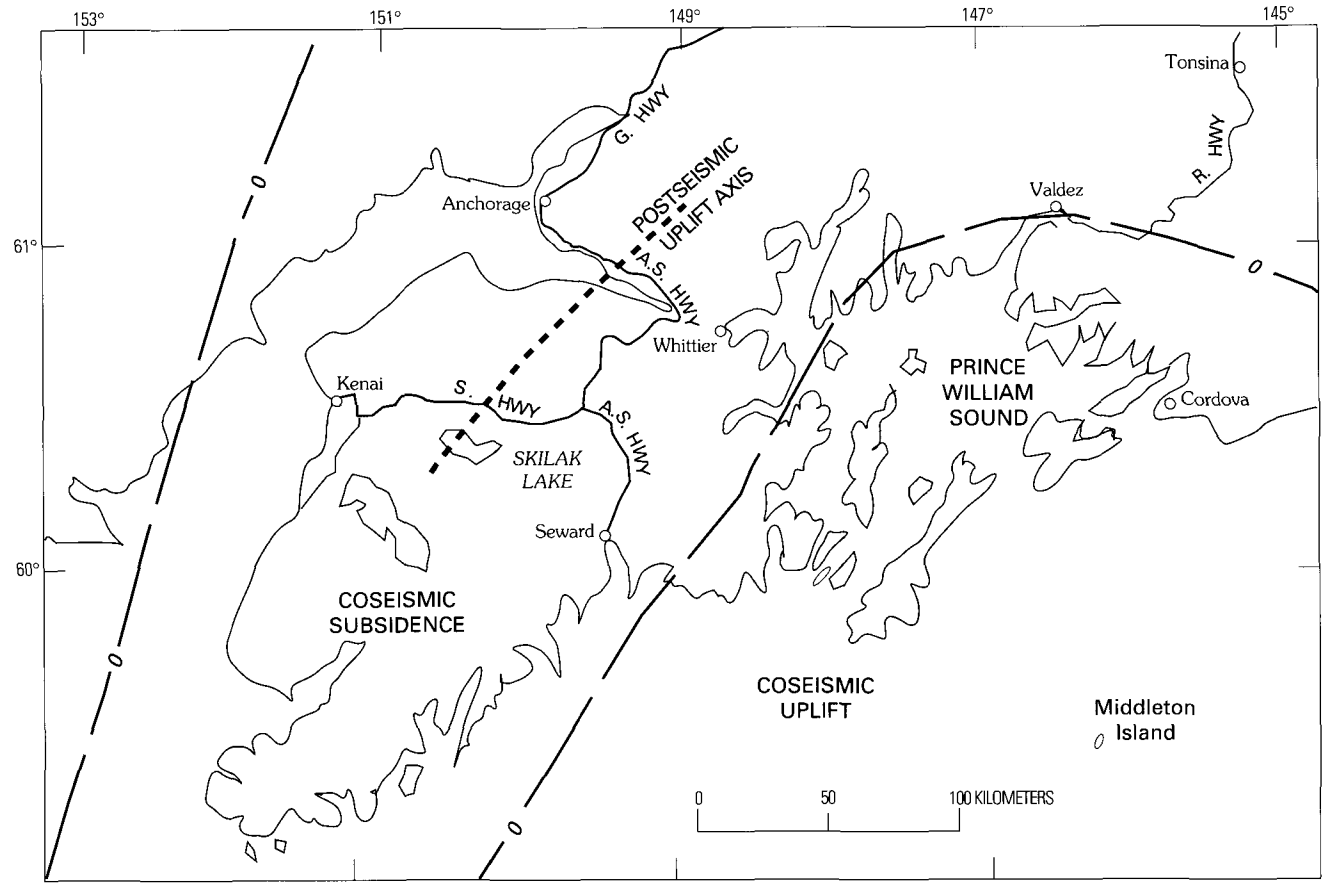

Figure 2. Map of area deformed in the 1964 Alaska eartnquake. Long dashes are zero isobase lines on borders of subsidence and uplift areas (Plafker, 1965). Dotted line within the coseismic subsidence area is axis of post-earthquake uplift (Brown and others, 1977; Cohen and Freymueller, 1997). Highways: R., Richardson; A.S., Anchorage-Seward; S., Sterling; G., Glenn.

stations were among the first stations reoccupied after the 1964 earthquake. The preliminary results indicated a small, probable free-air gravity change suggesting no loss or addition of underlying mass (Barnes, 1965). The possibilities for measuring post-earthquake changes along this traverse once seemed good (Rice, 1969), although there had been some minor scatter in base ties for the early measurements. Later measurements were made in 1965, 1972, and 1981, but each of these reoccupation attempts encountered more missing base stations (Barnes, 1968, p. 9C), which thus increased the uncertainty in defining gravity changes.

During the late 1970's the Alaska pipeline was constructed along the route and a new highway was built. In 1990 only short segments of the original road could be found, and virtually all of the original mile posts that marked station locations had been destroyed. Further measurement of the gravity change was considered impossible along this road. In other areas and airports, more frequent visits have enabled us to observe the potential loss of base stations and establish new bases by ties to nearby bases—thus it was possible to keep track of gravity changes. However, establishing new satellite bases probably increases the uncertainty of gravity differences relative to distant bases. Problems associated with measurement at specific satellite bases are, thus, briefly mentioned in the following text.

Anchorage Gravity Change

The nearly 1-m subsidence of the land near Anchorage was recognized soon after the earthquake (Grantz and others, 1964). When I first returned to the city less than a month after the earthquake, I expected to be able to measure a gravity increase of 0.2 to 0.3 mGal, depending on the tectonic process that caused the subsidence. However, data collected at that time immediately suggested a much smaller increase of <0.05 mGal. Larger gravity changes were soon measured elsewhere, and the small change at Anchorage was long considered evidence of inadequate pre-quake data. The small change was shown in the Barnes (1965) graph of gravity change versus elevation change but was ignored in the discussion. Four years later, Rice (1969) reported additional pre-earthquake data, including a 1963 Air Force gravimeter calibration effort with seven LaCoste and Romberg gravimeters, that yielded a value of pre-earthquake Anchorage gravity very close to my own and also an earthquake change of 0.05 mGal, which was less than what he considered the uncertainty of the measurements. His data thus supported my own conclusion that the coseismic gravity increase was only about 0.04 mGal. This may have been less than the uncertainty of the measurements, but even this change (as well as the uncertainty)

was less than the magnitude of the change expected from application of either the free-air or Bouguer gradients to the measured elevation change. It was also significantly smaller than the changes measured elsewhere in the quake area, particlarly along the highway system north and east of the city of Anchorage (stations described in Barnes, 1968, p. 7-C and 8-C).

The reason for the small gravity change at Anchorage gradually became apparent after the earthquake. Less than a year after the earthquake, Plafker (1965) suggested the hypothesis that the quake was the result of an overthrust movement toward the Aleutian trench and along a shallow-dipping fault that outcropped along the trench. Anchorage is near the zone of elastic expansion that provided the push for this movement. Whitcomb (1976) showed that density changes can significantly reduce the gravity change expected from elevation changes, and, a few years later, Jachens (1979) published a graph showing that, for elastic expansion and compression with a Poisson's ratio near 0.25, the resulting gravity change could be very small. The gravity data from the Anchorage area thus provides further support for Plafker's hypothesis, which is now a well-accepted aspect of plate tectonics.

In some ways, the small gravity change at Anchorage was very convenient because the city is the prime transportation hub for Alaska, so any measured changes in gravity differences with respect to other cities suggested that the change had probably occurred at the distant city. Furthermore, the base network could be expanded without making corrections for changes at its principal bases (Anchorage bases are described in Barnes, 1968, p. 6-C). Preparation of a State gravity map did provide multiple opportunities for measuring the gravity differences between stations at Anchorage airport and those at other airports within the State. Although the measurements show some scatter at all stations, the only evidence of a steady trend indicating a temporal gravity change was measured at other airports in the earthquake area. Post-earthquake ties to such distant cities as Fairbanks, McGrath, and Bethel show a scatter of ±0.5 mGal, but no evidence of change. The importance of Anchorage as a transportation hub and reference point for temporal changes elsewhere led to an absolute gravity measurement by free-fall apparatus (Marson and Alasia, 1980). The measurement has not been repeated because there has been no other evidence of a post-earthquake Anchorage gravity change.

The tide-gage data from Anchorage (Savage and Plafker, 1981) also show small, post-earthquake sea-level changes of <3 mm/yr or less than a total of 5 cm in the 25 years since the earthquake. This would cause a free-air gravity change of <0.2 mGal, which is less than the standard deviation of the various ties to other airports and base stations in Alaska. Thus, a detectable post-earthquake gravity change would not be expected from the tide-gage data.

Gravity Change South of Anchorage

The area of small or undetectable coseismic and postseismic gravity change seems to extend over a considerable area south and west of the city, although only limited data are available. Few pre-earthquake gravity data were available for the Seward Highway along the Turnagain Arm southeast of Anchorage, but in 1965 a first-order level line and two sets of gravity measurements by both the U.S. Coast and Geodetic Survey (USC&GS) and the USGS were made along the road. The USC&GS leveling between Anchorage and Portage was repeated the following year, in 1968, and again in 1975 (some gravity measurements were also made in 1975). The leveling showed a domal uplift centered about 40 km southeast of Anchorage with a maximum amplitude of about 50 cm (Brown and others, 1977). However, the gravity changes did not show a consistent relationship to vertical movements and had the same magnitude as the scatter of the data. Hoping to reduce the uncertainty, I repeated many of the 1965 USGS gravity measurements (base stations described in Barnes, 1968, p. 3-B) along the same highway in 1977 with very similar results. Figure 3 shows a plot of distance versus uplift, measured gravity changes, and the gravity changes that might be expected by applying the Bouguer gravity gradient to the measured uplift. The measured changes are much smaller than the calculated Bouguer changes and are approximately the same magnitude as the data scatter. The post-quake uplift south of Anchorage is thus accompanied by a very small gravity change similar to that which accompanied the coseismic subsidence at Anchorage during the 1964 earthquake. Brown and others (1977) used the dislocation program of Savage and Hastie (1966) to explain the uplift as the result of elastic creep and compression above a flexure of the thrust fault that ruptured in 1964. Seismic data suggest that the dip of this fault steepens significantly beneath the uplift area and thus causes compression in the overthrusting, overlying North American plate. The small gravity change is thus the result of horizontal elastic compression just as elastic expansion near Anchorage caused the small coseismic gravity change and subsidence.

Kenai Peninsula Gravity Change

Recent GPS measurements (Cohen and others, 1995; Cohen 1996; Cohen and Freymueller, 1997) along other highway level lines on the Kenai Peninsula have shown that this post-earthquake uplift extends southwest from the Anchorage-Seward highway and is as much as 90 cm near the center of the Peninsula along the Sterling highway. No public, pre-quake gravity data were available against which to measure the coseismic gravity changes. The first-order level survey was made along the highway in 1964, and both the USGS and USC&GS made gravity measurements along the highway in 1965. In 1981, I reoccupied six of the USGS gravity base stations (Barnes, 1968, p. 4-B) and measured small gravity decreases ranging from 0.01 to 0.12 mGal and averaging 0.05 mGal. However, only one gravimeter was used for these measurements and the drift control for the traverse was poor. Without the present evidence of uplift, the gravity decrease was not considered significant. In 1990, only one base station, at Skilak Lake near the center of the uplift, was reoccupied (within approximately 3 m of the original station) with two gravimeters. These readings suggest that the gravity at that station decreased by either 0.03 or 0.15 mGal, but new base stations were used for the reoccupation and the two values may not be comparable. Furthermore, the difference between the two measurements is large and shows significant scatter. The change in gravity, if any, is certainly smaller than the

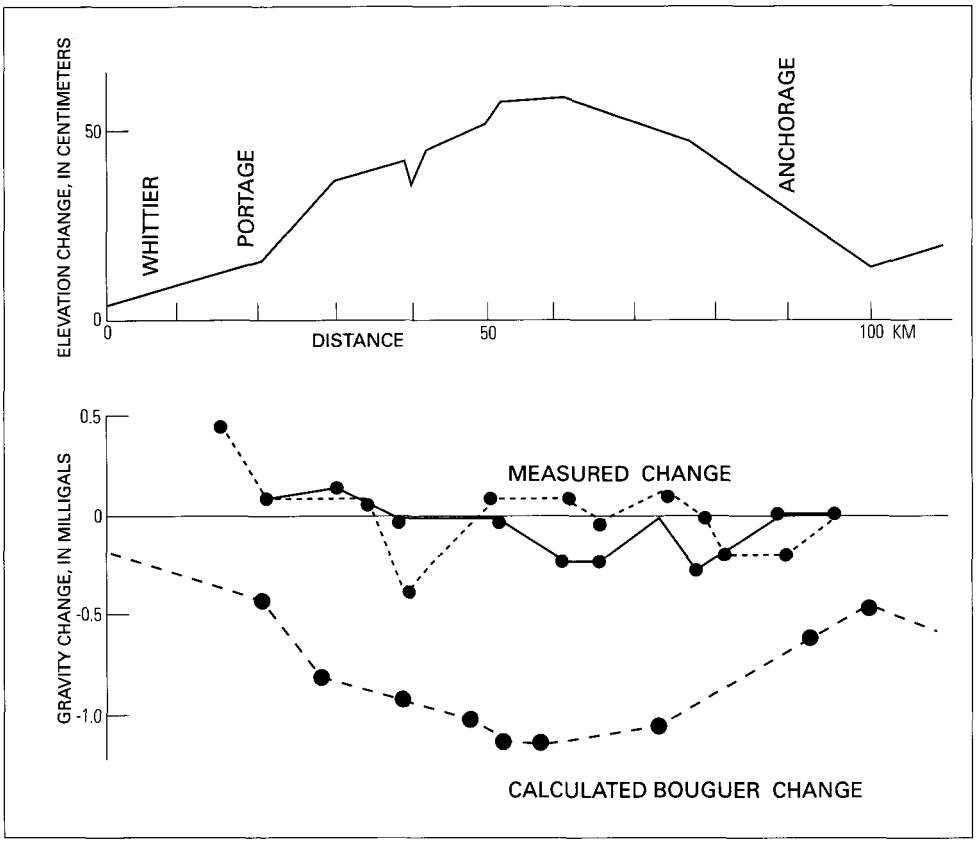

Figure 3. Plot of post-earthquake elevation change, measured gravity change, and calculated Bouguer change (calculated from the elevation change) as a function of distance along the Anchorage-Seward Highway, southeast of Anchorage. The solid and short-dashed lines are separate data sets and show the measurement scatter.

nearly 0.3 mGal that might be expected from the measured elevation change and Bouguer gradient.

Somewhat different processes may be active on the northwest edge of this post-earthquake uplift dome. This area along the northern shore of the Kenai Peninsula and central Cook Inlet is marked by a major gravity low with a Bouguer amplitude below –140 mGal, which represents a very large thickness of Mesozoic and Cenozoic sedimentary rock. The entire gravity low lies within the 1964 coseismic subsidence area, and the earthquake may have been one more episode in a long history of downwarping that created the sedimentary basin. However, the axis of maximum 1964 coseismic subsidence is south of the present gravity low. In 1965, the year following the earthquake, I thought I successfully reoccupied a station reported by Thiel and others (1958) at Kenai Airport. I measured, in a tie to Anchorage, a coseismic gravity increase of 0.05 mGal, which seemed consistent with the nearly 1 m of coseismic subsidence later reported at the nearby Nikiski tide gauge (Small and Wharton, 1969). The large gravity difference between Anchorage and Kenai may have increased the uncertainty of the measurement. Thiel had described the station as "Pacific Northern Airlines terminal on ground 40 feet from field entrance" and, after the earthquake, I decided that this spot was also the end of a concrete walkway south of the building. However, when I next returned to the airport in 1981, I wondered whether this had actually been the field entrance, so the reoccupation could have been questionable. By then the building had been converted to a gift shop and the airlines were using a new terminal building nearly a mile to the north along the single runway.

A new station, "KENT," with an aluminum marker, was established at the Kenai terminal and was tied to both the old terminal station and to Anchorage. This station was reoccupied and again retied to Anchorage in 1990. Comparison of the two ties suggests a gravity increase of 0.07 mGal at Kenai Airport during the 9-year interval. However, different base stations had to be used at Anchorage, and the suggested change is nearly the same as the measurement scatter. The change, if any, is certainly not well established. This questionable gravity increase would suggest a small subsidence at Kenai Airport between 1981 and 1990. In contrast, a 9-year record of tide-gage data between 1970 and 1979 at nearby Nikiski (Savage and Plafker, 1981) indicated a sea-level fall or land uplift of 19 mm/yr or nearly 17 cm in that 9-year period. However, Cohen and Freymueller (1997) have recently reported GPS data that make the tidal data suspect.

Cordova Gravity Change

In contrast to the Anchorage-Kenai area, there is better evidence of a post-quake gravity change at Cordova, where there were nearly 2 m of uplift and 0.5 mGal of gravity decrease during the earthquake. Repetitive measurements at this city were

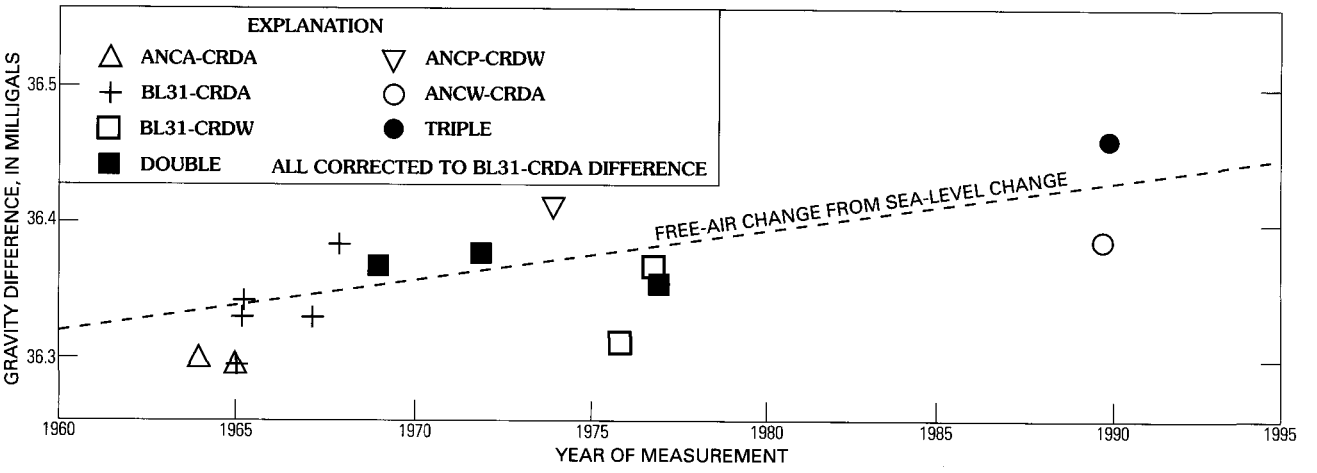

Figure 4. Graph of measured gravity differences between Anchorage and Cordova as a function of date of measurement. Symbols represent station pairs used in measurement (see text). Solid symbols indicate multiple differences. Dashed line is free-air gravity change calculated from tidal data.

easier than at most points in the earthquake area because, during different periods, Cordova was often a commercial air stop between Anchorage and the USGS California headquarters. However, frequent airport improvements and changing security regulations sometimes made reoccupations of the same base stations difficult. Although multiple bases were used at both airports, each station was either well tied to the previous base or to other known bases in these cities, so that the record of gravity change was adequately maintained. The standard deviation of these local ties, either within the airport or within the city, was 0.03 mGal. Figure 4 shows a graph of the gravity difference between Anchorage and Cordova airports plotted versus the date of measurement for the period 1964 to 1990. The difference plotted is for the station pair BL31 in Anchorage and CRDA at Cordova airport, but the symbols show which station pair was actually measured on that date and whose differences were later converted to the BL31-to-CRDA differences. The four-character station designations are those used in the USGS Alaskan gravity base station network reports (Barnes, 1968, 1972). From 1966 to the late 1980's, BL31 was the principal USGS gravity base at Anchorage airport where the gravity meter was read above USC&GS benchmark L31 at the base of a flagpole outside the post office. The station, flagpole, and post office were demolished in the late 1980's, but, by that time, the station had been well tied to other stations in the city (Barnes, 1968, p. 6-C). CRDA at Cordova was initially described as "on asphalt apron northwest of the field steps to log cabin air terminal and above a USGS gravity marker" (Barnes, 1968). Five years after the 1964 earthquake, a new concrete terminal was built and the old log terminal was moved closer to the new apron where it served as an annex. For several years, gravity was measured in the same place relative to the building steps, but in its new location; this station was renamed CRDW. However, increased security regulations gradually made access to this spot difficult, and another station, CRDH, was established on the road outside the new concrete terminal next to a fire hydrant. At the time of my 1990 visit, all three stations could still be reoccupied, although airport security police would only permit access to the older stations when commercial aircraft were not at the airport.

Figure 4 shows a 25-year increase of slightly more than 0.1 mGal in the gravity difference between Anchorage and Cordova airports, which must be caused by a gravity increase at Cordova because we have no present evidence of a gravity change at Anchorage. Cordova tide-gage data summarized by Savage and Plafker (1981) showed a sea-level rise or land subsidence of 9.7 mm/yr between 1965 and 1989 or 14 cm in the 25-year period. The dashed line in figure 4 shows the free-air gravity change that would result from this subsidence rate if no underlying material is lost, and it provides a fairly good fit to the observed data. Thus, a post-earthquake process of subsidence involving minimal mass transfer, but probable density change, is indicated. Such processes might include a phase change at the base of the crust for isostatic compensation as discussed by Broecker (1962). Another possibility is a mechanism of elastic relaxation involving a density change without transfer of mass, but I have not found a good reference for such a process.

Gravity Change at Prince William Sound Transition Area

Available data indicate both very small coseismic and even smaller, if any, postseismic gravity changes at Anchorage in the coseismic subsidence area. However, a significantly larger gravity decrease during the earthquake at Cordova, in the coseismic uplift area, was followed from 1965 to 1990 by a gravity increase and accompanying subsidence. Both coseismic and postseismic gravity-change data between these two zones are very limited. Only a few gravity measurements had been made on the islands of Prince William Sound before the earthquake, and only one of these stations was successfully reoccupied after the earthquake (Barnes, 1965). Following the earthquake, both the USGS and the U.S. Coast and Geodetic Survey made detailed surveys to determine the gravity field in the vicinity of the epicenter (Case and others, 1966; Rice, 1969; respectively). Most of the

USGS stations were inadequately described for accurate reoccupation, and the base-station control (Barnes, 1968, p. 2-B) on this ship-supported survey was inadequate for the measurement of gravity change. The other survey (i.e., the USC&GS survey) was made by aircraft flights from Anchorage, and the stations were better marked. However, that survey's prime base station at Anchorage airport has been destroyed, and the possibility of making an adequate repeat survey may depend on how well that station can be recovered from local ties in the Anchorage area. Access to the original data sheets would probably be necessary before evaluating the probable value of repeating parts or all of this survey.

Middleton Island Gravity Change

There may be better evidence for gravity change at Middleton Island on the northern edge of the Aleutian Trench. Here, Plafker (1969) reported a series of five marine terraces that represent successive uplifts extending over a period of more than 4,000 years. Thiel and others (1958) reported one pre-earthquake measurement made on the island in 1954 while an aircraft-weather and flight-control station was under construction. The station description by Thiel and others (1958) involved buildings that were removed after the construction, but, after a series of phone calls, I learned that the the spot could be closely relocated by the defining roadway and runway intersection (Dan Scroggs, Federal Aviation Administration, oral commun., September 1965). Commercial air flights were then available from Cordova to Middleton Island every second weekend, so a tie was made to the island and a gravity decrease of 0.6 mGal was measured. The gravity difference from Cordova was less than 14 mGal, and the meter drift on the flight was 0.03 mGal. Plafker (1969) had used raised barnacle and vegetation lines to measure a coseismic uplift of more than 3 m at the island. These data were not shown on the Barnes (1965) graph of coseismic gravity change versus elevation but provided an additional point along the Bouguer line at the lower right hand corner of figure 1 (this report). Readings were also made at two of the tidal benchmarks that had been recently placed on the island.

Rice (1969) later reported that the Coast and Geodetic Survey had used a twin-engine Piper Aztec to make post-earthquake gravity ties between Anchorage and Middleton Island in 1964, 1965, and 1967. Between 1964 and 1965, a gravity decrease of 0.17 mGal (equivalent to an uplift of 0.3 m) was recorded, but the 0.03-mGal increase between 1965 and 1967 was within the uncertainty of the measurements. The uplift was believed to have stabilized, and no further measurements have been reported. The USC&GS base station at Anchorage airport has been destroyed, and reoccupations of a cited reference station have been unsatisfactory. However, Prescott and Lisowski (1977) reported tilt measured on Middleton Island by repeated leveling in 1964, 1969, 1972, and 1975 and, thus, suggested a small continued movement of the island.

In 1990, I was anxious to repeat the 1964 gravity tie and measure any changes that might have happened since my 1965 measurement. Commercial aircraft no longer visited Middleton Island, and the only available transportation, without a prohibitively expensive charter flight, was a biweekly resupply flight for the aviation controllers and seismologists then occupying the island. Although I was able to arrange passage on the flight, I knew that its departure from Kenai instead of Cordova or Anchorage presented additional problems. I thought that the base value at Kenai air terminal could be adequately rechecked, although some of the ties to Anchorage showed evidence of change, as discussed earlier. The gravity difference between Middleton Island and Kenai is, however, much larger (more than 131 mGal) than the difference between the island and either Cordova (about 14 mGal) or Anchorage (about 42 mGal); therefore, calibration posed a problem. After leaving Kenai, the plane climbed to more than 4,000 m altitude enroute to the island—this pressure drop may have increased the gravimeter drift. The two gravimeters showed unusually high drift on the flight (0.19 mGal by meter G-8 and 0.27 mGal by meter D-26). The tide- and drift-corrected gravity difference measured by G-8 was 131.57 mGal between stations KENT at Kenai and MID6 (tidal benchmark 6) at Middleton Island and 131.36 mGal for D-26. Applying the mean of these differences to the best gravity value at Kenai Airport on the old 1960 datum, as used in 1965, gives a gravity value at the Middleton Island benchmark of 981,968.27 which is more than 0.3 mGal lower than the value of 981,968.58 measured at the same benchmark in 1965. Meter G-8, which had the smaller drift, would give an observed gravity about 0.1 mGal higher than the mean value, but even that value suggests a gravity decrease of about 0.2 mGal during the 25-year period. The gravity measurements are not directly comparable with the Coast and Geodetic Survey measurements in 1965–67 (Rice, 1969) because Rice did not identify the stations used on the island, although tidal benchmarks are presumed.

When this gravity decrease was first presented (Barnes, 1993) the uplift of the island was considered doubtful. However in 1995, Plafker (oral commun., January 1998) revisited the island and could no longer see a barnacle line visible during his earlier 1964 visit, but he estimated an uplift of at least 0.5 m. More recently Savage and others (1998) have reported evidence from GPS measurements that the island was rising at a rate of 20 mm/yr between 1993 and 1997. If this rate had been constant through the earlier 25-year period of 1965 to 1990 covered by the gravity measurements, the gravity change would have been only 0.10 or 0.15 mGal, depending on whether the uplift is either a Bouguer or free-air process involving the addition of underlying mass or no change in underlying mass, respectively. The fact that the measured gravity change is at least 50 percent larger makes the gravity measurements very doubtful. However, if the rate of gravity change reported by Rice (1969) for the 1964-to-1965 interval had extended over the whole 25-year period, the gravity change might have been more than 0.40 mGal or even higher than that measured by meter D-26, which had such a large drift during the trip to the island. The gravity-change data do suggest that the uplift of the island involves a very different geologic process than the post-earthquake uplift south of Anchorage, where no gravity change has been measured.

References Cited

Barnes, D.F., 1965, Gravity changes during the Alaska earthquake: Journal of Geophysical Research, v. 71, no. 2, p. 451–456.

Barnes, D.F., 1968, Alaskan gravity base station network: U.S. Geological Survey Open-File Report 68-4, 44 p.

Barnes, D.F., 1970, Alaskan Bouguer gravity anomalies, *in* U.S. Geological Survey, The National Atlas of the United States of America, p. 69, scale 1:38,500,000.

Barnes, D.F., 1972, Southeast Alaska gravity base station network: U.S. Geological Survey Open-File Report 72-18, 42 p.

Barnes, D.F., 1977, Bouguer gravity map of Alaska: U.S. Geological Survey Geophysical Investigations Map GP-913, 1 sheet, scale 1:2,500,000.

Barnes, D.F., 1993. Small gravity changes indicate that different processes are involved in post-1964 Alaska earthquake elevation changes [abs.]: EOS—Transactions, American Geophysical Union, Fall Meeting, p. 95.

Barnes, D.F., Oliver, H.W., and Robbins, S.L., 1969, Standardization of gravimeter calibrations in the Geological Survey: EOS—Transactions, American Geophysical Union, v. 50, no.10, p. 526–527.

Barnes, D.F, Mariano, John, Morin, R.L., Roberts, C.W., and Jachens, R.C., 1995, Incomplete isostatic anomaly map of Alaska, *in* Plafker, G.W., and Berg, H.C., eds, Geology of Alaska: Geological Society of America, Decade of North America Geology Volume, 1055 p., [plate 9, scale 1:2,500,000].

Broeker, W.L., 1962, The contribution of pressure induced phase changes to glacial rebound: Journal of Geophysical Research, v. 67, no. 10, p. 4837–4842.

Brown, L.D., Reilinger, R.E., Holdahl, S.R., and Balazs, G.I., 1977, Postseismic crustal uplift near Anchorage, Alaska: Journal of Geophysical Research, v. 67, p. 3369–3378.

Carter, W.E., Sasagawa, Glen, and Richter, Bernard, 1997, Researchers explore possibilities of microgal gravimetry: EOS—Transactions, American Geophysical Union, v. 78, no. 36, p. 383–385.

Case, J.E., Barnes, D.F., Plafker, G.W., and Robbins, S.L., 1966, Gravity survey and regional geology of the Prince William Sound epicentral region, Alaska: U.S. Geological Survey Professional Paper 543-C, 12 p.

Cohen, S.C., 1996, Time-dependent uplift of the Kenai Peninsula and adjacent regions of south-central Alaska since the 1964 Prince William Sound earthquake: Journal of Geophysical Research. v. 101, no. B4, p. 8595–8604.

Cohen, S.C., Holdahl, S.R, Caprette, Douglas, Hilla, Stephen, Safford, Robert, and Schultz, Donald, 1995, Uplift of the Kenai Peninsula since the 1964 Prince William Sound earthquake: Journal of Geophysical Research, v. 100, no. B2, p. 2031–2038.

Cohen, S.C., and Freymueller, J.T., 1997, Deformation of the Kenai Peninsula: Journal of Geophysical Research., v. 102, no. B9, p. 20479–20487.

Gilpin, Lou, and Carver, Gary, 1994, Tidal benchmark readings and postseismic rebound of Kodiak Islands. SW extent of the 1964 great Alaskan earthquake rupture [abs.]: Seismological Research Letters, v. 65, no. 1, p. 65.

Grantz, Arthur, Plafker, G.W., and Kachadoorian, Reuben, 1964, Alaska's Good Friday earthquake, March 27, 1964: A preliminary evaluation: U.S. Geological Survey Circular 491, 35 p.

Jachens, R.C, 1979, Temporal gravity changes as applied to studies of crustal deformation, *in* Everden, J.L., convener, Proceedings of Conference VII, Stress and Strain Measurements Related to Earthquake Prediction: U.S. Geological Survey Open-File Report 79-370, p. 222–243.

Krauskopf, K.B., 1972, The great Alaska earthquake of 1994 [preface], *in* The Great Alaska Earthquake of 1964: Seismology and Geodesy: National Academy of Sciences, 996 p.

Marson, Iginio, and Alasia, Franco, 1980, Absolute gravity measurements in the United States of America: [Final report contract AFOSR-80-6157 to Air Force Geophysics Laboratory, Hanscom AFB, Mass., unpub. report].

Plafker, George, 1965, Tectonic deformation associated with the 1964 Alaska earthquake: Science, v. 148, no. 3678, p. 1675–1687.

Plafker, George, 1969, Tectonics of the March 27, 1964, Alaska earthquake. *U.S. Geological Survey Professional Paper* 543-I, 74 p.

Prescott, W.H., and Lisowski, Michael, 1977, Deformation of Middleton Island, Alaska during the decade after the Alaskan earthquake of 1964: Bulletin, Seismological Society of America, v. 67, no. 3, p. 579–586.

Rice, D.A., 1969, Gravity Observations in Alaska, 1964–1965, including some repeat observations, *in* Leipold, L.E., ed., The Prince William Sound, Alaska, Earthquake of 1964 and Aftershocks: U.S. Goast and Geodetic Survey Publication 10-3, p. 5–20.

Savage, J.C., 1984, Local gravity anomalies produced by dislocation sources: *Journal of Geophysical Research*, v. 89, no. B3, p. 1945–1952.

Savage, J.C., and Hastie, L.M., 1966, Surface deformation with dip-slip faulting: Journal of Geophysical Research, v. 71, no. 20, p. 4897–4904.

Savage, J.C., and Plafker, G.W., 1981, Tide-gage measurements of uplift along the south coast of Alaska: Journal of Geophysical Research, v. 96, p. 4325–4335.

Savage, J.C., Svarc, J.L., Prescott, W.H., and Gross, W.K., 1998, Deformation across the rupture zone of the 1964 Alaska earthquake 1993–1997: Journal of Geophysical Research, v. 103, no. B9, p. 21275–21284.

Small, J.B., and Wharton, L.C., 1969, Vertical displacements determined by surveys after the Alaskan earthquake of March 1964, *in* Leipold, L.E., ed., The Prince William Sound, Alaska, earthquake of 1964 and aftershocks: U.S. Coast and Geodetic Survey Publication 10-3, p. 21–33.

Thiel, Edward, Bonini, W.E., Ostenso, N.A., and Woollard, G.P., 1958, Gravity measurements in Alaska: Woods Hole, Mass., Woods Hole Oceanographic Institution Reference 58-54, 104 p.

Walsh, J.B., and Rice, J.R., 1979, Local changes in gravity resulting from deformation: *Journal of Geophysical Research*, v. 84, no. B1, p. 165–170.

Whitcomb, T., 1976, New vertical geodesy: Journal of Geophysical Research, v. 81, no. 26, p. 4937–4944.

Woollard, G.P., Ostenso, N.A., Thiel, Edward, and Bonini, W.E., 1960, Gravity anomolies, crustal structure and geology in Alaska: Journal of Geophysical Research, v. 65, no. 3, p. 1021–1037.

Woollard, G.P., and Rose, J.C., 1963, International gravity measurements: Dallas, Society of Exploration Geophysicists, 518 p.

Reviewers: Jim Savage, Bob Jachens.

Geologic Studies in Alaska by the
U.S. Geological Survey, 1997
U.S. Geological Survey Professional Paper 1614

Metal Cycling Along the Northwestern Seward Peninsula, Alaska: A Possible Natural Cause of Metal Contamination in the Arctic

By Cynthia C. Parnow, Richard J. Goldfarb, Karen D. Kelley, *and* Geoff S. York

Abstract

The northwestern Seward Peninsula was targeted for detailed geochemical study after evaluation of data collected during the NURE reconnaissance-level program indicated anomalously high arsenic (60–635 ppm) concentrations in stream sediments. The arsenic is associated with tin skarn, greisen, and replacement deposits in the western Seward Peninsula. Surficial sampling of waters and sediments indicate that arsenic is being transported detritally but that solution transport is insignificant. Our new data indicate that sediments downstream from these tin occurrences are characterized by anomalous values of As (85–530 ppm) and Sn (14–36 ppm), as well as consistent anomalies of Ag, Be, Cu, Sb, and W. Stream sediments collected from drainages underlain by slate, but distal to the exposed tin occurrences, are characterized by background levels of As (10–60 ppm), Li (16–80 ppm), Sn (5–14 ppm), and W (5–10 ppm). These background levels for As and Sn are much higher than concentrations in typical slates and suggest a broad, weak hydrothermal alteration during mineral-deposit formation in much of the study area. A consistent pattern of Ca>>Mg>Na>K and generally alkaline pH (7.2–8.2) characterize waters throughout the study area. Dissolved sulfate concentrations range from 10 to 40 ppm for waters draining slates and from 3 to 20 ppm for water draining carbonates. The waters collected in areas of known tin occurrences in the Potato Mountain area are characterized by increased dissolved sulfate (43–75 ppm) and are generally acidic (pH 4.7–6.5), but most trace metals are at or below detection limits. Dissolved arsenic concentrations in the areas of known tin occurrences are at or below 2 ppb. Our data suggest that detrital arsenic and tin from mineral occurrences may be naturally entering the nearshore marine environment.

Introduction

A geochemical study to determine natural background concentrations of metals in surficial materials was carried out on the northwestern Seward Peninsula near the village of Wales, Alaska (fig. 1). This part of the Seward Peninsula was targeted for detailed study after assessment of regional element distribution maps, which were compiled from stream- and lake-sediment geochemical data collected during the National Uranium Resource Evaluation (NURE) program (Hoffmann and Buttleman, 1996). Interpretation of the NURE data indicated that some drainages feeding Lopp Lagoon (fig. 1) had anomalously high arsenic (60–635 ppm) and tin (60–144 ppm) concentrations in sediments, compared to regional background concentrations (between 5–60 ppm for As and 7–12 ppm for Sn).

The presence of relatively metal rich sediments, soils, or waters in the northwestern Seward Peninsula may be significant for a number of reasons. The population of Wales relies heavily on the local ecosystem for food sources. Plants are harvested throughout the summer from the tundra adjacent to the village, and fish are collected from nearby Lopp Lagoon—a body of water that receives most of the surface runoff and sediment load from the northwestern corner of the Seward Peninsula. Also, the proximity of the study area to the Bering Strait allows for rapid cycling of any eroding metals into the nearshore marine ecosystem.

Locally anomalous concentrations of many trace metals occur in tin-rich granites and adjacent metasedimentary rocks at scattered locations across the northwestern Seward Peninsula. The anomalous arsenic values observed in the NURE sediments are, at least in part, erosional products of metalliferous granites and adjacent skarn and replacement bodies. Dispersion of arsenic and other genetically associated ore metals, Sn, Be, and W, from bedrock sources into local soils, stream sediments, and surface waters is a normal part of the processes of weathering and erosion.

The aim of the present study is to better understand the element dispersion along the northwestern side of the York Mountains by sampling surface waters and stream sediments. Resulting local geochemical background data are critical for any future environmental impact assessment, land-use planning, pollution monitoring, and mineral-resource-assessment work in the area. These data may help identify areas of the tundra that

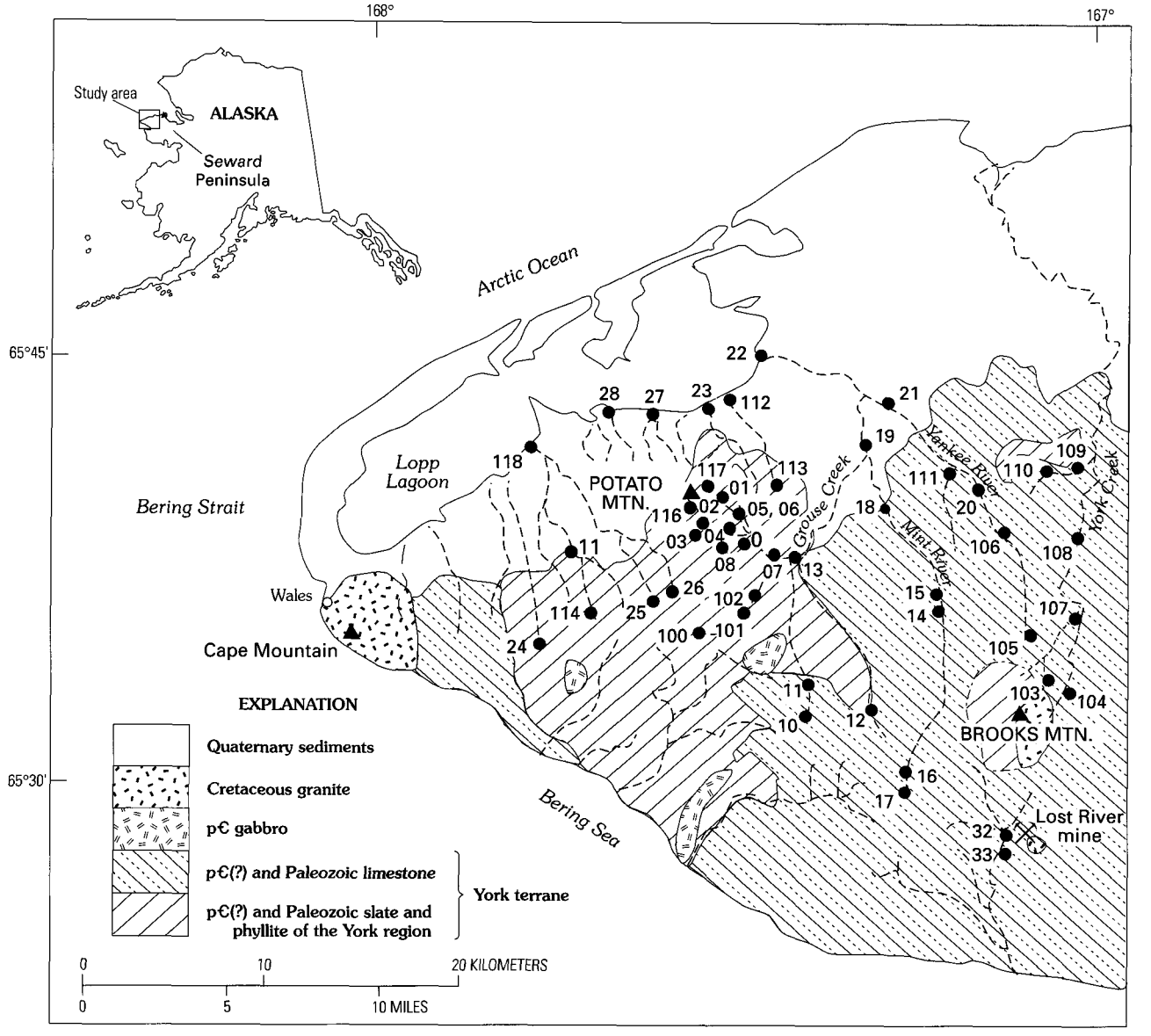

Figure 1. Site locations for stream-sediment and water samples collected in northwestern Seward Peninsula, Alaska. (Geology from Sainsbury, 1972)

should be avoided for plant harvesting. If metal levels in sediments or waters are relatively high near the mouths of the streams and rivers, then this might signal the need for detailed study of any effects on organisms in Lopp Lagoon. Certainly, at least, the possibility of biomagnification of metals within the food chain exists in the Wales area. Atmospherically transported, anthropogenic As, Cd, Hg, and other contaminants in high-latitude arctic ecosystems are now widely recognized in the tissue and organs of large marine mammals and native populations (Pearce, 1997). Identification of any significant natural metal cycling into the food chain in this part of the Seward Peninsula is a first step in determining whether regional geological processes may also be contributing contaminants to the environment. Also, data from this study may prove useful in better defining new areas of tin, uranium, and other granite-related mineral resources in this part of Alaska.

General Geology

Sainsbury (1972) mapped the geology of the western portion of the Seward Peninsula at a scale of 1:250,000. The area consists mainly of Precambrian(?) and early Paleozoic argillaceous and dolomitic limestones, shales, slates, and phyllites (fig. 1), which are referred to as slate of the York region. Much of this unit was mapped by Sainsbury (1972) as Precambrian in age, but it is lithologically similar to Lower Ordovician rocks found elsewhere on the Seward Peninsula (Till and Dumoulin, 1994). The weakly metamorphosed units were deposited in shallow marine to restricted carbonate platform sedimentary environments. The York terrane may be subdivided into two major units: (1) the slate of the York region—an informal name for graphitic, slaty, or phyllitic rocks that originally consisted mainly of

carbonaceous siltite, but also contained diverse laminated to thin-bedded mudstone, siltstone, fine-grained sandstone, calcareous sandstone, and carbonaceous limestone (Sainsbury, 1972)—and (2) a thick sequence of fossiliferous limestone, dolomitic limestone, and argillaceous limestone.

The York terrane was subsequently intruded by highly evolved, tin-rich granites and syenogranites between about 80–70 Ma. Seven of nine tin-enriched granite plutons are exposed and two are inferred at depth in the northwestern Seward Peninsula (Hudson and Arth, 1983). Three of these, Cape Mountain, Brooks Mountain, and an inferred pluton at Potato Mountain, occur within our study area. These granites are similar to granites exposed in eastern Siberia (Swanson and others, 1990) and, therefore, are likely to occur beneath the waters of the Bering Strait.

On the Seward Peninsula, tin lodes are generally found as cassiterite in greisenized plutonic cupolas and in pyroxene-garnet-tourmaline-axinite-cassiterite skarn in adjacent marbles (Swanson and others, 1990; Hudson and Reed, 1997). Uranium, tungsten, and rare-earth-element (REE) enrichments are commonly associated with many of these evolved plutons. Hudson and Arth (1983) report as much as 20 to 30 ppm U for representative samples of some plutons. Recognized sulfide and oxide mineral phases include pyrrhotite, arsenopyrite, fluorite, tetrahedrite, scheelite, cassiterite, stannite, wolframite, chalcopyrite, thorite, zeunerite, and many Be-bearing phases (West and White, 1952; Sainsbury, 1963; Sainsbury and others, 1968; Swanson and others, 1990).

About 3,000 metric tons (t) of tin have been recovered from lodes and related placers of the Seward Peninsula, representing more than 90 percent of Alaska's historic production. Past production is dominated by 1,676 t of tin from the Cape Mountain placer deposit, 1,000 t of tin from the Potato Mountain placer deposit, and 314 t of tin from the Lost River lode deposit (Hudson and Reed, 1997). Lode reserves remaining at the Lost River deposit include 22.3 million metric tons of 0.15 percent tin, 16.3 percent fluorite, and 0.03 percent WO_3 (Bundtzen and others, 1994). In addition, beryllium-fluorite-rich veins that replaced limestone at the Lost River deposit contain 4,500 t of beryllium, one of the world's largest reserves (Sainsbury, 1988).

Sainsbury and others (1968) carried out stream-sediment, soil, and plant-geochemical surveys around tin occurrences in the Brooks Mountain and Lost River areas. Although the data were generally semiquantitative and often below analytical determination limits, some stream sediments near the Lost River mine tailings contained as much as 160 ppm Be, 1,100 ppm Sn, 70 ppm W, 150 ppm Cu, 150 ppm Pb, 300 ppm Zn, 3,000 ppm As, 700 ppm B, and 3,000 ppm Li. Concentrations for soils in the Lost River valley were of equivalent magnitude. Various tundra plants in the valley showed Cu, Pb, B, and, less consistently, Ag and Zn enrichment. However, As, Be, and Sn were not strongly concentrated in the studied plant species.

Field and Laboatory Methods

Water samples were collected at 49 sites in the drainage basins of Potato Mountain and along and to the west of the Mint, York, and Yankee Rivers (fig. 1) during July 1997. Stream-sediment samples were collected from 48 sites, but at two of the sites there was not enough material collected for subsequent analysis. At each sample site, pH and conductivity of stream water were measured with portable meters. Three 60-mL water samples were collected in high-density polyethylene (HDPE) bottles at each site. Two samples, one filtered and one unfiltered, were taken for cation analysis. The unfiltered sample was analyzed for total metals, dissolved plus suspended cations. The second sample was passed through a 0.45-µm filter to determine dissolved-cation concentrations. Both samples were acidified with concentrated nitric acid to a pH of less than 2. A third filtered, unacidified sample was taken for anion analysis. This sample was packed in ice for shipping and then refrigerated until analyzed. Stream sediments were sieved in the field to minus-10-mesh (2 mm). Panned heavy-mineral-concentrate samples were collected at 29 sites.

In the laboratory, the stream sediments were dried at room temperature and sieved to minus-80-mesh (1 mm), pulverized, and chemically analyzed. The panned concentrates were dried and sieved to minus-18-mesh (<1 mm). The heavy minerals in each sample were then gravity-separated using bromoform (specific gravity > 2.86). The heavy-mineral concentrates were separated into magnetic, paramagnetic, and nonmagnetic fractions. The nonmagnetic fraction was further separated into two splits. One split was pulverized and chemically analyzed; the remaining split was retained for optical mineralogic examination.

Analytical Techniques

The filtered and unfiltered water samples were analyzed for major and minor cations and trace elements by inductively coupled plasma–mass spectrometry (ICP-MS) (Meier and others, 1994). Anion concentrations were determined on the unacidified, filtered water samples using ion chromatography as described by d'Angelo and Ficklin (1996). Total alkalinity was measured by titration as bicarbonate (HCO_3^-).

Stream sediments were digested in a total decomposition process using a mixture of hydrochloric, nitric, perchloric, and hydrofluoric acids at low temperature (Crock and others, 1983). The resulting solution was analyzed for 40 major, minor, and trace elements by inductively coupled plasma–atomic emission spectrometry (ICP-AES). Additionally, a 10-element ICP-AES (Motooka, 1996) method was applied that utilizes a partial digestion of the sample in a hydrochloric acid-hydrogen peroxide solution. These data are useful because of lower detection limits for Ag, Cd, Mo, and Sb, whose concentrations were below the detection limit utilizing the 40-element ICP-AES method. Se, W, and Hg were determined using the chemical methods outlined by Arbogast (1996). The nonmagnetic heavy-mineral-concentrate samples were analyzed by semiquantitative emission spectrography (ES) for 36 elements (Grimes and Marranzino, 1968). Analytical results of the stream sediment data are listed in Parnow and others (in press).

Geochemistry of Stream Sediment Samples

A summary table of basic statistics for the 45 stream-sediment samples (table 1) lists the median, minimum, and maximum values for elements that have detection ratios greater

than 0.5 (detection ratio equals the number of unqualified results divided by the total number of samples in the data set). The data for the sample (site 32; fig. 1) collected from below the Lost River mine tailings were excluded from the basic statistics because the extremely high concentrations of many elements would bias the mean statistics. This sample was collected from the Lost River immediately downstream from the main tailings pile along the river bank and is not representative of natural background geochemistry of the area. However, this sample is useful for defining the geochemical signature representative of tin-bearing skarn deposits in the western Seward Peninsula. The metalliferous sediment sample contained 13 percent Ca, 4.3 percent Mg, 3 ppm Ag, 1,435 ppm As, 106 ppm Bi, 21 ppm Cd, 285 ppm Cu, 768 ppm Li, 766 ppm Pb, 14 ppm Sb, 136 ppm Sn, 210 ppm W, and 5,200 ppm Zn. Many of these values are several times greater than the maximum concentrations from the remaining data set.

The sediment samples taken in the area underlain by the slate unit of the York terrane are characterized by background levels of 10–60 ppm As, 5–14 ppm Sn, <0.1 ppm Ag, <10 ppm Bi, 0.06–0.8 ppm Cd, 18–40 ppm Cu, 16–80 ppm Li, 25–31 ppm Pb, 1–9 ppm Sb, and 5–10 ppm W. Background values were estimated from visual evaluation of histograms of the geochemical data. The background values for As, Li, and Sn are quite high relative to average values for stream sediments derived from shales and slates (Levinson, 1980), reflecting a broad hydrothermal enrichment possibly associated with tin granite alteration haloes. Typical calcium concentrations of 0.2 to 0.5 percent characterize sediments derived from the slates, but calcium concentrations are locally higher due to calcareous silt and carbonaceous limestone interbedded in the slates.

Sediment samples taken from the upper reaches of streams draining Potato Mountain (fig. 1), an area of known tin occurrences, are consistently anomalous in As (85–530 ppm; fig. 2*A*).

Table 1. Statistical summary of selected elements from 45 stream-sediment samples (minus-80-mesh) from the western Seward Peninsula, Alaska.

[All concentrations in ppm unless otherwise noted; detection ratio is the number of samples with unqualified values divided by the total number of samples; values below detection limit were set equal to 0.7 times the lower detection limit. All elements were analyzed by 40-element inductively coupled plasma–mass spectrometry (ICP-AES), except for Cd, Mo, and Sb, which were analyzed by 10-element ICP-AES because of lower detection limits. Selenium was analyzed by hydride generation; tungsten was analyzed by neutron activation analysis (NAA). Samples were also analyzed for Ag and Au by 10-element ICP-AES, but more than 60 percent of the data were below the lower determination limit. All analyses done by USGS contract lab, XRAL Inc., Ontario, Canada]

Element analyzed	Detection ratio	Median	Minimum	Maximum	85th percentile	90th percentile	Geometric mean	Geometric deviation
Al (%)	1	7	1.1	8.6	7.9	8.2	6.1	1.5
Ca (%)	1	.68	0.18	22	11	16	1.5	5.4
Fe (%)	1	4.8	0.73	6.9	5.9	6	4.2	1.6
K (%)	1	1.9	0.34	2.5	2.3	2.3	1.7	1.5
Mg (%)	0.96	1.3	0.67	6.5	3.1	3.7	1.5	1.7
Na (%)	1	.65	0.05	1.1	0.93	0.94	.56	1.8
P (%)	1	.07	0.01	0.13	0.11	0.12	.07	1.7
Ti (%)	1	.41	0.05	0.95	0.54	0.61	.32	1.9
As	0.87	32	10	530	95	101	33	2.9
Ba	1	353	38	2510	995	1460	439	2.2
Cd	1	0.2	0.05	1.6	0.6	0.8	0.2	2.4
Ce	1	82	7	361	115	118	70	1.9
Co	1	19	3	32	27	28	17	1.7
Cr	1	95	13	140	123	125	84	1.6
Cu	1	23	3	59	30	41	22	1.7
Ga	1	21	14	31	26	26	21	1.2
Hg	1	0.063	0.014	0.287	0.174	0.212	0.06	2.2
La	1	38	4	132	51	54	32	1.8
Li	1	61	9	132	80	96	57	1.6
Mn	1	744	175	3660	1010	1180	726	1.7
Mo	1	0.7	0.3	8.2	2.8	3.1	1	2.2
Nd	0.96	36	10	199	56	59	34	1.8
Ni	1	50	8	76	61	66	46	1.5
Pb	1	25	4	86	30	31	23	1.6
Sb	0.51	0.7	1	26	9	9	1.5	3.0
Sc	1	15	3	21	19	19	13	1.5
Se	0.91	0.3	0.2	1	0.6	0.8	0.3	1.7
Sn	0.64	7	5	62	14	16	7	2.0
Sr	1	86	53	470	302	337	119	1.9
V	1	142	17	298	166	180	131	1.6
W	1	6.7	4	17	10	10	6.9	1.4
Y	1	14	4	24	17	18	14	1.3
Zn	1	100	15	155	120	133	90	1.5

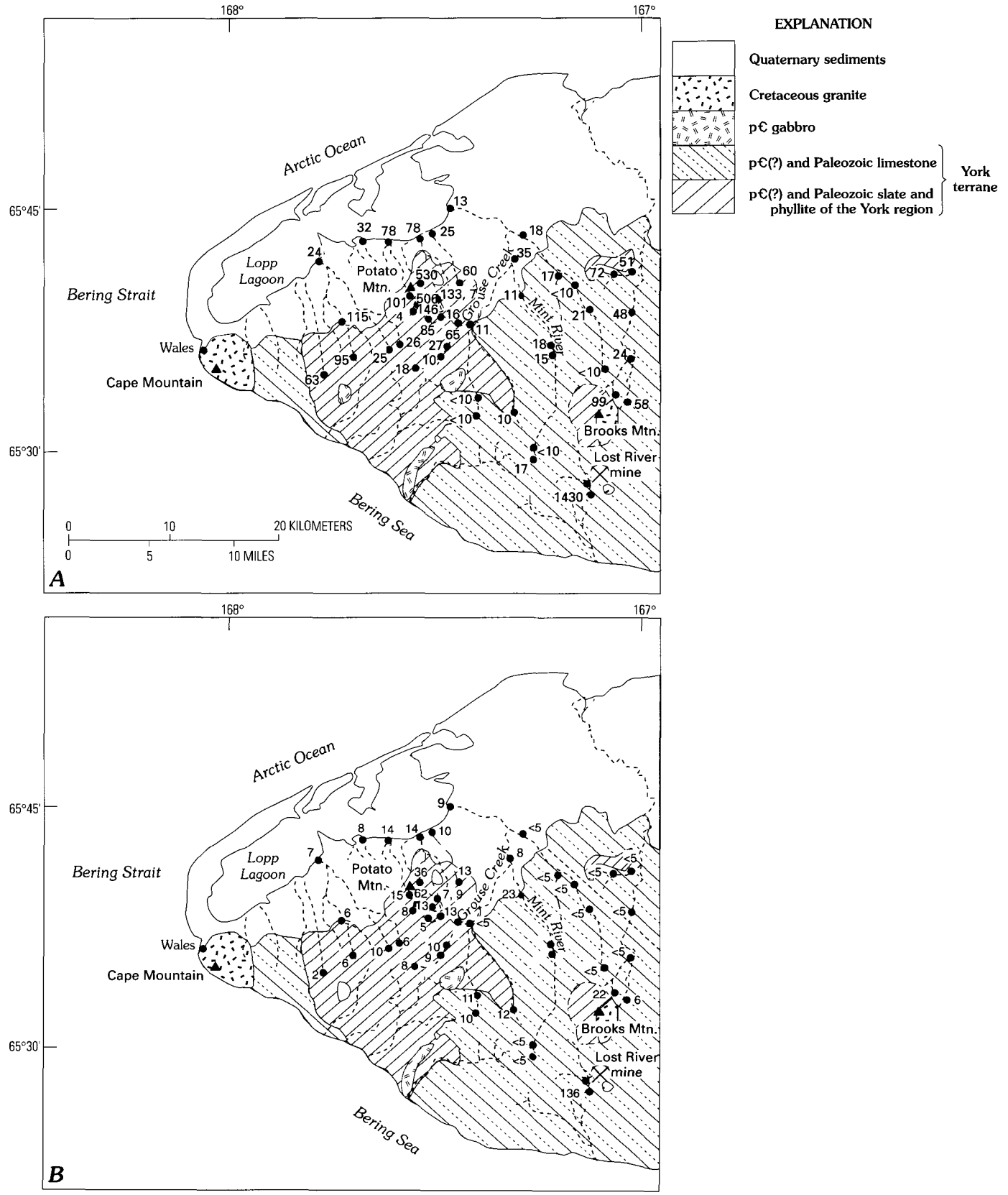

Figure 2. *A*, Concentrations of arsenic in ppm in stream sediments. *B*, Concentrations of tin in ppm in stream sediments.

Also, they show consistent anomalies for tin (fig. 2*B*), as well as enrichments of Ag, Be, Cu, Ni, Sb, and W. The sediment samples collected in the same drainages, but at lower elevations flowing through the Quaternary sediments directly upstream from Lopp Lagoon (sites 23, 27, 28, 112, and 118; fig. 1), generally contain background tin and arsenic concentrations. However, two of the five samples (sites 23 and 27) collected in the lower reaches contain As concentrations of 78 ppm. In addition,

Table 2. Factor loadings for selected elements for 45 stream-sediment samples collected from the western Seward Peninsula, Alaska.

[Leaders (--) indicate loadings less than |0.5|; negative loadings in boldface type]

Element	Factor 1	Factor 2	Factor 3	Factor 4
Al	0.92	--	--	--
Ca	**–0.81**	--	--	--
Fe	0.95	--	--	--
K	0.89	--	--	--
Mg	**–0.82**	--	--	--
Na	0.89	--	--	--
P	0.93	--	--	--
Ti	0.88	--	--	--
Mn	0.72	--	--	--
As	--	--	0.84	--
Ba	--	0.89	--	--
Cd	--	0.87	--	--
Ce	0.86	--	--	--
Co	0.88	--	--	--
Cr	0.93	--	--	--
Cu	0.50	0.68	--	--
Ga	--	--	--	--
Hg	--	--	--	–0.66
La	0.83	--	--	--
Li	0.79	--	--	--
Mo	--	0.87	--	--
Nd	0.85	--	--	--
Ni	0.82	--	--	--
Pb	0.69	--	--	--
Sb	--	--	0.87	--
Sc	0.94	--	--	--
Se	--	0.71	--	--
Sn	--	--	0.72	--
Sr	**–0.63**	0.55	--	--
V	0.83	0.51	--	--
W	0.03	--	0.62	--
Y	0.62	0.54	--	--
Zn	0.87	--	--	--

the most western of these (site 118) contains 361 ppm Ce, 8 ppm Eu, 132 ppm La, and 199 ppm Nd, the highest concentrations of these elements from the study area.

The samples collected in the eastern portion of the study area, which is underlain by the dolomitic part of the limestone unit of the York terrane, had mainly background concentrations of Ag (<0.8 ppm), As (10–50 ppm), Ba (400–1,000 ppm), Cu (5–30 ppm), Cd (0.3–0.8 ppm), Ni (30–60 ppm), Pb (15–30 ppm), Sb (<1 ppm), Sn (<5 ppm), V (80–180 ppm), Zn (56–130 ppm), and W (5–10 ppm). Background populations were again defined through visual inspection of histograms of the data for the sediments draining the limestone unit. Locally high concentrations of Ba (1,460–2,510 ppm), Cd (0.8–1.6 ppm), Mo (3.1–5.4 ppm), and V (180–225 ppm) primarily reflect material weathered from argillaceous interbeds.

Two samples (sites 109 and 110; fig. 1) collected from a small tributary of York Creek along the eastern border of the study area contained arsenic concentrations of 51 and 72 ppm (fig. 2*A*), respectively, suggesting possible hydrothermal mineralization even though there are no known granites in the area. The sample with 72 ppm As also contained detectable gold and silver, further suggesting hydrothermal mineralization distal to any known granite. Anomalous Mo (6.8–8.2 ppm) and V (298–235 ppm) in the two samples can best be attributed to argillaceous units within the limestone-dominant unit.

One of the sediment samples collected from a stream on the northeast side of Brooks Mountain (site 103; fig. 1) had a tin value of 22 ppm. This sample also had anomalous values for As (99 ppm), Cu (49 ppm), Li (110 ppm), Ni (66 ppm), Pb (86 ppm), and Sb (9 ppm). These enrichments reflect the known tin occurrences upstream and nearer to the peak of Brooks Mountain. This is further supported by a concentration of 26 ppm Sb at an adjacent site (site 104; fig. 1).

Factor Analysis of Stream-Sediment Data

Element associations for the 45 stream sediments (not including the Lost River site) were determined by factor analysis. R-mode factor analysis with Varimax rotation was used to identify dominant geochemical associations in the sediment data. The data were log-transformed prior to analysis, as most geochemical data are log-normally distributed (Koch and Link, 1970). The log transformation attempts to normalize the distribution so that the statistical analysis is valid. Resulting factors often delineate suites of elements that are geochemically associated with specific rock types or mineral deposits. Factor loadings may be interpreted in much the same way as correlation coefficients. A high factor loading indicates a strong association of the particular variable (element) with the given factor. The association of each sample within a given factor is analyzed by its score onto that factor. The greater the absolute score of a given sample, the stronger the correlation to the element or suite of elements defined by the factor.

A four-factor model, which accounts for 82 percent of the total variance, was chosen as the most appropriate for summarizing the data set. Table 2 lists the factor loadings for all of the elements that had a detection ratio of greater than 0.5 and were, therefore, included in the factor analysis. Gold and silver, although elements of economic interest, were among those elements deleted from the factor analysis due to low detection ratios.

Factors 1and 2 (figs. 3*A* and 3*B*) reflect geochemical signatures of the dominant lithologies of the study area. Factor 1 has high positive loadings for Al, Fe, K, Na, P, Ti, Mn, Ce, Co, Cr, Cu, La, Li, Nd, Ni, Pb, Sc, V, Y, and Zn, and negative loadings for Ca, Mg, and Sr. Plots of the factor scores (fig. 3*A*) indicate that samples with positive scores for factor 1 are located mainly in the western portion of the study area, which is underlain by slates. All of the sites having strong negative scores for factor 1 are located along the Mint River, Yankee River, and York Creek, or their tributaries, and are underlain by carbonate rocks. Factor 2 has high positive loadings for Ba, Cd, and Mo, (>0.85), and slightly lower positive loadings (0.5–0.71) for Cu, Se, Sr, V, and Y. The samples with highest scores onto factor 2 (fig. 3*B*) were collected from the streams and rivers that are underlain by carbonates; thus, the geochemical signature must reflect the

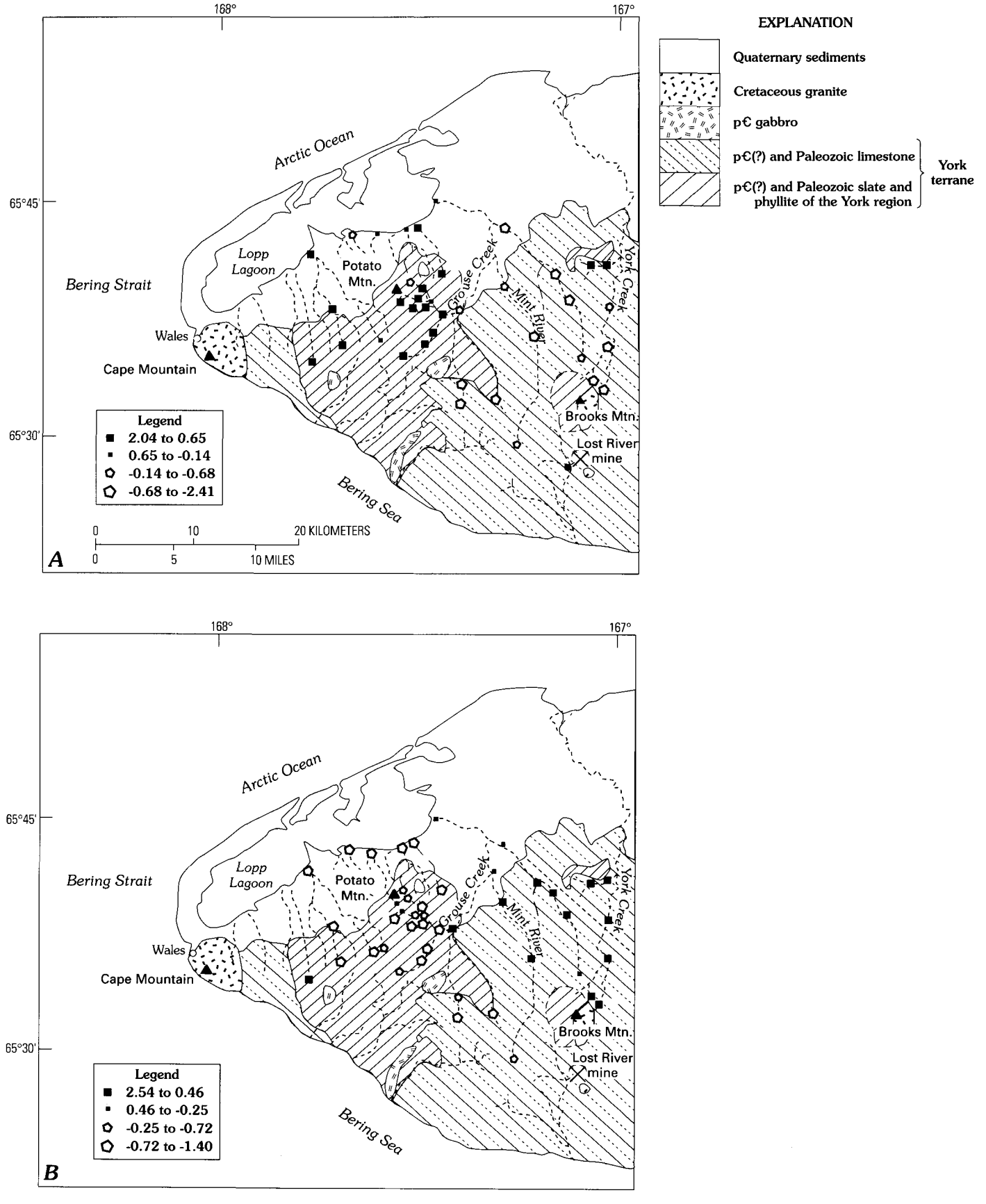

Figure 3. *A*, Plot of scores for factor 1 (positive loadings for Al, Fe, K, Na, P, Ti, Mn, Ce, Co, Cr, Cu, La, Li, Nd, Ni, Pb, Sc, V, Y, and Zn and negative loadings for Ca, Mg, and Sr). *B*, Plot of scores for factor 2 (positive loadings for Ba, Cd, Cu, Mo, Se, Sr, V, and Y).

abundance of argillaceous interbeds. Sites 109 and 110 (fig. 1) have high positive scores for factor 1, but also have positive scores for factor 2. These two samples sites reflect sediment contributions from both the slates and the carbonates in an area along the west side of York Creek.

Factor 3 shows a strong positive correlation between As, Sb, Sn, and W. This group of elements defines the geochemical signature of sediments influenced by tin occurrences of the region. Ten of the samples with high scores (>0.4) for factor 3 (fig. 4) were collected in the stream drainages of Potato Mountain. Other samples with high factor-three scores were collected from drainages northeast of Brooks Mountain (sites 103 and 104; fig. 1) and from southwest of Potato Mountain (sites 24 and 114; fig. 1). Although none of these sites contained elevated tin concentrations in the stream sediments, most had anomalous As and W, which are indicator elements for hydrothermal tin granites. Possibly, the data from sites 24 and 114 indicate additional undiscovered tin occurrences between Potato Mountain and Cape Mountain. Stream-sediment samples collected from a small tributary of York Creek (sites 109 and 110; fig. 1) had low scores for factor 3 and low concentrations of tin, although heavy-mineral-concentrate samples contained greater than 2,000 ppm tin and detectable tungsten (150 ppm) collected from the same sites.

Factor 4 was defined by a loading for mercury of –0.66. Analysis of the raw data indicates that this is due to minor variation in the mercury concentrations due to differences in lithology.

Geochemistry and Mineralogy of Heavy-Mineral-Concentrate Samples

Basic statistics for the heavy-mineral concentrates are listed in table 3. Eight of the fourteen samples collected in the drainages of the Potato Mountain area (fig. 1) contained greater than 2,000 ppm Sn. Three of these samples (sites 04, 116, and 117; fig. 1) showed significant amounts of As (500 ppm), B (1,000–2,000 ppm), Bi (20–2,000 ppm), and Be (2–5 ppm), but similar

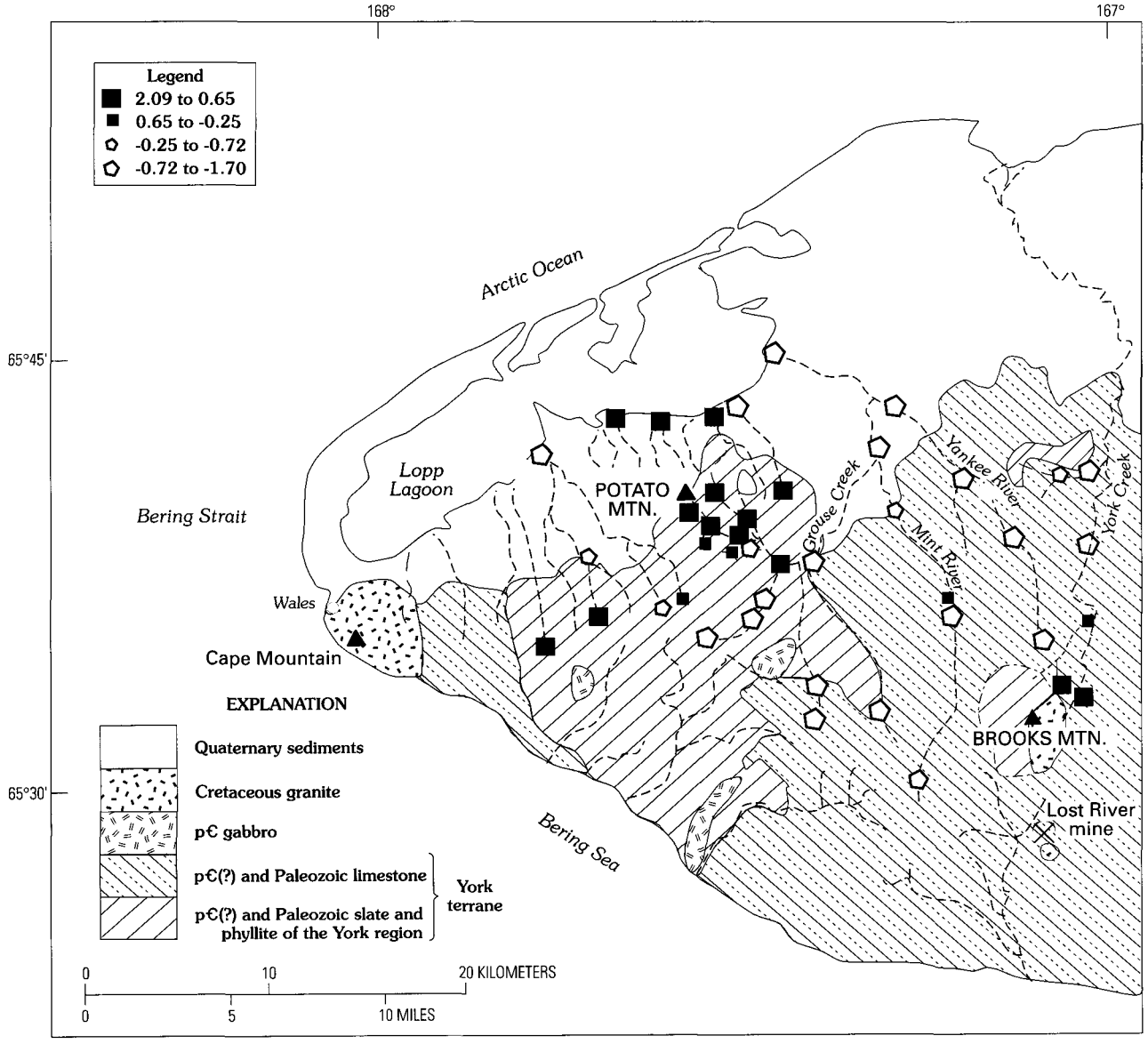

Figure 4. Plot of scores for factor 3 (positive loadings for As, Sb, Sn, and W).

Table 3. Basic statistics for 29 heavy-mineral-concentrate samples collected from the western Seward Peninsula.

[All concentrations in ppm unless otherwise noted; detection ratio is the number of samples with unqualified values divided by the total number of samples; N, number of samples qualified with "N" (not detected at lower detection limit); L, number of samples qualified with "L" (less than lower detection limit); G, number of samples qualified with "G" (greater than detection limit); geometric mean calculated using all data—values with "N" were set equal to 0.5 times the lower detection limit; values of L were set equal to 0.7 times the lower detection limit; and values of G were set to 1.3 times the upper detection limit]

Element	Detection ratio	N	L	G	Median	Minimum	Maximum	85th percentile	90th percentile	Geometric mean	Geometric deviation
Ca (%)	1	0	0	0	2	0.1	15	10	10	2.39	0.65
Fe (%)	1	0	0	0	0	0.2	5	2	2	0.94	0.30
Mg (%)	1	0	0	0	1	0.07	7	2	2	0.78	0.46
P (%)	0.72	3	5	0	1	0.7	3	2	2	0.91	0.34
Ti (%)	0.76	0	0	7	1	0.03	2.6	2.6	2.6	0.90	0.45
B	0.97	1	0	0	700	20	2000	1500	2000	295	0.11
Ba	0.97	0	0	1	500	50	13000	5000	7000	705	0.72
Co	0.69	2	8	0	20	20	70	30	50	21	0.67
Cr	0.93	0	2	0	50	20	200	100	100	48	0.21
Cu	0.93	0	2	0	15	15	100	50	50	20	0.27
Ga	0.59	5	7	0	10	10	20	15	15	9	0.29
La	0.55	2	4	7	200	100	2600	2600	2600	357	0.17
Mn	1	0	0	0	500	50	700	500	700	325	0.65
Ni	0.72	2	6	0	20	15	150	70	100	22	0.29
Pb	0.45	2	14	0	14	20	100	50	50	21	0.35
Sc	0.83	1	4	0	15	10	100	30	50	16	0.27
Sn	0.66			10	1000	20	2600	2600	2600	471	0.77
Sr	0.83	3	2	0	500	300	1000	1000	1000	480	0.33
V	0.97	0	1	0	70	50	200	100	100	69	0.20
Y	0.97	0	1	0	70	30	100	100	100	61	0.24
Zr	1	0	0	0	300	50	2000	1000	1500	359	0.40

concentrations of Cu (15–50 ppm), Ni (20–100 ppm), and Pb (20–100 ppm) when compared to the stream sediments. Two of the samples also contained 200–300 ppm tungsten.

The samples that were collected in the eastern portion of the study area, which is underlain by carbonate rocks, typically had barium concentrations of 3,000 to greater than 10,000 ppm. This is supportive of the presence of detrital barite. But, in addition, the sample collected from the stream northeast of Brooks Mountain (site 103; fig. 1) contained 500 ppm As and 200 ppm Sn. The two samples from a tributary of York Creek (sites 109 and 110; fig. 1) contained greater than 2,000 ppm Sn and detectable W (150 ppm). These data support the existence of exposed tin-bearing occurrences in these drainage basins.

Concentrate samples with anomalous tin and arsenic values were microscopically examined for identification of associated mineral phases. Because of the highly weathered nature of the grains, it was not possible to optically determine if the dominant sulfide in the concentrates was pyrite or arsenopyrite. Emission spectrographic analyses of the sulfide grains indicate that the samples contained concentrations of greater than 20,000 ppm As. This suggests that arsenopyrite is the dominant sulfide mineral. Metal-rich samples collected at sites in the Potato Mountain area and from streams northeast of Brooks Mountain contained cassiterite, pyrite, monazite, zircon, titanite, tourmaline, and rutile, in addition to arsenopyrite. Two of the samples also contained minor amounts of scheelite. Two samples (109 and 110; fig. 1) collected in a tributary of the York River contained cassiterite, monazite, rutile, tourmaline, sphene, and some pyrite/arsenopyrite.

The samples that were collected in the eastern part of the study area, in the drainages underlain by argillaceous and dolomitic limestone, contained appreciable amounts of barite and zircon, and fragments of limestone and dolomite. One sample (site 12; fig. 1), collected in the upper reaches of Skookum Creek at the contact between slates and carbonates, contained 2,000 ppm Mo, which indicates an upstream molybdenite-bearing occurrence.

Geochemistry of Water Samples

Water samples were collected at 49 sites. Table 4 lists the basic summary statistics for the water samples collected during this study. Samples collected near the Lost River mine were excluded from the tabulation because they would strongly skew the data. Field pH measurements (table 5) indicate that most surface waters are slightly alkaline, with values ranging from 7.5–8.2. Conductivity, also measured in the field, varied over almost an order of magnitude, ranging between 51 and 729 micromhos/s (table 5). The lowest values reflect headwater seeps that have limited flowpaths and thus relatively little water/rock interaction (sites 02, 08, and 103; fig. 1). Analytical results for filtered water samples (Parnow and others, in press) indicate a consistent pattern of Ca>>Mg>Na>K in both the areas underlain by slate and carbonate units of the York terrane. There are no appreciable differences in dissolved calcium and magnesium levels, regardless of whether the samples were collected in streams underlain by slate or limestone. This is indicative of

Table 4. Data for dissolved constituents in filtered, acidified stream-water samples collected from the western Seward Peninsula.

[All concentrations in ppb unless otherwise noted]

Element analyzed	Detection ratio	Median	Minimum	Maximum	85th percentile	90th percentile	Geometric mean	Geometric deviation
Ca (ppm)	1	20	1.8	84	38	46	18	0.32
Mg (ppm)	1	6.4	0.30	19	11	13	5.22	0.38
Na (ppm)	1	3.2	0.76	5.9	4.4	4.9	2.76	0.24
SiO_2 (ppm)	0.64	2	1	9.6	4	5	1.1	0.33
K	1	280	54	830	430	510	245	0.28
Al	0.85	5	0.83	1100	100	100	14	1.49
Ag	0.66	0.07	0.01	100	100	100	0.52	0.46
As	0.26	0.14	0.20	2	0.30	0.60	0.20	0.30
Ba	1	5	0.10	66	18	28	5.59	0.56
Co	0.62	0.02	0.01	8.9	0.07	0.10	0.03	0.65
Fe	1	31	7	160	59	85	31	0.33
Li	0.87	1.2	0.20	100	2.1	3.7	1.32	0.43
Mn	1	0.33	0.01	120	8.5	29	0.47	1.09
Mo	0.55	0.04	0.10	0.51	0.40	0.40	0.07	0.54
Ni	1	0.40	0.1	20	1.0	1.2	0.51	0.46
P	0.51	10	1	100	39	100	11.38	0.56
Rb	0.98	0.30	0.2	100	1.4	2.5	0.34	0.66
Sb	0.55	0.03	0.02	0.30	0.10	0.20	0.03	0.42
Sc	0.83	0.30	0.10	100	0.50	0.5	0.31	0.22
Se	0.53	0.2	0.2	0.6	0.3	0.4	0.22	0.19
Sr	1	100	9.2	320	170	210	83	0.33
U	0.74	0.04	0.008	5.80	1.10	1.30	0.06	1.05

Table 5. Field-measured pH and conductivity for 49 stream-water samples collected from the western Seward Peninsula.

Site no.	pH	Conductivity (µS/cm)
01	4.9	145
02	5.7	56
03	6.1	132
04	7.3	282
05	6.5	216
06	7.0	323
07	6.9	258
08	6.5	82
09	7.0	270
10	7.0	137
11	7.4	265
12	8.2	241
13	7.2	277
14	8.1	364
15	8.0	206
16	8.1	165
17	8.4	108
18	8.2	246
19	8.1	260
20	8.2	341
21	8.0	386
22	8.3	257
23	7.5	172
24	7.9	388
25	7.6	231
26	7.2	450
27	5.5	99
28	6.7	145
32	8.3	163
33	8.0	167
100	6.7	322
101	7.5	243
102	7.4	142
103	8.7	51
104	8.4	165
105	8.1	106
106	7.5	416
107	9.0	321
108	7.9	496
109	7.5	729
110	7.6	635
111	7.8	447
112	7.3	335
113	7.7	190
114	7.6	159
115	7.4	173
116	7.3	234
117	4.7	165
118	8.0	160

interbedded carbonates within the slates of the York terrane contributing significant amounts of calcium to dissolved loads. This is further supported by the variation of bicarbonate in the area underlain by slate (fig. 5*A*). Dissolved sulfate levels for waters collected in streams underlain by slates are typically in the range of 20–38 ppm, and the waters collected in the areas underlain by carbonates have sulfate concentrations <20 ppm (fig. 5*B*). Dissolved iron generally ranges between 20–40 ppb in both areas, but most trace metals were always below analytical determination limits; these include <0.2 ppb As, <0.05 ppb Be, <0.02 ppb Cd, <0.5 ppb Cu, <10 ppb Mn, <0.2 ppb Mo, <1 ppb Ni, <0.05 ppb Pb, <0.02 ppb Sb, <0.05 ppb Sn, and <3 ppb Zn.

Two water samples were collected at the Lost River mine, located south of the study area. Samples were collected from a small seep at the base of the main tailings piles (site 33; fig. 1) and from Lost River, immediately downstream from the mine workings (site 32; fig. 1). Resulting analytical data provided geochemical signatures characteristic of waters that have interacted with tin-rich mineralized rock typical of the western Seward Peninsula. Conductivity values were at background levels (167 and 163 micro-mhos/s) and were comparable to those from elsewhere in the study area. The carbonate host rock buffered the water such that the pH's were alkaline despite the abundance of sulfide minerals in the tailings. The seep in the tailings, despite the alkaline pH, does show significant enrichment of metals when compared to the waters collected from the areas of known, but undeveloped, occurrences in the Potato Mountain area. However, all absolute concentrations remain extremely low. The filtered water sample from site 33 (fig. 1) contained only 3.2 ppm sulfate, but 180 ppb As, 90 ppt Cd, 0.7 ppb Cu, 8.9 ppb Mo, 1.5 ppb Sb, 0.4 ppb W, and 10 ppb Zn. A large volume of suspended material in the water is indicated by elevated concentrations of metals in the unfiltered samples from the same site (4.4 ppm Al, 2.5 ppm Fe, 470 ppb As, 3.1 ppb Be, 2.7 ppb Cd, 38 ppb Cu, 420 ppb Mn, 5.5 ppb Mo, 2.2 ppb Ni, 270 ppb Pb, 6.2 ppb Sb, 8 ppb Sn, 23 ppb Ti, and 600 ppb Zn)

Most of the water samples collected in the drainages surrounding Potato Mountain contained background concentrations of all metals, including the same metals that were anomalous in sediments collected from these sites. However, waters at sites 04–07 and 116–117 (fig. 1) showed enrichments in As (0.2–0.7 ppb) and Sb (0.2–0.3 ppb) concentrations, both which are indicator elements for tin deposits. Also, samples collected at sites 01 and 117, located just north of Potato Mountain (fig. 1) were acidic (pH 4.85 and 4.73, respectively) and had relatively high concentrations of dissolved Al (1,100 and 360 ppb), Cu (2 and 6 ppb), Mn (120 and 71 ppb), and Ni (20 and 12 ppb). Sites 01 and 117 had very low alkalinity (3.3 and 1.0 ppm) relative to the other samples collected near Potato Mountain, signifying a decrease in the buffering ability of the water. This may be due to weathering of sulfides, which would decrease the pH. However, there was no significant increase in dissolved iron, although sample 117 did have measurable arsenic (0.7 ppb). Dissolved sulfate concentrations ranged between 40–75 ppm in the waters collected from areas of known tin occurrences. Increased sulfate concentrations may be the best hydrogeochemical indicators of the Potato Mountain tin-bearing occurrences.

The sites located in the carbonate-dominated unit of the York terrane, along the eastern margin of the studied area that had anomalous arsenic and tin in stream sediments and heavy-mineral concentrates, also contained slightly elevated metal concentrations in water samples. Sites 109 and 110, located within the York Creek watershed (fig. 1), had the highest conductivities of any samples (729 and 635 micro-mhos/s), but pH was slightly alkaline (7.5 and 7.6). Relatively high concentrations of Fe (85–160 ppb) and Mg (13–19 ppm) at these sites

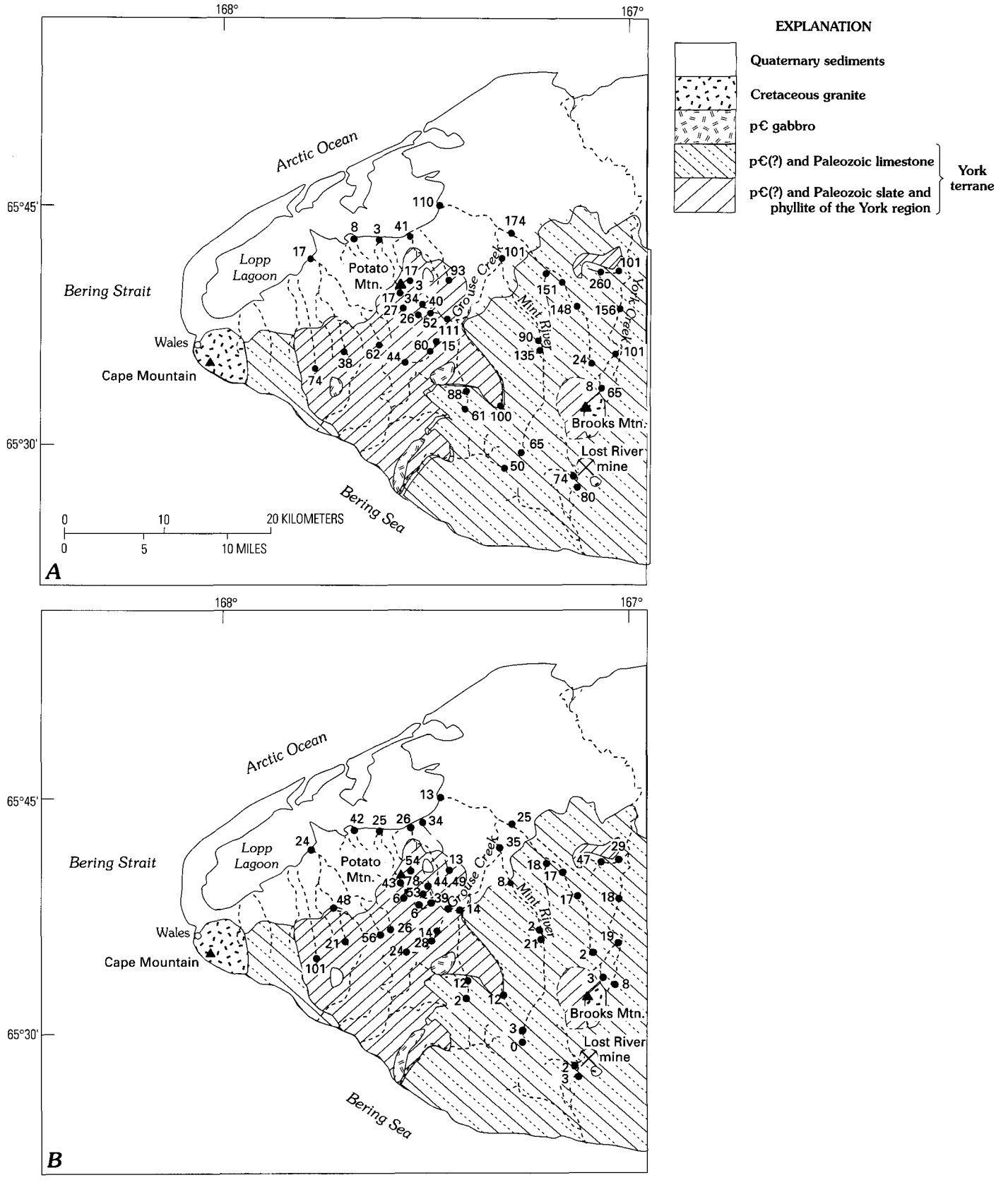

Figure 5. *A*, Concentrations of bicarbonate in ppm in filtered water samples. *B*, Concentrations of dissolved sulfate in ppm in filtered water samples.

could be due to lithologic variations, representative of water-rock interaction with both the slates and the carbonates, as there is a small outcrop of slate to the north of the two sites (fig. 1). However, slight enrichments in dissolved tin (0.1 ppb at site 110) and arsenic (0.5 ppb at site 109) are consistent with a tin-mineralized source. Sites 103 and 104, in the headwaters of

York Creek (fig. 1) and also characterized by previously described anomalies in other sample media, contained 1–2 ppb dissolved arsenic and 0.2 ppb dissolved tin.

Six samples were collected from the mouths of streams at Lopp Lagoon. The waters had a broad variation in pH ranging from 5.5–8.3. Five of the six samples were collected from streams draining Potato Mountain, and that from site 22 was collected at the mouth of the Mint River. Sites 27, 28, and 118 were sulfate-dominated waters, whereas sites 22, 23, and 112 (fig. 1) were bicarbonate-dominated waters. The sulfate-dominated waters may indicate greater input from waters that have interacted with the tin occurrences and their associated sulfide minerals. Site 27 had the lowest pH (5.53) and had corresponding high concentrations of dissolved cations (99 ppb Al, 47 ppb Mn, 8.3 ppb Ni, and 8 ppb Zn) and detectable levels of As (0.3 ppb). Sites 27 and 112 contained elevated concentrations of Fe (110–150 ppb) and Mn (47 and 29 ppb). The elevated iron and manganese at these two sites compared to the rest of the study area may be due to particulates in the water that are smaller than the 0.45-μm filter that was used. The increased particulates may be due to greater biologic activity in the lower reaches of the stream, which increases respiration and causes oxidation of the sediments. This is further supported by the total iron concentrations at these sites, which are an order of magnitude greater than the average iron concentration (250–280 ppm, avg = 64 ppm). Only two of the water samples (sites 23 and 27) collected at the mouths of the streams contained detectable arsenic concentrations (0.3 ppb). These sites also contained the highest arsenic concentrations (78 ppm) in the stream sediments collected from near Lopp Lagoon.

Discussion

An understanding of the distribution of trace metals in the environment along the western Seward Peninsula is critical for a number of reasons. The tin granites and their associated mineral occurrences represent a potentially significant metal source that is directly eroded into Lopp Lagoon and the Bering Sea. Furthermore, geophysical evidence suggests that these metalliferous intrusive systems continue beneath the Bering Strait (Rick Saltus, oral commun., 1997). If correct, then additional mineralized material is exposed across this shallow part of the Bering Sea. Metals such as Cd, As, and Hg have been recognized at elevated levels in marine mammals off Alaska's west coast (for example, see Taylor and others, 1989; Becker and others, 1995). This may simply be natural biomagnification of such metals by the large mammals, but these high metal concentrations may, in part, reflect more local contributions from metalliferous locations on the western Seward Peninsula. Also of concern is whether metals are being enriched in plants or in fish in Lopp Lagoon, both of which the villagers of Wales depend on as a food source.

The first step in identifying any potential environmental problems within the local ecosystem is to determine background levels for the metals. Arsenic and tin appear to be the elements with the greatest natural fluctuation in this studied area of western Alaska. Our stream-sediment data identify natural arsenic levels in stream sediments of as much as 530 ppm downstream from known, but undeveloped, mineral occurrences in the higher elevations of Potato Mountain. To the east, concentrations of about 100 ppm As characterize streams draining Brooks Mountain, and stream sediments with as much as 72 ppm As occur in tributaries of lower York Creek. The former anomalies are also associated with known mineral occurrences, whereas the latter suggest the presence of exposed, but unrecognized, occurrences. To the west, in the lower elevations approaching the village of Wales, a concentration of 95 ppm As was determined at site 114 (fig. 1), also distal from any recognized tin-bearing occurrences. The data collected in 1997 were not able to duplicate the NURE-reported concentration of 635 ppm As for stream sediments just upstream from Lopp Lagoon, but concentrations of as much as 78 ppm As confirm that significant amounts of arsenic are reaching the lagoonal muds.

Tin, while not usually an element of environmental concern, has been found in elevated concentrations (19–35 ppm dry weight) in the livers and kidneys of walruses harvested from the Bering Sea (Warburton and Seagars, 1993). The average concentration of tin in most rock types ranges between 1 and 3 ppm (Levinson, 1980), and sediments eroded from such rocks will typically have similar tin concentrations. Due to the tin-rich alteration of rocks throughout this part of the Seward Peninsula, resulting sediments from our studied area consistently contain greater than 5 ppm Sn. Highest concentrations are again in sediments on Potato Mountain, with measured concentrations of as great as 62 ppm, and below Brooks Mountain with 22 ppm. All six sediment samples collected along Lopp Lagoon contained 7–14 ppm Sn, indicating that detrital tin is likely accumulating along this part of the coastline. In addition, 15 ppm Sn characterizes sediments from site 114 in the western part of our studied area (fig. 1).

Other elements that are commonly enriched in the tin-bearing occurrences, such as Ag, Cu, F, Pb, W, and Zn, are not anomalous in stream sediments of the western Seward Peninsula, excluding the anthropogenic enrichments below the large Lost River mine tailings pile. Beryllium, a signature element for many of the tin occurrences in the Seward Peninsula, rarely shows significant enrichment in stream sediments. A few samples from the study area contained 1–2 ppm Be, but the remainder contained less than 1 ppm Be. All samples contained less than 0.3 ppm Hg, and all except one sample contained less than 0.8 ppm Cd. The only sample with a greater cadmium concentration (1.6 ppm) was collected at site 103 below Brooks Mountain (fig. 1).

Extremely low concentrations of dissolved trace elements characterize all waters from the study area. Many trace elements become slightly more soluble in the acidic surface flow (pH 5–6) near the top of Potato Mountain. Dissolved species in the Potato Mountain samples include 1.1 ppm Al, 2 ppb As, 200 ppb Be, 300 ppb Cd, 6 ppb Cu, 71 ppb Mn, 20 ppb Ni, 300 ppb Sb, and 10 ppb Zn. Similar concentrations of these elements also characterize acidic streamflow just above Lopp Lagoon at site 27. The reason for the pH-5.5 water at this low elevation, far from any exposed bedrock, is uncertain. Perhaps it identifies (a) a large influx of ground water from higher elevation recharge zones to the south, or (b) a possible acidic input from the breakdown of organics. Many of the unfiltered water samples from throughout the study area contain 2–5 times more iron than filtered water samples from the same sites. Concentrations of 100–250 ppb Fe in these unfiltered waters reflect minor amounts of colloidal

oxyhydroxides. Arsenic is not soluble at the pH range of our study area, but may adsorb onto oxyhydroxides. However, the data shows no correlation between increased total iron and increased arsenic.

Conclusions

Results from our study indicate that solution transport of metal phases from the tin-bearing occurrences of the western Seward Peninsula is extremely insignificant. Furthermore, acidic water drainage in this area poses little problem due to the natural buffering of waters by carbonate units of the York terrane. However, detrital transport of tin- and arsenic-enriched mineral grains is significant, as is indicated by relatively high concentrations of the elements in stream sediments surrounding Potato Mountain. Enrichments in sediments are traceable as far north as the edge of Lopp Lagoon. Future study should examine any further dispersion through the local ecosystem, such that arsenic or tin enrichments can be traced into lagoonal muds, fish, and seals within the lagoon or into local plant species harvested by the villagers of Wales. Other inorganic contaminants that may be of environmental concern along the Bering Sea, such as mercury and cadmium, do not have any obvious point sources within our studied area.

Acknowledgments

We would like to thank the following people for their support: Toby Anungazuk of the Wales Native Corporation, Wales, Alaska; Dale Taylor, Laurie Balistrieri, Barrett Cieutat, Pete Theodorakis, Steve Sutley, Al Meier, and Rich Wanty of the USGS.

References Cited

Arbogast, B.F., ed., 1996, Analytical methods manual for the Mineral Resource Surveys Program of the United States Geological Survey: U.S. Geological Survey Open-File Report 96-525, 184 p.

Becker, P., Mackey, E.A., Demiralp, R., Koster, B.J., Greenburg, R.R., Wise, S.A., and Muir, D.C.G., 1995, Concentrations of chlorinated hydrocarbons, heavy metals, and other elements in tissues banked by the Alaska marine mammal tissues archive project: National Institute of Standards and Technology, NISTIR 5620, 80 p.

Bundtzen, T.K., Swainbank, R.C., Clough, A.H., Henning, W.W., and Hansen, E.W., 1994, Alaska's mineral industry 1993: Alaska Division of Geological and Geophysical Surveys Special Report 48, 84 p.

Crock, J.G., Lichte, F.E., and Briggs, P.H., 1983, Determination of elements in National Bureau of Standards' Geological Reference Materials SRM278 Obsidian and SRM 688 Basalt by inductively coupled argon plasma–atomic emission spectrometry: Geostandards Newsletter, v. 7, p. 335–340.

d'Angelo, W.M., and Ficklin, W.M., 1996, Fluoride, chloride, fluoride, nitrate, and sulfate in aqueous solution by chemically suppressed ion chromatography, *in* Arbogast, B.F., ed., Analytical Methods Manual for the Mineral Resource Surveys Program of the United States Geological Survey: U.S. Geological Survey Open-File Report 96-525, p. 149–153.

Grimes, D.J., and Marranzino, A.P., 1968, Direct-current arc and alternating-current spark emission spectrographic field methods for quantitative analysis of geologic materials: U.S. Geological Survey Circular 591, 6 p.

Hoffmann, J.D., and Buttleman, K., 1996, National geochemical database: 1. National Uranium Resource Evaluation (NURE) hydrogeochemical and stream sediment reconnaissance (HSSR) data for Alaska: U.S. Geological Survey Digital Data Series DDS-18-B, CD-ROM.

Hudson, T.L., and Arth, J.G., 1983, Tin granites of Seward Peninsula, Alaska: Geological Society of America Bulletin, v. 94, p. 768–790.

Hudson, T.L., and Reed, B.L., 1997, Tin deposits in Alaska: Economic Geology Monograph 9, p. 450–465.

Koch, G.S., Jr., and Link, R.F., 1970, Statistical analysis of geological data: New York, Dover Publications, 438 p.

Levinson, A.A., 1980, Introduction to exploration geochemistry: Wilmette, Illinois, Applied Publishing, 613 p.

Meier, A.L., Grimes, D.J., and Ficklin, W.H., 1994, Inductively coupled plasma–mass spectrometry—A powerful analytical tool for mineral resource potential and environmental studies [abs.], *in* Carter, L.M.H., Toth, M.I., and Day, W.C., eds., U.S. Geological Survey Research on Mineral Resources—1994, Part A—Program and Abstracts, V. E. McKelvey Forum on Mineral and Energy Resources, 9th, Tucson, Ariz., February 22–25, 1993: U.S. Geological Survey Circular 1103-A, p. 67–68.

Motooka, J.M., 1996, Organometallic halide extraction for 10 elements by inductively coupled plasma–atomic emission spectrometry, *in* Arbogast, B.F., ed., Analytical methods manual for the Mineral Resource Surveys Program of the United States Geological Survey: U.S. Geological Survey Open-File Report 96-525, p. 102–108.

Parnow, C.C., Kelley, K.D., Goldfarb, R.J., Meier, A.L, Sutley, S.J, and Theodorakos, P.M., in press, Analytical results of stream sediment, heavy-mineral concentrates, and water data collected from northwestern Seward Peninsula, Alaska: U.S. Geological Survey Open-File Report.

Pearce, F., 1997, Why is the apparently pristine Arctic full of toxic chemicals that started off thousands of kilometers away?: New Scientist, v. 29, no. 2, p. 24–27.

Sainsbury, C.L., 1963, Beryllium deposits of the western Seward Peninsula, Alaska: U.S. Geological Survey Circular 479, 18 p.

Sainsbury, C.L., 1972, Geologic map of the Teller quadrangle, western Seward Peninsula, Alaska: U.S. Geological Survey Miscellaneous Investigations Series Map I-685, 4 p., scale 1:250,000.

Sainsbury, C.L., 1988, Vertical and horizontal zoning from tin to beryllium deposits, Lost River district, Alaska, *in* Kisvarsanyi, G., and Grant, S.K., eds., North American Conference on Tectonic Control of Ore Deposits and the Vertical and Horizontal Extent of Ore Systems, Proceedings Volume: University of Missouri-Rolla, p. 80–91.

Sainsbury, C.L., Hamilton, J.C., and Huffman, C., Jr., 1968, Geochemical cycle of selected trace elements in the tin-tungsten-beryllium district, western Seward Peninsula, Alaska—A reconnaissance study: U.S. Geological Survey Bulletin 1242-F, 41 p.

Swanson S.E., Newberry, R.J., Coulter, G.A., and Dyehouse, T.M., 1990, Mineralogical variation as a guide to the petrogenesis of the tin granites and related skarns, Seward Peninsula, Alaska: Geological Society of America Special Paper 246, p. 143–159.

Taylor, D., Schliebe, S., and Metsker, H., 1989, Contaminants in blubber, liver, and kidney tissues of Pacific walruses: Marine Pollution Bulletin, v. 20, no. 9, p. 465–468.

Till, A.B., and Dumoulin, J.A., 1994, Geology of the Seward Peninsula and Saint Lawrence Island, *in* Plafker, G., and Berg, H.C., eds., The Geology of Alaska: Boulder, Colo., Geological Society of America, The Geology of North America, v. G-1, p. 141–152.

Warburton, J., and Seagars, D., 1993, Metal concentrations in liver and kidney tissues of Pacific walrus: Continuation of a baseline study: U.S. Fish and Wildlife Service Technical Report R7/MMM 93-1, 23 p.

West, W.S., and White, M.G., 1952, The occurrence of zuenerite at Brooks Mountain, Seward Peninsula, Alaska: U.S. Geological Survey Circular 214, 7 p.

Reviewers: Helen W. Folger, James G. Crock.

Geologic Studies in Alaska by the
U.S. Geological Survey, 1997
U.S. Geological Survey Professional Paper 1614

Major-Element, Trace-Element, and Strontium-Isotope Systematics of Natural Waters in the Fairbanks Mining District: Constraints from Local Geology

By Richard J. Goldfarb, G. Lang Farmer, Barrett A. Cieutat, *and* Allen L. Meier

Abstract

The chemical characteristics of natural waters were studied over a large area north of Fairbanks, Alaska, within the Yukon-Tanana terrane. Waters dominated by calcium, bicarbonate, and sulfate from seeps and streams within areas underlain by rocks of the Fairbanks Schist typically had pH levels of 7.2–8.2, conductivities of 100–200 μS/cm, and concentrations of 13–20 ppm Ca, 4–7 ppm Mg, 0.7–1.2 ppm K, and 8–36 ppm sulfate. In contrast, waters that interacted with mid-Cretaceous granitoids intruding the schist were characterized by more acidic pH's of 6.8–7.1, much lower conductivities, and <9 ppm Ca, 0.6–0.7 ppm Mg, 0.3–0.4 ppm K, and ≤2 ppm sulfate. These waters were also enriched in dissolved Si, F^-, and U relative to those in contact with schist. Dissolution of relatively soluble Ca-Mg silicates in eclogite, the dominant lithology of the Chatanika assemblage, were responsible for highly alkaline surface waters that contain as much as 61 ppm Ca, 22 ppm Mg, 2.6 ppm K, and 140 ppm sulfate. Strontium isotopic ratios varied from 0.7146 to 0.7182 for waters in contact with granites to 0.7282–0.7364 for those in contact with schist; those draining eclogite were intermediate to these two ranges. Ground and surface waters that had contacted eolian overburden have less predictable hydrogeochemical signatures.

Introduction

Fairbanks is Alaska's second largest city, with a 1997 population of about 80,000. Many inhabitants rely on ground water from private domestic wells for their drinking supply. Therefore, background hydrogeochemical data for surface and ground water in the Fairbanks region are critical for land-use planning, regulatory considerations, and prioritization. In the mid-1970's, extremely high concentrations of dissolved arsenic were found to be present locally near Fairbanks, both in ground water near Ester dome and in a belt extending northeast along the Goldstream Creek valley (fig. 1*A*). Dissolution of widespread arsenopyrite, and its oxidation product scorodite, within many aquifers was shown to contribute to natural background concentrations of dissolved arsenic in ground water at as much as 10 ppm (Hawkins and others, 1982), 200 times greater than the 50 ppb maximum contaminant level recommended by the State of Alaska (Alaska Department of Environmental Conservation, 1996). This has caused many homeowners in affected areas to use distillation, reverse osmosis, or activated alumina to remove much of the arsenic

Despite the abundance of information on dissolved arsenic content, published data for other low-level trace metals in ground water across the area are relatively uncommon. Some multielement hydrogeochemical data have been recently collected from areas proximal to specific ore deposits, due to renewed interest in lode gold mining in the Fairbanks area. For example, Fairbanks Gold Mining, Inc., has collected a wealth of such data from wells and streams surrounding the Fort Knox gold mine (i.e., Fairbanks Gold Mining, Inc., Water Quality Data, 1992–1994, unpub. company report). In addition, government agencies have begun to collect background data for waters surrounding active placer (Ray and others, 1992) and abandoned lode (Goldfarb and others, 1997) gold mines. However, as additional commercial and residential development takes place in the Fairbanks area, detailed hydrogeochemical data will be needed for areas other than those directly adjacent to present or past mining activities.

The aim of this investigation is to obtain major- and trace-element hydrogeochemical and Sr isotopic data that will serve as a baseline for Fairbanks ground and surface waters. In addition, these data will provide constraints on the source lithologies of specific ground-water chemical characteristics (e.g., high arsenic content). Such information will be important for future assessments of water supply and quality in the Fairbanks area, as well as for human health studies. Furthermore, bedrock exposures in central Alaska are limited, due to low relief and thick loess cover, and, as a result, the subsurface geology of the region is difficult to constrain. However, because the chemical and isotopic compositions of the ground waters are mainly a function of the underlying geology and the amount of water-rock interaction, hydrogeochemical signatures in the region could help identify unexposed rock units, including felsic igneous rocks that are spatially associated with many of the Fairbanks gold deposits.

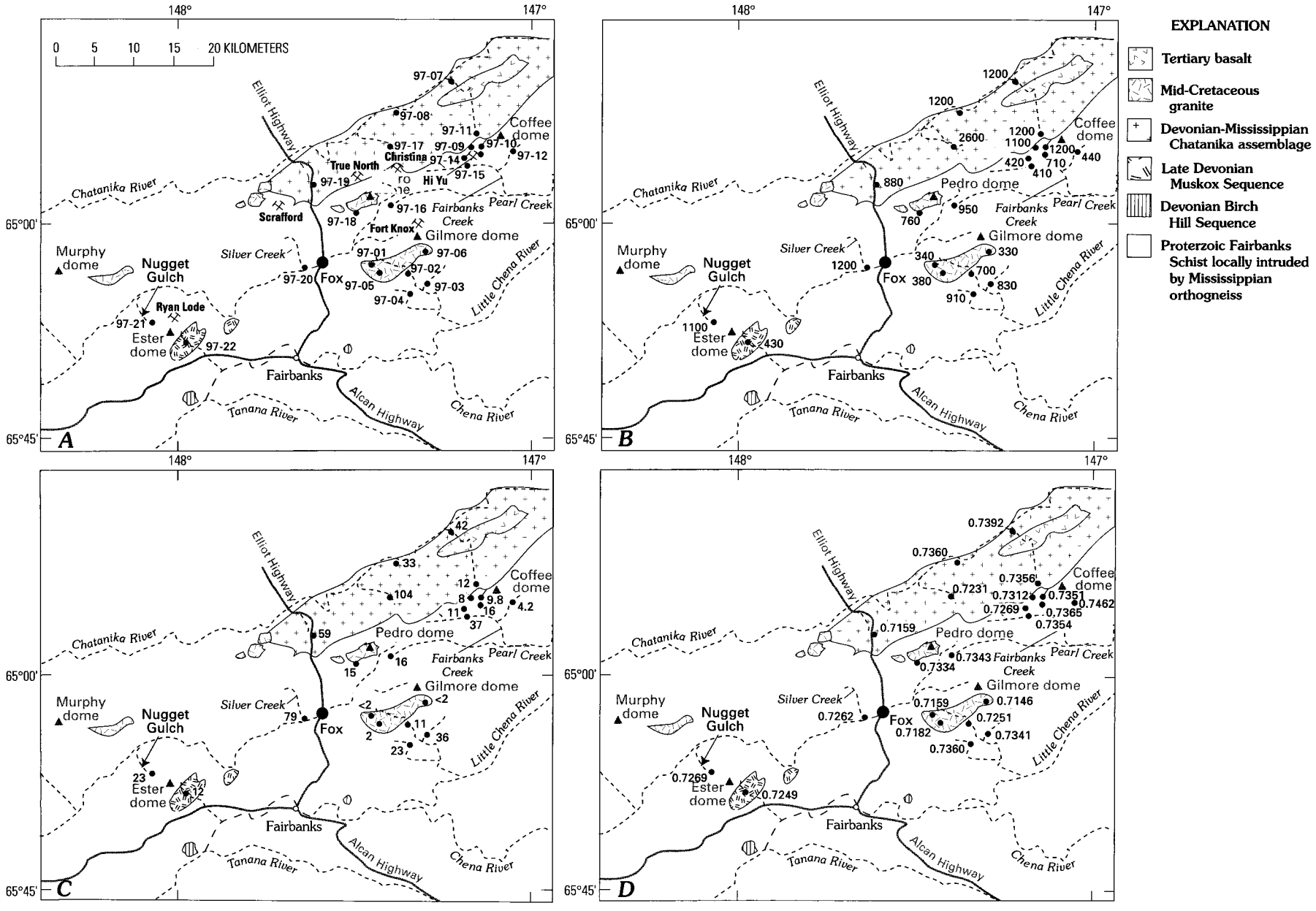

Figure 1. *A*, Site locations for water samples from the Fairbanks area within the Yukon-Tanana terrane. Local bedrock geology of this part of the terrane is generalized from Newberry and Bundtzen (1996). *B*, Concentrations of potassium in ppb for filtered water. *C*, Concentrations of sulfate in ppm for filtered water samples. *D*, Ratios of $^{87}Sr/^{86}Sr$ for filtered water samples.

Regional Geology

The Fairbanks area (fig. 1*A*) is underlain by metamorphosed rocks of the Yukon-Tanana terrane, which have been described in detail most recently by Robinson and others (1990) and Newberry and Bundtzen (1996). The area's structurally highest rocks, belonging to the more northerly Chatanika assemblage, include Devonian to Mississippian quartzite, schist, marble, and amphibolite. A calc-silicate mineral assemblage is common throughout these oceanic rocks, which have been regionally metamorphosed to eclogite facies. The underthrust parautochthonous metasedimentary rocks of the Proterozoic Fairbanks Schist are mainly composed of quartzite and quartz-muscovite schist, with lesser amphibolite and rare marble. They have been locally intruded by Mississippian granodioritic orthogneiss. The entire Fairbanks Schist package was metamorphosed to amphibolite facies at the end of the Paleozoic, followed by greenschist-grade retrograde metamorphism in the Early Cretaceous (Newberry and Bundtzen, 1996). A few local lithologic sequences have been distinguished in fault contact with the Fairbanks Schist near the Fairbanks city limits. Greenschist-facies phyllites of the Ordovician(?) to Devonian Birch Hill Sequence crop out along the northern and western borders of the city limits. Amphibolite-facies metavolcanic rocks and schists of the Upper Devonian Muskox Sequence are mainly recognized about 10 km west of the city.

Mid-Cretaceous intrusive bodies and early Tertiary olivine basalts are scattered throughout the Chatanika assemblage and the Fairbanks Schist (Robinson and others, 1990; Newberry and Bundtzen, 1996). The intrusive rocks are granitic, granodioritic, or tonalitic in composition; range in age from 94–88 Ma; and comprise the topographic domes that are responsible for much of the local relief (e.g., Pedro, Ester, and Gilmore domes). Many of the epigenetic gold-bearing quartz veins and stockworks of the Fairbanks mining district are spatially associated with these igneous bodies. The olivine basalts are tholeiitic in composition, range in age from about 56–50 Ma, and represent subaerial and lacustrine extrusions (Newberry and Bundtzen, 1996).

More than 8 million ounces of gold have been recovered historically from the placer fields of the Fairbanks region. More recently, low-grade bulk-tonnage deposits, the probable source for much of the alluvial gold, have become important new mining targets in the district. Mining has commenced at the Fort Knox deposit (>7 million oz gold), and additional large targets exist at the True North and Ryan Lode properties. Deposits are hosted by porphyritic granitic bodies (i.e., Fort Knox), the Fairbanks Schist (i.e, Hi-Yu, Christina, and Scrafford), and the Chatanika assemblage (i.e., True North). In addition to gold, most deposits contain an average of one percent arsenopyrite, variable pyrite, common stibnite, and local minor scheelite, molybdenite, pyrrhotite, loellingite, sulfosalts, and base-metal sulfides (McCoy and others, 1997). Consequently, hydrothermally altered rocks are irregularly enriched in Fe, As, and (or) Sb, with grab samples of sedimentary rocks commonly containing many tens to hundreds of parts-per-million arsenic and antimony and finely disseminated sulfides (Metz, 1991). The widespread sulfidation of all lithologic units within the Fairbanks area is of concern with regard to ground-water quality, given that oxidation of the sulfide minerals can result in production of acidic waters with high contents of arsenic and other metals.

Methods

Description of Studied Sites

We visited 22 sites within the Fairbanks area between July 1–4, 1997. Weather during this period was exceptionally warm and dry, except for a few brief thunderstorms. Sites were selected such that samples would be representative of waters in contact with various lithologic units within the Fairbanks region (fig. 1*A*). Our sampling was restricted to ground-water seeps and stream headwater regions north and east of Fox and, to a lesser extent, near Ester dome. We did not sample the lower elevations along the Goldstream Creek valley because private wells in this location had been already sampled by previous workers such as Hawkins and others (1982) and Weber (1986). Also, we wanted to develop a better understanding of the more regional hydrogeochemical patterns over a broader region north of Fairbanks. Resulting data could then be compared with the arsenic-rich ground waters already recognized along the Goldstream Creek valley.

Because the Fairbanks Schist composes much of the bedrock geology in the area, about half of the selected sites were from areas partly or totally underlain by this unit. Discharge derived from the metasedimentary schist and metavolcanic amphibolite of the Fairbanks Schist (Newberry and Bundtzen, 1996) was not distinguished because these two lithologies are complexly interbedded throughout the study area. Five samples were collected from streams within the Chatanika assemblage (sites 97-07, -08, -11, -17, -19); one of these also partly drains Tertiary basalt (site 97-07). Samples from sites 97-01, -05, and -06 represent flow discharging from areas exclusively underlain by mid-Cretaceous granites, whereas five other sites in the Fairbanks Schist (sites 97-02, -03, -04, -18, -21) contain some granite outcrops upstream from the sample locations. Site 97-16 was selected because waters there exclusively drain Mississippian orthogneiss intruding the Fairbanks Schist. Sample 97-22 is representative of waters interacting solely with rocks of the Muskox Sequence.

Whenever possible, we attempted to place sites as high in elevation as possible within a given catchment. Therefore, many of the samples are essentially springs, located by tracing flowing streams up to their headwaters where the initial discharge was seeping from the ground. In other cases, we collected samples farther downstream either because of difficulty of access (sites 97-08, 97-18 to 97-22), or to examine the impact on the water compositions of changes in rock composition within a given basin (sites 97-02 to 97-04, -07, -13, -15). In all of these cases, sample sites were located on the upstream side of access roads.

Field Methods

Water temperature, pH, and conductivity were measured at each of the sampled sites (table 1) using standard meters and

probes, and calibrating instruments at each site. Three filtered water samples were collected in polyethylene bottles at each location using a 0.45-μm filter and a portable battery-operated pump. An acid-rinsed 60-mL bottle was filled with filtered water for dissolved-cation analyses, and the sample was acidified in the field to a pH <2 with ultrapure concentrated nitric acid. An unacidified, filtered 125-mL sample was collected for determination of anions. A 1-L acid-rinsed bottle was filled with sample for isotopic analysis, and it too was acidified with ultrapure concentrated nitric acid. All samples were kept cool with ice until they were returned to Denver, where they were then refrigerated prior to analysis.

Analytical Methods

Concentrations for more than 60 trace, minor, and major elements were determined by inductively coupled plasma–mass spectrometry (ICP-MS) using the methodology of Meier and others (1994). This analytical method is characterized by analytical determination limits down to the parts-per-trillion level for most elements. Laboratory quality control was confirmed by analysis of one duplicate sample for every ten samples, as well as a number of U.S. Geological Survey Water Resources Division quality-control water standards. Anions were determined by ion chromatography as described in d'Angelo and Ficklin (1996). Alkalinity as $CaCO_3$ was measured in the laboratory by titration. These cation and anion data are shown in tables 2 and 3, respectively.

For the Sr isotopic analyses, five 50-mL aliquots of each water sample were dried in a Teflon beaker in a class-100 clean-room environment, and the residues were passed through conventional cation-exchange columns to separate Sr. Total procedural blanks for Sr were approximately 1 ng, with $^{87}Sr/^{86}Sr$=0.720. Because an average of 1,200 ng of Sr was processed for each sample, the blank contribution to each measured $^{87}Sr/^{86}Sr$ ratio was inconsequential (<0.00002). The Sr isotopic compositions were obtained using a 6-collector Finnigan MAT 261 thermal ionization mass spectrometer at the University of Colorado, Boulder. Repeated measurements of the NBS-987 Sr standard during the study period produced a mean ratio of 0.710312±2 (2σ; n=8), which is ~0.00003 higher than accepted values for this standard. As a result, the Sr isotopic data reported in table 4 have been corrected downward by this increment.

Interpretation of Water Data

Hydrogeochemistry in Areas of Cretaceous Granite

Waters in contact with mid-Cretaceous granitic rocks at Gilmore dome have a characteristic and consistent hydrogeochemical signature. Seeps in granite at the head of Nugget (site 97-01), Rex (site 97-05), and Pearl (site 97-06) Creeks were observed in the field to have relatively low conductivities (40–65 μS/cm) compared to waters draining metasedimentary units (table 1). The pH values for these seeps were essentially neutral, ranging between 6.8 and 7.1, with relatively low alkalinities between 27 and 32 mg/L (table 3). Rainwater is slightly acidic in the Fairbanks area as noted from the pH measurement of 6.27 at site 95-20 from Goldfarb and others (1997), and, therefore, we interpret slightly more alkaline measurements for the seeps on Gilmore dome to reflect waters that have interacted with mid-Cretaceous granitic bedrock.

As suggested by the low conductivity measurements, many of the major cations have relatively low concentrations. Calcium concentrations of less than 9 ppm, Mg of about 0.6–0.7 ppm, and K between 330 to 380 ppb are relatively low compared to most samples in the Fairbanks area (table 2; fig. 1*B*). These waters also have distinctively low sulfate levels (2 ppm or less; fig. 1*C*) but have the highest levels of dissolved silica observed in the study area, with concentrations as high as 17 ppm Si in the headwaters of Nugget Creek (site 97-01; table 2) . In addition, two of the three "granite" seeps (sites 97-01 and -06) have relatively high fluoride concentrations of 0.6–0.9 ppm, compared to typical background levels over much of the study area of 0.1–0.2 ppm. Uranium concentrations of 3.9 and 4.7 ppb at these two sites are 1 to 2 orders of magnitude greater than background levels of most waters collected away from granite, which have uranium concentrations in the parts-per-trillion range.

With increasing distance south of the crest of Gilmore dome (sites 97-02, -03, -04), Ca, Mg, and K concentrations in surface waters increase dramatically, presumably reflecting the fact that these waters have interacted considerably with metasedimentary units of the Fairbanks Schist, the predominant bedrock in the lower elevations of these catchments. As a result, these major-element data provide little indication that the headwaters of each watershed are underlain by granitic rocks. However, surface waters at site 97-02, several kilometers down Nugget Creek from site 97-01, do have high U (7.8 ppb) and F^- contents (0.4 ppm), suggesting that these elements may provide a fingerprint of the upstream granitic rocks, which can be recognized even after the addition of significant dissolved material from the Fairbanks Schist.

Ground water that has interacted with the granitic rocks does not, however, invariably have elevated U and F^- concentrations. Water sampled at the crest of Gilmore dome at site 97-05 (Rex Creek) lacks U and F^- enrichments, despite its low Mg and Ca contents (and low $^{87}Sr/^{86}Sr$; see below) that we consider characteristic of ground waters that have interacted with granitic rocks. Most likely, given the similar neutral pH and low conductivity values for the waters from sites 97-01, -05 and -06, the lower concentrations of the U and F^- at site 95-05 may reflect local changes in granite chemical characteristics. Alternatively, the seep at Rex Creek may simply reflect waters that have more limited flow distances through the bedrock at this location and, therefore, have interacted less with the granitic rocks. It is also interesting to note that the Rex Creek seep contains 48 ppb As, a value much higher than any other seep in the study area (table 2). This may be an indication that igneous rocks at depth are more highly sulfidized at Rex Creek (site 97-05) than in other portions of Gilmore dome, and, therefore, this region represents a potential target for precious-metal mineralization. We also note that surface waters within Nugget Gulch, on the northwest side of Ester dome (site 97-21), contain only 7 ppm Ca and 3 ppm Mg. This suggests that much of the flow may be derived from areas underlain by the poorly exposed, upstream mid-Cretaceous granite.

Table 1. Field measurements and site descriptions for hydrogeochemical sampling sites in the Fairbanks area.

[Leaders (--) signify no measurement at a given site]

Site no.	pH	Temp. (°C)	Conductivity (µS/cm)	Site description	Geology
97-01	7.1	5	40	Spring at head of Nugget Creek	Mid-Cretaceous granite
97-02	7.3	8	133	Nugget Ck, 0.5 km above junction with Smallwood Ck	Fairbanks Schist; granitic headwaters
97-03	7.5	5	200	Gay Gulch, 0.5 km above junction with Smallwood Ck	Fairbanks Schist; granitic headwaters
97-04	7.3	7	161	Rex Ck, 0.8 km above junction with Smallwood Ck	Fairbanks Schist; granitic headwaters
97-05	6.9	10	65	Spring at head of Rex Creek	Mid-Cretaceous granite
97-06	6.8	3	55	Spring at head of Pearl Creek	Mid-Cretaceous granite
97-07	6.9	12	201	Alder Ck on upstream side of Steese Highway	Chatanika assemblage and Tertiary basalt
97-08	7.6	10	181	Pilot Ck on upstream side of Steese Highway	Chatanika eclogite
97-09	8.2	6	150	Spring at head of Alder Creek	Fairbanks Schist
97-10	7.7	5	165	Spring at head of Ginger Creek	Fairbanks Schist
97-11	7.4	7	183	Spring at head of Kokomo Creek	Chatanika assemblage
97-12	6.8	10	52	Spring at head of Deep Creek	Fairbanks Schist
97-13	7.2	3.5	165	Ginger Creek at 1,300-ft elevation	Fairbanks Schist; marble in headwaters
97-14	7.7	3	115	Moose Creek above Hi-Yu mill tailings; same as 96-15	Fairbanks Schist
97-15	7.3	9	179	Moose Ck at base of Hi-Yu mill tailings; same as 96-16	Fairbanks Schist
97-16	7.2	2	132	Tributary on south side of Pedro Creek	Orthogneiss
97-17	--	3	555	Dora Ck on upstream side of Steese Highway	Chatanika assemblage
97-18	7.2	7	143	Flume Creek at 1,200-ft elevation	Fairbanks Schist; minor granite in headwaters
97-19	7.4	15	392	Creek at about Mile 7.5 along Dome Ck Road	Chatanika assemblage
97-20	7.7	9	395	Silver Creek on upstream side of Goldstream Rd	Fairbanks Schist
97-21	7.0	3	108	Nugget Creek at 1,000-ft elevation	Fairbanks Schist
97-22	7.0	4	69	Eastern tributary to Ready Bullion Ck at 1,050-ft elevation	Muskox Sequence

Table 2. Concentrations of dissolved cations in filtered, acidified waters collected in the Fairbanks region.

[All data in ppb except for Ca, Mg, and Na, which are in ppm]

Sample site	Ca	Mg	Na	K	Si	Fe	Al	Mn	Co	Ni	Cu	Pb	Zn	Cd	As	Sb	U
97-01	5.6	0.61	2.5	340	17	150	13	11	0.1	0.4	0.5	<0.05	2	<0.02	2	0.1	3.9
97-02	16	2.9	3.2	700	13	150	17	73	0.2	0.8	0.6	<0.05	1	<0.02	2	0.1	7.8
97-03	17	6.8	2.4	830	10	300	8.6	120	0.4	0.7	0.6	<0.05	1	<0.02	4	0.2	0.21
97-04	11	5.5	2.6	910	12	200	8.0	62	0.2	0.8	0.5	<0.05	0.9	<0.02	3	0.1	0.08
97-05	7.3	0.72	1.7	380	14	88	9.9	17	0.08	0.3	<0.5	<0.05	1	<0.02	48	0.4	0.57
97-06	8.9	0.67	1.8	330	13	15	8.6	0.41	<0.02	0.1	<0.5	<0.05	1	<0.02	0.6	0.02	4.7
97-07	17	6.6	3.1	1200	10	1400	15	230	1.1	1.6	0.8	<0.05	2	<0.02	1	0.2	0.13
97-08	17	6.5	1.8	1200	10	300	8.6	38	0.1	1.0	0.7	<0.05	1	<0.02	1	0.2	0.33
97-09	16	3.9	0.58	1100	6	25	1.9	0.06	<0.02	0.2	<0.5	<0.05	0.5	<0.02	5	0.1	0.15
97-10	18	4.8	0.63	1200	5	27	1.2	0.06	<0.02	0.2	<0.5	<0.05	0.7	<0.02	9	0.3	0.36
97-11	20	4.3	0.59	1200	5	29	6.4	0.13	0.02	0.3	<0.5	<0.05	0.5	<0.02	1	0.4	0.27
97-12	3.8	1.4	0.61	440	8	11	9.5	0.09	<0.02	0.6	<0.5	<0.05	0.9	<0.02	1	0.05	0.01
97-13	17	5.8	0.83	710	6	27	5.7	0.22	0.02	0.3	<0.5	<0.05	<0.5	0.02	4	0.50	0.47
97-14	13	2.7	0.85	410	8	19	4.9	0.13	<0.02	0.4	<0.5	<0.05	2	0.78	12	0.86	0.04
97-15	14	4.6	1.1	420	10	170	11	220	0.4	9.6	1.0	0.3	140	<0.02	78	8.0	0.04
97-16	14	2.9	1.8	950	10	22	7.0	0.08	<0.02	0.3	<0.5	<0.05	0.5	<0.02	0.4	0.06	0.41
97-17	61	22	1.9	2600	11	90	6.5	1.0	0.04	2.8	0.9	<0.05	1	<0.02	0.5	0.07	7.3
97-18	14	3.0	2.8	760	12	68	10	13	0.2	1.1	<0.5	<0.05	0.5	<0.02	2	0.1	0.29
97-19	32	13	2.9	880	9	730	20	130	0.3	2.0	1.0	<0.05	0.7	<0.02	1	0.06	0.18
97-20	38	14	5.5	1200	9	300	6.4	30	0.1	1.3	1.0	<0.05	0.9	<0.02	1	0.2	2.4
97-21	7.0	4.1	1.9	1100	13	16	5.5	1.9	0.03	1.2	<0.5	<0.05	1	<0.02	2	0.1	0.01
97-22	4.3	2.3	1.8	430	13	26	18	0.46	0.02	0.8	0.5	<0.05	0.9	<0.02	5	0.73	0.01

Table 3. Concentrations of dissolved anions in filtered water from the Fairbanks region.

[All samples were also analyzed for Br^- and HPO_4^{2-}, with all values below lower determination limits of 0.2 ppm and 1 ppm, respectively. All data in ppm; alkalinities in mg/L $CaCO_3$]

Sample site	F^-	NO_3^-	Cl^-	SO_4^{2-}	Measured alkalinity
97-01	0.6	<0.4	0.2	<2.0	27
97-02	0.4	<0.4	0.5	11	61
97-03	0.2	0.7	0.3	36	55
97-04	0.2	1.0	0.3	23	45
97-05	0.2	<0.4	0.2	2.0	30
97-06	0.9	3.4	0.2	<2.0	32
97-07	0.1	<0.4	0.3	42	47
97-08	0.2	0.6	0.3	33	52
97-09	0.1	1.3	0.3	8.0	67
97-10	0.7	0.8	0.3	9.8	74
97-11	0.1	0.8	0.3	12	74
97-12	0.1	1.7	0.2	4.2	17
97-13	0.1	1.0	0.3	16	67
97-14	0.1	2.7	0.3	11	44
97-15	0.1	1.6	0.2	37	33
97-16	0.1	1.3	0.3	16	46
97-17	0.4	0.9	0.4	140	166
97-18	0.1	0.8	0.3	15	51
97-19	0.2	0.4	0.2	59	100
97-20	0.2	0.9	0.4	79	122
97-21	0.2	3.3	0.4	23	21
97-22	0.1	1.3	0.3	12	15

Waters that have interacted with the granites at Gilmore dome also have a unique strontium isotope signature (table 4). Measured $^{87}Sr/^{86}Sr$ values from the three seeps in the granites (sites 97-01, -05, and -06) range between 0.7146 and 0.7182. These values are much less radiogenic than waters draining metasedimentary rock lithologies (figs. 1*D*, 2). Water collected at site 97-02, noted above to contain high concentrations of U and F^- that may have been inherited from upstream granitic rocks, has a high strontium concentration (174 ppm) and a $^{87}Sr/^{86}Sr$ ratio of 0.7251. The strontium isotopic composition is intermediate between that of waters that interacted exclusively with granites and those that have interacted exclusively with schist (fig. 1*D*), which suggests that the higher strontium concentration in water from Nugget Creek was derived from the schist. Farther downstream in this drainage, at sites 97-03 and -04, isotopic ratios are more radiogenic and waters no longer retain an isotopic signature characteristic of the upstream igneous units (fig. 1*D*).

Hydrogeochemistry in Areas of Fairbanks Schist

Water samples collected from springs and streams within the Fairbanks Schist typically have pH values of 7.2–8.2 and conductivities of 100–200 µS/cm. Concentrations of dissolved major ions are high compared to those of seeps in granites, with typical concentrations from areas within the schist of 13–20 ppm Ca, 4–7 ppm Mg, 700–1,200 ppb K (fig. 1*B*), and 8–36 ppm sulfate (fig. 1*C*). Trace-element concentrations vary little from those that characterize waters in contact with granites,

Table 4. Sr elemental and isotopic data for surface waters from the Fairbanks area.

Site	Sr (ppb)	$^{87}Sr/^{86}Sr$
97-01	64	0.7159
97-02	174	0.7251
97-03	158	0.7341
97-04	102	0.7360
97-05	63	0.7182
97-06	53	0.7146
97-07	126	0.7392
97-08	108	0.7360
97-09	37	0.7312
97-10	45	0.7351
97-11	54	0.7356
97-12	28	0.7461
97-13	71	0.7364
97-14	29	0.7287
97-15	70	0.7354
97-16	99	0.7343
97-17	258	0.7231
97-18	117	0.7334
97-19	171	0.7159
97-20	277	0.7282
97-21	39	0.7296
97-22	27	0.7249

except for the consistent relatively lower U and F^- contents. Strontium-isotope compositions are typically much more radiogenic than those of waters that have interacted with granitic rocks. The $^{87}Sr/^{86}Sr$ values range between 0.7282 and 0.7364, with the one spring on the south side of Coffee dome having the highest value measured from any surface water or seep in the study area (0.7461; fig. 1*D*).

In spite of some similar characteristics, there is significant variability in waters draining the Fairbanks Schist. For instance, a comparison of data from the Smallwood Creek watershed (sites 97-03 and -04) with those from the north side of Fairbanks Creek (sites 97-09, -10, -12, -13, -14) indicates that, although similar in Ca, Mg, and K concentrations, the waters in the Fairbanks Creek area are significantly lower in dissolved Fe, Al, Mn, Si, and sulfate. One possibility could be more limited interaction between ground water and the Fairbanks Schist in the Fairbanks Creek area. However, because conductivities and many of the major elements show similar concentrations in waters from both areas, we favor local mineralogical differences in the schist as the most likely cause of the hydrogeochemical variability.

It is noteworthy that there is little difference in the hydrogeochemistry between water from site 97-10, at the head of Ginger Creek, and site 97-13, located 1.5 km downstream (fig. 3). A large lens of limestone within the Fairbanks Schist on the western side of the basin (Newberry and Bundtzen, 1996) has no obvious affect on the dissolved load or $^{87}Sr/^{86}Sr$ value; in fact, the measured pH of the stream decreased by one-half a pH unit below the limestone. Most likely, ground waters within the Ginger Creek watershed have not interacted to any significant degree with the limestone.

There are anomalous concentrations of metals in waters from some sites underlain by the schist. As expected and observed in a previous study (Goldfarb and others, 1997), Moose

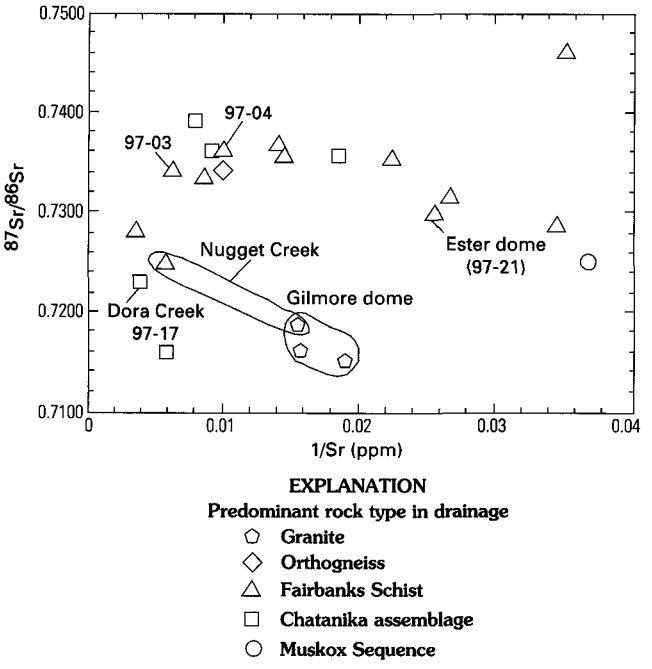

Figure 2. Plot of $^{87}Sr/^{86}Sr$ vs. 1/Sr for surface waters in the Fairbanks area. Note the isotopically low values for waters draining granite and the possible mixing relationship downstream of granites along Nugget Creek. Even though the strontium isotope data vary with lithology, absolute strontium concentrations do not show a similar relationship.

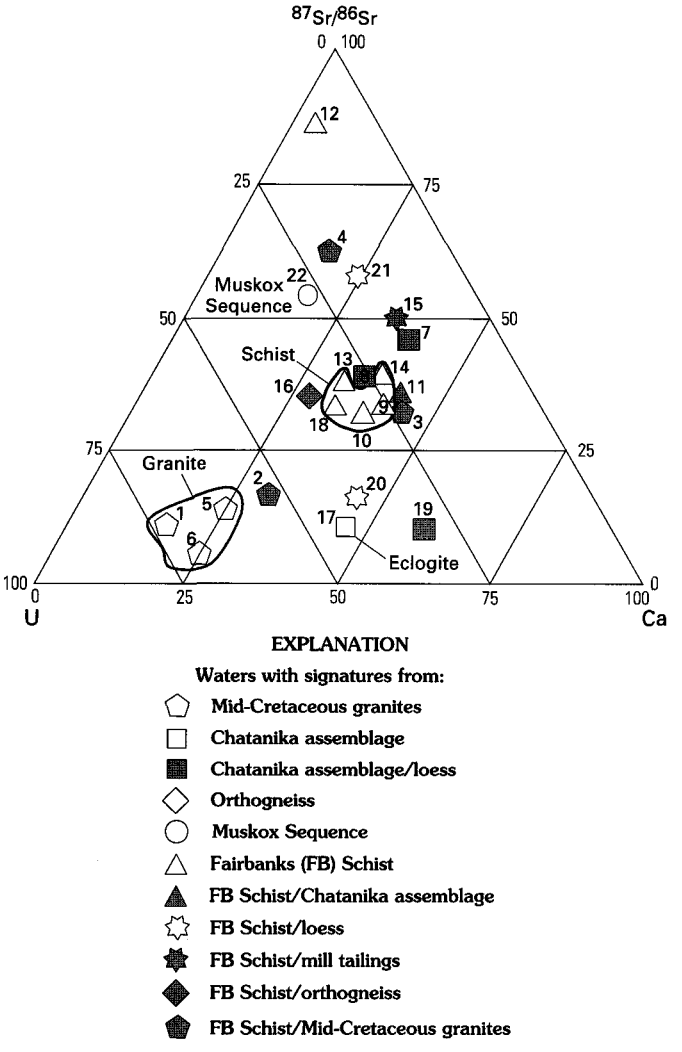

Figure 3. Triangular plot showing fields that best characterize waters that have interacted with granite (sites 1, 5, and 6), schist (sites 9, 10, 13, 14, and 18), and eclogite (site 17), based on uranium and calcium concentrations (in percent) and strontium isotopic values. Mixed signatures reflect waters that have also interacted with loess, mining waste, or multiple lithologies, and specific sites are described throughout the text.

Creek below the Hi-Yu mill tailings is enriched in many dissolved components including As, Cd, Co, Fe, Mn, Ni, Pb, Sb, and Zn. The sampled water was significantly less acidic in 1997 (site 97-15, pH 7.3) than in 1995 (site 95-16, pH 5.18; Goldfarb and others, 1997), and the absolute concentrations of the dissolved metal species are also significantly lower. A few hundred meters upstream from the tailings (site 97-14), where seep discharge into Moose Creek represents the initial surface-water flow in the creekbed during this time of year, concentrations of dissolved K were only 410 ppb. This is the lowest value measured for waters interacting with the schist. Once again, this is thought to reflect local mineralogical variations within the schist.

Two samples hint at the presence of nearby, unexposed granite. The spring at the head of Ginger Creek (site 97-10) contained 0.7 ppm F^-, a level consistent with measurements for waters from samples draining granitic rocks (sites 97-01 and -06). In addition, the spring on the south side of Coffee dome (site 97-12) had low concentrations of Ca, Mg, K (fig. 1*B*), and sulfate (fig. 1*C*) relative to all other samples collected from the Fairbanks Schist. But the relatively high $^{87}Sr/^{86}Sr$ ratio (0.7461) for this latter water (fig. 1*D*) is atypical of those that have interacted exclusively with mid-Cretaceous granites (fig. 3).

Water at site 97-20, from Silver Creek immediately above its junction with Goldstream Creek, is characterized by a relatively low pH and high levels of Mg, Ca, Na, Cu, U, Sr, and sulfate. It also has a $^{87}Sr/^{86}Sr$ ratio of 0.7282, a value marking the low end of the range for waters collected from areas underlain by the Fairbanks Schist. The sampled site is notable in that it is downstream from an extensive accumulation of eolian silt that overlies bedrock throughout most of the Silver Creek watershed. Contributions from eolian deposits appear to significantly increase dissolved loads such that water chemistry will not simply reflect local bedrock lithology, and, thus, data for site 97-20 plot far from the field typical of waters that have interacted with the schist (fig. 3).

Site 97-16 was purposely located where a body of orthogneiss underlies the lower part of a small drainage basin on the south side of Pedro Creek within the Fairbanks Schist. Hydrogeochemical data measured for the sample are indistinguishable from those collected elsewhere within the schist (fig. 3). The $^{87}Sr/^{86}Sr$ ratio of 0.7343 is typical of waters from the schist (figs. 1*D*, 2). Because of the present limited data, we cannot determine what, if any, hydrogeochemical differences distinguish waters that have interacted with the orthogneiss from those that have interacted with the schist. Perhaps most of the discharge at site 97-16 actually reflects ground water that has been in contact with upstream schist and had only limited flow through the orthogneiss.

Hydrogeochemistry in Areas of Muskox Sequence

A large area throughout the southeast side of Ester dome is underlain by interbedded schist, amphibolite, and metarhyolite of the Muskox Sequence (Newberry and Bundtzen, 1996). In the center of the area, we collected a water sample (site 97-22) on a small tributary to Ready Bullion Creek. Similar to the samples in equilibrium with the granites, this water was characterized by relatively low levels of potassium (430 ppb) and calcium (4.3 ppm) and a low alkalinity of 15 mg/L. In addition, the sample had extremely low concentrations of strontium (27 ppb) and uranium (0.01 ppb). Higher magnesium (2.3 ppm) and sulfate (12 ppm) concentrations for the water were in sharp contrast to the extremely low levels for waters in equilibrium with granites. The $^{87}Sr/^{86}Sr$ value of 0.7249 is partly between that of waters that have interacted with the Fairbanks Schist and those that drain the granites (fig. 2). Although we only obtained one water sample from the area underlain by this rock sequence, initial interpretation of the resulting data suggests that waters that interacted with this sequence exhibit a unique geochemical signature (site 97-22; fig. 3).

Hydrogeochemistry in Areas of Chatanika Assemblage

The generally nonresistant nature of eclogite of the Chatanika assemblage results in the low-relief topography in the northern part of the study area (Newberry and Bundtzen, 1996). Because of the resulting topography, many of the stream valleys underlain by this lithology are filled with eolian loess. Waters from sites 97-07, -08, and -19, although all clearly collected from streams draining rocks of the Chatanika assemblage, have chemistries that are influenced by dissolution of material from the unconsolidated silt. The sampled spring at the headwaters of Kokomo Creek (site 97-11) was located within an area underlain by eclogite, but a minority of the recharge area is also underlain by Fairbanks Schist. The sample collected on Dora Creek at site 97-17 represents the one sample we feel reflects waters that interacted solely with eclogite.

The relatively soluble Ca-Mg silicate assemblage of eclogite has led to elevated dissolved loads in the waters of Dora Creek. At site 97-17, the conductivity was 555 µS/cm, and major ion concentrations included 61 ppm Ca, 22 ppm Mg, 2,600 ppm K, and 140 ppm sulfate. In addition, Ba, Cs, F^-, Li, Rb, Re, Ti, and U were detected at relatively elevated levels (table 2) (Goldfarb, unpub. data). A $^{87}Sr/^{86}Sr$ ratio of 0.7231 lies between that for waters that have interacted with the granites and the Fairbanks Schist (fig. 2). This was the most alkaline of the waters from the Fairbanks area, with a measured alkalinity of 166 mg/L.

The other four samples collected from streams draining rocks of the Chatanika assemblage are difficult to interpret. The spring at the headwaters of the Kokomo Creek drainage (site 97-11) has chemical attributes, including a strontium isotope signature, that are nearly identical to nearby springs that discharge from rocks of the Fairbanks Schist. Schist underlies only a small part of the upstream reaches of the watershed for site 97-11, but the hydrochemistry suggests a major influence by schist along the water flow path. Kokomo (site 97-07) and Pilot (site 97-08) Creeks also drain eclogite, but these waters flowed for a number of kilometers through loess, and the resulting hydrogeochemical signatures lack the characteristics of the Dora Creek water. A tributary to Dome Creek (site 97-19) drains a large area of loess, but concentrations of 13 ppm Mg, 730 ppb Fe, and 32 ppm Ca, as well as elevated Al, Ba, P, REE, and Ti, seem to be indicative of the underlying eclogite.

Site 97-07 on Kokomo Creek is only 1 km downstream from a large Tertiary basalt flow that seems to influence local water chemistry. Concentrations of 1,400 ppb Fe, 230 ppb Mn, and 1.1 ppb Co are apparently a function of water-basalt interaction, although an enriched $^{87}Sr/^{86}Sr$ ratio of 0.7392 (table 4) hints that interaction with the loess overwhelms the isotopic signature characterizing the relatively nonradiogenic basalt.

Discussion

Natural waters in the Fairbanks region may be fingerprinted by unique chemical signatures that, in large part, are a function of the underlying bedrock geology (fig. 3). Throughout the study area, calcium is consistently the dominant cation species (table 2, this paper; table 2, sites 11–24, Goldfarb and others, 1997; fig. 4, this paper), probably reflecting dissolution of calcite and plagioclase in metasedimentary rocks. Bicarbonate, defining most of the measured alkalinity, and sulfate are both significant anion species (table 3 and fig. 4, this paper; table 4, sites 11–24, Goldfarb and others, 1997). Bicarbonate concentrations in the Fairbanks area are equal to or two to three times greater than sulfate concentrations. Because much of the sulfidization of country rocks near gold deposits was accompanied by coeval and spatially overlapping carbonate alteration, sulfate does not notably predominate as the major anion species even where waters drain abandoned mine workings (site 97-15, this study; Goldfarb and others, 1997). Nevertheless, absolute sulfate concentrations are relatively high for most water samples from the Fairbanks area (fig. 1*C*), indicative of the extensive sulfidization of the rocks.

The greater solubility of plagioclase, relative to microcline or orthoclase, in addition to the well-defined cleavage in plagioclase, lead to its greater susceptibility to weathering (Ollier, 1969). As a result, potassium levels are relatively low compared to calcium for all water samples from the study area (fig. 4). Typically, dissolved calcium concentrations are an order of magnitude greater than those for sodium in waters draining metasedimentary rock units, suggesting the predominance of anorthite over albite and (or) significant dissolution of calcite from the schist.

Waters draining the granites are only about one-half of an order of magnitude enriched in calcium relative to sodium; absolute sodium concentrations are similar to those of waters from the metasedimentary rocks; and dissolved silica is notably elevated. We interpret this to indicate a relatively increased amount of dissolution of Na-rich feldspars. The amount of dissolved silica released into natural waters per hydrogen ion is much greater for Na-rich feldspars than for other major mineral phases in felsic to intermediate igneous rocks (Hem, 1992). The low conductivity and calcium concentrations for these waters indicates, however, that overall rock-dissolution rates are lower

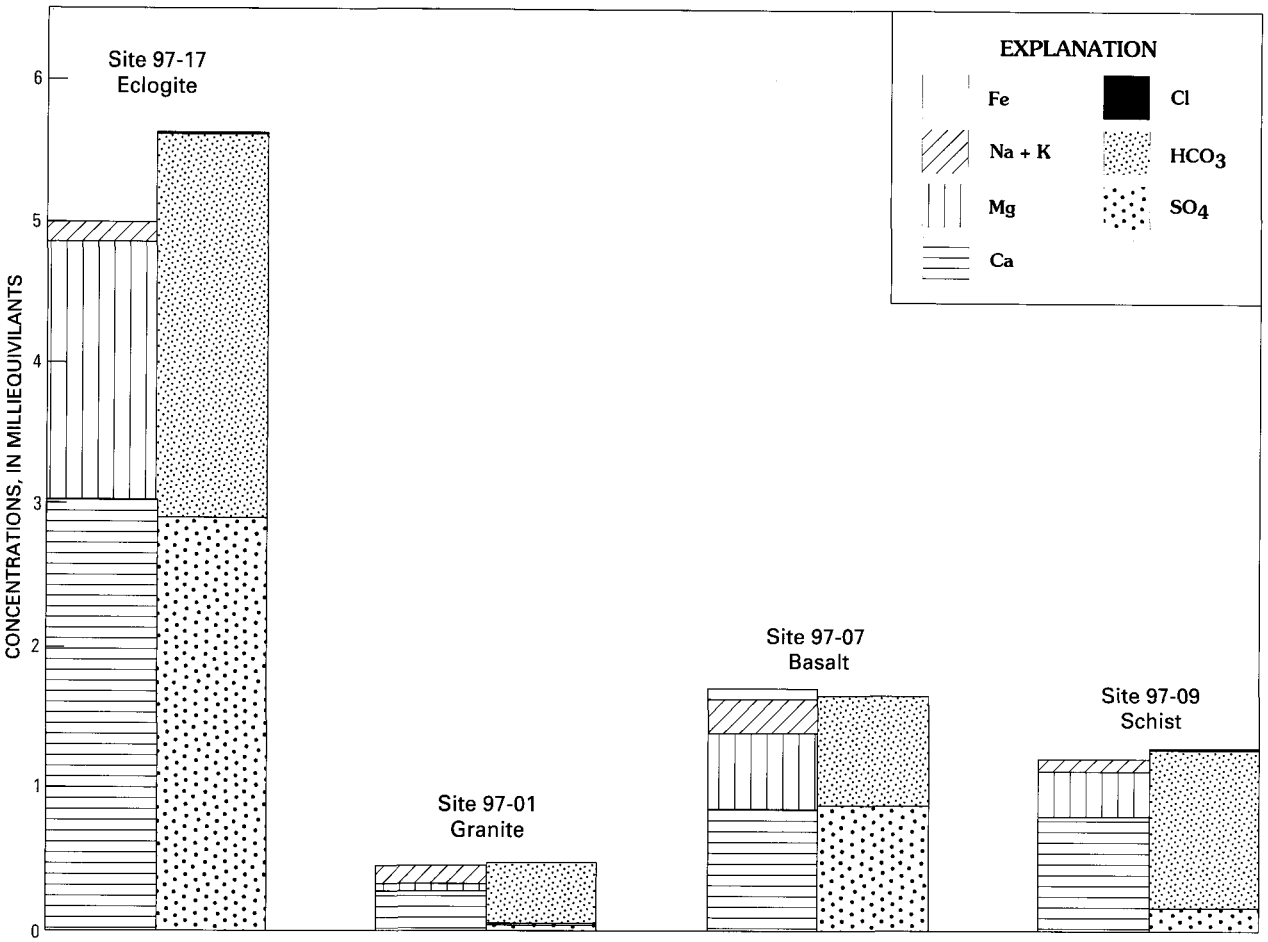

Figure 4. Sum of cations vs. anions for waters that have interacted with the various rock types in the Fairbanks area.

than in the schists. This is not surprising because the relatively low permeability and coarse-grained nature of the granitic rocks, compared to the schists, hinder rapid weathering of mineral grains.

Other chemical species that are enriched in waters that flowed through granites are unlikely to be derived from feldspar weathering. Weathering of biotite to vermiculite, for example, may have contributed fluorine to the ground waters. This possibility is consistent with the fact that biotite is the most abundant mafic mineral in the mid-Cretaceous granitic rocks of Pedro and Gilmore domes (Blum, 1985) and the fact that biotite has been demonstrated to have a significantly higher weathering rate (4× to 6×) than plagioclase (Blum and others, 1994). It is even possible that the somewhat higher $^{87}Sr/^{86}Sr$ ratio in our ground-water seeps (average= 0.7163), relative to the average equigranular and porphyritic facies of the Gilmore and Pedro domes granitic rocks (~0.7135; Blum, 1985), also reflects the preferential weathering of biotite. This is because biotite generally has high Rb/Sr ratios and, as a result, highly radiogenic strontium (Blum and others, 1994).

The greatest dissolved load in a water sample from this study, mainly reflected by elevated calcium, magnesium, sulfate, and bicarbonate concentrations, is for the sample from Dora Creek (site 97-17). The relatively abundant mafic silicate phases within the underlying Chatanika eclogite are easily broken down by circulating ground waters. Elevated trace-element concentrations in the waters at site 97-17, compared to those flowing through all other lithologies, clearly are the result of more extensive irreversible dissolution of bedrock. It is noteworthy that the major-element chemistry of the sample from Dora Creek is very similar to that of waters collected below mine-waste rock from the Scrafford mine (site 96-23, Goldfarb and others, 1997). The local geology around the Scrafford mine is mapped as Fairbanks Schist, but the hydrogeochemistry suggests an abundance of Ca- and Mg-rich mineral phases similar to those that characterizes the eclogite.

The one sample with a high dissolved-iron concentration is along Kokomo Creek (site 97-07), which was collected downstream from a large outcrop of basalt. This fine-grained mafic unit is relatively easily weathered and provides a unique fingerprint to waters that interact with it. Iron concentrations of 300–730 ppb for sites on Pilot Creek (site 97-08), a tributary to Dome Creek (site 97-19), and on Silver Creek (site 97-20) are also higher than those from any other waters in this study. Upstream parts of these watersheds all contain significant amounts of loess, suggesting that some of the iron may be derived from loess rather than bedrock. This implies that significant loess accumulations along Kokomo Creek may also be contributing some of the iron in sample 97-07.

Absolute trace-metal concentrations are extremely low (i.e., see table 2-1 in Levinson, 1974), even from Dora Creek (site 97-17), for waters collected from all units, and we interpret these concentrations to mainly reflect local background levels. As expected, an arsenic concentration of 78 ppb in Moose

Creek below the Hi-Yu mill tailings (site 97-15) likely represents an anthropogenic contribution. Above the mine workings, surface flows are above background levels, but only contain 12 ppb As (site 97-14). Values of 410–420 ppb K for waters at these two sites are much lower than those of any other samples draining the Fairbanks Schist. This could be indicative of the likely broad-scale alteration of rock units in the vicinity of the mesothermal gold-type mineralization. Sericitization of the schist would convert any K-bearing feldspars in rocks surrounding the auriferous quartz veins to muscovite, generally a more resistent mineral to chemical weathering (Ollier, 1969). Only the sample from near the head of Rex Creek (site 97-05), with 48 ppb As, contains a very high natural arsenic concentration and may define an unexposed zone of hydrothermal mineralization in granite on the southeast side of Gilmore dome.

The samples in this study were collected over a broad region, mostly a few tens of kilometers north of Fairbanks, and, typically, waters contained less than 10 ppb As. This is consistent with the findings of Weber (1986) who, in a detailed study of well waters, showed those waters with >10 ppb arsenic were confined to a 5-km-wide zone between Ester and Gilmore domes (location of site 97-05) and centered along Goldstream Creek. Despite the concentration of gold occurrences to the north of Fox, the lower arsenic concentrations in natural waters in this area indicates that widespread dissolution of sulfides in local aquifers is much less severe than for lithologies along Goldstream Creek.

Summary

The chemical composition of natural waters in the Fairbanks mining district is strongly influenced by the local geology. Dissolved species in all parts of the studied area are dominated by calcium, bicarbonate, and sulfate. However, calcium concentrations are consistently lower (<10 ppm) in waters draining granites and rocks of the Muskox Sequence, intermediate (13–20 ppm) throughout the Fairbanks Schist, and high (as much as 61 ppm) for waters that have interacted with the eclogite of the Chatanika assemblage. Sulfate varies from low (<2 ppm) in waters draining granite, to intermediate (8–36 ppm) in waters from the metasedimentary rocks, to high (140 ppm) for waters in contact with the eclogite. Similarly, dissolved Mg and K concentrations increase from granite to schist to eclogite.

The presence of unexposed granite within the Fairbanks area may be indicated by the chemical characteristics of surface discharge that has interacted with such buried rock. Uranium at the ppb level, fluorine concentrations of at least 0.5 ppm, or strontium isotopic ratios below about 0.720 within surface waters are good indicators of granitic rocks somewhere along the ground-water flow path. Except for the water collected below the Hi-Yu mill tailings at site 97-15, none of our samples contained dissolved arsenic concentrations above the State of Alaska maxium contaminant level (50 ppb; Alaska Department of Environmental Conservation, 1996). This confirms the fact that soluble and widespread arsenopyrite is mainly confined to aquifers in the area previously described by others (Hawkins and others, 1982; Weber, 1986) between Fairbanks and Fox.

Acknowledgments

Cynthia Parnow's assistance with measurement of anions and graphics is very much appreciated. We thank Lisa Campbell and Seth Mueller, University of Colorado, for their help in obtaining the Sr-isotope data.

References Cited

Alaska Department of Environmental Conservation, 1996, Drinking water regulations: State of Alaska, Department of Environmental Conservation Document 18 ACC 80, 199 p.

Blum, J.D., 1985, A petrologic and Rb-Sr isotopic study of intrusive rocks near Fairbanks, Alaska: Canadian Journal of Earth Sciences, v. 22, p. 1314–1321.

Blum, J.D., Erel, Y., and Brown, K., 1994, $^{87}Sr/^{86}Sr$ ratios of Sierra Nevada stream waters: Implications for relative mineral weathering rates: Geochimica et Cosmochimica Acta, v. 58, p. 5019–5025.

d'Angelo, W.M., and Ficklin, W.H., 1996, Fluoride, chloride, nitrate, and sulfate in aqueous solution by chemically suppressed ion chromatography, *in* Arbogast, B.F., ed., Analytical Methods Manual for the Mineral Resource Surveys Program, U.S. Geological Survey: U.S. Geological Survey Open-File Report 96-525, p. 149–153.

Goldfarb, R.J., Taylor, C.D., Jr., Meier, A.L., d'Angelo, W.M., and O'Leary, R.M., 1997, Hydrogeochemistry of mine-drainage waters associated with low-sulfide, gold-quartz veins in Alaska, *in* Dumoulin, J.A., and Gray, J.D., eds., Geologic Studies in Alaska by the U.S. Geological Survey, 1995: U.S. Geological Survey Professional Paper 1574, p. 3–17.

Hawkins, D.B., Forbes, R.B., Hok, C.I., and Dinkel, D., 1982, Arsenic in water, soil, bedrock, and plants of the Ester dome area of Alaska: Institute of Water Resources, University of Alaska, Fairbanks, Report IWR-103, 82 p.

Hem, J.D., 1992, Study and interpretation of the chemical characteristics of natural water: U.S. Geological Survey Water-Supply Paper 2254, 263 p.

Levinson, A.A., 1974, Introduction to exploration geochemistry: Wilmette, Illinois, Applied Publishing, 614 p.

McCoy, D., Newberry, R.J., Layer, P., DiMarchi, J.J., Bakke, A., Masterman, J.S., and Minehane, D.L., 1997, Plutonic-related gold deposits of interior Alaska, *in* Goldfarb, R.J., and Miller, L.D., eds., Mineral Deposits of Alaska: Economic Geology Monograph 9, p. 191–241.

Meier, A.L., Grimes, D.J., and Ficklin, W.H., 1994, Inductively coupled plasma mass spectrometry—A powerful analytical tool for mineral resource and environmental studies [abs.], *in* Carter, L.M.H., Toth, M.I., and Day, W.C., eds., USGS Research on Mineral Resources—1994, Part A—Program and Abstracts, Ninth V.E. McKelvey Forum on Mineral and Energy Resources: U.S. Geological Survey Circular 1103-A, p. 67–68.

Metz, P.A., 1991, Metallogeny of the Fairbanks district, Alaska, and adjacent areas: University of Alaska, School of Mineral Engineering, Minerals Research Industry Laboratory Report 90, 370 p.

Newberry, R.J., and Bundtzen, T.K., 1996, Preliminary geologic map of the Fairbanks mining district, Alaska: Alaska Division of Geological and Geophysical Surveys, Public-Data File 96-12, 14 p., 2 sheets.

Ollier, C.D., 1969, Weathering: New York, American Elsevier, 304 p.

Ray, S.R., Vohden, J., and Morgan, W., 1992, Investigation of trace metals related to placer mining on Fairbanks and Porcupine Creeks: Alaska Division of Geological and Geophysical Surveys, Public-Data File 92-13, 17 p.

Robinson, M.S., Smith, T.E., and Metz, P.A., 1990, Bedrock geology of the Fairbanks mining district, Alaska: Alaska Division of Geological and Geophysical Surveys Professional Report 106, 2 sheets, scale 1:63,360.

Weber, E.F., 1986, A stochastic model and risk analysis of arsenic, well depth, and well yield in the Fairbanks area, Alaska: University of Alaska, Fairbanks, unpub. M.S. thesis, 196 p.

Reviewers: P. Briggs, R. Eppinger.

Geologic Studies in Alaska by the
U.S. Geological Survey, 1997
U.S. Geological Survey Professional Paper 1614

U.S.Geological Survey Reports on Alaska Released in 1997

Compiled by John P. Galloway *and* Susan Toussaint

[Some reports dated 1994, 1995, or 1996 did not become available until 1997; they are included in this listing]

Ager, Thomas, 1997, How does climate change influence Alaska's vegetation? Insights from the fossil record: U.S. Geological Survey Fact Sheet FS-071-97, 2 p.

Bailey, E.A., Hines, M.E., and Gray, J.E., 1997, Mercury speciation in soils and vegetation, southwest Alaska, *in* Wanty, R.B., Marsh, S.P., and Gough, L.P., eds., 4th International Symposium on Environmental Geochemistry Proceedings: U.S. Geological Survey Open-File Report 97-496, p. 8.

Bailey, E.A., and Gray, J.E., 1997, Mercury in the terrestrial environment, Kuskokwim Mountains region, southwestern Alaska, *in* Dumoulin, J.A., and Gray, J.E., eds., 1997, Geologic Studies in Alaska by the U.S. Geological Survey, 1995: U.S. Geological Survey Professional Paper 1574, p. 41–56.

Bailey, E.A., Keith, W.J., Bickerstaff, Damon, Dempsey, David, and Miller, M.L., 1996, Analytical results and sample locality maps of stream-sediment, panned concentrate, stream-water, and soil samples from the Stuyahok study area, part of Holy Cross A-4 and A-5 quadrangles, Alaska : U.S. Geological Survey Open-File Report 96-505-C, 44 p., 1 diskette.

Bie, S.W., Arbogast, B.F., Light, T.D., and Weber, F.R., 1997, Analytical results of rock samples from the Livengood 1°x3° quadrangle, Alaska: U.S. Geological Survey Open-File Report 97-446, 131 p., 3 maps, scale 1:250,000.

Brabets, T.P., 1997, Geomorphology of the lower Copper River, Alaska: U.S. Geological Survey Professional Paper 1581, 89 p.

Brabets, T.P., 1997, Regional streamflow information in Alaska—An investment in the future: U.S. Geological Survey Open-File Report 96-630, 2 p.

Brew, D.A., 1997, Description and regional setting of the Silver Bay segment of the Sitka fault zone, southeastern Alaska, and evidence for possible sinistral separation, *in* Dumoulin, J.A., and Gray, J.E., eds., 1997, Geologic Studies in Alaska by the U.S. Geological Survey, 1995: U.S. Geological Survey Professional Paper 1574, p. 307–316.

Brew, D.A., 1997, Reconnaissance geologic map of the Petersburg A-2 quadrangle, southeastern Alaska: U.S. Geological Survey Open-File Report 97-156-A, 20 p., 1 map, scale 1:63,360.

Brew, D.A., 1997, Reconnaissance geologic map of the Petersburg A-3 quadrangle, southeastern Alaska: U.S. Geological Survey Open-File Report 97-156-B, 24 p., 1 map, scale 1:63,360.

Brew, D.A., 1997, Reconnaissance geologic map of the Petersburg B-1 quadrangle, southeastern Alaska: U.S. Geological Survey Open-File Report 97-156-C, 20 p., 1 map, scale 1:63,360.

Brew, D.A., 1997, Reconnaissance geologic map of the Petersburg B-2 quadrangle, southeastern Alaska: U.S. Geological Survey Open-File Report 97-156-D, 21 p., 1 map, scale 1:63,360.

Brew, D.A., 1997, Reconnaissance geologic map of the Petersburg B-3 quadrangle, southeastern Alaska: U.S. Geological Survey Open-File Report 97-156-E, 23 p., 1 map, scale 1:63,360.

Brew, D.A., 1997, Reconnaissance geologic map of the Petersburg B-4 quadrangle, southeastern Alaska: U.S. Geological Survey Open-File Report 97-156-F, 20 p., 1 map, scale 1:63,360.

Brew, D.A., 1997, Reconnaissance geologic map of the Petersburg B-5 quadrangle, southeastern Alaska: U.S. Geological Survey Open-File Report 97-156-G, 19 p., 1 map, scale 1:63,360.

Brew, D.A., 1997, Reconnaissance geologic map of the Petersburg C-1 quadrangle, southeastern Alaska: U.S. Geological Survey Open-File Report 97-156-H, 23 p., 1 map, scale 1:63,360.

Brew, D.A., 1997, Reconnaissance geologic map of the Petersburg C-3 quadrangle, southeastern Alaska: U.S. Geological Survey Open-File Report 97-156-I, 18 p., 1 map, scale 1:63,360.

Brew, D.A., 1997, Reconnaissance geologic map of the Petersburg C-4 quadrangle, southeastern Alaska: U.S. Geological Survey Open-File Report 97-156-J, 21 p., 1 map, scale 1:63,360.

Brew, D.A., 1997, Reconnaissance geologic map of the Petersburg C-5 quadrangle, southeastern Alaska: U.S. Geological Survey Open-File Report 97-156-K, 18 p., 1 map, scale 1:63,360.

Brew, D.A., 1997,Reconnaissance geologic map of the Petersburg D-4 quadrangle, southeastern Alaska: U.S. Geological Survey Open-File Report 97-156-L, 21 p., 1 map, scale 1:63,360.

Brew, D.A., 1997, Reconnaissance geologic map of the Petersburg D-5 quadrangle, southeastern Alaska: U.S. Geological Survey Open-File Report 97-156-M, 22 p., 1 map, scale 1:63,360.

Brew, D.A., compiler, 1997, Geologic bibliography for the Atlin, Mount St. Elias, Skagway, and Yakutat quadrangles and adjacent areas of the Yukon and British Columbia: U.S. Geological Survey Open-File Report 97-159, 23 p.

Brew, D.A., and Grybeck, D.J., 1997, Combined description of map units and correlation of map units for the Petersburg-Wrangell area 1:63,360-scale geologic maps, southeastern Alaska: U.S. Geological Survey Open-File Report 97-156-O, 108 p.

Brew, D.A., Grybeck, D.J., Taylor, C.D., Jachens, R.C., Cox, D.P., Barnes, D.F., Koch, R.D., Morin, R.I., and Drinkwater, J.L., 1996, Undiscovered mineral resources of southeastern Alaska—Revised

mineral-resource-assessment-tract descriptions: U.S. Geological Survey Open-File Report 96-716, 131 p., 1 map, scale 1:1,000,000.

Brew, D.A., and Koch, R.D., 1997, Reconnaissance geologic map of the Bradfield Canal B-6 quadrangle, southeastern Alaska: U.S. Geological Survey Open-File Report 97-156-N, 22 p., 1 map, scale 1:63,360.

Campbell, D.L., and Nokleberg, W.J., 1997, Interpretation of aeromagnetic map and related geophysical data for Mount Hayes 1°x3° quadrangle, Alaska: U.S. Geological Survey Open-File Report 97-280, 64 p., 2 maps, scale 1:250,000.

Carlson, P.R., Kvenvolden, K.A., Hostettler, F.D., Rosenbauer, R.J., and Warden, Augusta, 1997, Fate of spilled oil in Prince William Sound: Diary of a forensic geology study: U.S. Geological Survey Open-File Report 97-518, 88 p.

Celebi, M., Page, R.A., and Seekins, Linda, 1995, Building safer structures: U.S. Geological Survey Fact Sheet FS-167-95, 2 p.

Dorava, J.M., and Liepitz, G.S., 1996, Balancing the three R's (regulation, research, and restoration) on the Kenai River, Alaska: U.S. Geological Survey Fact Sheet FS-160-96, 2 p.

Dorava, J.M., and Moore, G.W., 1997, Effects of boatwakes on streambank erosion Kenai River, Alaska: U.S. Geological Survey Water Resources Investigations Report 97-4105, 84 p.

Dover, James, 1997, Alaska resource data file: Arctic quadrangle: U.S. Geological Survey Open-File Report 97-292, 10 p.

Dover, James, 1997, Alaska resource data file: Table Mountain quadrangle: U.S. Geological Survey Open-File Report 97-293, 14 p.

Dover, James, 1997, Alaska resource data file: Christian quadrangle: U.S. Geological Survey Open-File Report 97-294, 6 p.

Dover, James, 1997, Alaska resource data file: Coleen quadrangle: U.S. Geological Survey Open-File Report 97-295, 39 p.

Dover, James, 1997, Alaska resource data file: Howard Pass quadrangle: U.S. Geological Survey Open-File Report 97-296, 47 p.

Dover, James, 1997, Alaska resource date file: Misheguk Mountain quadrangle: U.S. Geological Survey Open-File Report 97-297, 18 p.

Dumoulin, J.A., and Gray, J.E., eds., 1997, Geologic studies in Alaska by the U.S. Geological Survey, 1995: U.S. Geological Survey Professional Paper 1574, 328 p.

Dumoulin, J.A., and Harris, A.G., 1997, Kinderhookian (Lower Mississippian) calcareous rocks of the Howard Pass quadrangle, west-central Brooks Range, *in* Dumoulin, J.A., and Gray, J.E., eds., 1997, Geologic Studies in Alaska by the U.S. Geological Survey, 1995: U.S. Geological Survey Professional Paper 1574, p. 243–268.

Eppinger, R.G., Sutley, S.J., and McHugh, J.B., 1997, Environmental geochemical study of the Nabesna gold skarn and Kennecott stratabound copper deposits, Alaska, *in* Dumoulin, J.A., and Gray, J.E., eds., 1997, Geologic Studies in Alaska by the U.S. Geological Survey, 1995: U.S. Geological Survey Professional Paper 1574, p. 19–39.

Evans, K.R., 1997, Offshore geologic framework and sedimentology of the Gulf of Alaska: Selected bibliography of U.S. Geological Survey studies (1970-present): U.S. Geological Survey Open-File Report 97-26, 15 p.

Finch, W.I., 1996, Uranium provinces of North America—Their definition, distribution, and models: U.S. Geological Survey Bulletin 2141, 18 p., 2 plates.

Flores, R.M., Stricker, G.D., and Stiles, R.B., 1997, Tidal influence on deposition and quality of coals in the Miocene Tyonek Formation, Beluga coal field, upper Cook Inlet, Alaska, *in* Dumoulin, J.A., and Gray, J.E., eds., 1997, Geologic Studies in Alaska by the U.S. Geological Survey, 1995: U.S. Geological Survey Professional Paper 1574, p. 137–156.

Flowers, Chris, 1997, Observations of geothermal activitiy near Pavlof Volcano on the Alaska Peninsula during March and April of 1996: U.S. Geological Survey Open-File Report 97-146, 13 p.

Fountain, A.G., Krimmel, R.M., and Trabant, D.C., 1997, A strategy for monitoring glaciers: U.S. Geological Survey Circular 1132, 19 p.

Frenzel, S.A., 1997, Cook Inlet basin, Alaska, National Water-Quality Assessment Program: U.S. Geological Survey Fact Sheet 97-153, 4 p.

Galloway, J.P., and Carter, L.D., 1997, A selected bibliography of sand and gravel resources Arctic Coastal Plain, Alaska: U.S. Geological Survey Open-File Report 97-702, 12 p.

Galloway, J.P., and Toussaint, Susan, 1997, Reports about Alaska in non-USGS publications released in 1995 that include USGS authors, *in* Dumoulin, J.A., and Gray, J.E., eds., 1997, Geologic Studies in Alaska by the U.S. Geological Survey, 1995: U.S. Geological Survey Professional Paper 1574, p. 323–328.

Galloway, J.P., and Toussaint, Susan, 1997, U.S. Geological Survey reports on Alaska released in 1995, *in* Dumoulin, J.A., and Gray, J.E., eds., 1997, Geologic Studies in Alaska by the U.S. Geological Survey, 1995: U.S. Geological Survey Professional Paper 1574, p. 317–321.

Glass, R.L., 1996, Alaska wetland resources *in* Fretwell, J.D., Williams, J.S., and Redman, P.J., compilers, National Water Summary on Wetland Resources: U.S. Geological Survey Water-Supply Paper 2425, p. 107–114.

Goldfarb, R.J., Taylor, C.D., Meier, A.L., d'Angelo, W.M., and O'Leary, R.M., 1997, Hydrogeochemistry of mine-drainage waters associated with low-sulfide, gold-quartz veins in Alaska, *in* Dumoulin, J.A., and Gray, J.E., eds., 1997, Geologic Studies in Alaska by the U.S. Geological Survey, 1995: U.S. Geological Survey Professional Paper 1574, p. 3–17.

Gough, L.P., and Crock, J.G., 1997, Distinguishing between natural geologic and anthropogenic trace element sources, Denali National Park and Preserve, *in* Dumoulin, J.A., and Gray, J.E., eds., 1997, Geologic Studies in Alaska by the U.S. Geological Survey, 1995: U.S. Geological Survey Professional Paper 1574, p. 57-71.

Gough, L., Day, W., Crock, J., Gamble, B., and Henning, M., 1997, Placer-gold mining in Alaska—Cooperative studies on the effect of suction dredge operations on the Fortymile River: U.S. Geological Survey Fact Sheet FS-155-97, 4 p.

Grauch, V.J.S., and Castellanos, Esther, 1995, Revised digital aeromagnetic data for areas in and adjacent to the National Petroleum Reserve Area (NPRA), North Slope, Alaska: U.S. Geological Survey Open-File Report 95-835, 11 p.

Gray, J.E., 1997, Environmental geochemistry and mercury speciation of abandoned mercury mines in southwestern Alaska, *in* Wanty, R.B., Marsh, S.P., and Gough, L.P., eds., 4th International Symposium on Environmental Geochemistry Proceedings: U.S. Geological Survey Open-File Report 97-496, p. 31.

Gray, J.E., Folger, P.F., and Hageman, P.L., 1997, Map showing the distribution of anomalous concentrations of mercury, antimony, and arsenic in stream sediment, heavy-mineral concentrate, and aquatic moss in the Iditarod quadrangle, Alaska: U.S. Geological Survey Miscellaneous Field Studies Map MF 2219-C, 1 map, scale 1:250.000.

Gray, J.E., Kelley, K.D., Goldfarb, R.J., and Taylor, C.D., 1997, Environmental studies of mineral deposits in Alaska, *in* Wanty, R.B., Marsh, S.P., and Gough, L.P., eds., 4th International Symposium on Environmental Geochemistry Proceedings: U.S. Geological Survey Open-File Report 97-496, p. 31.

Gray, J.E., Motooka, J.M., and O'Leary, R.M., 1997, Map showing the distribution of anomalous concentrations of gold and silver in stream sediment, heavy-mineral concentrate, and aquatic moss in the

Iditarod quadrangle, Alaska: U.S. Geological Survey Miscelllaneous Field Studies Map MF 2219-D, 1 map, scale 250,000.

Gray, J.E., Ryder, J.L., and Taylor, C.D., 1997, Map showing the distribution of anomalous concentations of copper, lead, zinc, tin, and tungsten in stream sediment and heavy-mineral concentrate in the Iditarod quadrangle, Alaska: U.S. Geological Survey Miscellaneous Field Studies Map MF 2219-E, 1 map, scale 1:250,000.

Gray, J.E., and Theodorakos, P.M., 1997, Areas favorable for metallic mineral resources and newly discovered mineral occurrences in the Buckstock Mountains area, southwestern Alaska, *in* Dumoulin, J.A., and Gray, J.E., eds., 1997, Geologic Studies in Alaska by the U.S. Geological Survey, 1995: U.S. Geological Survey Professional Paper 1574, p. 111–123.

Gray, J.E., Theodorakos, P.M., Lee, G.K., Hageman, P.L., and Sutley, S.J., 1997, Analytical data of stream-sediment and heavy-mineral-concentrate samples collected from the Buckstock Mountains and surrounding areas, Sleetmute quadrangle, southwest Alaska: U.S. Geological Survey Open-File Report 97-743-A, 147 p., plus 97-743-B, 1 diskette.

Grommé, Sherman, and Hillhouse, J.W., 1997, Paleomagnetic results from Devonian and Permian rocks at Saginaw Bay, Kuiu Island, southeastern Alaska, *in* Dumoulin, J.A., and Gray, J.E., eds., 1997, Geologic Studies in Alaska by the U.S. Geological Survey, 1995: U.S. Geological Survey Professional Paper 1574, p. 295–306.

Haeussler, P.J., and Anderson, R.S., 1997, The "Twin Peaks fault:" Not a tectonic or seismogenic structure, *in* Dumoulin, J.A., and Gray, J.E., eds., 1997, Geologic Studies in Alaska by the U.S. Geological Survey, 1995: U.S. Geological Survey Professional Paper 1574, p. 93–99.

Harris, A.G., Brenckle, P.L., Baesemann, J.F., Krumhardt, A.P., and Gruzlovic, P.D., 1997, Comparison of conodont and calcareous microfossil biostratigraphy and lithostratigraphy of the Lisburne Group (Carboniferous), Sadlerochit Mountains, northeast Brooks Range, Alaska, *in* Dumoulin, J.A., and Gray, J.E., eds., 1997, Geologic Studies in Alaska by the U.S. Geological Survey, 1995: U.S. Geological Survey Professional Paper 1574, p. 195–219.

Kaufman, D.S., and Stilwell, K.B., 1997, Preliminary evaluation of emergent postglacial shorelines, Naknek and Iliamna Lakes, southwestern Alaska, *in* Dumoulin, J.A., and Gray, J.E., eds., 1997, Geologic Studies in Alaska by the U.S. Geological Survey, 1995: U.S. Geological Survey Professional Paper 1574, p. 73–81.

Keith, W.J., and Miller, M.L., 1997, Alaska resource data file: Sleetmute quadrangle: U.S. Geological Survey Open-File Report 97-32, 38 p.

Kelley, J.S., 1997, Alaska resource data file: Demarcation Point quadrangle: U.S. Geological Survey Open-File Report 96-678, 14 p.

Kelley, J.S., 1997, Alaska resource data file: Umiat quadrangle: U.S. Geological Survey Open-File Report 96-679, 6 p.

Kelley, J.S., 1997, Alaska resource data file: Mount Michelson quadrangle: U.S. Geological Survey Open-File Report 96-681, 21 p.

Kelley, Karen, 1997, Alaska resource data file: Chandler Lake quadrangle: U.S. Geological Survey Open-File Report 97-265, 24 p.

Kelley, Karen, 1997, Alaska resource data file: Killik River quadrangle: U.S. Geological Survey Open-File Report 97-266, 20 p.

Kelley, K.D., 1997, Natural acid drainage associated with shale-hosted Ag-Pb-Zn massive sulfide deposits in the Brooks Range, Northern Alaska, USA, *in* Wanty, R.B., Marsh, S.P., and Gough, L.P., eds., 4th International Symposium on Environmental Geochemistry Proceedings: U.S. Geological Survey Open-File Report 97-496, p. 44.

Kelley, K.D., Bailey, E.A., Briggs, P.H., Motooka, J.M., and Meier, A.L., 1996, Digital release of stream-sediment, heavy-mineral-concentrate, soil, water, and rock geochemical data collected in the Howard Pass 1°x3° quadrangle, Alaska: U.S. Geological Survey Open-File Report 96-711, $3^1/_2$"-diskette for IBM PC or compatible.

Kelley, K.D., Taylor, C.D., and Cieutat, B.A., 1997, Silver-lead-zinc mineral occurrences in the Howard Pass quadrangle, Brooks Range, Alaska, *in* Dumoulin, J.A., and Gray, J.E., eds., 1997, Geologic Studies in Alaska by the U.S. Geological Survey, 1995: U.S. Geological Survey Professional Paper 1574, p. 101–110.

Kennedy, B.W., Mayo, L.R., Trabant, D.C., and March, R.S., 1997, Air temperature and precipitation data, Gulkana Glacier, Alaska, 1968-96: U.S. Geological Survey Open-File Report 97-358, 144 p.

Kleinman, J.W., Iwatsubo, E.Y., Power, J.A., and Endo, E.T., 1997, Geodetic studies in the Novarupta area, Katmai National Park, Alaska, 1990 to 1995, *in* Dumoulin, J.A., and Gray, J.E., eds., 1997, Geologic Studies in Alaska by the U.S. Geological Survey, 1995: U.S. Geological Survey Professional Paper 1574, p. 83–92.

Light, T.D., Barnwell, C.E., and Andrade, Julio, 1997, Livengood quadrangle GeoExplorer: U.S. Geological Survey Open-File Report 97-484-E, 1 CD-ROM.

Light, T.D., and Lee, G.K., 1997, Map showing distribution and occurrence of gold-bearing samples from the Livengood quadrangle, Alaska: U.S. Geological Survey Open-File Report 97-484-C, 21 p., 1 map, scale 1:250,000.

Lilly, M.R., DePalma, K.L., and Benson, S.L., 1995, Selected environmental and geohydrologic reports for the Fort Wainwright and Fairbanks areas, Alaska, as of July 1995: U.S. Geological Survey Open-File Report 95-420, 62 p.

Lorenson, T.D., and Kvenvolden, K.A., 1997, Methane in coastal sea water, sea ice, and bottom sediments, Beaufort Sea, Alaska—Results from 1995: U.S. Geological Survey Open-File Report 97-54, 77 p.

March, R.S., Mayo, L.R., and Trabant, D.C., 1997, Snow and ice volume on Mount Spurr Volcano, Alaska, 1981: U.S. Geological Survey Water-Resources Investigations Report 97-4142, 36 p., 2 maps, scale 1:50,000.

March, R.S., and Trabant, D.C., 1997, Mass balance, meteorological, ice motion, surface altitude, and runoff data at Gulkana Glacier, Alaska, 1993 balance year: U.S. Geological Survey Water Resources Investigations Report 96-4299, 30 p.

McCammon, R.B., Light, T.D., Rinehart, C.D., Weber, F.R., Lee, G.K., and Bie, S.W., 1997, Map showing mineral resource potential of the Livengood quadrangle, Alaska: U.S. Geological Survey Open-File Report 97-484-B, 47 p., 1 map, scale 1:250,000.

McGimsey, R.G., and Neal, C.A., 1996, 1995 volcanic activity in Alaska and Kamchatka: Summary of events and response of the Alaska Volcano Observatory: U.S. Geological Survey Open-File Report 96-738, 22 p.

Miller, L.D., Goldfarb, R.J., Snee, L.W., McClelland, W.C., and Klipfel, P.D., 1997, Paleocene molybdenum mineralizaiton in the eastern Coast batholith, Taku River region, and new age constraints on batholith evolution, *in* Dumoulin, J.A., and Gray, J.E., eds., 1997, Geologic Studies in Alaska by the U.S. Geological Survey, 1995: U.S. Geological Survey Professional Paper 1574, p. 125–135.

Moore, T.E., Hemming, Sidney, and Sharp, W.D., 1997, Provenance of the Carboniferous Nuka Formation, Brooks Range, Alaska: A multicomponet isotope provenance study with implications for age of cryptic crystalline basement, *in* Dumoulin, J.A., and Gray, J.E., eds., 1997, Geologic Studies in Alaska by the U.S. Geological Survey, 1995: U.S. Geological Survey Professional Paper 1574, p. 173–194.

Morin, R.L., 1997, Gravity models of Abby Creek and Bion barite deposits, Howard Pass quadrangle, northwestern Brooks Range, Alaska: U.S. Geological Survey Open-File Report 97-704, 15 p.

Morin, R.L., 1997, Gravity and magnetic maps of part of the Drenchwater Creek stratiform zinc-lead-silver deposit, Howard Pass quadrangle, northwestern Brooks Range, Alaska: U.S. Geological Survey Open-File Report 97-705, 9 p.

Mull, C.G., Harris, A.G., and Carter, J.L., 1997, Lower Mississippian (Kinderhookian) biostratigraphy and lithostratigraphy of the western Endicott Mountains, Brooks Range, Alaska, *in* Dumoulin, J.A., and Gray, J.E., eds., 1997, Geologic Studies in Alaska by the U.S. Geological Survey, 1995: U.S. Geological Survey Professional Paper 1574, p. 221–242.

Neal, Christina, 1997, What is the Alaska Volcano Observatory?: U.S. Geological Survey Open-File Report 97-443, 2 p.

Neal, C.A., Casadevall, T.J., Miller, T.P., Hendley, J.W., II, and Stauffer, P.H., 1997, Volcanic ash—Danger to aircraft in the north Pacific: U.S. Geological Survey Fact Sheet 030-97, 2 p.

Neal, Christina, and McGimsey, Robert, 1996, Volcanoes of the Wrangell Mountains and Cook Inlet region, Alaska—Selected photographs: U.S. Geological Survey Digital Data Series DDS-39, 1 CD-ROM.

Neal, Christina, and McGimsey, Robert, 1997, Volcanoes of the Alaska Peninsula and Aleutian Islands, Alaska—Selected photographs: U.S. Geological Survey Digital Data Series DDS–40, 1 CD-ROM.

Neal, C.A., and McGimsey, R.G., 1997, 1996 volcanic activity in Alaska and Kamchatka: Summary of events and response of the Alaska Volcano Observatory: U.S. Geological Survey Open-File Report 97-433, 34 p.

Neal, E.G., 1998, Hydrologic investigation of the Ophir Creek watershed near Yakutat, Alaska: U.S. Geological Survey Open-File Report 98-199, 33 p.

Nelson, Steven, 1997, Alaska resource data file: Ambler River quadrangle: U.S. Geological Survey Open-File Report 97-856, 98 p.

Newberry, R.J., and Brew, D.A., 1997, The upper Triassic Greens Creek VMS (volcanogenic massive sulfide) deposit and Woewodski Island VMS prospects, southeastern Alaska: Chemical and isotopic data for rocks and ores demonstrate similarity of these deposits and their host rocks: U.S. Geological Survey Open-File Report 97-539, 49 p.

Nokleberg, W.J., Bundtzen, T.K., Dawson, K.M., Eremin, R.A., Goryachev, N.A., Koch, R.D., Ratkin, V.V., Rozenblum, I.S., Shpikerman, V.I., Frolov, Yu.F., Gorodinsky, M.E., Melnikov, V.D., Ognyanov, N.V., Petrachenko, E.D., Petrachenko, R.I., Pozdeev, A.I., Ross, K.V., Wood, D.H., Grybeck, D., Khanchuck, A.I., Kovbas, L.I., Nekrasov, I.Ya., and Sidorov, A.A., 1996, Significant metalliferous and selected non-metalliferous lode deposits and placer districts for the Russian Far East, Alaska, and the Canadian Cordillera: U.S. Geological Survey Open-File Report 96-513-A, 385 p.

Nokleberg, W.J., Parfenov, L.M., Monger, J.W.H., Baranov, B.V., Byalobzhesky, S.G., Bundtzen, T.K., Feeney, T.D., Fujita, K., Gordey, S.P., Grantz, A., Khanchuk, A.I., Natal'in, B.A., Natapov, L.M., Norton, I.O., Patton, W.W., Jr., Plafker, G., Scholl, D.W., Sokolov, S.D., Sosunov, G.M., Stone, D.B., Tabor, R.W., Tsukanov, N.V., and Vallier, T.L., 1997, Summary Circum-North Pacific tectonostratigraphic terrane map: U.S. Geological Survey Open-File Report 96-727, 1 map, scale 1:10,000,000.

O'Sullivan, P.B., Plafker, George, and Murphy, J.M., 1997, Apatite fission-track thermotectonic history of crystalline rocks in the northern Saint Elias Mountains, Alaska, *in* Dumoulin, J.A., and Gray, J.E., eds., 1997, Geologic Studies in Alaska by the U.S. Geological Survey, 1995: U.S. Geological Survey Professional Paper 1574, p. 283–293.

Patton, W.W., Jr., and Moll-Stalcup, E.J., 1996, Geologic map of the Unalakleet quadrangle, west-central Alaska: U.S. Geological Survey Miscellaneous Investigations Map I-2559, 1 map, scale 1:250,000, 39 p.

Richter, D.H., Moll-Stalcup, Elizabeth, Duffield, W.A., and Shew, Nora, 1997, Geologic map of the Nabesna A-6 quadrangle, Alaska: U.S. Geological Survey Open-File Report 97-475, 1 map, scale 1:63,360, 1 pamphlet, variously paged.

Rickman, R.L., 1996, Effect of ice formation and streamflow on salmon incubation habitat in the lower Bradley River, Alaska: U.S. Geological Survey Water Resources Investigations Report 96-4202, 63 p.

Rickman, R.L., and Rosenkrans, D.S., 1997, Hydrologic conditions and hazards in the Kennicott River basin, Wrangell-St. Elias National Park and Preserve, Alaska: U.S. Geological Survey Water Resources Investigations Report 96-4296, variously paged.

Riehle, J.R., Fleming, M.D., Molnia, B.F., Dover, J.H., Kelley, J.S., Miller, M.L., Nokleberg, W.J., Plafker, George, and Till, A.B., 1997, Digital shaded-relief image of Alaska: U.S. Geological Survey Miscellaneous Investigations Series Map 2585, 1 sheet, scale 1:2,500,000, plus explanatory pamphlet, 11 p.

Rinehart, C.D., Light, T.D., and Shew, N.B., 1997, Petrography and radiometric ages for selected rocks from the Livengood quadrangle, Alaska: U.S. Geological Survey Open-File Report 97-484-D, 22 p.

Roush, James, and Brease, Phil, 1997, Glacier monitoring in Denali National Park and Preserve, Alaska: Integrating field study and remote sensing *in* Williams, R.S., Jr., and Ferrigno, J.G., compilers, Final Report of the Workshop on Long-Term Monitoring of Glaciers of North America and Northwestern Europe: U.S. Geological Survey Open-File Report 98-31, p. 91.

Rowan, E.L., 1997, Basin evolution, and the timing and extent of oil generation, Canning River region, North Slope, Alaska: Preliminary Basin2 calculations assuming a conductive thermal history: U.S. Geological Survey Open-File Report 97-711, 61 p.

Saltus, R.W., and Simmons, G.C., 1997, Composite and merged aeromagnetic data for Alaska: A web site for distribution of gridded data and plot files: U.S. Geological Survey Open-File Report 97-520, 15 p.

Saltus, R.W., Meyer, J.F., Jr., Barnes, D.F., and Morin, R.L., 1997, Tectono-geophysical domains of interior Alaska as interpreted from new gravity and aeromagnetic data compilations, *in* Dumoulin, J.A., and Gray, J.E., eds., 1997, Geologic Studies in Alaska by the U.S. Geological Survey, 1995: U.S. Geological Survey Professional Paper 1574, p. 157–171.

Schneider, J.L, ed., 1997, 1996 annual report on Alaska's mineral resources: U.S. Geological Survey Circular 1142, 70 p.

Silberling, N.J., Grant-Mackie, J.A., and Nichols, K.M., 1997, The late Triassic bivalve *Monotis* in accreted terranes of Alaska: U.S. Geological Survey Bulletin 2151, 32 p.

Snyder, E.F., 1997, Water-resources activities of the U.S. Geological Survey in Alaska, 1997: U.S. Geological Survey Fact Sheet 028-97, 4 p.

St. John, J.M., and Babcock, L.E., 1997, Late Middle Cambrian trilobites of Siberian aspect from the Farewell terrane, southwestern Alaska, *in* Dumoulin, J.A., and Gray, J.E., eds., 1997, Geologic Studies in Alaska by the U.S. Geological Survey, 1995: U.S. Geological Survey Professional Paper 1574, p. 269–281.

Symonds, R.B., Ritchie, B.E., McGimsey, R.G., Ort, M.H., Poreda, R.J., Evans, W.C., and Janik, C.J., 1997, Investigations of gas seeps and springs in the vicinity of the Gas Rocks, south shore Becharof Lake, Alaska: U.S. Geological Survey Open-File Report 97-127, 27 p.

Trabant, D.C., and Hawkins, D.B., 1997, Glacier ice-volume modeling and glacier volumes on Redoubt Volcano, Alaska: U.S. Geological Survey Water-Resources Investigations Report 97-4187, 29 p.

Trabant, D.C., with contributions from workshop participants Benson, C.S., Echelmeyer, Keith, Brease, Phil, and Roush, James, 1997, Data base and geographical perspective for monitoring glaciers of

Alaska *in* Williams, R.S., Jr., and Ferrigno, J.G., compilers, Final Report of the Workshop on Long-Term Monitoring of Glaciers of North America and Northwestern Europe: U.S. Geological Survey Open-File Report 98-31, p. 28–37.

U.S. Geological Survey, 1994, National Marine and Coastal Geology Program: A plan for geologic research on environmental hazards and resources issues affecting the Nation's coastal realms and marine federal lands: U.S. Geological Survey, 65 p.

U.S. Geological Survey, 1996, U.S. Geological Survey programs in Alaska: U.S. Geological Survey Fact Sheet FS-001-96, 4 p.

U.S. Geological Survey, Volcano Hazards Team, 1997, Volcano Hazards Program five-year science plan—1998 to 2002: U.S. Geological Srvey Open-File Report 97-680, 20 p.

Waitt, R.B., and Begét, J.E., *with contributions from* Juergen Kienle, 1996, Provisional geologic map of Augustine Volcano, Alaska: U.S. Geological Survey Open-File Report 96-516, 44 p., 1 map, scale 1:25,000.

Wang, Bronwen, 1997, Trace elements in the Kuskokwim River, Alaska, *in* Wanty, R.B., Marsh, S.P., and Gough, L.P., eds., 4th International Symposium on Environmental Geochemistry Proceedings: U.S. Geological Survey Open-File Report 97-496, p. 95.

Wanty, R.B., Wang, B., and Vohden, J., 1997, Studies of suction dredge gold-placer mining operations along the Fortymile River, eastern Alaska: U.S. Geological Survey Fact Sheet FS-154-97, 2 p.

Waythomas, C.F., Miller, T.P., McGimsey, R.G., and Neal, C.A., 1997, Preliminary volcanic-hazard assessment for Pavlof Volcano, Alaska: U.S. Geological Survey Open-File Report 97-135, 1 map, scale 1:250,000.

Weber, F.R., Wheeler, K.L., Rinehart, C.D., and Light, T.D., 1997, Generalized geologic map of the Livengood quadrangle, Alaska: U.S. Geological Survey Open-File Report 97-484-A, 1 map, scale 1:250,000.

Williams, R.S., Jr., and Ferrigno, J.G., workshop coordinators, 1997, Final report of the workshop on long-term monitoring of glaciers of North America and northwestern Europe: U.S. Geological Survey Open-File Report 98-31, 144 p.

Wilson, F.H., 1997, Alaska resource data file: Cold Bay quadrangle: U.S. Geological Survey Open-File Report 97-168, 17 p.

Wilson, F.H., 1997, Alaska resource data file: False Pass quadrangle: U.S. Geological Survey Open-File Report 97-169, 16 p.

Wilson, F.H., Weber, F.R., Dochat, T.M., Miller, T.P., and Detterman, R.L., 1997, Revised geologic map of the Cold Bay and False Pass quadrangles, Alaska Peninsula: U.S. Geological Survey Open-File Report 97-866, 34 p., 1 sheet, scale 1:250,000.

Yeend, Warren, 1997, Reconnaissance geologic map of surficial deposits for the Mount McKinley quadrangle, Alaska: U.S. Geological Survey Open-File Report 97-138, 1 map, scale 1:250,000.

Geologic Studies in Alaska by the
U.S. Geological Survey, 1997
U.S. Geological Survey Professional Paper 1614

Reports About Alaska in Non-USGS Publications Released in 1997 that Include USGS Authors

Compiled by John P. Galloway *and* Susan Toussaint

[Some reports dated 1995 or 1996 did not become available until 1997; they are included in this listing. USGS authors are marked with asterisks (*)]

*Adams, K.E., Mull, C.G., and Crowder, R.K., 1997, Permian deposition in the north central Brooks Range, Alaska: Constraints for tectonic reconstructions: Journal of Geophysical Research, v. 102, no. B9, p. 20727–20748.

Ashleman, J.C., *Taylor, C.D., and Smith, P.R., 1997, Porphyry molybdenum deposits of Alaska, with emphasis on the geology of the Quartz Hill deposit, southeastern Alaska, *in* Goldfarb, R.J., and Miller, L.D., eds., 1997, Mineral Deposits of Alaska: Economic Geology Monograph 9, p. 334–354.

*Bacon, C.R., *Neal, C.A., Nye, C.J., and *McGimsey, R.G., 1997, Pre-eruptive temperatures for postcaldera magmas of Aniakchak Volcano, Alaska [abs.]: Eos (American Geophysical Union Transactions), v. 78, no. 46, supplement, p. 792.

Bahr, D.B., Meier, M.F., and *Peckham, S.D., 1997, The physical basis of glacier volume-area scaling: Journal of Geophysical Research, v. 102, no. B9, p. 20355–20362.

Bence, A.E., *Kvenvolden, K.A., and Kennicutt, M.C., II, 1996, Organic geochemistry applied to environmental assessments of Prince William Sound, Alaska, after the *Exxon Valdez* oil spill—A review: Organic Geochemistry, v. 24, p. 7–42.

*Brew, D.A., 1997, "The coast range megalineament" in southeastern Alaska—How does it differ from the "coast shear zone?" [abs.]: Geological Society of America, Abstracts with Programs, v. 29, no. 6, p. 81.

*Brew, D.A., 1997, Geologic mapping in the Wrangell-Petersburg area, southeastern Alaska—A case history illustrating evolution of geologic studies [abs.]: Geological Society of America, Abstracts with Programs, v. 29, no. 6, p. 425.

*Bufe, C.G., *Varnes, D.J., and Nishenko, S.P., 1996, Time-to-failure in the Alaska-Aleutian region: An update [abs.]: Eos (American Geophysical Union Transactions), v. 77, no. 46, supplement, p. 456.

Bundtzen, T.K., and *Miller, M.L., 1997, Precious metals associated with Late Cretaceous–early Tertiary igneous rocks of southwestern Alaska, *in* Goldfarb, R.J., and Miller, L.D., eds., 1997, Mineral Deposits of Alaska: Economic Geology Monograph 9, p. 242–286.

Cai, Jinkui, Powell, R.D., Cowan, E.A., and *Carlson, P.R., 1997, Lithofacies and seismic-reflection interpretation of temperate glacimarine sedimentation in Tarr Inlet, Glacier Bay, Alaska: Marine Geology, v. 143, p. 5–37.

Cai, Jinkui, Powell, R.D., Cowan, E.A., and *Kayen, R.E., 1996, Lithofacies, physical properties and seismic-reflection characteristcs of temperate glaciomarine deposits in Glacier Bay, Alaska [abs.]: Eos (American Geophysical Union Transactions), v. 77, no. 46, supplement, p. 332.

*Carlson, P.R., and *Kvenvolden, K.A., 1996, Tracking *Exxon Valdez* oil from beach to deepwater sediments of Prince William Sound, Alaska, *in Exxon Valdez* Oil Spill Symposium, Anchorage, Alaska, 1993, Proceedings: American Fisheries Society Symposium 18, p. 109–120.

*Carlson, P.R., *Stevenson, A.J., *Bruns, T.R., *Mann, D.M., and Huggett, Quentin, 1996, Sediment pathways in Gulf of Alaska from beach to abyssal plain *in* Gardner, J.V., Field, M.E., and Twichell, D.C., eds., Geology of the United States' Seafloor—The View from GLORIA: New York, Cambridge University Press, p. 255–277.

*Chouet, B.A., 1997, Hydrothermal pressure instabilites related to magmatic steam injection and reflected in long-period seismicity [abs.]: Eos (American Geophysical Union Transactions), v. 78, no. 46, supplement, p. 764–765.

*Cole, Frances, *Bird, K.J., Toro, Jaime, Roure, François, O'Sullivan, P.B., Pawlewicz, Mark, and *Howell, D.G., 1997, An integrated model for the tectonic development of the frontal Brooks Range and Colville Basin 250 km west of the Trans-Alaska Crustal Transect: Journal of Geophysical Research, v. 102, no. B9, p. 20685–20708.

Cole, F., Toro, J., *Bird, K.J., and Roure, F., 1996, A forward model for thrusting and sedimentation in the north-central Brooks Range, Alaska [abs.]: Eos (American Geophysical Union Transactions), v. 77, no. 46, supplement, p. 642.

*Collett, T.S., 1996, Sources of surficial methane flux associated with natural gas hydrate accumulations in northern Alaska [abs.]: Eos (American Geophysical Union Transactions), v. 77, no. 46, supplement, p. 184.

*Collett, T.S., 1997, Gas hydrate resources of northern Alaska: Bulletin of Canadian Petroleum Geology, v. 45, p. 317–338.

Dobson, M.R., *Karl, H.A., and *Vallier, T.L., 1996, Sedimentation along the fore-arc region of the Aleutian Island Arc, Alaska *in* Gardner, J.V., Field, M.E., and Twichell, D.C., eds., Geology of the United States' Seafloor—The View from GLORIA: New York, Cambridge University Press, p. 279–304.

Dreher, S.T., Faust, J.L., *Miller, T.P., and *Bacon, C.R., 1997, Chemical characteristics of the Aniakchak Caldera ash-flow sheet [abs.]: Eos (American Geophysical Union Transactions), v. 78, no. 46, supplement, p. 180.

*Dumoulin, J.A., Watts, K.F., and *Harris, A.G., 1997, Stratigraphic contrasts and tectonic relationships between Carboniferous successions in the Trans-Alaska Crustal Transect corridor and adjacent areas, northern Alaska: Journal of Geophysical Research, v. 102, no. B9, p. 20709–20726.

Eichelberger, J.C., *Keith, T.C., and Nye, C.J., 1996, New monitoring and geological investigations in the central Aleutian Arc, Alaska [abs.]: Eos (American Geophysical Union Transactions), v. 77, no. 46, supplement, p. 771.

Elias, S.A., Short, S.K., and *Waythomas, C.F., 1996, Late Quaternary environments, Denali National Park and Preserve, Alaska: Arctic, v. 49, no. 3, p. 292–305.

*Evans, K.R., *Stevenson, A.J., *Barnes, P.W., *Carlson, P.R., *Hampton, M.A., and *Marlow, M.S., 1996, Sea-floor sediments in the Gulf of Alaska: New map compilation for studies of benthic biohabitats [abs.]: Eos (American Geophysical Union Transactions), v. 77, no. 46, supplement, p. 409.

*Fierstein, J., Houghton, B.F., Wilson, C.J.N., and *Hildreth, W., 1997, Complexities of Plinian fall deposition at vent: An example from the 1912 Novarupta eruption (Alaska): Journal of Volcanology and Geothermal Research v. 76, p. 215–227.

Foley, J.Y., *Light, T.D., *Nelson, S.W., and Harris, R.A., 1997, Mineral occurrences associated with mafic-ultramafic and related alkaline complexes in Alaska, *in* Goldfarb, R.J., and Miller, L.D., eds., 1997, Mineral Deposits of Alaska: Economic Geology Monograph 9, p. 396–449.

*Fuis, G.S., *Murphy, J.M., *Lutter, W.J., *Moore, T.E., *Bird, K.J., and Christensen, N.I., 1997, Deep seismic structure and tectonics of northern Alaska: Crustal-scale duplexing with deformation extending into the upper mantle: Journal of Geophysical Research, v. 102, no. B9, p. 20873–20896.

*Goldfarb, R.J., 1997, Metallogenic evolution of Alaska, *in* Goldfarb, R.J., and Miller, L.D., eds., 1997, Mineral Deposits of Alaska: Economic Geology Monograph 9, p. 4–34.

*Goldfarb, R.J., and Miller, L.D., eds., 1997, Mineral deposits of Alaska: Economic Geology Monograph 9, 482 p.

*Goldfarb, R.J., Miller, L.D., *Leach, D.L., and *Snee, L.W., 1997, Gold deposits in metamorphic rocks of Alaska, *in* Goldfarb, R.J., and Miller, L.D., eds., 1997, Mineral Deposits of Alaska: Economic Geology Monograph 9, p. 151–190.

*Gray, J.E., *Gent, C.A., *Snee, L.W., and *Wilson, F.H., 1997, Epithermal mercury-antimony and gold-bearing vein lodes of southwestern Alaska, *in* Goldfarb, R.J., and Miller, L.D., eds., 1997, Mineral Deposits of Alaska: Economic Geology Monograph 9, p. 287–305.

Greninger, M.L., Klemperer, S.L., and *Nokleberg, W.J., 1996, Geographic information system (GIS) database of the geology, geophysics, deep-crustal structure, and tectonics of the Russian Far East, Alaska, Canadian Cordillera, and adjacent offshore regions [abs.]: Eos (American Geophysical Union Transactions), v. 77, no. 46, supplement, p. 669.

*Guffanti, Marianne, and *Ewert, J.W., 1997, Improvements in real-time monitoring of US volcanoes [abs.]: Eos (American Geophysical Union Transactions), v. 78, no. 46, supplement, p. 37.

*Haeussler, P.J., and Bruhn, R.L., 1996, Evidence for Holocene or late Pleistocene folding in Cook Inlet, Alaska [abs.]: Eos (American Geophysical Union Transactions), v. 77, no. 46, supplement, p. 686.

*Hammond, W.R., *Lockhart, A.B., *Neal, C.A., *McGimsey, R.G., and *Paskievitch, J.F., 1997, Seismic monitoring at Aniakchak Volcano, Alaska [abs.]: Eos (American Geophysical Union Transactions), v. 78, no. 46, supplement, p. 816.

*Hammond, W.R., *Paskievitch, J.F., *Power, J.A., *Lockhart, A.B., Estes, S.A., Tytgat, G., and Benevento, J., 1996, The AVO central Aleutian expansion: Seismic monitoring and instrumentation [abs.]: Eos (American Geophysical Union Transactions), v. 77, no. 46, supplement, p. 451–452.

*Harris, A.G., Brenckle, P.A., Baesemann, J.F., and Krumhardt, A.P., 1997, Conodont and calcareous microfossil biostratigraphy of the Lisburne Group (Carboniferous), Sadlerochit Mts., NE. Brooks Range, Alaska [abs.]: Geological Society of America, Abstracts with Programs, v. 29, no. 2, p. 12–13.

*Healy, J.H., *Dewey, J.W., Kossobokov, V.G., and Romashkova, L.L., 1996, Intermediate-term changes of seismicity in advance of the 10 June 1996 Delarof Islands earthquake [abs.]: Eos (American Geophysical Union Transactions), v. 77, no. 46, supplement, p. 502.

*Heinrichs, T.A., *Mayo, L.R., Echelmeyer, K.A., and Harrison, W.D., 1996, Quiescent-phase evolution of a surge-type glacier: Black Rapids Glacier, Alaska, U.S.A.: Journal of Glaciology, v. 42, p. 110–122.

*Hildenbrand, T.G., *Blakely, R.J., *Jachens, R.C., and *Saltus, R.W., 1997, Insights on crustal structures based on new regional magnetic anomaly data in Western U.S.A.: Eos (American Geophysical Union Transactions), v. 78, no. 17, supplement, p. 118.

*Hill, D.P., and *Guffanti, Marianne, 1997, Issues in volcano hazards mitigation: Eos (American Geophysical Union Transactions), v. 78, no. 17, supplement, p. 47.

*Hodge, S.M., 1997, Glacier mass balances suggest recent changes in Pacific hemisphere teleconnections [abs.]: Eos (American Geophysical Union Transactions), v. 78, no. 46, supplement, p. 101.

Hudson, T.L. and *Reed, B.L., 1997, Tin deposits in Alaska, *in* Goldfarb, R.J., and Miller, L.D., eds., 1997, Mineral Deposits of Alaska: Economic Geology Monograph 9, p. 450–465.

Jolly, A.D., McNutt, S.R., Coombs, M.L., Sthiler, S.D., and *Paskievitch, J., 1997, Seismicity in the vicinity of the Katmai group of volcanoes, Katmai National Park, Alaska; July 1995–March 1997 [abs.]: Eos (American Geophysical Union Transactions), v. 78, no. 46, supplement, p. 442.

Jolly, A.D., McNutt, S.R., Wiener, S., and *Lahr, J.C., 1996, An evaluation of b-value spatial mapping techniques based on an analysis of seismicity at Mt. Spurr, Alaska, and synthetic data [abs.]: Eos (American Geophysical Union Transactions), v. 77, no. 46, supplement, p. 514.

*Karl, H.A., *Carlson, P.R., and *Gardner, J.V., 1996, Aleutian Basin of the Bering Sea: Styles of sedimentation and canyon development *in* Gardner, J.V., Field, M.E., and Twichell, D.C., eds., Geology of the United States' Seafloor—The View from GLORIA: New York, Cambridge University Press, p. 305–332.

*Karl, H.A., and *Carlson, P.R., 1996, Alaskan EEZ *in* Gardner, J.V., Field, M.E., and Twichell, D.C., eds., Geology of the United States' Seafloor—The View from GLORIA: New York, Cambridge University Press, p. 251–254.

*Kayen, R.E., *Lee, H.J., *Kvenvolden, K.A., and *Lorenson, T.D., 1997, Glacial episodes, gas hydrate, and mass wasting of the contrinental slope: Eos (American Geophysical Union Transactions), v. 78, no. 17, supplement, p. 189.

*Keith, T.E.C., 1997, Real-time monitoring and eruption warning responses by the Alaska Volcano Observatory [abs.]: Eos (American Geophysical Union Transactions), v. 78, no. 46, supplement, p. 37.

*Keith, T.E.C., Nye, C.J., Eichelberger, J.C., *Miller, T.P., and *Power, J.A., 1996, March 1996 seismic crisis at Akutan Volcano, central Aleutian Arc, Alaska [abs.]: Eos (American Geophysical Union Transactions), v. 77, no. 46, supplement, p. 815.

*Kelley, K.D., and *Taylor, C.D., 1997, Environmental geochemistry of shale-hosted Ag-Pb-Zn massive sulfide deposits in northwest Alaska: Natural background concentrations of metals in water from mineralized areas: Applied Geochemistry, v. 12, p. 397–409.

Kusky, T.M., *Bradley, D.C., *Haeussler, P.J., and *Karl, Sue, 1997, Controls on accretion of melange and flysch belts, Chugach terrane, south-central Alaska: Eos (American Geophysical Union Transactions), v. 78, no. 17, supplement, p. 320.

Kusky, T.M., *Bradley, D.C., *Haeussler, P.J., and *Karl, Sue, 1997, Controls on accretion of flysch and mélange belts at convergent margins: Evidence from the Chugach Bay thrust and Iceworm mélange, Chugach accretionary wedge, Alaska: Tectonics, v. 16, p. 855–878.

*Lilly, M.R., Hinzman, L.D., and Wegner, M.A., 1997, Characteristics of ground-water and surface-water interactions in a subarctic basin in central Alaska [abs.]: Eos (American Geophysical Union Transactions), v. 78, no. 46, supplement, p. 311.

*Lorenson, T.D., and *Kvenvolden, K.A., 1996, Nonmethane hydrocarbon gases in permafrost [abs.]: Eos (American Geophysical Union Transactions), v. 77, no. 46, supplement, p. 184.

*Lorenson, T.D., *Kvenvolden, K.A., *Collett, T.S., and *Kayen, R.E., 1997, The search for gas hydrate in northern Alaska and the Beaufort Sea: Eos (American Geophysical Union Transactions), v. 78, no. 17, supplement, p. 189.

*MacKevett, E.M. Jr., *Cox, D.P., Potter, R.W., II, and *Silberman, M.L., 1997, Kennecott-type deposits in the Wrangell Mountains, Alaska: High-grade copper ores near a basalt-limestone contact, *in* Goldfarb, R.J., and Miller, L.D., eds., 1997, Mineral Deposits of Alaska: Economic Geology Monograph 9, p. 66–89.

*McCarthy, K.A., Hinzman, L.D., Braddock, J.F., *Lilly, M.R., Richmond, S.A., and Wegner, M.A., 1997, A hydrological, geochemical, and microbiological characterization of a trichloroethylene-contaminated alluvial aquifer in subarctic Alaska [abs.]: Eos (American Geophysical Union Transactions), v. 78, no. 46, supplement, p. 211.

McLaughlin, E.A., Lilley, M.D., Olson, E.J., *Kvenvolden, K.A., and *Lorenson, T.D., 1996, Methane oxidation in the Beaufort Sea [abs.]: Eos (American Geophysical Union Transactions), v. 77, no. 46, supplement, p. 187–188.

McNutt, S.R., Benoit, J., Christensen, D., Estes, S., Tytgat, G., Stihler, S., Weimer, S., Jolly, A., Robinson, M., Hansen, R., Lindquist, K., Garces, M., *Lahr, J., *Hammond, R., *Power, J., and *Paskievitch, J., 1997, Broadband seismology at the Alaska Volcano Observatory, 1993–1997 [abs.]: Eos (American Geophysical Union Transactions), v. 78, no. 46, supplement, p. 429.

Miller, L.D., and *Goldfarb, R.J., 1997, Preface, *in* Goldfarb, R.J., and Miller, L.D., eds., 1997, Mineral Deposits of Alaska: Economic Geology Monograph 9, p. 1–3.

*Miller, T.P., Begét, J.E., *Stephens, C.D., and *Moore, R.B., 1996, Geology and hazards of Iliamna Volcano, Alaska [abs.]: Eos (American Geophysical Union Transactions), v. 77, no. 46, supplement, p. 815.

*Miller, T.P., *Richter, D.H., *Smith, R.L., and Dreher, S.T., 1997, Caldera-forming events at Aniakchak Volcano, Alaska [abs.]: Eos (American Geophysical Union Transactions), v. 78, no. 46, supplement, p. 816.

*Molnia, B.F., 1996, Kettle formation in 1994 flood deposits —Bering Glacier, Alaska [abs.]: Eos (American Geophysical Union Transactions), v. 77, no. 46, supplement, p. 194.

Monger, J.W.H., and *Nokleberg, W.J., 1996, Evolution of the northern North American Cordillera: Generation, fragmentation, displacement and accretion of successive North American plate-margin arcs, *in* Coyner, A.R., and Fahey, P.L., eds., Geology and Ore Desposits of the American Cordillera: Geological Society of Nevada Symposium Proceedings, Reno/Sparks, Nevada, April 1995, p. 1133–1152.

*Moore, T.E., *Aleinikoff, J.N., and *Harris, A.G., 1997, Stratigraphic and structural implications of conodont and detrital zircon U-Pb ages from metamorphic rocks of the Coldfoot terrane, Brooks Range, Alaska: Journal of Geophysical Research, v. 102, no. B9, p. 20797–20820.

*Moore, T.E., Wallace, W.K., Mull, C.G., *Adams, K.E., *Plafker, George, and *Nokleberg, W.J., 1997, Crustal implications of bedrock geology along the Trans-Alaska Crustal Transect (TACT) in the Brooks Range, northern Alaska: Journal of Geophysical Research, v. 102, no. B9, p. 20645–20684.

*Morrissey, M.M., 1997, Long-period seismicity at Redoubt Volcano, Alaska, 1989–1990 related to magma degassing: Journal of Volcanology and Geothermal Research v. 75, p. 321–335.

*Morrissey, M.M., and *Chouet, B.A., 1997, A numerical investigation of choked flow dynamics and its application to the triggering mechanism of long-period events at Redoubt Volcano, Alaska: Journal of Geophysical Research, v. 102, p. 7965–7983.

Mortera-Gutierrez, C.A., and *Geist, E., 1996, The subducted high relief of Rat fracture zone beneath the Aleutian accretionary prism [abs.]: Eos (American Geophysical Union Transactions), v. 77, no. 46, supplement, p. 659.

*Neal, C.A., *McGimsey, R.G., *Miller, T.P., Nye, C.J., *Bacon, C.R., and *Felger, T.J., 1997, New geologic map of Aniakchak Caldera, Alaska [abs.]: Eos (American Geophysical Union Transactions), v. 78, no. 46, supplement, p. 816.

Newberry, R.J., Crafford, T.C., Newkirk, S.R., Young, L.E., *Nelson, S.W., and Duke, N.A., 1997, Volcanogenic massive sulfide deposits of Alaska, *in* Goldfarb, R.J., and Miller, L.D., eds., 1997, Mineral Deposits of Alaska: Economic Geology Monograph 9, p. 120–150.

Nishenko, S.P., *Bufe, C., *Dewey, J., *Varnes, D., *Healy, J., Jacob, K., and Kossobokov, V., 1996, 1996 Delarof Islands earthquake—A successful earthquake forecast/prediction? [abs.]: Eos (American Geophysical Union Transactions), v. 77, no. 46, supplement, p. 456.

*Nokleberg, W.J., Parfenov, L.M., Monger, J.W.H., Norton, I.O., Khanchuk, A.I., Stone, D.B., *Scholl, D.W., and Fujita, Kazuya, 1997, Tectonic evolution of the Russian Northeast and mainland Alaska [abs.]: Eos (American Geophysical Union Transactions), v. 78, no. 46, supplement, p. 664.

Nye, C.J., *Miller, T.P., and Layer, P.W., 1997, Chemically and temporally distinct magma series at Aniakchak Volcano and the role of crustal mixing [abs.]: Eos (American Geophysical Union Transactions), v. 78, no. 46, supplement, p. 816.

*Oppenheimer, D., *Bittenbinder, A., *Bogaert, B., *Dietz, L., *Ellsworth, W., *Jensen, E., *Kohler, W., *Van Schaack, J., *Buland, R., *Benz, H., Hansen, R., *Weaver, C., Malone, S., and *Okubo, P., 1997, CREST: Consolidated reporting of earthquakes and tsunamis [abs.]: Eos (American Geophysical Union Transactions), v. 78, no. 46, supplement, p. 46.

*O'Sullivan, P.B., Murphy, J.M., and Blythe, A.E., 1997, Late Mesozoic and Cenozoic thermotectonic evolution of the central Brooks Range and adjacent North Slope foreland basin, Alaska: Including fission track results from the Trans-Alaska Crustal Transect (TACT): Journal of Geophysical Research, v. 102, no. B9, p. 20821–20845.

*Phillips, R.L., and *Grantz, Arthur, 1997, Quaternary history of sea ice and paleoclimate in the Amerasia Basin, Arctic Ocean, as recorded

in the cyclical strata of Northwind Ridge: Geological Society of America Bulletin, v. 109, p. 1101–1115.

*Plafker, George, and *Mooney, W.D., 1997, Introduction to special section: The Trans-Alaska Crustal Transect (TACT) across Arctic Alaska: Journal of Geophysical Research, v. 102, no. B9, p. 20639–20643.

*Power, J.A., Jolly, A.D., Harbin, M.L., and Nye, C.J., 1997, Deep long-period events associated with the 1992 eruptions of Crater Peak vent, Mount Spurr, Alaska [abs.]: Eos (American Geophysical Union Transactions), v. 78, no. 46, supplement, p. 438.

*Power, J.A., *Paskievitch, J.F., *Richter, D.H., *McGimsey, R.G., Stelling, P., Jolly, A.D., and Fletcher, H.J., 1996, 1996 seismicity and ground deformation at Akutan Volcano, Alaska [abs.]: Eos (American Geophysical Union Transactions), v. 77, no. 46, supplement, p. 514.

Queen, L.K., Nye, C.J., Benoit, J.P., Dean, K.G., Engle, K., Lindquist, K.G., Servilla, M.S., and *Hammond, W.R., 1997, Near-real time volcano monitoring via the Internet at the Alaska Volcano Observatory [abs.]: Eos (American Geophysical Union Transactions), v. 78, no. 46, supplement, p. 46.

*Riehle, J.R., *Waitt, R.B., *Meyer, C.E., and *Calk, L.C., 1996, Age of Kaguyak caldera, eastern Aleutian arc, Alaska, estimated by tephrochronology [abs.]: Eos (American Geophysical Union Transactions), v. 77, no. 46, supplement, p. 772.

*Rosenbaum, J.G.,*Reynolds, R.L., *Muhs, D.R., *Harlan, S.S., and Beget, J.E., 1997, Geochemical constraint on the interpretation of magnetic property variations in loess/paleosol sequences from central Alaska [abs.]: Eos (American Geophysical Union Transactions), v. 78, no. 46, supplement, p. 171.

Scarpa, R., and *Tilling, R.I., eds., 1996, Monitoring and mitigation of volcano hazards: New York, Springer-Verlag, 841 p.

*Schmidt, J.M., 1997, Shale-hosted Zn-Pb-Ag and barite deposits of Alaska, *in* Goldfarb, R.J., and Miller, L.D., eds., 1997, Mineral Deposits of Alaska: Economic Geology Monograph 9, p. 35–65.

*Schmidt, J.M., 1997, Strata-bound carbonate-hosted Zn-Pb and Cu deposits of Alaska, *in* Goldfarb, R.J., and Miller, L.D., eds., 1997, Mineral Deposits of Alaska: Economic Geology Monograph 9, p. 90–119.

*Schneider, D.J., Dean, K.G., Engle, K., and Worley, S.L., 1997, Monitoring and analyses of volcanic activity using remote sensing data at the Alaska Volcano Observatory [abs.]: Eos (American Geophysical Union Transactions), v. 78, no. 46, supplement, p. 777.

Seramur, K.C., Powell, R.D., and *Carlson, P.R., 1997, Evaluation of conditions along the grounding line of temperate marine glaciers: An example from Muir Inlet, Glacier Bay, Alaska: Marine Geology, v. 140, p. 307–327.

Snyder-Conn, Elaine, *Garbarino, J.R., *Hoffman, G.L., and Oelkers, Alan, 1997, Soluble trace elements and total mercury in arctic Alaskan snow: Arctic, v. 50, no. 3, p. 201–215.

*Starratt, S.W., 1995, Latest Quaternary foraminifers and sediment transport in Pervenets Canyon, Bering Sea: Marine Micropaleontology, v. 26, p. 233–243.

Stevens, C.H., Davydov, V.I., and *Bradley, Dwight, 1997, Permian Tethyan Fusulinina from the Kenai Peninsula, Alaska: Journal of Paleontology, v. 71, p. 985–994.

*Svarc, J.L., *Savage, J.C., *Prescott, W.H., *Lisowski, M., and *Gross, W.K., 1997, Deformation across the Alaska collision zone near Prince William Sound, Alaska 1993–1997 [abs.]: Eos (American Geophysical Union Transactions), v. 78, no. 46, supplement, p. 162.

*Trabant, D.C., and *Mayo, L.R., 1997, Predicted responses of glaciers to climate change along the Gulf of Alaska [abs.]: Eos (American Geophysical Union Transactions), v. 78, no. 46, supplement, p. 250.

Truffer, M., Harrison, W.D., Echelmeyer, K.A., Gorda-DeMallie, J, and *Heinrichs, T.A., 1996, Velocity variations of surge type Black Rapids Glacier [abs.]: Eos (American Geophysical Union Transactions), v. 77, no. 46, supplement, p. 213.

*Vallier, T.L., Mortera-Gutierrez, C.A., *Karl, H.A., Masson, D.G., Prueher, Libby, and *Chase, T.E., 1996, Geology of the Kula paleo-plate, North Pacific Ocean *in* Gardner, J.V., Field, M.E., and Twichell, D.C., eds., Geology of the United States' Seafloor—The View from GLORIA: New York, Cambridge University Press, p. 333–353.

*von Huene, R., and Klaeschen, D., 1997, Strain partitioning across the Kodiak margin [abs.]: Eos (American Geophysical Union Transactions), v. 78, no. 46, supplement, p. 627.

Wallace, W.K., *Moore, T.E., and *Plafker, George, 1997, Multistory duplexes with forward dipping roofs, north central Brooks Range, Alaska: Journal of Geophysical Research, v. 102, no. B9, p. 20773–20796.

*Waythomas, C.F., and *Neal, C.A., 1997, Tsunami generation during the 3500 yr B.P. caldera-forming eruption of Aniakchak Volcano [abs.]: Eos (American Geophysical Union Transactions), v. 78, no. 46, supplement, p. 816.

White, J.M., *Ager, T.A., *Adam, D.P., Leopold, E.B., Liu, G., Jette, H., and Schweger, C.E., 1997, An 18 million year record of vegetation and climate change in northwestern Canada and Alaska: Tectonic and global climatic correlates: Palaeogeography, Palaeoclimatology, Palaeoecology, v. 130, p. 293–306.

Wolf, L.W., Stone, D.B., Fujita, K., *Brocher, T., and Klemperer, S., 1997, A crustal model of the Bering Strait: Implications for tectonic reconstructions [abs.]: Eos (American Geophysical Union Transactions), v. 78, no. 46, supplement, p. 628.

Young, L.E., St. George, Phil, and Bouley, B.A., 1997, Porphyry copper deposits in relation to the magmatic history and palinspastic restoration of Alaska, *in* Goldfarb, R.J., and Miller, L.D., eds., 1997, Mineral Deposits of Alaska: Economic Geology Monograph 9, p. 307–333.

☆ U.S. GOVERNMENT PRINTING OFFICE: 1999 — 573-047 / 20173 Region No. 8